

**COLLECTED PAPERS**  
**ON**  
**COHERENT QUANTUM OPTICS AND TECHNOLOGY**

**Volume 7**  
**August 1991—July 1992**

**Professor**  
**Motoichi OHTSU**

**TOKYO INSTITUTE OF TECHNOLOGY**  
**Interdisciplinary Graduate School of Science and Engineering**  
**4259 Nagatsuta, Midori-ku, Yokohama,**  
**Kanagawa 227, JAPAN**

各位殿

拝啓 時下ますますご清祥のこととお慶び申し上げます。

さて、このたび、前回に引き続きまして、最近の私どもの発表論文をまとめましたので、ここにお送り致します。よろしくご査収下されば幸いです。

いずれも未熟な論文ばかりですので、ご意見、ご批評を賜ればと、お待ちしております。今後ともご指導ご鞭撻のほど、宜しく願い申し上げます。

敬具

平成4年8月

東京工業大学 総合理工学研究科

大津 元一



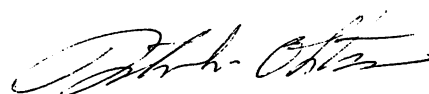
## PREFACE

In order to realize the ultimate status of light and matter, M. Ohtsu aims at the following three research subjects:

- (1) Laser frequency control
- (2) Application of highly coherent semiconductor lasers .
- (3) Photon scanning tunneling microscope.

The papers related to the subject (1) cover several progress in the study on high- $T_c$  oxide super-conducting film for an ultrafast photo-detector and development of a highly accurate optical frequency counting system, which have been made recently. Furthermore, studies on nonlinear optical frequency conversions of semiconductor lasers and on the frequency control of a semiconductor laser-pumped YAG laser have been started to realize a Peta-Hz-class coherent optical sweep generator and a master oscillator for the interferometer of the gravitational wave detection. and these two results will be reviewed in the forthcoming volume. The papers related to the subject (2) cover the development of commercial products of a semiconductor laser-pumped rubidium atomic clock and a passive ring resonator-type fiber gyroscope, which are supported by Research Development Corporation of Japan ( JRDC ) with the cooperation of industries. The subject (3) is devoted to develop a super-resolution optical microscope for diagnostics of micro-devices and biological samples, high-density optical recording, spatially localized spectroscopy, and so on. The final goal of the subject (3) is the manipulation of a single neutral atom by using an optical fiber probe of the photon scanning tunneling microscope as an optical tweezer.

August 1992



Motoichi OHTSU

\* Back numbers of the collected papers are still available on request.

## MEMBERS

### Professor

Motoichi OHTSU ( Dr. Eng. )

### Research Associate

Ken'ichi NAKAGAWA ( Dr. Sci. )

### Graduate Students ( Doctor Candidates )

Shudong JIANG ( M. Eng. ) ( - 03/1992 )

Motonobu KOUROGI ( M. Eng. )

Mituru MUSHA ( M. Sci. )

Togar PANGARIBUAN ( M. Eng. )

Weizhi WANG ( M. Eng. )

### Graduate Students ( Master Course )

Yoshihiko FUJIE ( B. Sci. )<sup>a)</sup> ( - 03/1992 )

Yasumasa KIKUNAGA ( B. Sci. )<sup>b)</sup> ( - 03/1992 )

Keiji YAMAMOTO ( B. Sci. ) ( - 03/1992 )

Yoshinari AWAJI ( B. Eng. )

Madoka KAWAI ( B. Sci. )

Yukitaka SIMIZU ( B. Sci. )

Yasunobu TODA ( B. Eng. )

Takeshi KATSUDA ( B. Sci. ) ( 04/1992 - )

Mikio KOZUMA ( B. Sci. ) ( 04/1992 - )

Shyuji SAYAMA ( B. Eng. ) ( 04/1992 - )



## Undergraduate Students

Takeshi YAMASHITA	
Kazunobu YAMADA	( - 03/1992 )
Takashi ENAMI	( 04/1992 - )
Junichi ICHIHASHI	( 04/1992 - )
Taketo UENO	( 04/1992 - )

## Research Students

Toru IMAI<sup>c)</sup>  
Naoto KITABAYASHI<sup>d)</sup>

## Visiting Scientists

Vitaly Valentino VASILJEV <sup>e)</sup>	( - 10/1991 )
Shudong JIANG <sup>f)</sup>	( 04/1992 - )
Hisao OHSAWA <sup>g)</sup>	

## Secretaries

Sanae OKAMOTO	( 10/1991 - )
Yuko YABE	( - 12/1991 )
Kaoru OGURA	

a) Presently with Recruit Corp.

b) Presently with Toshiba Corp.

c) Permanent affiliation : Tokyo Aircraft Instrument Co. Ltd., Tokyo, Japan

d) Permanent affiliation : Research Lab., Nihon Musen Co. Ltd., Saitama, Japan

e) Permanent affiliation : P.N. Lebedev Physical Institute, Moscow, Russia

f) Permanent affiliation : Shaanxi Institute of Mechanical Engineering

g) Permanent affiliation : Research Lab., NIKON Co. Ltd., Tokyo, Japan

## LIST OF PAPERS

### [I] LASER FREQUENCY CONTROL

#### (a) Journal Papers

[1] K. Nakagawa, M. Teshima, and M. Ohtsu, "Injection Locking of a Highly Coherent and High-power Diode Laser at 1.5  $\mu\text{m}$ ", Opt. Lett., Vol.16, No.20, Oct. 1991, pp.1590-1592

[ pp.1 - 3 ]

[2] T. Senoh, Y. Fujino, Y. Tanabe, M. Hirano, M. Ohtsu, and K. Nakagawa, "Direct Modulation of Blue Radiation from Frequency-doubled AlGaAs Laser Diode Using the Electro-optic Effect in a  $\text{KNbO}_3$  Nonlinear Crystal", Appl. Phys. Lett., Vol.60, No.10, March 1992, pp.1172-1174

[ pp.4 - 6 ]

[3] K. Nakagawa, M. Kouroggi, and M. Ohtsu, "Frequency Noise Reduction of a Diode Laser by Using the FM Sideband Technique", Opt. Lett., Vol.17, No.13, July 1992, pp.934-936

[ pp.7 - 9 ]

[4] M. Ohtsu, "Reduction of the Field Spectral Linewidth of a Semiconductor Laser", Oyo-Buturi ( J. Jpn. Soc. Appl. Phys. ), Vol.60, No.9, Sept. 1991, pp.935-936 ( Review paper, in Japanese )

[ pp.10 - 11 ]

[5] M. Ohtsu, "Wideband Optical Frequency Sweep Generator", Gakujutu Geppo ( Japanese Scientific Monthly ), Vol.45, No.5, May 1992, pp.500 ( Review paper, in Japanese )

[ pp.12 ]

(b) International Conferences

[1] Y. Harada, K. Narushima, M. Sano, M. Sekine, Y. Higashino, and M. Ohtsu, "Optical Response of  $\text{YBa}_2\text{Cu}_3\text{O}_{7-x}$  Epitaxial Thin Films", Proceedings of the 4th International Symposium on Superconductivity ( ISS'91 ), ed. by H. Hayakawa and N. Koshizuka, ( Springer-Verlag, Tokyo 1992 ), ( October 14-17, 1991, Tokyo ), pp.763-766

[ pp.13 - 16 ]

[2] M. Ohtsu, C.-H. Shin, S. Jiang, M. Kouroggi, and K. Nakagawa, "Ultra-narrow Linewidth Semiconductor Lasers and Their Applications", Conference Digest of IEEE Lasers and Electro-Optics Society 1991 Annual Meeting, ( November 4-7, 1991, San Jose, CA ), pp.25 ( Invited )

[ pp.17 ]

[3] T. Fujii, K. Nemoto, R. Ishikawa, A. Awaji, and M. Ohtsu, "Visible Semiconductor Laser for Application to Isotope Separation", Conference Digest of IEEE Lasers and Electro-Optics Society 1991 Annual Meeting, ( November 4-7, 1991, San Jose, CA ), pp.44

[ pp.18 ]

[4] K. Yoshida, M. Kouroggi, K. Nakagawa, and M. Ohtsu, "1/8 Correction Factor of Schawlow-Townes Limit in FM Noise of Negative Frequency Feedback Lasers", Proceedings of the International Conference on Noise in Physical Systems and 1/f Fluctuations", ed. by T. Musha, S. Sato, and M. Yamamoto ( Ohmsya, Tokyo, 1991 ), ( November 24-27, 1991, Kyoto ), pp.349-352

[ pp.19 - 22 ]

[5] M. Kozuma, M. Kouroggi, M. Ohtsu, and H. Hori, "Linewidth Reduction and Fine Detuning of a Semiconductor Laser, Using Velocity-selective Optical Pumping of Atomic Resonance Line", Tech. Digest of Quantum Electronics and

Laser Science Conference, ( Opt. Soc. Am., Washington, D.C., 1992 ), ( May 10-15, Anaheim, CA ), pp.54-55

[ pp.23 - 24 ]

[6] A.M. Akulshin, A. A. Celikov, K. Nakagawa, M. Ohtsu, V.L. Velichansky, "Using Resonances Induced by Coherent Population Trapping for Frequency Difference Stabilization and Microwave Generation", Tech. Digest of the 18th International Quantum Electronics Conference, ( June 14-19, 1992, Vienna ), pp.42-43

[ pp.25 - 26 ]

[7] M. Kourogi, K. Nakagawa, and M. Ohtsu, "A Wideband Optical Frequency Comb Generator for a Highly Accurate Laser Frequency Measurement", Tech. Digest of the 18th International Quantum Electronics Conference, ( June 14-19, 1992, Vienna ), pp.110-112

[ pp.27 - 29 ]

[8] Y. Harada, K. Narushima, M. Sano, M. Sekine, and M. Ohtsu, "Nonbolometric Optical Response of  $\text{DyBa}_2\text{Cu}_3\text{O}_{7-x}$  Epitaxial Thin Films for a Wavelength-Insensitively Fast Photo-Detector", Tech. Digest of the 18th International Quantum Electronics Conference, ( June 14-19, 1992, Vienna ), pp.314-315

[ pp.30 - 31 ]

## [II] APPLICATION OF HIGHLY COHERENT SEMICONDUCTOR LASERS

### (a) Journal Papers

[1] H. Furuta and M. Ohtsu, "Estimation of Frequency Accuracy and Stability in a Diode Laser-Pumped Rubidium Beam Atomic Clock Using a Novel Microwave Resonant Method", Jpn. J. Appl. Phys., Vol.30, No.11A, Nov. 1991, pp.2921-2931

[ pp.32 - 42 ]

[2] M. Ohtsu, "What Time Does Your Clock Have?", Parity ( Japanese Version of Physics Today ), Vol.6, No.10, Oct. 1991, pp.28-34 ( Review paper, in Japanese )

[ pp.43 - 49 ]

(b) International Conferences

[1] T. Imai, K. Nishide, H. Ochi, and M. Ohtsu, "The Passive Ring Resonator Fiber Optic Gyro Using Modulatable Highly Coherent Laser Diode Module", Proceedings of the SPIE Vol.1585, Fiber Optic Gyros: 15th Anniversary Conference, ( Sept. 4-6, 1991, Boston, MA. ), pp.153-162

[ pp.50 - 59 ]

[III] A PHOTON SCANNING TUNNELING MICROSCOPE

(a) Journal Papers

[1] S. Jiang, N. Tomita, H. Ohsawa, and M. Ohtsu, "A Photon Scanning Tunneling Microscope Using an AlGaAs Laser", Jpn. J. Appl. Phys., Vol.30, No.9A, Sept. 1991, pp.2107-2111

[ pp.60 - 64 ]

[2] S. Jiang, H. Ohsawa, K. Yamada, T. Pangaribuan, M. Ohtsu, K. Imai, and A. Ikai, "Nanometric Scale Biosample Observation Using a Photon Scanning Tunneling Microscope", Jpn. J. Appl. Phys., Vol.31, No.7, July 1992, pp.2282- 2287

[ pp.65 - 70 ]

[3] M. Ohtsu, S. Jiang, and H. Ohsawa, "Photon Scanning Tunneling Microscope", Laser Kenkyu ( The Review of Laser Engineering ), Vol.19, No.8, Aug. 1991, pp.839-848 ( Review paper, in Japanese )

[ pp.71 - 80 ]

[4] M. Ohtsu, "Ultrafine Fabrication Technique by a Photon STM", *Kinzoku (Metals and Technology)*, Vol.62, No.3, March 1992, pp.39-44 ( Review paper, in Japanese )

[ pp.81 - 86 ]

[5] M. Ohtsu, "Control of Atomic Motion by Light", *Seimitsu ( J. of the Jpn. Soc. for Precision Engineering )*, Vol.58, No.3, March 1992, pp.410-411 ( Review paper, in Japanese )

[ pp.87 - 91 ]

[6] M. Ohtsu, "What can be done by a Photon STM", *Electronics*, Vol.37, No.4, April 1992, pp.68-72 ( Review paper, in Japanese )

[ pp.92 - 96 ]

(b) International Conferences

[1] S. Jiang, H. Ohsawa, and M. Ohtsu, "Photon Scanning Tunneling Microscope Using Diode Lasers", *Tech. Digest of Optical Society of America Annual Meeting*, ( Nov. 3-8, 1991, San Jose, CA ), pp.65

[ pp.97 ]

[2] M. Ohtsu, "Photon STM, Application to Biotechnology and Single Atom Crystal Growth", *Proceedings of OITDA Second International Forum on New Trends on Scanning Optical Microscopy*, ed. by S. Minami, ( Jan. 8-10, 1992, Naha ), pp. 67-71 ( Invited paper )

[ pp.98 - 102 ]

[3] M. Ohtsu, "Photon STM", *Proceedings of the Second Symposium on "Nanosopic" Science & Technology for Low-Dimensional Materials*, ( April 24, 1992, Wako-shi ), pp.5 ( Invited paper )

[ pp.103 ]

[4] H. Hori, S. Jiang, M. Ohtsu, and H. Ohsawa, "A Nanometer-Resolution Photon Scanning Tunneling Microscope and Proposal of Single Atom Manipulation",

Tech.Digest of the 18th International Quantum Electronics Conference ( June 14-19, 1992, Vienna ) pp.48-49

[ pp.104 - 105 ]

#### PUBLISHED BOOKS

[1] M. Ohtsu, "Coherent Optical Frequency Sweep Generator by Semiconductor Lasers", Chapter 2 in Advanced Non-Linear Optical Organic Materials II, edited by T. Kobayashi, S. Umegaki, H. Nakanishi, and A. Nakamura, CMC Corporation, Tokyo, 1991, pp.121-127 ( In Japanese )

[2] M. Ohtsu, "Optical Properties of Semiconductor Lasers and Their Measurement Techniques", Chapter 3 in Semiconductor Lasers and Optical Measurements, edited by I. Yamaguchi and Y. Tsunoda, Gakkai Shyuppan Center, Tokyo, 1992, pp.31-45 ( In Japanese )

#### AWARDS

[1] M. Ohtsu: K. Sakurai Memorial Award, Optoelectronic Industry and Technology Development Association ( to the achievement of developing super-resolution photon scanning tunneling microscope ), Dec. 19, 1991

[2] M. Ohtsu: Development Award, Teshima Foundation for Industrial Education ( to the achievement of developing a photon scanning tunneling microscope ), March 18, 1992

#### PRESENTED PH.D. THESES

[1] S. Jiang, "A Photon Scanning Tunneling Microscope Using a Semiconductor Laser", January 1992 ( In Japanese )

[2] S. Yamaguchi, "Study on Frequency- and Power-controls of Semiconductor Lasers by Spectroscopic Techniques", January 1992 ( In Japanese )



# Injection locking of a highly coherent and high-power diode laser at 1.5 $\mu\text{m}$

K. Nakagawa, M. Teshima,\* and M. Ohtsu

Graduate School at Nagatuta, Tokyo Institute of Technology, 4259, Nagatsuta-cho, Midori-ku, Yokohama 227, Japan

Received June 10, 1991

Injection locking has been employed to improve the coherence of a high-power diode laser at 1.5  $\mu\text{m}$ . The injected high-power laser emitted in a single mode with a side-mode suppression ratio of larger than 30 dB and an output power of 40 mW. The FM noise of the slave laser was nearly the same as that of the submegahertz-linewidth master laser. We have also demonstrated the coherent addition of the master and the injection-locked slave laser with a residual phase error of  $\delta\phi < 0.2$  rad.

There are growing needs for high-power and highly coherent diode lasers in many applications such as second-harmonic generation, optical communications, and laser spectroscopy. Recent advances in diode-laser devices enable one to achieve a spectral linewidth of less than 1 MHz in the free-running condition,<sup>1</sup> and an active frequency stabilization technique makes it possible to achieve a linewidth of as narrow as 7 Hz.<sup>2</sup> The output power of diode lasers has been continually increasing, and more than 3-W cw output power can be obtained by high-power gain-guided diode-laser arrays or broad-area diode lasers. However, in general, these high-power diode lasers show multitransverse- and longitudinal-mode oscillation. By using an injection-locking technique, the spectral and spatial coherence of these lasers can be drastically improved, and single-mode and single diffraction-limited lobe emission can be obtained.<sup>3-8</sup> Further high power is expected by using the coherent addition of two or more injection-locked high-power diode lasers.<sup>8</sup>

In contrast to many studies of injection-locked high-power GaAlAs diode lasers in the 0.8- $\mu\text{m}$  region,<sup>4-8</sup> there have been few studies of injection locking of InGaAsP high-power diode lasers in the 1.3-1.5- $\mu\text{m}$  region. In this wavelength region, available tunable cw high-power lasers are only color-center lasers, which generally require cryostats and high-power ion lasers as pumping sources. If the diode lasers have high power and highly coherent properties in this wavelength region, these diode lasers will be useful light sources for many applications such as the nonlinear spectroscopy of atoms and molecules, the frequency-stabilized laser at the landmark of the frequency chain between infrared and visible lasers,<sup>9</sup> and the local oscillator of coherent optical communication systems.

Here we present what is to our knowledge the first demonstration of the injection locking of a high-power diode laser at 1.5  $\mu\text{m}$ . The master laser is a multiple-quantum-well distributed-feedback (DFB) diode laser,<sup>1</sup> which emits as much as 10 mW of power at 1.54  $\mu\text{m}$  in a single mode with a linewidth of  $\sim 680$  kHz in the free-running condition.<sup>10</sup> The

high-power slave laser is a single-stripe diode laser (Oki OL503A-65),<sup>11</sup> which emits as much as 65 mW of power at 1.54  $\mu\text{m}$  in a multilongitudinal mode. A schematic diagram of the injection-locking experiment is shown in Fig. 1. The output of the master laser was introduced into the slave laser through two-stage optical isolators (isolation ratio  $> 60$  dB) to avoid optical feedback. A Faraday rotator and polarization beam splitter were used as the optical circulator. The temperature fluctuations of both lasers were reduced to less than 1 mK for stable injection locking. A part of the slave-laser output was introduced into the optical spectrum analyzer to measure the spectral profile of the slave laser.

Figure 2(a) shows the multilongitudinal-mode oscillation of the high-power slave laser in a free-running condition. Under injection locking, the spectrum of the slave laser was single longitudinal mode with a side-mode suppression ratio of larger than 30 dB [Fig. 2(b)]. In this case, the slave laser was biased at  $I/I_{\text{TH}} = 5.9$ , and the output power was  $\sim 40$  mW, which was measured in front of the slave-laser collimator lens. The injected master laser power was 1.5 mW, which was measured in front of the slave laser. Estimated by the relative power of  $\sim 30$  longitudinal modes around the main mode [Fig. 2(b)], the main mode power contained  $\sim 99.6\%$  of the total output power of the slave laser. Figure 3 shows the dependence of the power concentration ratio on injection power. The power concentration ratio is defined as the ratio of the main mode power to the total output power. At a low injection power of less than 0.8 mW, the side modes were not completely suppressed, and the side-mode power decreased as the injection power increased. A maximum power concentration ratio of 99.6% was obtained when the injection power was larger than 0.8 mW. The locking bandwidth was wider than 1 GHz at an injection power of  $\sim 1$  mW, which was estimated by measuring the capture range of the slave-laser injection current.

We have measured the frequency noise (FM noise) of the injection-locked slave laser. The laser FM noise was converted to intensity noise by using

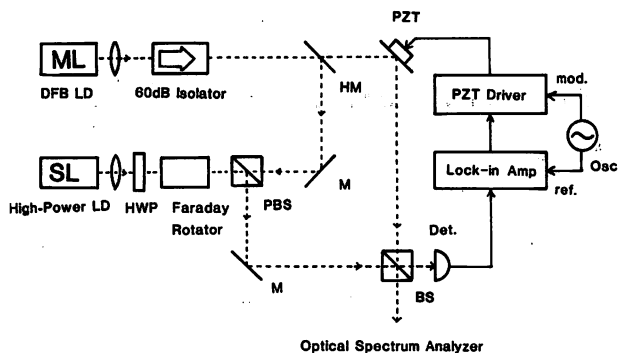


Fig. 1. Schematic diagram of the injection-locking experiment. ML, master laser; SL, slave laser; HWP, half-wave plate; PBS, polarizing beam splitter; HM, half-mirror; LD, laser diode; M's, mirrors; PZT, piezoelectric transducer.

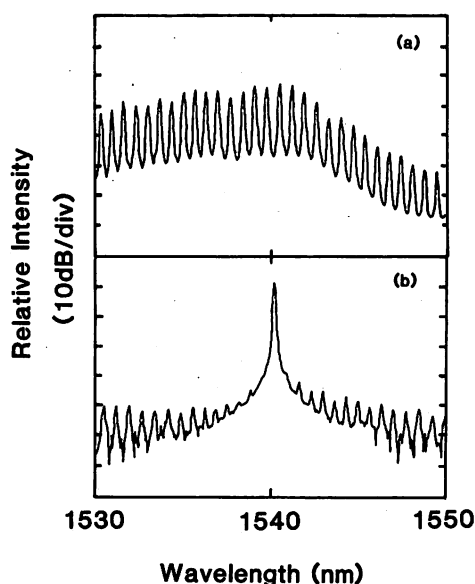


Fig. 2. Spectra of the high-power slave laser: (a) free running, (b) injection locked. The measurements were limited by the 0.1-nm resolution of the optical spectrum analyzer.

the side of a reflection fringe of a 2-GHz étalon (finesse 20).<sup>10</sup> Figure 4(a) shows the FM noise power spectral density of the master laser. We have derived the field spectral profile from this FM noise spectrum and have estimated its spectral linewidth to be  $\sim 680$  kHz.<sup>10</sup> The FM noise spectrum of the injection-locked slave laser was nearly the same as that of the master laser [Fig. 4(b)]. As a result, we have estimated that the spectral linewidth of the slave laser was nearly the same as that of the master laser ( $\sim 680$  kHz).

The relative phase noise between two lasers was estimated by the interference signal between the master and slave lasers (Fig. 5, right side). There is large phase noise in the low-frequency region. This phase noise is caused by the fluctuation and drift of the optical path length. The active servo system effectively reduced this low-frequency phase noise (Fig. 5, left side) to achieve coherent addition between the master and injection-locked slave lasers. We applied a small modulation at 1 kHz and a

low-frequency feedback signal to the piezoelectric-transducer-mounted mirror. The residual phase noise was less than 0.2 rad for over 40 min by estimating the fringe (Fig. 5, inset). This method enables one to maintain a dark fringe at the photodetector side of the beam splitter, whereas the other side has a bright fringe. The coherent addition of two laser powers is given by  $I_{\max} = TI_m + RI_s + 2(RTI_m I_s)^{1/2}$ , where  $I_m$  and  $I_s$  are the master- and slave-laser powers, respectively, and  $T$  and  $R$  are the power transparency and reflectivity of the beam splitter, respectively. If we use a power ratio  $I_m/I_s$  of 0.33 and the 50% beam splitter ( $T = R = 0.5$ ), the fringe visibility, defined as  $V = (I_{\max} - I_{\min}) / (I_{\max} + I_{\min})$ , is expected to be 0.87, whereas the observed value was  $\sim 0.43$  (Fig. 5). This discrepancy is mainly due to the imperfect mode matching between two lasers.

This injection-locked high-power laser can be employed in the saturation spectroscopy of molecular absorption lines in the 1.5- $\mu\text{m}$  region, which will be used as the stable frequency references in many applications such as optical frequency standards and

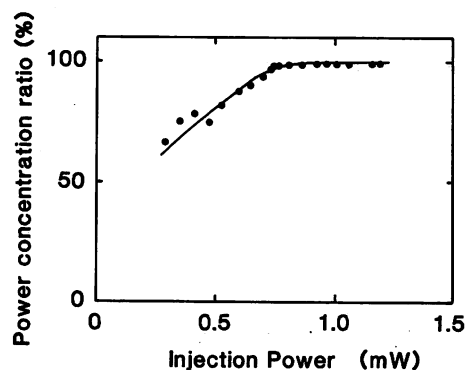


Fig. 3. Power concentration ratio of the main mode power to the total power versus injection power.

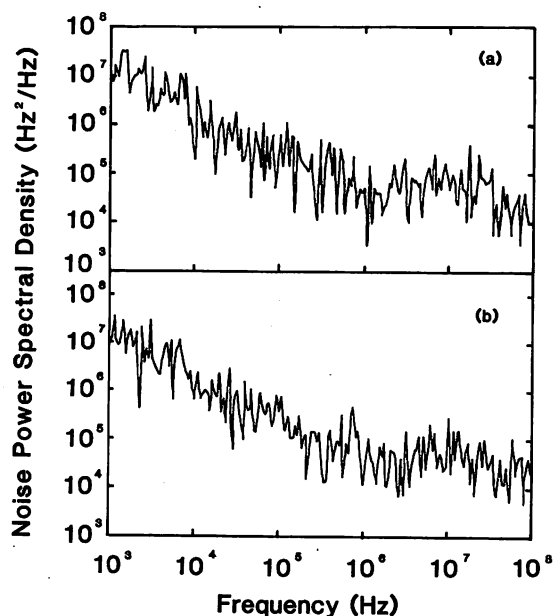


Fig. 4. Power spectral density of the FM noise of (a) the master laser and (b) the injection-locked slave laser.

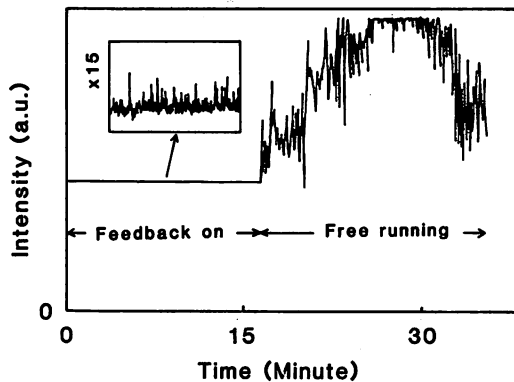


Fig. 5. Relative phase noise between the master and the slave lasers under free-running condition and with the servo control on. The inset is a vertically magnified (15 $\times$ ) trace of the left side.

optical communication.<sup>9,12</sup> Previous studies showed no saturation effects in the case of  $\text{NH}_3$  (Ref. 13) and  $\text{HCN}$  (Ref. 14) molecules when using low-power (<5 mW) modest-linewidth (>30 MHz) DFB lasers. The required saturation conditions are estimated to be more than 50 mW of power and less than 1 MHz in linewidth, which are nearly satisfied by use of the present lasers. This laser will also be applied for an efficient frequency doubling of 1.5- $\mu\text{m}$  lasers, which are used for the frequency chain between 1.5- and 0.78- $\mu\text{m}$  diode lasers<sup>15</sup> and also the recently proposed novel frequency chain methods.<sup>16-18</sup>

In conclusion, injection locking of a high-power laser at 1.5  $\mu\text{m}$  has been achieved with an output power of 40 mW in a single mode and a linewidth of less than 1 MHz. We have also achieved the coherent addition of master and slave lasers with a residual phase error of less than 0.2 rad.

We thank M. Okai of Hitachi Central Laboratory for supplying the submegahertz-linewidth multiple-quantum-well DFB laser and N. Kitabayashi of Japan Radio Company, Ltd., for the loan of the optical spectrum analyzer. We also thank M. Kourogi

of the Tokyo Institute of Technology for helpful advice and discussions about the experiments.

\*Present address, NTT Transmission System Laboratories, 1-2356, Take, Yokosuka 238-03, Japan.

## References

1. M. Okai, T. Tsuchiya, K. Uomi, N. Chinone, and T. Harada, *IEEE Photon. Technol. Lett.* **2**, 529 (1990).
2. C.-H. Shin and M. Ohtsu, *Opt. Lett.* **15**, 1455 (1990).
3. S. Kobayashi and T. Kimura, *IEEE J. Quantum Electron.* **17**, 681 (1981).
4. L. Goldberg, H. F. Taylor, J. F. Weller, and D. R. Scifres, *Appl. Phys. Lett.* **46**, 236 (1985).
5. L. Goldberg and M. K. Chun, *Appl. Phys. Lett.* **53**, 1900 (1988).
6. G. L. Abbas, S. Yang, V. W. S. Chan, and J. G. Fujimoto, *IEEE J. Quantum Electron.* **24**, 609 (1988).
7. S. Q. Shang and H. J. Metcalf, *Appl. Opt.* **28**, 1618 (1989).
8. L. R. Brewer, *Appl. Opt.* **30**, 317 (1991).
9. D. A. Jennings, F. R. Petersen, and K. M. Evenson, *Opt. Lett.* **4**, 129 (1979).
10. M. Kourogi, C.-H. Shin, and M. Ohtsu, *IEEE Photon. Technol. Lett.* **3**, 496 (1991).
11. H. Horikawa, S. Oshiba, A. Motoba, and Y. Kawai, *Appl. Phys. Lett.* **50**, 374 (1987).
12. S. Sudo, Y. Sakai, H. Yasaka, and T. Ikegami, *IEEE Photon. Technol. Lett.* **1**, 281 (1989).
13. K. Nakagawa, Ph.D. dissertation (University of Tokyo, Tokyo, 1989).
14. H. Sasada, *J. Chem. Phys.* **88**, 797 (1988).
15. M. Ohtsu and E. Ikegami, *Electron. Lett.* **25**, 22 (1989).
16. T. Sato, S. Swartz, and J. L. Hall, in *Digest of International Quantum Electronics Conference* (Optical Society of America, Washington, D.C., 1990), paper QTHD3.
17. H. R. Telle, D. Meschede, and T. W. Hänsch, *Opt. Lett.* **15**, 532 (1990).
18. M. Kourogi, K. Nakagawa, C.-H. Shin, M. Teshima, and M. Ohtsu, in *Digest of Conference on Lasers and Electro-Optics* (Optical Society of America, Washington, D.C., 1991), paper CThR57.

# Direct modulation of blue radiation from frequency-doubled AlGaAs laser diode using the electro-optic effect in a KNbO<sub>3</sub> nonlinear crystal

T. Senoh, Y. Fujino, Y. Tanabe, and M. Hirano

Asahi Glass Co., Ltd., Research Center, 1150 Hazawa, Kanagawa-ku, Yokohama 221, Japan

M. Ohtsu and K. Nakagawa

Tokyo Institute of Technology, Graduate School at Nagatsuta, 4259 Nagatsuta, Midori-ku, Yokohama 227, Japan

(Received 29 July 1991; accepted for publication 2 December 1991)

A novel method for modulating frequency-doubled blue radiation from an AlGaAs laser diode was developed utilizing the electro-optic effect in a KNbO<sub>3</sub> nonlinear crystal. Stable blue radiation was obtained from an external ring resonant cavity containing a KNbO<sub>3</sub> crystal. The weakly excited counterpropagating mode in the resonant cavity was re-injected into the laser diode to establish self-locking. Nearly 100% intensity modulation was observed when a 3 kV/cm ac electric field was applied parallel to the *c* axis of the KNbO<sub>3</sub> crystal.

Since several demonstrations of direct doubling of the frequency of radiation from a laser diode utilizing a resonant cavity containing a KNbO<sub>3</sub> crystal together with either an electrical or an optical feedback technique,<sup>1-3</sup> blue lasers realized by these techniques have been considered promising for practical applications. They are simple in structure, small in size, and in particular, they have high-conversion efficiency. However, direct or internal modulation of the blue-doubled radiation, which greatly enhances some applications including optical data storage<sup>4</sup> and laser printing, has not been reported so far.

In this letter, we report a novel method for direct modulation of the frequency-doubled blue radiation.<sup>5</sup> Very stable radiation up to 6.6 mW was obtained by an optical feedback self-locking technique using a ring buildup cavity. The blue radiation was directly modulated, for the first time, utilizing the electro-optic effect (EO effect) of a KNbO<sub>3</sub> nonlinear crystal.

An *a*-cut KNbO<sub>3</sub> crystal, having a high nonlinear susceptibility, was used as a second-harmonic generation crystal, which was grown by the top-seeded solution growth method in our laboratory.<sup>6-9</sup> The crystal size was 3×3×2 mm. Phase matching was achieved by temperature tuning; that is, noncritical phase matching for 860 nm fundamental radiation of the laser diode was realized at room temperature, where the nonlinear susceptibility *d*<sub>32</sub> was used.<sup>6-8</sup>

The experimental setup for modulating the frequency-doubled radiation is schematically shown in Fig. 1. An AlGaAs laser oscillating in the single-mode at 862 nm with about a 100 mW output was mode-matched to a triangular ring-buildup cavity. A 3-mm-long KNbO<sub>3</sub> crystal was placed in the beam waist of the cavity. The locking of the laser diode to the cavity resonance frequency was achieved by an optical feedback technique, where the counterpropagating fundamental mode excited at one facet of the KNbO<sub>3</sub> crystal was re-injected into the laser diode. To stabilize the self-locking, the optical path length between the diode laser and the ring cavity was precisely controlled by

employing proportional and integration (*P-I*) feedback PZT mounted mirrors. The maximum output of the second harmonic was about 6.6 mW when fundamental radiation of 90 mW is introduced into the resonant cavity.

Figure 2 shows the fluctuation of the second harmonic output power fluctuates with time. When the *P-I* control loop was closed, the fluctuation was remarkably reduced to less than 0.1% over several hours.

In order to modulate the stable CW output, an electric field was applied to the KNbO<sub>3</sub> crystal in the cavity. As shown in Fig. 3, electrodes were fixed on *c* planes of the crystal so that an applied electric field was directed parallel to the *c* axis. The laser beam propagated along the *a* axis with the polarization parallel to the *b* axis. Thus, the second harmonic was polarized parallel to the *c* axis.

When the electric field was applied, the refractive index *n<sub>b</sub>* for the fundamental radiation, remained practically unchanged, while *n<sub>c</sub>* for the second-harmonic generation changed because the electro-optic coefficient *r*<sub>33</sub> for the blue radiation is about 50 times larger than *r*<sub>23</sub> for the IR

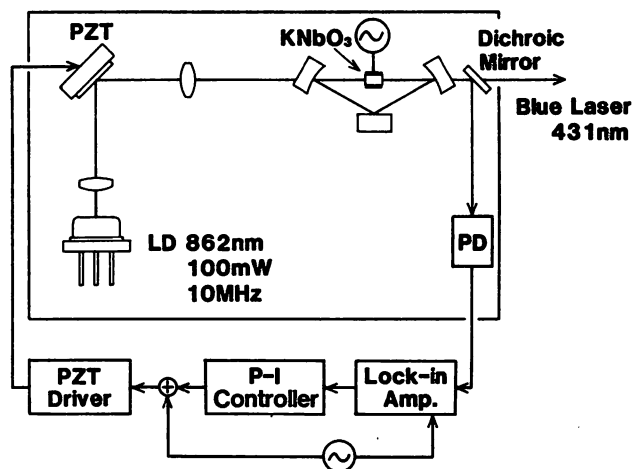


FIG. 1. Experimental setup for modulating frequency-doubled radiation.

**Stability < 0.1%**

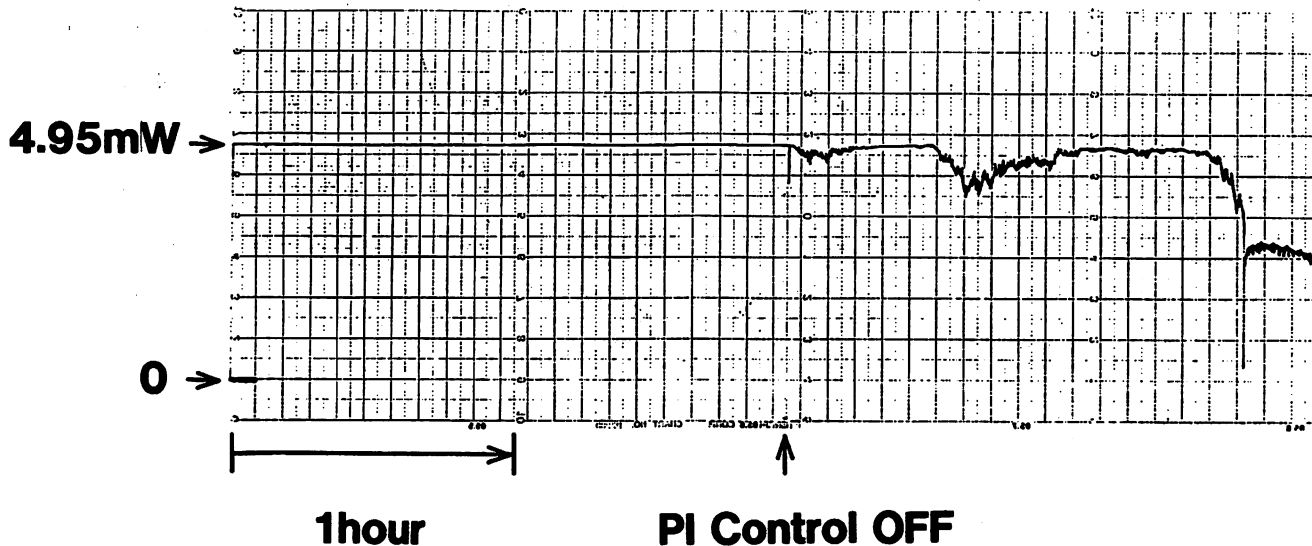


FIG. 2. Fluctuation of the second-harmonic output with and without *P-I* control.

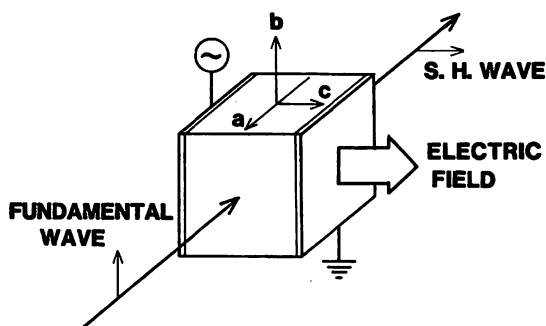


FIG. 3. Geometric configuration of light propagation and applied electric field with respect to crystal axes.

radiation. Therefore, the phase-matching condition for the frequency doubling was violated by applying the electric field, while the very stable frequency locking remained. As a result, the blue radiation was selectively modulated due to the electric-field application.

Figure 4 shows oscilloscope traces of the second harmonic as well as the fundamental when a rectangular electric field of 3 kV/cm was applied to the KNbO<sub>3</sub> crystal. It can be clearly seen that the blue radiation was deeply modulated, keeping the frequency locking unchanged. Figure 5 shows the applied field dependence of the modulation depth. The depth increased with the electric field, and the second-harmonic radiation was fully modulated when the field exceeded more than 3 kV/cm. The repetition rate in this figure was 0.3 kHz, which was limited by switching frequency of the driving circuit. Wideband characteristics

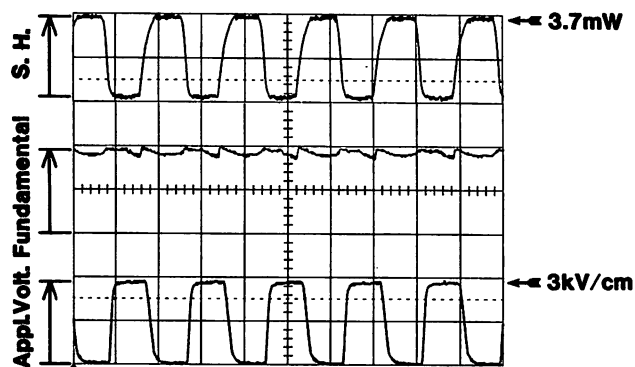


FIG. 4. Oscilloscope traces of the second harmonic and the fundamental when the electric field is applied to the KNbO<sub>3</sub> crystal.

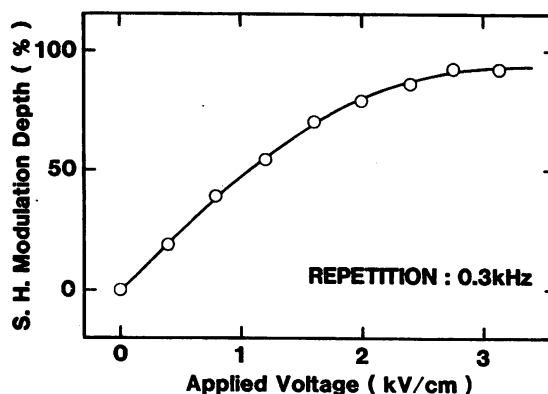


FIG. 5. Applied electric-field dependence of the modulation depth.

are generally expected in the switching mechanism due to the electro-optic effect. Therefore, improvements of the electric circuit will allow the increase of modulation frequency up to GHz range.

Modulated small size blue lasers with high-conversion efficiency and stable output are very promising for practical applications such as optical data storage and printing light sources.

<sup>1</sup>G. J. Dixon, C. T. Tanner, and C. E. Wieman, *Opt. Lett.* **14**, 731 (1989).

<sup>2</sup>L. Goldberg and M. Chun, *Appl. Phys. Lett.* **55**, 218 (1989).

<sup>3</sup>W. J. Kozlovsky, W. Lenth, E. E. Latta, A. Moser, and G. L. Bona, *Appl. Phys. Lett.* **56**, 2291 (1990).

<sup>4</sup>D. Ruger, C. J. Lin, and R. Geiss, *IEEE Trans. Magn. MAG-23*, 2263 (1987).

<sup>5</sup>T. Senoh, Y. Fujino, Y. Tanabe, M. Ohtsu, and K. Nakagawa, in *Technical Digest of Conference on Laser and Electro-Optic* (Optical Society of America, Washington, DC, 1991), paper CWA 6.

<sup>6</sup>P. Günter, *Appl. Phys. Lett.* **34**, 650 (1979).

<sup>7</sup>P. Günter, P. M. Asbeck, and S. K. Kurtz, *Appl. Phys. Lett.* **35**, 461 (1979).

<sup>8</sup>J. C. Baumert, P. Günter, and H. Melchior, *Opt. Commun.* **48**, 215 (1983).

<sup>9</sup>P. Günter, *Electro-optics/Laser Proceedings International '76 UK*, edited by H. G. Jerrard (IPC Science and Technology, England, 1976), p. 121.

*Published without author corrections*

# Frequency noise reduction of a diode laser by using the FM sideband technique

K. Nakagawa, M. Kourogi, and M. Ohtsu

Graduate School at Nagatsuta, Tokyo Institute of Technology, 4259, Nagatsuta-cho, Midori-ku, Yokohama 227, Japan

Received February 13, 1992

The frequency of a 1.5- $\mu\text{m}$  three-electrode multiple-quantum-well distributed-feedback diode laser was stabilized to a reference Fabry-Perot cavity by using a current-modulated FM sideband technique. The low-frequency AM noise imposed on the frequency error signal was effectively reduced with this technique, and the power spectrum density of the FM noise was reduced to less than  $25 \text{ Hz}^2/\text{Hz}$  at a Fourier frequency of less than 10 kHz, which corresponded to a Lorentz spectral half-linewidth of approximately 80 Hz.

Improvement of the spectral purity in diode lasers has been an area of growing interest in many applications such as optical communications, optical precision measurements, and high-resolution spectroscopy.<sup>1</sup> The spectral linewidths of commercial diode lasers are typically 5–100 MHz, which is mainly due to the low-quality factors of laser cavities. Optical feedback from a high-finesse cavity is one of the effective methods to reduce the linewidth of diode lasers to approximately 20 kHz.<sup>2</sup> The negative electrical feedback (NEF) method, which uses injection current feedback and an external reference Fabry-Perot cavity, also makes it possible to reduce the linewidth to 250 Hz.<sup>3</sup> Recently a linewidth of 7 Hz has been achieved by using the NEF method, in which the optical feedback was employed in an auxiliary way to extend the feedback bandwidth.<sup>4</sup> In addition, recent improvements in semiconductor fabrication techniques have resulted in the development of submegahertz diode lasers.<sup>5</sup>

Here we present a novel frequency-noise-reduction technique of diode lasers by using a FM sideband technique known as the Pound-Drever method.<sup>6</sup> The laser frequency was modulated by the injection current instead of using an external electro-optic modulator. In our previous experiments on frequency noise reduction with the NEF method we locked the laser frequency to the side of the fringe of a reference cavity for use as a frequency discriminator, and the residual frequency noise under the feedback was due mainly to the low-frequency laser amplitude noise.<sup>3,4</sup> The advantage of the FM sideband technique is that one can easily obtain shot-noise-limited high sensitivity. We could effectively reduce the amplitude noise in the frequency error signal and obtain better frequency stability by using this technique.

A schematic diagram of our experiment is shown in Fig. 1. We used a three-electrode multiple-quantum-well (MQW) distributed-feedback (DFB) diode laser operating at 1.54  $\mu\text{m}$ .<sup>5</sup> A dc injection current was divided and fed into all three electrodes. This laser showed stable single-mode oscillation with its output power of as much as 10 mW at

the bias level of  $I/I_{\text{th}} = 3$ . Its spectral linewidth was approximately 680 kHz under the free-running condition.<sup>3</sup> The output of the laser was introduced into a reference Fabry-Perot cavity through two-stage optical isolators (isolation ratio >60 dB). The reference cavity was a commercial confocal spectrum analyzer with a free spectral range of 300 MHz and a finesse of greater than 150. The efficiency of the reflection mode of this cavity was approximately 60%. Considering the cavity linewidth of approximately 2 MHz and the wide feedback bandwidth, we used a FM modulation frequency ( $f_m$ ) of 20 MHz. The modulation current was fed into a side electrode. The FM responses of the middle and side electrodes are approximately 600 and 80 MHz/mA, respectively.<sup>3</sup> A reflected light from the reference cavity was detected with an InGaAs p-i-n photodiode. Typical detected power was 1 mW. The photocurrent was amplified with a low-noise pre-amplifier and demodulated with a double-balanced mixer (DBM). The  $2f_m$  (40 MHz) component was eliminated with a band-elimination filter (BEF) before the mixer. The high-frequency ( $f > 10 \text{ kHz}$ ) component of feedback signal was directly fed back to the middle electrode. The low-frequency

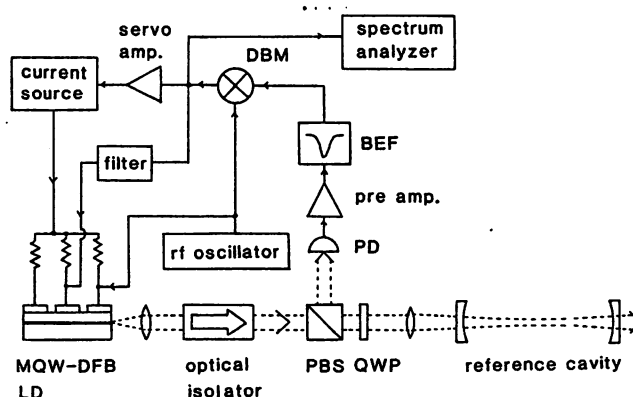


Fig. 1. Schematic diagram of the experimental setup. LD, laser diode; PBS, polarizing beam splitter; QWP, quarter-wave plate; PD, photodetector; BEF, band-elimination filter at  $2f_m$ .

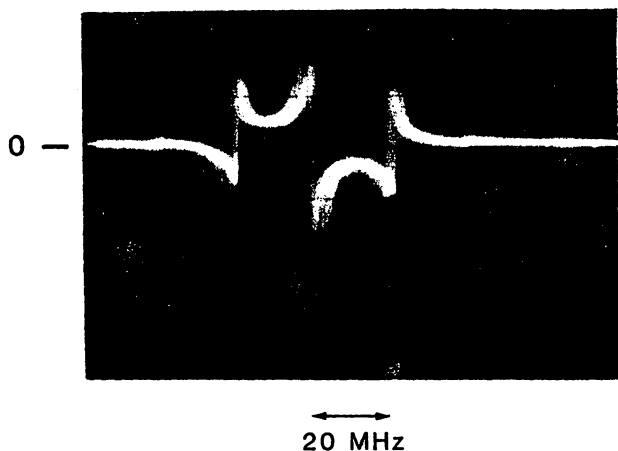


Fig. 2. Oscilloscope trace of the demodulated dispersion signal of the reference cavity.

( $f < 10$  kHz) component was amplified and fed back to all electrodes through a dc current source.

The demodulated signal is shown in Fig. 2. The modulation index was approximately 0.5. By adjusting the length of a coaxial cable between a rf oscillator and the DBM, the dispersive resonance signal profile of the reference cavity was obtained. This signal shows a sharp carrier component at the center and clearly resolved FM sideband components at both sides.

The problem of the injection current modulation of diode lasers is that it causes a simultaneous frequency and amplitude modulation of the laser output.<sup>7</sup> As a result, the detection sensitivity is limited by this AM effect in current-modulated diode-laser FM spectroscopy. The amplitude-modulated and frequency-modulated laser light field is given by

$$E(t) = E_0[1 + A \cos(2\pi f_m t + \delta)] \times \exp[i2\pi\nu_0 t + iM \sin(2\pi f_m t)], \quad (1)$$

where  $\nu_0$  is the laser carrier frequency,  $f_m$  is the modulation frequency,  $A$  is the AM index, and  $M$  is the FM (or phase-modulation) index. Considering the instantaneous laser frequency  $\nu(t) = \nu_0 + Mf_m \cos(2\pi f_m t)$ , we define  $\delta$  as the phase difference between AM and FM. After the reflection from the reference cavity, this amplitude-modulated and frequency-modulated light possesses the information of the response characteristics of the reference cavity, which is represented by a complex transfer function  $H_{FP}(\nu_0)$ . When  $\nu_0$  is near the cavity resonance frequency, and the cavity linewidth is narrower than  $f_m$ , the ac component of the photocurrent at  $f_m$  is

$$I(t) = 2I_0(\text{Re}[H_{FP}(\nu_0)]A[-\sin \delta(1 + M^2/2) \times \sin(2\pi f_m t) + \cos \delta \cos(2\pi f_m t)] + \text{Im}[H_{FP}(\nu_0)]M\{[1 - (A^2 \sin^2 \delta)/2] \times \sin(2\pi f_m t) + (A^2 \sin \delta \cos \delta) / 2 \cos(2\pi f_m t)\}), \quad (2)$$

where  $I_0$  is the dc component of the photocurrent. The imaginary part  $\text{Im}[H_{FP}(\nu_0)]$  gives the dispersive

signal used as the frequency discriminator. However, the real part  $\text{Re}[H_{FP}(\nu_0)]$  gives the nonzero background signal that contains the low-frequency AM noise. If the phase difference  $\delta$  is zero, the real and imaginary parts of  $H_{FP}(\nu_0)$  are out of phase, and the pure dispersive signal can be obtained with no background.<sup>8</sup> On the other hand, if the AM index ( $A$ ) is much smaller than the FM index ( $M$ ), the background contribution is also negligible. In Fig. 2, this AM-induced background signal is sufficiently small. We believe that this was because the real and imaginary parts of  $H_{FP}(\nu)$  are out of phase. This was confirmed by the FM response characteristic of this three-electrode DFB diode laser, which showed a nearly flat FM response and a phase difference  $\delta$  of nearly zero up to 100 MHz.<sup>3,9</sup> We believe that the sensitivity of the frequency error signal is limited by the AM noise at the modulation frequency  $f_m = 20$  MHz, where the AM noise of the diode laser is within 10 dB above the shot-noise level.

Figure 3(a) shows the power spectrum density of the frequency noise under free-running (upper trace) and feedback (lower trace) conditions, respectively. The feedback bandwidth was approximately 6 MHz, and the 60-dB frequency noise reduction was achieved at a Fourier frequency of  $f = 1$  kHz. For

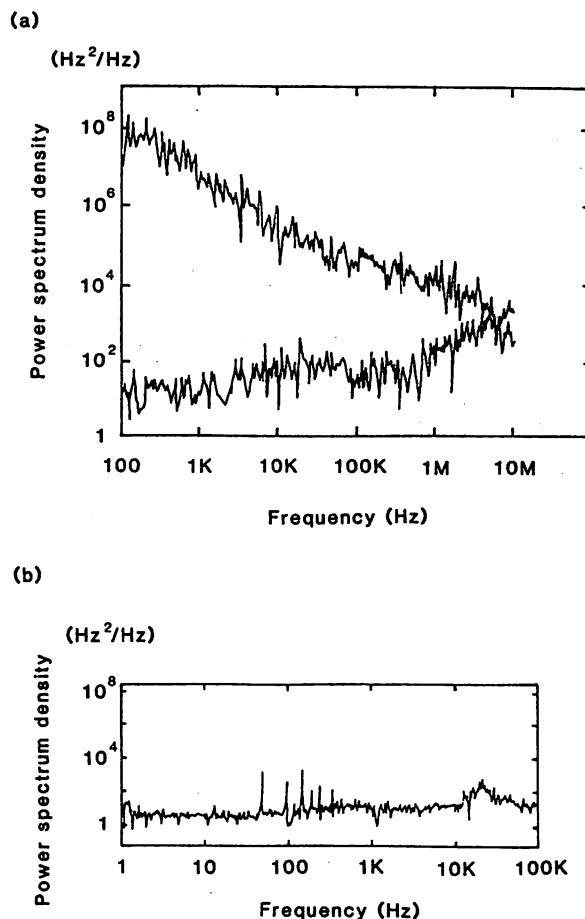


Fig. 3. Power spectral density of the frequency noise. The upper and lower curves in (a) show the frequency noise of the free-running and stabilized laser, respectively. The low-frequency (1–100 kHz) component of the frequency noise is shown in (b).



$f < 10$  kHz [Fig. 3(b)], the frequency noise was fully reduced to lower than approximately  $25 \text{ Hz}^2/\text{Hz}$ . Our previous experiment, which used fringe side locking, showed that the frequency noise was increasing at  $f < 10$  kHz and was approximately 40 dB higher than the present noise level at  $f = 1$  Hz because of the low-frequency AM noise.<sup>3</sup> The laser half-linewidth under feedback was estimated to be approximately 80 Hz from the relation between the power spectral density of the frequency noise  $S$  ( $\text{Hz}^2/\text{Hz}$ ) and the Lorentzian spectral half-linewidth  $\Delta\nu$  (Hz) of  $\Delta\nu = \pi S$ . This is to our knowledge the narrowest linewidth achieved by the NEF method. The power concentration ratio within the feedback bandwidth (6 MHz) was estimated to be roughly 99%.<sup>4</sup> The residual frequency noise was still higher than the calculated shot-noise limit of approximately  $10^{-3}$  ( $\text{Hz}^2/\text{Hz}$ ). This is partly due to the residual AM noise caused by the inadequate phase adjustment of the rf oscillator. Further improvement of the frequency stability should require not only the accuracy of the phase adjustment but also the acoustic, mechanical, and thermal isolation of the present reference cavity, which was made of super Invar and was directly mounted on the optical stage.

The present narrow-linewidth FM diode laser is useful for highly sensitive and high-resolution spectroscopy as Doppler-free FM spectroscopy.<sup>10,11</sup> The absolute laser frequency can be stabilized with high accuracy by using saturation absorptions of atoms<sup>12</sup> or molecules in the  $1.5\text{-}\mu\text{m}$  region. When the FM output is an obstacle to some applications, one can use a transmitted light from a reference cavity. The cavity acts as the passive bandpass filter, and the sideband components can be effectively reduced when the modulation frequency is high enough compared with the cavity linewidth.

In conclusion, we have demonstrated fre-

quency noise reduction of a three-electrode multiple-quantum-well distributed-feedback diode laser by using the FM sideband technique. The frequency noise under the feedback was not affected by the low-frequency AM noise on the laser and was reduced to less than  $25 \text{ Hz}^2/\text{Hz}$  below 10 kHz, which gave the Lorentzian half-linewidth as narrow as 80 Hz.

The authors thank N. Chinone and M. Okai, Central Research Laboratory, Hitachi, Ltd., for supplying the distributed-feedback diode laser and their helpful discussions. This research was supported by a Grant-in-Aid for Scientific Research (No. 03250205) from the Ministry of Education, Science, and Culture of Japan.

## References

1. M. Ohtsu, *Highly Coherent Semiconductor Lasers* (Artech House, Boston, Mass., 1992).
2. B. Dahmani, L. Hollberg, and R. Drullinger, *Opt. Lett.* **12**, 876 (1987).
3. M. Kourogi, C.-H. Shin, and M. Ohtsu, *IEEE Photon. Technol. Lett.* **3**, 496 (1991).
4. C.-H. Shin and M. Ohtsu, *Opt. Lett.* **15**, 1455 (1990).
5. M. Okai, T. Tsuchiya, K. Uomi, N. Chinone, and T. Harada, *IEEE Photon. Technol. Lett.* **3**, 427 (1991).
6. R. W. P. Drever, J. L. Hall, F. V. Kowalski, J. Hough, G. M. Ford, A. J. Munley, and H. Ward, *Appl. Phys. B* **31**, 97 (1983).
7. W. Lenth, *IEEE J. Quantum Electron.* **QE-20**, 1045 (1984).
8. W. Lenth and M. Gehrtz, *Appl. Phys. Lett.* **47**, 1263 (1985).
9. O. Ishida and H. Toda, *Electron. Lett.* **23**, 1161 (1987).
10. J. L. Hall, L. Hollberg, T. Baer, and H. G. Robinson, *Appl. Phys. Lett.* **39**, 680 (1981).
11. G. P. Barwood, P. Gill, and W. R. C. Rowley, *Opt. Commun.* **80**, 359 (1991).
12. A. J. Lucero, Y. C. Chung, S. Reilly, and R. W. Tkach, *Opt. Lett.* **16**, 849 (1991).



# 半導体レーザー

東工大総理工 大津元一

## 1. まえがき

光通信、さらにはパリティ非保存の検証などの基礎物理学への応用において、スペクトル線幅の狭い半導体レーザーが必須光源となりつつある。レーザーの周波数揺らぎを広帯域にわたり抑圧すれば線幅が狭く化される。半導体レーザーはその共振器損失が大きいため、大きな周波数揺らぎを有するが、一方、注入電流(つまり活性層内のキャリア密度)を変調すると屈折率が、したがって周波数が変調される。この変調の効率は大きく、帯域は広い。この特徴を利用すれば、線幅狭く化が可能である。以下ではこの方法について述べる。

## 2. 電氣的制御法

周波数揺らぎを光周波数復調器により検出し、復調信号を半導体レーザーの注入電流に負帰還する。この方法はレーザー周波数のドリフトを抑え、かつ高利得制御が可能という特長を有する。制御帯域は制御ループ長によって制限されるが、最近では100MHz以上の帯域が実現し、ループ長よりもむしろ半導体レーザーの群遅延特性により制限されるまで広帯域化されている<sup>1)</sup>。

高感度の光周波数復調器としては、ファブリー・ペロー(FP)共振器が有望である。特にFP共振器中に偏光コントローラーを設置し、光平衡検出器で復調する方法では、強度揺らぎの影響の除去、高利得・広帯域、広キャプチャーレンジ、FP共振器の他の使い方よりも周波数揺らぎ抑圧の際のショット雑音限界が小さい、光ファイバーなどを用いてコンパクト化可能、などの際立った利点を有する<sup>2)</sup>。さらに、最近ではフィネス $1 \times 10^6$

以上のFP共振器も実現しており、高い復調感度を得られる。

電氣的制御の場合には、広い変調周波数範囲にわたり、半導体レーザーの周波数変調効率が均一であることが望ましい。最近では、DFBレーザーの電極を分割したものが、このような均一性を示すことが確かめられている<sup>3)</sup>。このレーザーを用い、図1に示すように線幅250Hz

が得られている。このとき、制御帯域内へのパワー集中度は99%以上に達することも確認されている<sup>3)</sup>。

## 3. 光學的制御法

図2に光學的制御法の一例を示す<sup>4)</sup>。共焦点型FP共振器からの戻り光をレーザーに再注入する。この光によりキャリア密度、したがってレーザー周波数が変化する。戻り光量はレーザー周波数がFP共振器の共振周波数に合致したとき最大となるので、この光帰還によりレーザー周波数はFP共振器の共振周波数に引き込まれ、線幅が狭く化される。

約10kHzの線幅を得ることが可能である。この方法は構造が簡単であるが、

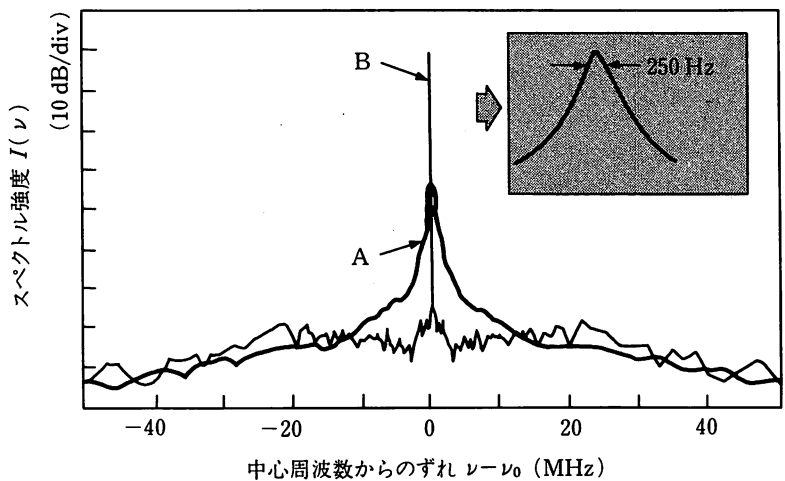


図1 波長1.5 μm DFBレーザーのスペクトル形状<sup>3)</sup>。A: 非制御時、B: 電氣的制御時。

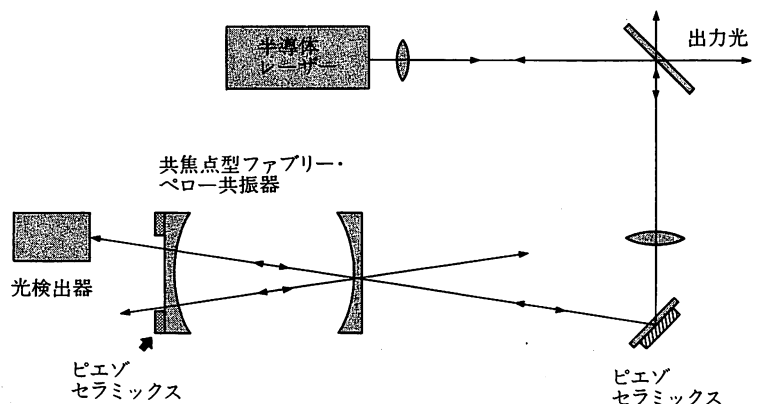


図2 共焦点型ファブリー・ペロー共振器を用いた光學的制御法の原理<sup>4)</sup>。

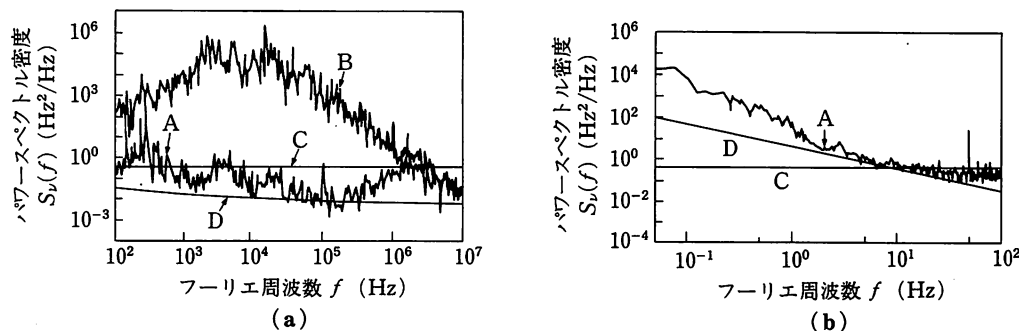


図3 電気・光学的制御時のAlGaAsレーザー(波長0.8 $\mu\text{m}$ )の周波数揺らぎのパワースペクトル密度の測定結果<sup>7)</sup>。(a)フーリエ周波数100Hz~10MHzにおける値。(b)フーリエ周波数50mHz~100Hzにおける値。A:最大利得帯域の場合。B:利得帯域、ともに低い制御の場合。C:幅1Hzのローレンツ型スペクトル形状をもつレーザーの周波数揺らぎの値。D:レーザーのパワー揺らぎの影響により制限される周波数揺らぎ検出限界。

周波数ドリフトは抑圧できない。-3 dB 利得制御帯域は、FP共振器の共振スペクトル線幅の半分に対応する。

制御利得は2.の方法に比べ小さいが、帯域を広くとることが可能である。例えば、微小半球やファイバーを用いることにより、自由スペクトル域の大きなFP共振器を作れば<sup>5)</sup>、制御帯域は半導体レーザーの緩和振動周波数以上の値にもなりうる。最近では、このような周波数選択性のある外部反射体を集積化したレーザー素子の製作も試みられ、線幅7kHzが得られている<sup>6)</sup>。

#### 4. 電気・光学的制御法

3.の光学的制御法は広い制御帯域をもつが、周波数ドリフトを抑圧できず、また制御利得も低い。この欠点を解決するには電氣的制御法を適用するのが不可欠である。すなわち、予備的に光学的制御を施し、さらに同時に電氣的制御を施す。この電氣的制御法により、高安定、広帯域、高利得制御が初めて実現する。

図3(a), (b)中の曲線Aは、それぞれこのような電気・光学的制御法の結果得られた周波数揺らぎのパワースペクトル密度を、フーリエ周波数100Hz~10MHzおよび、50mHz~100Hzにわたって測定した結果を示す<sup>7)</sup>。

図3の曲線Aの値から推定されるレーザーの線幅は7Hz、さらに制御帯域内でのパワー集中度98%以上であること

が確認されている<sup>7)</sup>。特にフーリエ周波数500Hz~2MHzの範囲では、曲線Aのパワースペクトル密度の値は、線幅1Hzのローレンツ型スペクトルをもつ光の周波数揺らぎ値(曲線C)より小さい。すなわち、このレーザーを応用するシステムの使用帯域が500Hz~2MHzに限られているとき、このレーザーの線幅は1Hz以下に対応する。今後、装置の改良により、数mHzの線幅の実現が可能と試算されている。

#### 5. むすび

上記の制御方式により、線幅狭く化の実験が著しく進歩している。一方、空間的ホールバーニングを抑圧したDFB、多重量子井戸、長共振器、などの構造を導入し、レーザー素子自身の線幅を狭くする試みも活発に行われている。実際のシステムにこれらのレーザーを使用する多くの場合にも、種々の制御が重要であり、また、このような制御を施すことにより、さらに線幅が狭く化される。線幅が1Hz以下になると、新しい量子光学研究用や新型発光素子開発用の光源として威力を発揮するので、今後一層の研究の進展が期待されている。

- 1) M. Kouroggi, C.-H. Shin and M. Ohtsu: IEEE Photon. Technol. Lett. 3, 270 (1991).
- 2) M. Kouroggi and M. Ohtsu: Opt.

Commun. 81, 204 (1991).

- 3) M. Kouroggi, C.-H. Shin and M. Ohtsu: IEEE Photon. Technol. Lett. 3, No.6 (1991) 印刷中.
- 4) B. Dahmani, L. Hollberg and R. Drullinger: Opt. Lett. 12, 876 (1987).
- 5) C.-H. Shin, M. Teshima, M. Ohtsu, T. Imai, J. Yoshida and K. Nishide: IEEE Photon. Technol. Lett. 2, 167 (1990).
- 6) D. A. Ackerman, M. I. Danbura, Y. Shani, C. H. Henry, R. C. Kisler, R. Y. Kazarinov and C. Y. Kuo: Appl. Phys. Lett. 58, 449 (1991).
- 7) C.-H. Shin and M. Ohtsu: Opt. Lett. 15, 1455 (1990).

分類番号 7.7, 7.1  
Semiconductor lasers. Motoichi OHTSU.  
Graduate School at Nagatsuta, Tokyo  
Institute of Technology.

科学研究費補助金（試験研究）成果の紹介（光学系技術）

## 超広帯域光スイープジェネレータ

東京工業大学大学院総合理工学研究科 教授 大津 元一

紫外～赤外領域にわたり周波数可変で、かつ周波数揺らぎの少ない光を発する装置は光エレクトロニクス、生命理工学、分析化学、などの広い分野の発展のために古くからその実現が望まれている夢の光源である。本研究では我々が過去に蓄積した半導体レーザー制御技術、及び非線形光学技術を駆使してそのような光源、すなわち超広帯域光スイープジェネレータを開発することを目標としている。

図1にそのシステムの概念を示す。いろいろな周波数で発振可能な複数の半導体レーザーを周波数制御して周波数揺らぎを抑圧し、非線形光学結晶を用いてそのレーザー光の周波数を変換し、さらに複数個のレーザー間での光混合により光位同期を実現して広帯域にわたり光周波数変換を行う。これにより波長  $1.66 \mu\text{m} \sim 0.31 \mu\text{m}$ 、すなわち光周波数に換算すると750テラヘルツにわたる光周波数掃引可能な光源を実現する。必要な非線形光学結晶も自作する。

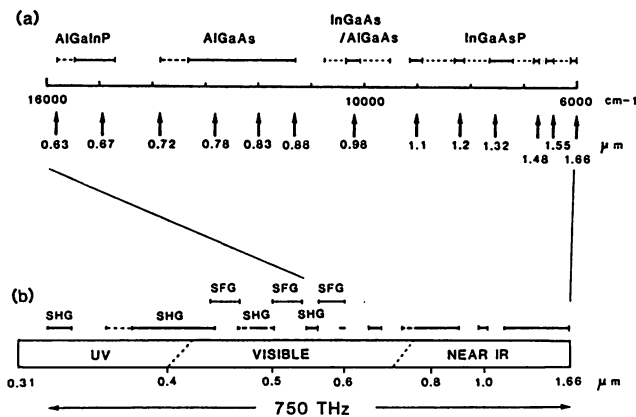


図1 光スイープジェネレータの原理。(a)半導体レーザーの種類とその発振波長。(b)和周波数(SFG)、第二高調波(SHG)などの発生により実現し得る波長範囲の概略。

まず、半導体レーザーの自動制御により光周波数揺らぎが減少し、レーザーの発振スペクトル線幅として世界最小の値、7ヘルツを得た。図2はその発振スペクトル線幅狭化の進歩の様子を示す。また、酸化物非線形光学結晶により波長  $1.56 \mu\text{m}$ の半導体レーザーの第二高調波を発生させた後、この光と波長  $0.78 \mu\text{m}$ の光との位同期ループを実現した。赤、青、緑、さらには紫外、の光を半導体レーザーと非線形光学結晶により発生させた。

将来有望な非線形光学結晶として有機材料を用い、写真に示すような大面積単分子軸配向薄膜の作成に成功した。

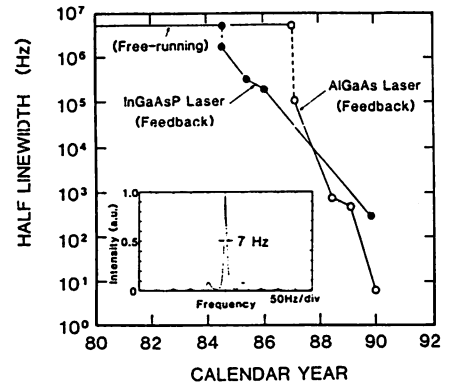


図2 発振スペクトル幅狭化の進歩の様子。内挿図は7ヘルツの幅をもつ発振スペクトル形状。

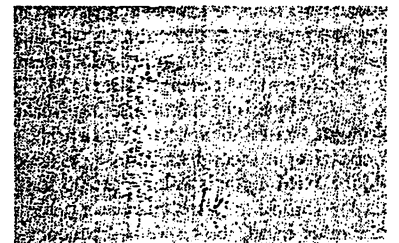


写真 光パラメトリック発振器用に製作したMNA単結晶薄膜。面積  $12 \text{ cm}^2$ 、厚み  $1 \mu\text{m}$ 。

試験研究課題名： 半導体レーザーの光混合による超広帯域光スイープジェネレータの試作（課題番号 01850015）  
 成果の発表： IEEE, Conference on Lasers and Electro-Optics（1990年5月）  
 International Union of Radio Science, The XXIII-th General Assembly of the International Union of Radio Science（1990年8月）  
 Optics Letters 15巻 24号 Optical Society of America（1990年12月）  
 Photonics Technology Letters 3巻 3号 IEEE（1991年3月）

# Optical Response of $\text{YBa}_2\text{Cu}_3\text{O}_{7-x}$ Epitaxial Thin Films

Y. HARADA<sup>1</sup>, K. NARUSHIMA<sup>1</sup>, M. SANO<sup>1</sup>, M. SEKINE<sup>1</sup>, Y. HIGASHINO<sup>2</sup>, and M. OHTSU<sup>1</sup>

<sup>1</sup> The Graduate School at Nagatsuta, Tokyo Institute of Technology, Yokohama, 227 Japan

<sup>2</sup> Yokogawa Electronic Corporation, Musashino, Tokyo, 180 Japan

## ABSTRACT

We have studied the optical response of epitaxial thin films of  $\text{DyBa}_2\text{Cu}_3\text{O}_{7-x}$  by irradiation of semiconductor laser at the wavelength of 830 nm.  $\text{DyBa}_2\text{Cu}_3\text{O}_{7-x}$  superconducting thin films are prepared on MgO (100) by molecular beam epitaxy (MBE). These are confirmed c-axis oriented epitaxial thin films using X-ray analysis and *in-situ* RHEED observation. We have investigated the output signals (i.e. optical response) under the irradiation of laser light, whose frequency can be modulated up to 100 MHz. We have obtained the evidence of nonbolometric response under irradiation of laser at the modulation frequency of 100 MHz.

KEY WORDS: optical detector,  $\text{DyBa}_2\text{Cu}_3\text{O}_{7-x}$  thin film, nonbolometric response

## INTRODUCTION

Since the discovery of high- $T_C$  superconductors, the feasibility of optical and infrared detection using these materials has been much investigated as one of the promising electronic applications [1-5]. As they are used as optical detectors, they can be classified into two types; bolometric or nonbolometric devices due to the operation principle. Microbolometers are well known as the typical bolometric devices. Their theoretical and experimental investigations are advanced by P. L. Richards *et al.* [6,7]. They have shown that a high- $T_C$  superconducting bolometer can be potentially two orders of magnitude more sensitive than any other infrared detector operating in the liquid nitrogen temperature at its wavelengths longer than 20  $\mu\text{m}$ . This means that a high- $T_C$  superconducting bolometric detector operate as the broadband detector. However its response time is generally late compared with other nonbolometric superconducting detectors. As regards a nonbolometric high- $T_C$  superconducting detector, a lot of works were reported [3,4,5,8,9]. In general, it is considered that the response time of mostly nonbolometric superconducting devices is faster than that of bolometric ones. This is because their response time is decided by quantum mechanics. However its operating mechanism is still not clear, and it is doubtful whether nonbolometric response of high- $T_C$  superconducting thin films exists.

In this paper, we have investigated optical response of epitaxial  $\text{DyBa}_2\text{Cu}_3\text{O}_{7-x}$  superconducting thin films under the irradiation of laser light at the wavelength of 830 nm.  $\text{DyBa}_2\text{Cu}_3\text{O}_{7-x}$  superconducting epitaxial thin films are grown by molecular beam epitaxy (MBE). We have investigated the optical response under the irradiation of laser light, whose frequency can be modulated up to 100 MHz. We have obtained the evidence of nonbolometric response.

## EXPERIMENTAL

$\text{DyBa}_2\text{Cu}_3\text{O}_{7-x}$  superconducting thin films are deposited on MgO (100) substrate by MBE in an ultrahigh vacuum system [10]. We set the temperature of the effusion cells for Dy, Ba, and Cu to about 950 °C, 600 °C, and 1000 °C, respectively. The substrate is heated to 650 °C with a graphite carbon heater. Activated oxygen species by rf-discharge plasma are introduced to the substrate. The growth rate is 0.06 nm/sec. The critical temperature of these films with a thickness of 30 nm is 88 K measured by standard four-point probe method. From the X-ray diffraction pattern, these films are a high degree of c-axis orientation with a c-axis parameter of 11.71 Å. By means of *in-situ* RHEED observation, fine streak patterns appeared from the initial crystal growth, so it has been proved that an atomically smooth surface is epitaxially grown.

Fabrication process of samples is the following way.  $\text{DyBa}_2\text{Cu}_3\text{O}_{7-x}$  superconducting thin films on MgO (100) with the thickness of 100 nm is prepared by MBE as mentioned above. Patterning of sample's configuration is used standard photolithography and Ar ion milling. Fabricated samples have constrictions with a size of 20  $\mu\text{m}$  width and 400  $\mu\text{m}$  length. The critical temperature of samples is 65 K. As samples are damaged during the fabrication process, its critical temperature is low compared with that of thin films.

The experimental arrangement for the study of the optical response is shown in Fig. 1. GaAlAs laser diode whose wavelength is 830 nm is used as the light source and its average power is 3.5 mW. A sample is mounted on the stage in the cryostat which can cool down to 20 K. A sample is biased by constant dc current from the current source. Laser

light is introduced perpendicularly to a sample through the window of the cryostat. Laser diode can be modulated by a dc-biased sinusoidal signal current and its modulation frequency can be varied from 1 kHz to 100 MHz. We have measured the output electrical signals through the lock-in amplifier under the irradiation of laser light. In this experimental arrangement, the output signals can't be detected even up to the laser modulation frequency of 200 kHz. The output signals at the modulation frequency from 200 kHz to 100 MHz is measured using the another experimental arrangement as shown in Fig.2. In this arrangement, a double balanced mixer (DBM) is used to beat down the output signals to 10 kHz.

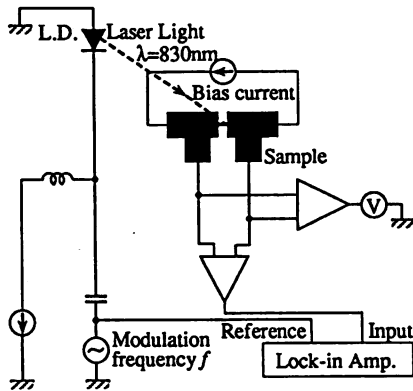


Fig. 1 Arrangement of optical response in  $\text{DyBa}_2\text{Cu}_3\text{O}_{7-x}$  superconducting thin films by irradiation of laser light whose frequency can be modulated up to 200 kHz.

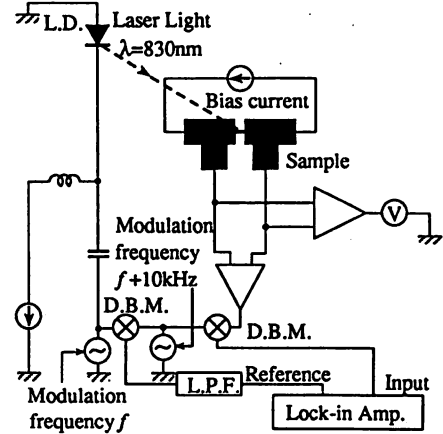


Fig. 2 Arrangement of optical response in  $\text{DyBa}_2\text{Cu}_3\text{O}_{7-x}$  superconducting thin films by irradiation of laser light whose frequency can be modulated from 200 kHz to 100 MHz.

## RESULTS AND DISCUSSIONS

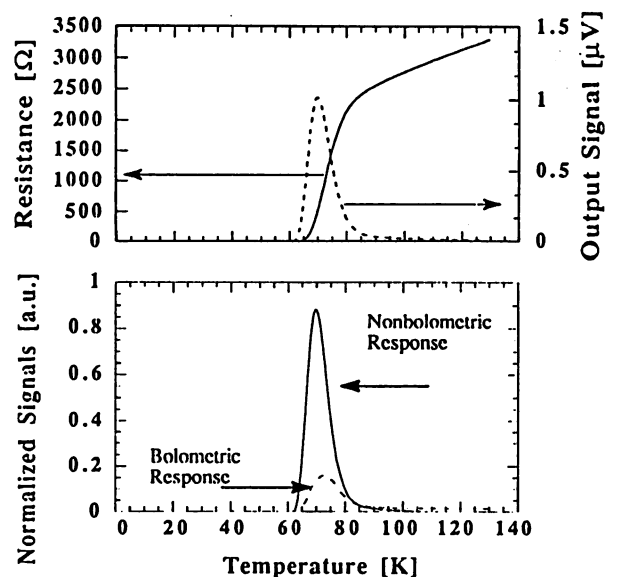
The upper part of Figs. 3 shows the temperature dependence of resistivity of a sample film (solid line) and output voltage (i.e. photo response) under the irradiation of laser light (break line). The modulation frequency of the laser is 1

MHz, and the biased current of the sample is 0.1 mA. The critical temperature of this sample is found 65 K from this figure. The maximum value of the optical response is obtained at the temperature of 70 K. This optical response includes both the bolometric and nonbolometric ones as mentioned in introduction. This relation is expressed as the following way,

$$\delta V = I_B \frac{\partial R}{\partial T} \Delta T + R \frac{\partial I}{\partial T} \Delta T \quad (1)$$

where  $\delta V$  represents the output voltage produced from the laser irradiation,  $I_B$  and  $R$  are a bias current and the resistance of a sample, respectively.  $\Delta T$  means the rising temperature by heating effect due to the laser irradiation. The first term of right hand in this equation indicates bolometric response which result from an increase of the sample's temperature by the laser irradiation. On the other hand, the second term of right hand in this equation means nonbolometric response. Recently some theories are suggested as the explanation of the mechanism on nonbolometric response [11-13].

The lower part of Fig. 3 shows the magnitude of both the bolometric and the nonbolometric signal under laser irradiation. Both signals are normalized by some factor. These values are calculated according to the expression (1). It is assumed that at the region of high temperature beyond  $T_C$ , the total signal equals the bolometric signal. From this figure, it is found that when the modulation frequency of the laser diode is 1



Figs. 3 The optical response of a sample under the irradiation of laser at the wavelength of 830 nm with the modulation frequency of 1 MHz.

MHz, the nonbolometric response is about 5.5 larger than the bolometric one. It is considered that the bolometric signal is so late that it can't follow the modulation of the laser source.

Figures 4 also show the optical response of the same sample under the irradiation of laser like Figs. 3. But the modulation frequency of laser is different from that of Figs.3, and its frequency is 100 MHz. Clearly, the ratio of a bolometric signal,  $S_B$ , to nonbolometric one,  $S_N$ , is smaller than that of Figs. 3. In other words, it is considered that the bolometric signal decreases at a higher modulation frequency of the laser.

To confirm this assumption, we have investigated the frequency dependence of the ratio,  $S_B / S_{TOTAL}$  ( $S_{TOTAL} = S_B + S_N$ ), as shown in Fig. 5. At the region of low modulation frequency, this ratio is constant. This is because the bolometric signal dominates over the total signals and the nonbolometric signal doesn't contribute because of its rapid response. But it is found that the bolometric signal gradually decrease from the modulation frequency of about 100 kHz and in stead of bolometric signal, nonbolometric one dominates at the higher frequency. According to the theory of nonequilibrium superconductivity, which is based on the BCS theory, it can be calculated that nonbolometric response time is about several ten picosecond, which corresponds to several hundred GHz [14].

As additional facts, it is found that the peak temperature of the nonbolometric response is shifted toward a lower temperature compared with that of the

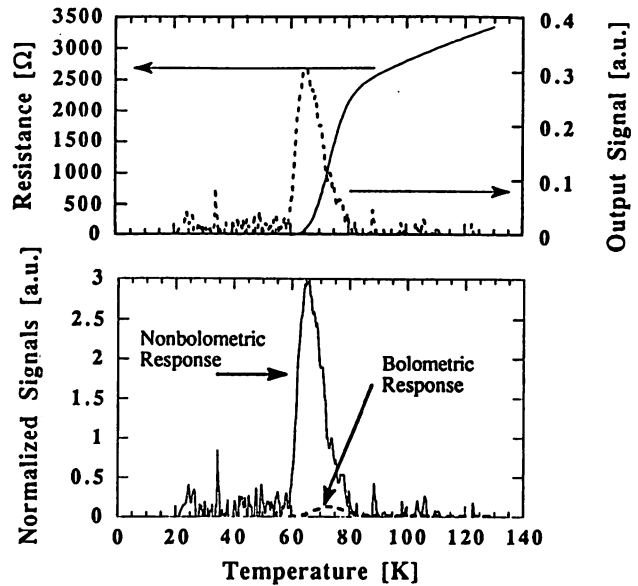


Fig. 4 The optical response of a sample under the irradiation of laser at the wavelength of 830 nm with the modulation frequency of 100 MHz. Bias current of this sample is 0.5 mA.

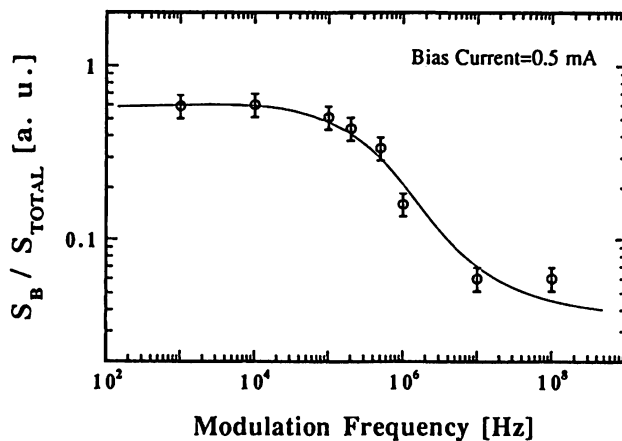


Fig. 5 Modulation frequency dependence of ratio of a bolometric signal to the total one,  $S_B / S_{TOTAL}$ .

bolometric response. This reason is not evident, but it may be related to the mechanism of the high- $T_c$  superconductivity. We have also studied the bias current dependence of the optical response. Up to now, the evident relations between the bias current and optical response can't be observed.

## CONCLUSIONS

We have investigated the optical response of  $DyBa_2Cu_3O_{7-x}$  thin films under the irradiation of laser light ( $\lambda=830$  nm), whose modulation frequency can be varied from 1 kHz to 100 MHz.  $DyBa_2Cu_3O_{7-x}$  thin films are prepared by MBE and they are highly c-axis oriented epitaxial thin films. We have observed both bolometric and nonbolometric signal from  $DyBa_2Cu_3O_{7-x}$  thin films under the laser irradiation. At the lower modulation frequency, the bolometric signal dominates the total optical response by the irradiation of laser light, but as the modulation frequency goes up, the bolometric signal decreases. At the modulation frequency of 100 MHz, the large part of total optical response is the

nonbolometric signal. To confirm this fact, we have also investigated the frequency dependence of the ratio  $S_B / S_{TOTAL}$ . It is found that this ratio becomes small as the modulation frequency becomes higher. As the result, we have obtained that the optical response includes the nonbolometric signal in evidence. However origin of the nonbolometric signals is not obvious. From our experiments, it can be stated that the nonbolometric response time is shorter than 10 ns and the bolometric response time of our sample size (constriction with the size of  $20 \mu\text{m} \times 400 \mu\text{m}$ ) is within several nanoseconds.

## REFERENCES

1. Forrester MG, Gottlieb M, Gavalier JR, Braginski AI (1988) *Appl. Phys. Lett.* 53: 1332-1334
2. Brocklesby WS, Monroe D, Levi AFJ, Hong M, Liou SH, Kwo J, Rice CE (1989) *Appl. Phys. Lett.* 54: 1175-1177
3. Frenkel A, Saifi MA, Venkatesan T, Lin C, Wu XD, Inam A (1989) *Appl. Phys. Lett.* 54: 1594-1596
4. Tanabe K, Enomoto Y, Suzuki M, Iwata T, Yamaji A (1990) *Jpn. J. Appl. Phys.* 29: L466-469
5. Han SG, Vardeny ZV, Wong KS, Symko OG, Koren G (1990) *Phys. Rev. Lett.* 65: 2708-2711
6. Richards PL, Clarke J, Leoni R, Lerch P, Verghese S, Beasley MR, Geballe TH, Hammond RH, Rosenthal P, Spielman SR (1989) *Appl. Phys. Lett.* 54: 283-285
7. Hu Q, Richards PL (1989) *Appl. Phys. Lett.* 55: 2444-2446
8. Chibane F, Bonnel de Longchamp N, Martin R, Perrière J, Hauchecorne G, Kerhervé F, Maneval JP (1989) *Solid State Commun.* 69: 907-909
9. Zeldov E, Amer NM, Koren G, Gupta A (1989) *Phys. Rev.* B39: 9712-9714
10. Higashino Y, Umezawa T, Mizobuchi K (1991) Proceedings of the third International Superconducting Electronics Conference (ISEC '91), Glasgow
11. Zeldov E, Amer NM, Gupta A, Gambino RJ, McElfresh MW (1989) *Phys. Rev. Lett.* 62: 3093-3098
12. Tanabe K, Enomoto Y, Suzuki M, Kubo S, Asano H, Iwata T, Tajima Y, Yamaji A (1990) Proceedings of the third International Symposium on Superconductivity (ISS '90), Tokyo
13. Kadin AM, Leung M, Smith AD, Murduck JM (1990) *Appl. Phys. Lett.* 57: 2847-2849
14. Kaplan SB, Chi CC, Langenberg DN, Chang JJ, Jafarey S, Scalapino DJ (1976) *Phys Rev.* B14: 4854-4873



**TUESDAY, NOVEMBER 5, 1991**

**▶ SADL4: APPLICATIONS OF NARROW LINEWIDTH  
LASERS (JOINT SESSION WITH EOS AND OSM)  
ROOM J4**

**SADL4.1  
10:30am  
ULTRA-NARROW LINEWIDTH SEMICONDUCTOR  
LASERS AND THEIR APPLICATIONS**

M. OHTSU, C.-H. SHIN\*, S. JIANG, M. KOUROGI, and K. NAKAGAWA

Graduate School at Nagatsuta, Tokyo Institute of Technology,

4259 Nagatsuta, Midori-ku, Yokohama 227, JAPAN

Phone : +81-45-922-1111 (ext) 2526. FAX : +81-45-921-1156

\* Presently, with National Mokpo Merchant Marine College,  
Mokpo, Chun-Nam, KOREA

A DFB InGaAsP lasers with a 250 Hz spectral linewidth has been achieved by using the negative electrical feedback (NEF) method. The power concentration ratio within the controlled bandwidth was higher than 99 %. By NEF and optical feedback from an external confocal cavity, the linewidth an AlGaAs laser was reduced to 7 Hz with the power concentration ratio higher than 98 %. It was estimated that the shot noise-limited linewidth of the order of 1 mHz would be realized in the near future by utilizing an optical balanced detector. Homodyne and heterodyne optical phase locked loops ( OPLL ) were realized to reduce the phase error variance to 0.02 rad<sup>2</sup>. The bandwidth of the homodyne OPLL was expanded to 134 MHz by using the NEF method. An accurate and wideband optical frequency sweep generator was proposed by combining the coherent semiconductor lasers, methods of OPLL and nonlinear optical frequency conversion. Organic nonlinear optical waveguides were fabricated for this frequency conversion. The frequency sweep range as wide as 700 THz is expected, ranging from the near infrared to the ultraviolet regions.

As applications of these lasers to advanced photonics systems, performances of our photon STM for super-resolution microscope and for single-atom-level crystal growing machine, an optical frequency counter, a rubidium atomic clock, and a passive ring resonator fiber gyro will be demonstrated.

SADL6.4

4:45pm

VISIBLE SEMICONDUCTOR LASER FOR APPLICATION TO ISOTOPE SEPARATION

T. Fujii, K. Nemoto, R. Ishikawa, *Central Research Institute of Electric Power Industry, Tokyo, Japan*; A. Awaji, M. Ohtsu, *Tokyo Institute of Technology, Kanagawa, Japan*

We have already proposed the application of a visible semiconductor laser (VSL) to isotope separation, especially of uranium [1]. As the absorption band frequencies of isotopes are close to each other and often have hyperfine structures (hfs), chirping reduction of the pulsed VSL and frequency tuning to the hfs are strongly required. A pulsed laser with a pulse duration of about 50 nsec is required to obtain high peak power in many cases of laser isotope separation. However, to achieve efficient isotope separation employing a VSL, it is very important to suppress frequency chirping when the VSL is pulse operated.

In order to realize narrow linewidth of a pulsed VSL, we propose an optical feedback system utilizing a phase conjugate wave (PCW) [2] generated by four-wave mixing (FWM) from another VSL. At the first step, to demonstrate the above-mentioned system, we made what is to our knowledge the first successful attempt to generate a PCW from a visible AlGaInP laser, as shown in Fig.1. The PCW was generated with a bandwidth as wide as 2.8 GHz. The PCW reflectivity at the resonance peak observed at detuning of about  $\pm 1.5$  GHz, which was referred to relaxation oscillation, was about 100 times. The bandwidth and reflectivity of the PCW were sufficiently broad and high to reduce the linewidth by its optical feedback. Although the above-mentioned FWM is induced by interband relaxation, we have also succeeded in generation of a PCW with a bandwidth of more than 1THz by a FWM induced by intraband relaxation using an AlGaAs laser.

Next, we propose an easy and convenient method of frequency tuning to hfs using a frequency shift of the VSL by high-speed and high-efficiency direct modulation. Time-resolved measurement of the frequency shift of a visible AlGaInP laser with sinusoidal direct modulation has been carried out by observing the real-time variation of the interference fringe obtained with a Fabry-Perot etalon by means of an image intensifier and a camera. Figure 2 shows the frequency shift against time on the 2-MHz sinusoidal direct modulation. The laser frequency varied slightly following the current variation, and a frequency shift of 7 GHz within 300 nsec was achieved. In the case of uranium isotope separation, a frequency shift of 1-10 GHz is required within 50 nsec, which is the laser pulse duration. From this result, it is expected that the broad bandwidth frequency shift required for uranium isotope separation will be realized with direct modulation of a VSL.

"References"

- [1] M. Ohtsu et al.: *J. Appl. Phys.*, Vol. 29 (1990) L1463
- [2] M. Ouhayoun et al.: *IEEE J. Quantum Electron.*, Vol. QE-22 (1986) 2150

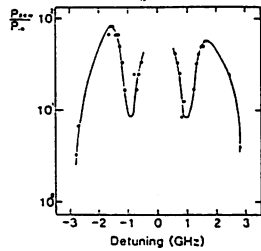


Fig.1 PCW reflectivity versus detuning between probe and pump beams. Pump power = 7.0 mW. Pin: probe power = 3.0µW and Ppcw: PCW power.

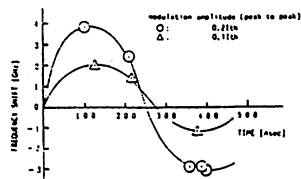


Fig.2 Frequency shift versus time on 2 MHz sinusoidal direct modulation. Ith: threshold current = 33.2 mA and bias current = 1.21th.

## 1/8 CORRECTION FACTOR OF SCHAWLOW-TOWNES LIMIT IN FM NOISE OF NEGATIVE FREQUENCY FEEDBACK LASERS

K.Yoshida<sup>1</sup>, M.Kourog<sup>2</sup>, K.Nakagawa<sup>2</sup> and M.Ohtsu<sup>2</sup>

<sup>1</sup> Faculty of Engineering, Toin University of Yokohama,  
 1614 Kurogane-cho, Midori-Ku, Yokohama-shi, 227 Japan

<sup>2</sup> Graduate School at Nagatsuta, Tokyo Institute of Technology,  
 4259 Nagatsuta-cho, Midori-Ku, Yokohama-shi, 227 Japan

### Abstract

A limit of the frequency modulation (FM) noise in a negative frequency feedback laser using a Fabry-Perot interferometer (FP) as a frequency discriminator is equal to the modified Schawlow-Townes limit of the laser having the same Fabry-Perot resonator by a correction factor. We show that this correction factor is 1/8 which results from no gain noise, half vacuum noise and doubled energy of resonator as compared with a laser resonator.

### 1. Introduction

A limit of the frequency modulation (FM) noise in a negative frequency feedback laser using a Fabry-Perot interferometer (FP) as an optical frequency discriminator has been well known. The limit, which is determined by the zero-point field fluctuations introduced by the discriminator and the power divider[1], is equal to the modified Schawlow-Townes limit of the laser having the same Fabry-Perot resonator by a correction factor which is ambiguous for various ways of parameter definitions. This correction factor is important for practical use of such a laser in a gravitational wave detection, coherent optical transmission system, and so on. We point out that this factor is 1/8 which results from no gain noise, half vacuum noise and doubled energy of resonator as compared with a laser resonator.

### 2. Schawlow-Townes limit of FM noise

When we can ignore the relaxation oscillation in a laser, we have

$$da/dt = -(i\omega_c + (\tau_c - G(n))/2)a + \sqrt{\tau_c}(f_i + f_g), \quad f_o = \sqrt{\tau_c}a - f_i, \quad (1)$$

$$[a, a^\dagger] = 1, \quad [f_i, f_i^\dagger] = [f_o, f_o^\dagger] = \delta(t-s), \quad r_c[f_g, f_g^\dagger] = -(dRe(nG)/dn)\delta(t-s)$$

where  $\omega_c$ ,  $\tau_c$ ,  $a$  and  $n$  are an angular frequency, a power damping rate, an annihilation operator and a photon number  $a^\dagger a$  of the resonator's quasi-mode respectively.  $G$  is a gain,  $f_g$  is the gain noise,  $f_i$  is an incoming photon flux and  $f_o$  is an outgoing photon flux[2]. Furthermore, if  $f_i$  is in a vacuum state, the so-called  $\alpha$  parameter is zero and a pumping level is high, then we get

$$\langle Re^2(f_i) \rangle = \langle Im^2(f_i) \rangle = \langle Re^2(f_g) \rangle = \langle Im^2(f_g) \rangle = 1/4,$$

$$\langle dRe(nG)/dn \rangle = 0, \quad \langle dIm(G)/dn \rangle = 0$$

where  $Re$  ( $Im$ ) is a real (imaginary) part, and the averaged value  $\langle XY \rangle$  means

$$\langle X(t)Y(s) \rangle = \langle XY \rangle \delta(t-s).$$

Fig.1(a) shows a laser using a FP resonator with two output ports, and  $f_i$  and  $f_o$  in eq.(1) are

$$f_i = (f_{v1} + f_{v2})/\sqrt{2}, \quad f_o = (f_{o1} + f_{o2})/\sqrt{2}.$$

For small fluctuations of  $(A, F_i, F_o, F_g) := \exp(i\omega t)(a, f_i, f_o, f_g)$  where  $\omega$  is an optical angular frequency(':= ' means a definition), we can linearize eq.(1) about the steady-state mean values, and get

$$A = \sqrt{n}e^{-i\phi} \approx \langle A \rangle (1 + \delta n / \langle 2n \rangle - i\delta\phi), \quad F_o = \sqrt{N}e^{-i\Psi} \approx \langle F_o \rangle (1 + \delta N / \langle 2N \rangle - i\delta\Psi), \quad (2)$$

$$d\delta\phi/dt = -(r_c/n)^{1/2} \text{Im}(F_i + F_g), \quad \delta\Psi = \delta\phi + (r_c n)^{-1/2} \text{Im}(F_i) \quad (3)$$

where we take  $\langle A \rangle$  as real( $\delta$  means a fluctuation part). Therefore, the side-band power spectrum  $S_\omega$  of the angular frequency fluctuation  $d\delta\Psi/dt$  of out-going light is

$$S_\omega = \langle N \rangle^{-1} (\tau_c^2 + (2\pi\nu)^2/2) d\nu \approx (\hbar\omega/P_o) \tau_c^2 d\nu \quad (2\pi\nu \ll r_c) \quad (4)$$

where  $\hbar\omega$  is an energy of a photon,  $P_o$  is a power of the out-going light of the laser, and  $\nu$  is a Fourier frequency. The  $\tau_c^2 / \langle N \rangle$  is called the Schawlow-Townes limit of FM noise revised by [3], and the  $(2\pi\nu)^2 / \langle 2N \rangle$  is the so-called shot noise which can be ignored when  $2\pi\nu \ll r_c$ . The intensity fluctuation  $\delta N$ , which is a shot noise, can be also ignored when  $2\pi\nu \ll r_c$  because the power spectrum of  $d(\delta N / \langle 2N \rangle) / dt$  in eq.(2) is  $(2\pi\nu)^2 / \langle 2N \rangle$ .

### 3. Limit of FM noise in a negative frequency feedback laser

Fig.1(b) shows a negative frequency feedback laser with detection of the reflected light from a FP resonator which is used as an optical frequency discriminator. The laser's angular frequency  $\omega$  is locked to  $\omega_0$  using a slope of resonant profile of the FP where  $\omega_0$  is slightly detuned from the FP's resonant angular frequency  $\omega_c$ . The output current  $i(t)$  of the photo detector with the unit quantum efficiency is

$$i(t) = (eP_i/\hbar\omega)/(1 + r_c^2/4(\omega - \omega_c)^2) + i_n(t) \approx (eP_i/\hbar\omega)(2\Delta\omega_c/r_c)^2(1 - 2\Delta\omega/\Delta\omega_c) + i_n(t) \quad (5)$$

if  $r_c \gg |\Delta\omega_c| \gg |\Delta\omega|$  where  $\Delta\omega_c := \omega_c - \omega_0$ ,  $\Delta\omega := \omega - \omega_0$ ,  $r_c$  is the FP's power damping rate,  $P_i$  is a power of in-coming light to FP,  $i_n(t)$  is a shot noise by photo-electrons, and  $e$  is a electron charge. We lock  $\omega$  to  $\omega_0$  by maintainig  $i(t)$  constant, and have

$$\Delta\omega \approx (\Delta\omega_c / \langle 2i \rangle) i_n, \quad S_\omega \approx (\hbar\omega/\delta P_i) \tau_c^2 d\nu = (\text{Schawlow-Townes's limit})/\delta \quad (6)$$

because the side-band power spectrum of shot noise  $i_n$  is  $2e \langle i \rangle d\nu$ .

In order to explain why the factor  $1/\delta$  appears in eq.(6), we re-calculate the power spectrum  $S_\omega$  of FM noise by using quantum theory. In Fig.1(b),  $f_v$  is a photon flux(zero-point field fluctuation) incident on one mirror of the FP resonator. By the same definitions as above, we have

$$dA/dt = -(i\Delta\omega_c + r_c/2)A + \sqrt{r_c}(F_i + F_v)/\sqrt{2} \quad (A := \exp(i\omega_0 t)a, \quad \text{etc}), \quad (7)$$

$$F_r = \sqrt{r_c/2}A - F_i \approx 2i(\Delta\omega - \Delta\omega_c) \langle F_i \rangle / r_c + F_v \quad (8)$$

$$(\Delta\omega := d\delta\Psi/dt, \quad F_i \approx \langle F_i \rangle (1 - i\delta\Psi), \quad P_i = \hbar\omega |\langle F_i \rangle|^2),$$

$$i(t) = eF_r^+ F_r \approx (eP_i/\hbar\omega)(2\Delta\omega_c/r_c)^2(1 - (2\Delta\omega + \langle r_c/F_i \rangle \text{Im}(F_v))/\Delta\omega_c) \quad (9)$$

where we take  $\langle F_i \rangle$  as real(we ignored the intensity fluctuation  $\delta N$ ). Eq.(8) is derived from

$$F_r = -\sqrt{2/r_c}(d/dt + i\Delta\omega_c)A + F_r, \quad A = \sqrt{2/r_c}(F_i + F_v) - (2/r_c)(d/dt + i\Delta\omega_c)A$$

in which  $F_v$  and  $(d/dt + i\Delta\omega_c)$  are small quantities. By maintaining  $i(t)$  constant, we have

$$\Delta\omega \approx -\langle r_c/2F_i \rangle \text{Im}(F_v), \quad S_\omega = (\hbar\omega/\delta P_i) r_c 2d\nu = (\text{Schawlow-Townes's limit})/\delta \quad (10)$$

which is equal to eq.(6) in a classical treatment. Deleting the  $F_i$  in eq.(7), we get a following equation

$$d\delta\phi/dt = -(r_c/2n)^{1/2} \text{Im}(F_v), \quad r_c |\langle A \rangle|^2 = 2 |\langle F_i \rangle|^2 \quad (11)$$

which corresponds to eq.(3) in case of a laser, and is derived from

$$-\tau_c A/2 + \sqrt{\tau_c/2} F_i = -\sqrt{\tau_c/2} F_r \approx 2i \langle F_i \rangle \Delta\omega_c/\tau_c - \text{Re}(F_v).$$

Eq.(11) explains that the correction factor 1/8 in eq.(10) results from no gain noise, half vacuum noise and doubled energy of resonator as compared with a laser resonator.

Even if Fabry-Perot resonator has one output port, we can realize the same factor 1/8 by combining Mach-Zehnder interferometer and balanced detector with the FP resonator as Fig.1(c). Although we must adjust the arm length difference of the interferometer, we can lock the laser frequency to the center of a resonant spectral profile of the FP. From Fig.1(c), we have

$$\begin{aligned} dA/dt &= -\tau_c A/2 + \sqrt{\tau_c} F_1, & F_r &= \sqrt{\tau_c} A - F_1 \quad (F_1 := (F_i + F_v)/\sqrt{2}, \quad F_2 := i(F_i - F_v)/\sqrt{2}), \\ i(t) &= e(F_3^+ F_3 - F_4^+ F_4), & (F_3 &:= (F_r + F_2)/\sqrt{2}, \quad F_4 := (F_r - F_2)/\sqrt{2}). \end{aligned} \quad (12)$$

With the linearization and the Fourier series analysis[2], Eq.(12) leads to

$$\begin{aligned} F_i &= T^{-1/2} \sum a_k \exp(-i\Delta\omega_k t) = \langle F_i \rangle (1 + \delta N / \langle 2N \rangle - i\delta\Psi), \quad [a_k, a_k^+] = 1, \\ F_v &= T^{-1/2} \sum v_k \exp(-i\Delta\omega_k t), \quad [v_k, v_k^+] = 1, \quad \langle v_k^+ v_k \rangle = 0 \quad (\Delta\omega_k := \omega_k - \omega_c), \\ i(t) &= T^{-1/2} \sum \langle eF_i/2i \rangle (\tau_c/2 - i\Delta\omega_k)^{-1} (2i\Delta\omega_k (a_k - a_k^+) + \tau_c (v_k - v_k^+)) \exp(-i\Delta\omega_k t) \end{aligned} \quad (13)$$

where we take  $\langle F_i \rangle$  as real, and  $\Delta\omega_k := -\Delta\omega_k$ . We control  $\delta\Psi$  to maintain  $i(t)$  constant, and have

$$\begin{aligned} \delta\Psi_k &= (a_k - a_k^+) / \langle 2iF_i \rangle \approx \tau_c (v_k - v_k^+) / \langle 4\Delta\omega_k F_i \rangle \quad (\delta\Psi = T^{-1/2} \sum \delta\Psi_k \exp(-i\Delta\omega_k t)), \\ S_w &= 2\tau_c^2 \langle \text{Im}^2 F_v \rangle d\nu / \langle 4N \rangle = \tau_c^2 d\nu / \langle 8N \rangle. \end{aligned} \quad (14)$$

In eq.(14), the correction factor of the same 1/8 appears again and  $S_w \approx 0$  if  $F_v$  is in a squeezed vacuum-state ( $\langle \text{Im}^2 F_v \rangle \approx 0$ ). It is also remarkable that the FM noise of  $F_i$  has no shot noise component. Therefore the fluctuation of  $\text{Im}(F_i)$  is below the shot noise limit at  $2\pi\nu \gg \tau_c$  (squeezing. see appendix), while we can not take it out from this feedback system.

Finally, we point out that FM modulation method with FP resonator having one output port also leads to the same correction factor 1/8 as above when the modulation index is nearly zero. A method using a  $\lambda/4$  plate in the FP resonator which does not need any modulation techniques and adjustments of optical path-length is known[4], and leads to the same factor 1/8.

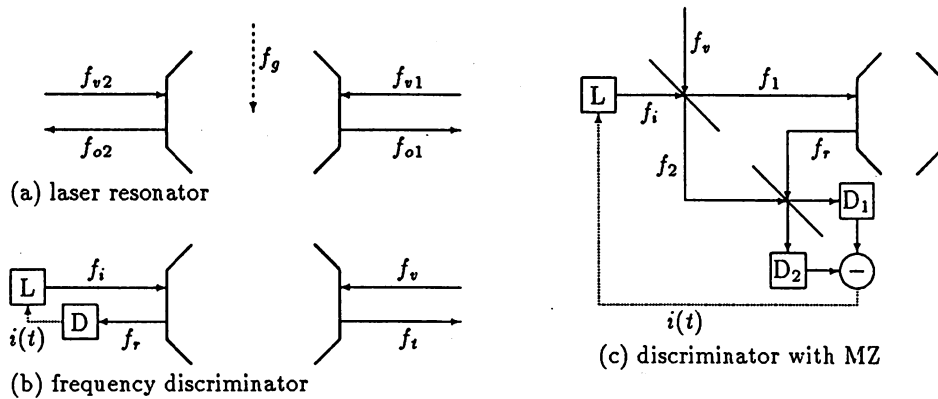


Figure 1: Photon flux at FP resonator

## Appendix:FM noise and squeezing

The power spectrum of phase fluctuation is also the squeezing spectrum. In fact, for a photon flux  $F(t)$ , we have with the linearization and the Fourier series analysis

$$F(t) := T^{-1/2} \sum a_k \exp(-i\Delta\omega_k t) \approx \langle F \rangle (1 + \delta N / \langle 2N \rangle - i\delta\Psi), \quad [a_k, a_k^\dagger] = 1.$$

$$\delta N_k = \langle F \rangle^* a_k + \langle F \rangle a_k^\dagger, \quad \delta\Psi_k = (\langle F \rangle^* a_k - \langle F \rangle a_k^\dagger) / \langle 2iN \rangle \quad (\Delta\omega_k := -\Delta\omega_k).$$

$$X(t) := \text{Re}(e^{-i\theta} \Delta F) = T^{-1/2} \sum x_k \exp(-i\Delta\omega_k t), \quad x_k := (e^{-i\theta} a_k + e^{i\theta} a_k^\dagger) / 2 = x_k^\dagger, \quad (k \neq 0).$$

A squeezing spectrum  $S(\Delta\omega_k, e^{i\theta})$  which is defined as a Fourier transform of  $\langle : X(t)X(0) : \rangle$  [5], and a side-band power spectrum  $S_\omega$  of FM noise are

$$S(\Delta\omega_k, e^{i\theta}) = \langle : x_k x_{k'} : \rangle = \langle x_k x_{k'} \rangle - 1/4,$$

$$S_\omega = 2 \langle |\Delta\omega_k \delta\Psi_k|^2 \rangle d\nu = 2 \langle \Delta\omega_k^2 / N \rangle (1/4 + S(\Delta\omega_k, i \langle F \rangle / |\langle F \rangle|)) d\nu.$$

Squeezed state can be generated by a degenerate parametric oscillator(DPO). However if we pump it by a laser light which has a large FM noise, then the FM noise of output light is not reduced. In fact, as is shown by ref.[6], we have Langevin equations and its linearizations such as

$$dA_1/dt = -r_1 A_1/2 + g A_1^\dagger A_2 + \sqrt{r_1} F_{i1}, \quad dA_2/dt = -r_2 A_2/2 - g^* A_1^2/2 + \sqrt{r_2} F_{i2},$$

$$F_{o1} = \sqrt{r_1} A_1 - F_{i1}, \quad F_{o2} = \sqrt{r_2} A_2 - F_{i2}.$$

$$\langle N_{i2} \rangle = (r_1 + \mu n_1)^2 / 8\mu, \quad \langle N_{o1} \rangle = r_1 n_1 \quad (\mu := 2|g|^2 / r_2, \quad n_1 := \langle A_1^\dagger A_1 \rangle),$$

$$\text{Im}(\delta F_{o1}) = \text{Im}(-\mu n_1 F_{i1} + \sqrt{2r_1 \mu n_1} \delta F_{i2}) / (\mu n_1 + r_1) \quad (|\Delta\omega_k| \ll \tau_1, \tau_2)$$

where  $F_{i2}$  is a pumping flux( $\omega_2 = 2\omega_1$ ). Therefore, when  $F_{i2}$  has a large FM noise, we get

$$\langle \delta\Psi_{o1}^2 \rangle = K/4\Delta\omega_k^2 + (1 - r_1^2 / (\mu n_1 + r_1)^2) / \langle 4N_{o1} \rangle \quad (\langle \delta\Psi_{i2}^2 \rangle := K/\Delta\omega_k^2 + 1 / \langle 4N_{i2} \rangle)$$

which means that we should use a DPO as a vacuum squeezer ( $\langle \text{Im}^2 F_{o1} \rangle = \langle N_{o1} \delta\Psi_{o1}^2 \rangle \approx 0$ ) when we pump a DPO by a light with large FM noise. The squeezed vacuum is valuable because the classical shot noise usually results from one quadrature component of zero-point field fluctuation of the vacuum.

## References

- [1] Y.Yamamoto, O.Nilson, S.Saito, 1985, "Theory of a Negative Frequency Feedback Semiconductor Laser", IEEE J. of Quantum Electronics, Vol.QE-21, No.12: 1919-1927
- [2] Y.Yamamoto, N.Imoto, 1986, "Internal and External Field Fluctuations of a Laser Oscillator: Part 1-Quantum Mechanical Langevin Treatment", IEEE J. of Quantum Electronics, Vol.QE-22, No.10: 2032-2042
- [3] A.Blaquiere, 1962, "Spectre d'un oscillateur maser; relation avec la th orie des autooscillateurs classiques", Compt. Rend., vol.26: 2929-2931
- [4] M.Kouroggi, M.Ohtsu, 1991, "Novel Optical Discriminator for FM Noise Reduction of Semiconductor Lasers", Optics Communications, Vol.81, No.3,4: 204-208
- [5] H.J.Carmichael, 1987, "Spectrum of Squeezing and Photocurrent Shot Noise: a Normally Ordered Treatment", J. Opt. Soc. Am B, Vol,4, No.10: 1588-1603
- [6] M.Dance, M.J.Collett, D.F.Walls, 1991, "Quantum-Nondemolition Measurement via Second-Harmonic Generation", Physical Review Letters, Vol.66, No.9: 1115-1118

Tuesday  
May 12, 1992  
Convention Center Room C3

MORNING  
QTuG

10:30 am Precision Spectroscopy  
Edward E. Eyler, *University of Delaware, President*

11:00 am

**QTuG2 Linewidth reduction and fine detuning of a semiconductor laser, using velocity-selective optical pumping of atomic resonance line**

M. Kozuma, M. Kourogi, M. Ohtsu, H. Hori\*  
*Graduate School of Nagatsuta, Tokyo Institute of Technology, 4259 Nagatsuta, Midori-ku, Yokohama 227, Japan*

This paper reports on a novel optical feedback method to control a semiconductor laser frequency by utilizing the velocity-selective optical pumping<sup>1</sup> of an atomic resonance line in order to meet the requirements of laser cooling and optical molasses experiments. These requirements are: (1) lasing frequency  $\nu$  should be stabilized and detuned from the atomic resonance frequency  $\nu_0$ , with detuning of  $\nu - \nu_0 \approx \pm \gamma/2$  ( $\gamma$  = natural linewidth of atomic resonance spectral line); and (2) linewidth must be narrow.

The present method has several advantages over previously reported optical feedback methods using atomic resonance lines.<sup>2,3</sup> It easily meets the two requirements, the setup is simple and compact, and the magnetic field does not have to be applied to the atom, by which the stabilized laser frequency is free from the magnetic-field fluctuations.

Figure 1 shows the experimental setup. An AlGaAs laser and a Rb vapor cell were used at room temperature. The total length of the setup was as short as 300 mm. The polarization of the probe beam was converted from linear to elliptic by passing it through the Rb vapor, because the circular dichroism was induced in the Rb vapor by a nonlinear interaction with the strong pump beam. Furthermore, the circularly polarized strong pump beam produces velocity-selective polarization in the Rb vapor and induces velocity-selective circular dichroism and birefringence in the probe beam reflected by a mirror (M3). In order to feed back the spectral selective probe beam to the laser, the Faraday rotator with rotation angle of 45° was used.

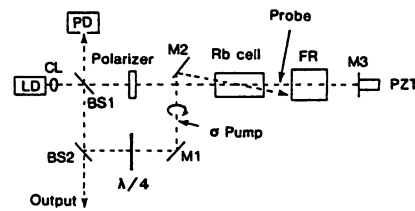
Figure 2(a) shows the Doppler-free spectral profile of the Rb- $D_2$  line due to hyperfine transitions from the  $F = 2$  level in the ground state measured by sweeping the laser injection current. Since this spectral profile took the peak at the resonance frequency, stable resonant optical feedback was achieved by injecting the reflected probe beam to the laser, i.e.,  $\nu$  was locked to  $\nu_0$ . Figure 2(b) shows the deformed Doppler-free spectral profile measured while injecting the reflected probe beam to the laser. The plateau at the center of the profile proves that  $\nu$  was locked to  $\nu_0$ , and the locking range was as wide as 200 MHz. The field spectral linewidth of this optical feedback laser was measured as 1 MHz, which was 20 times narrower than that of the free-running laser. While the series of measurements described above were performed,

the laser frequency stayed in the locking range so that the optical path length did not have to be controlled in this compact setup.

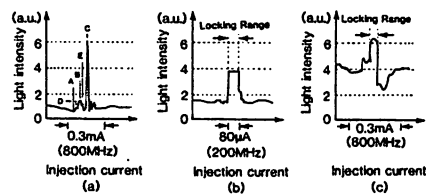
The stabilized frequency could be detuned from  $\nu_0 - \gamma/2$  to  $\nu_0 + \gamma/2$  by changing the Faraday rotation angle from 45° since this rotation could provide a dispersive spectral profile of Rb owing to the circular birefringence. Figure 2(c) shows the profile measured while injecting the reflected probe beam to the laser. The laser frequency  $\nu$  was locked at the plateau, which means that the stabilized laser frequency was detuned from  $\nu_0$ , with the magnitude of half the natural linewidth of the atomic resonance line, i.e.,  $\nu - \nu_0 \approx \pm \gamma/2$ .

\**Faculty of Engineering, Yamanashi University, 4 Takeda, Koufu-shi, Yamanashi 400, Japan*

1. M. Pinard *et al.*, *Phys. Rev. A* **19**, 2366 (1979).
2. D. Lee and J. C. Campbell, *Appl. Phys. Lett.* **58**, 995 (1991).
3. E. C. Valdez *et al.*, in *Proceedings of the IEEE/LEOS 1991 Annual Meeting* (San Jose, 1991), paper SADL4.4.



QTuG2 Fig. 1. Experimental setup: FR, Faraday rotator; PD, photodiode for monitoring the spectral profile of Rb vapor.



QTuG2 Fig. 2. Doppler-free spectral profile in Rb vapor measured as a function of the laser injection current: (a) Measured circular dichroism spectral profile by using a free-running laser. Spectral lines A, B, and C correspond to the transitions  $FF = 2 - 1, 2 - 2, 2 - 3$ , respectively. Spectral lines D and E correspond to the crossover resonances. (b) The result measured by injecting the reflected probe beam into the laser. For (a) and (b), the Faraday rotation angle was fixed at  $45^\circ$ . (c) Measured dispersive spectral profile while injecting the reflected probe beam into the laser. The Faraday rotation angle was changed from  $45^\circ$ .



of Sciences, Leninsky prospect 53, 117924 Moscow, Russia; <sup>(4)</sup>Graduate School at Nagatsuta, Tokyo Institute of Technology, 4259 Nagatsuta, Midori-ku, Yokogama 227, Japan

Laser diodes (LD) are comparatively simple and inexpensive devices so that it makes sense to use two LD with closely spaced optical frequencies for microwave generation.<sup>[1,2]</sup> Atoms of alkali metals provide a set of reference lines which are convenient for frequency stabilization. Many of the corresponding stabilized frequency differences fall within the microwave region with many possible applications in meteorology and communication systems.

We present results on investigating and using Doppler-free resonances in copropagating beams of the two highly coherent LDs as well as  $\Lambda$ -resonance induced by the coherent population trapping (CPT) for frequency difference stabilization and microwave generation. The experiments were carried out on D<sub>1</sub>, D<sub>2</sub> lines of Rb.

The main results are the following:

1. Peculiarities of the Doppler-free resonances in copropagating waves of the two LDs lines were analyzed. The absorption of bichromatic radiation was displayed as a function of frequency of the one laser while the frequency of the second one was not varied (Fig. 1). There are three and seven peaks due to optical pumping compensation on D<sub>1</sub> and D<sub>2</sub> lines respectively. The Doppler background is strongly suppressed and the contrast is actually larger. The resonances occur for definite differences of laser frequencies with frequencies itself being not fixed. The distances between adjacent resonances are equal either to HF splittings or their differences.

2. Various form (dispersion-like, different signs) of the narrow high contrast  $\Lambda$ -resonances have been observed in polarization scheme.

3. Frequency difference of the two LDs has been stabilized to the Doppler-free resonances induced by optical pumping compensation (the width is about 10 MHz) and by resonances occurring because of CPT (the width is about 100 kHz) with the frequency or Zeeman modulation technique. The beat note of the two lasers stabilized by  $\Lambda$ -resonance is shown in the Fig. 3.

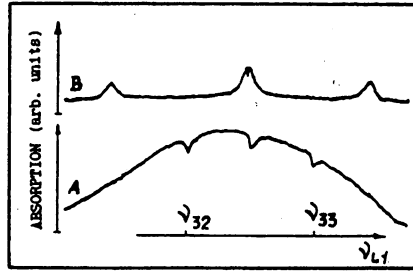
It will be possible to narrow the linewidth of microwave signal to ~10 Hz if the high contrast  $\Lambda$ -resonance and wide bandwidth servo system are utilized according to Ref. 3. To find out the limiting parameters of the  $\mu$ -wave generator and to compare them with the parameters of commercial Cs and Rb atomic clocks some additional experiments are to be carried out.

1. M. Tetu, B. Villence, N. Cyr, P. Tremblay, S. Theriaultand, and M. Breton, *J. of Lightwave Techn.* 7 (1989) 1540.
2. A. Akulshin, A. Celikov, and V. Velichansky, *Opt. Comm.* 84 (1991) 134.
3. C.-H. Shin and M. Ohtsu, *Opt. Lett.* 15, (1990) 1455.

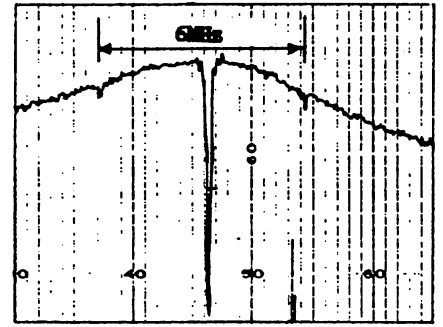
14:45 PM

**MoL3 Using Resonances Induced by Coherent Population Trapping for Frequency Difference Stabilization and Microwave Generation**

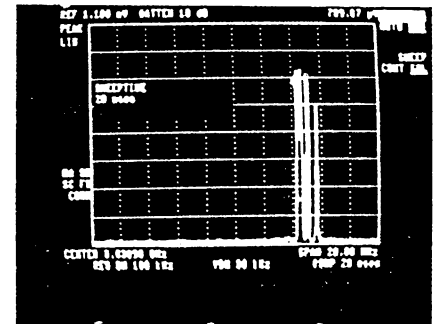
A. M. AKULSHIN, A. A. CELIKOV, K. NAKAGAWA\*, M. OHTSU\*, V. L. VELICHANSKY, and V. V. VASILJEV, P. N. Lebedev Physics Institute, Academy



MoL3 Fig. 1: Absorption spectrum on D<sub>1</sub>-line of <sup>85</sup>Rb displayed simultaneously: a) in the reference cell with the two counter propagating beams of the first laser; b) in the cell with the two copropagating beams of both lasers. The frequency of second LD was fixed while the first one was tuned over the Doppler profile of the transition 5S<sub>1/2</sub>(F=3)-5P<sub>1/2</sub>(F=2,3).



MoL3 Fig. 2: High contrast  $\Lambda$ -resonance on D<sub>2</sub> line of <sup>87</sup>Rb, to provide frequency scale one of the lasers was FM modulated at 3 MHz.



MoL3 Fig. 3: Frequency of microwave signal corresponding to HF splitting of the ground state of <sup>85</sup>Rb.

17:45 PM

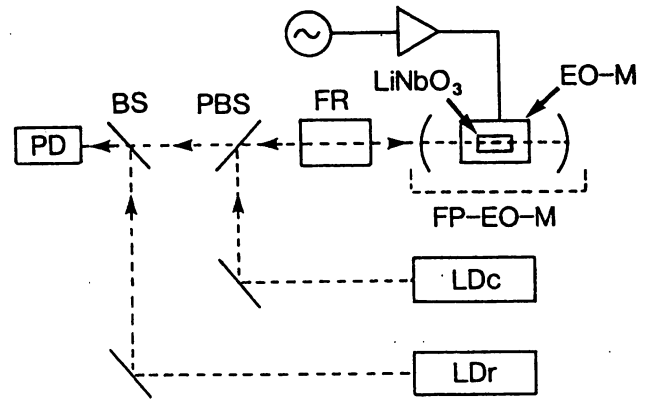
**TuM5 A Wideband Optical Frequency Comb Generator for a Highly Accurate Laser Frequency Measurement**

M. KOUROGI, K. NAKAGAWA, and M. OHTSU, Graduate School at Nagatsuta, Tokyo Institute of Technology, 259 Nagatsuta, Midori-ku, Yokohama, Kanagawa 227, Japan

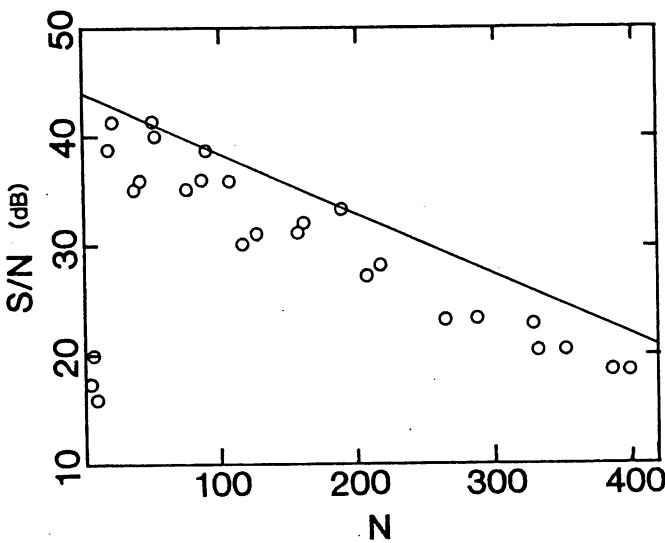
We have proposed recently a novel laser frequency measurement system at 1.5  $\mu\text{m}$  wavelength region with  $1 \times 10^{-10}$  accuracy.<sup>[1]</sup> This system is composed of two parts. One is the nonlinear optical frequency converters to phase-lock a 1.5- $\mu\text{m}$  wavelength semiconductor laser, used as a secondary standard, to two frequency-stabilized He-Ne lasers used as primary standards. Note that a similar phase locking has been also proposed by Telle, et al.<sup>[2]</sup> The other part is an "optical frequency comb generator" as a local oscillator to measure the frequency difference between the secondary standard laser and the laser under measurement.

A wideband optical frequency comb generator for the system mentioned above is demonstrated by employing an electro-optic (EO) modulator installed in Fabry-Perot (FP) cavity (i.e., FP-EO modulator<sup>[3]</sup>).

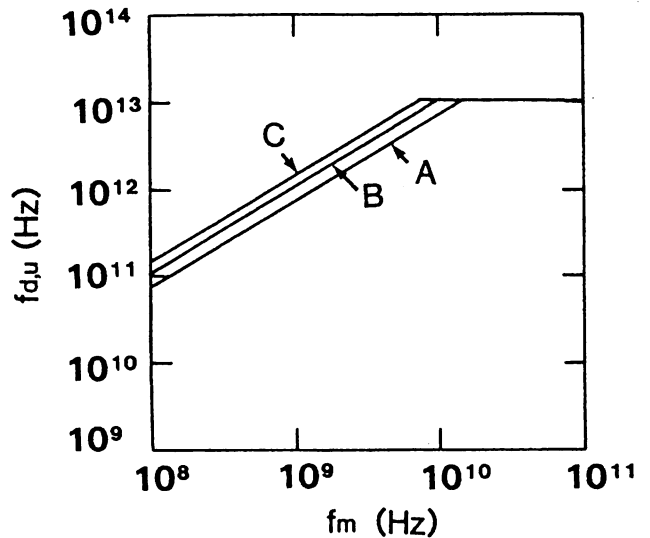
Experimental setup is shown by Fig. 1. The LD<sub>c</sub> and LD<sub>r</sub> were used as a laser for the comb generator and a reference, respectively. The modulation frequency ( $f_m$ ) of the FP-EO modulator was equal to twice the free-spectral-range of the FP cavity. The heterodyne signal between the LD<sub>r</sub> and the N-th sideband of the LD<sub>c</sub> generated by the FP-EO modulator was observed by a microwave spectrum analyzer. Figure 2 shows the signal-to-noise ratio (S/N) of the heterodyne signal measurement. Agreement between the experimental and calculation confirms the high reliability of the FP-EO modulator. The highest measured N was 400, corresponding to the absolute value of the frequency difference ( $f_d$ ) between the LD<sub>r</sub> and the optical



TuM5 Fig. 1: Experimental setup. LD<sub>c</sub> LD<sub>r</sub>: 10kHz linewidth 1.5μm DFB lasers. FP-EO-M: FP-EO modulator consisting of an EO modulator and FP cavity (Finesse = 150, Efficiency = 8 %). EO-M: EO modulator using a LiNbO<sub>3</sub> crystal installed in a microwave cavity (Modulation frequency = 1.25GHz. Modulation index = π/2-rad.). BS: Beam splitter. PBS: Polarization beam splitter. FR: Faraday rotator. PD: Photodiode.



TuM5 Fig. 2: Relation between the signal-to-noise ratio of the heterodyne signal measurement between the LD<sub>r</sub> and the N-th sideband of the LD<sub>c</sub>. Open circles and a solid line represents the results measured by a microwave spectrum analyzer with the resolution bandwidth of 10 kHz. A solid line represents the theoretical results.



TuM5 Fig. 3: Theoretical result of the measurable upper-limit of the frequency difference  $f_{d,u}$  given as a function of  $f_m$ . The curve A represents the result obtained by using the S/N value obtained by the present work. The curves B and C represent the values by assuming that additional increases of 20dB and 40dB, respectively.

carrier component of the LD<sub>c</sub> as high as 500 [GHz], which was limited only by the tunable range of the laser used. The S/N of 18-dB was obtained even though the 400-th sideband power was several 10-pW, due to low FM noises of the lasers. Such a S/N is sufficiently high for optical phase locking in our laser frequency measurement system. The  $N_{\max}$ , defined as the maximum of  $N$  corresponding to  $S/N = 0$ -dB, is estimated as 680, corresponding to the measurable upper-limit of  $f_d$  (i.e.,  $f_{d,u}$  given by  $N_{\max} \times f_m$ ) as high as 850-GHz. This is, to our knowledge, the largest among the directly measured values documented so far. If the shot-noise-limited detection and further FM noise reductions of the laser by employing our servocontrol method<sup>[4]</sup> are realized, additional 40-dB increase of the S/N is expected and  $N_{\max}$  can be increased to 1380, corresponding to  $f_{d,u}$  as high as 1.73-THz.

For a higher-order operation of the microwave cavity,<sup>[5]</sup> a highly efficient EO modulator was designed to increase the values of  $f_m$  and thus,  $f_{d,u}$ . Figure 3 shows the expected value of the  $f_{d,u}$  as a function of  $f_m$ . Due to the dispersion characteristics of the EO crystal,  $f_{d,u}$  keeps constant for  $f_m > 10$ -GHz.

The value of  $|f_{d,u}|$  as high as 10-THz is expected from this figure for  $f_m > 10$ -GHz. It means that the optical frequency comb generator here can be used for laser frequency measurement system which covers the 20-THz wide window region around 1.55- $\mu$ m wavelength, and thus, can be used as a highly accurate laser frequency calibrator indispensable for ultra-large capacity FDM coherent optical transmission systems.

1. M. Kourogi, K. Nakagawa, C. H. Shin, M. Teshima, and M. Ohtsu, Proc. CLEO'91, Baltimore, May 1991, paper number CThR57.
2. H. R. Telle, D. Meschede, and T. W. Hänsch, Opt. Lett. 15, 532 (1990).
3. T. Kobayashi, T. Sueta, T. Cho, and Y. Matsuo, Appl. Phys. Lett. 21, 341 (1972).
4. M. Kourogi, C.-H. Shin, and M. Ohtsu, IEEE Photon. Technol. Lett. 3, 496 (1991).
5. B. Y. Lee, T. Kobayashi, A. Morimoto, and T. Sueta, Proc. CLEO'91, Baltimore, May 1991, paper number CTuR4.

Since the discovery of high- $T_c$  superconductors, the feasibility of optical and infrared superconducting detectors has been much investigated as one of the promising electronic applications.<sup>11, 21</sup> In this paper, we have investigated optical response of epitaxial  $\text{DyBa}_2\text{Cu}_3\text{O}_{7-x}$  thin films to a GaAlAs diode laser light at the wavelength of 830 nm in order to use the thin film as a fast photo-detector for our laser frequency system with the accuracy as high as  $1 \times 10^{-10}$ .<sup>131</sup> We have, for the first time, succeeded in observing the optical response at the modulation frequency up to 100 MHz.

$\text{DyBa}_2\text{Cu}_3\text{O}_{7-x}$  superconducting thin films are deposited on MgO (100) substrate by MBE in an ultrahigh vacuum system.<sup>141</sup> The samples with the  $T_c=88$  K have constrictions with a size of 20  $\mu\text{m}$  width, 400  $\mu\text{m}$  length and 0.1  $\mu\text{m}$  thickness, which were fabricated by standard photolithography and Ar ion milling.

The modulation frequency of the dc-biased GaAlAs laser was varied from 1 kHz to 100 MHz. The sample is biased by constant dc current from the current source, and the output electrical signals were measured through the lock-in amplifier under the irradiation of modulated laser light.

The upper part of Fig. 1 shows the temperature dependence of resistivity of a sample film (solid line) under the irradiation of laser light (break line) and the output voltage (i. e. photo response). The modulation frequency of the laser is 1 MHz, and the biased current of the sample is 0.1 mA. This optical response (break line) includes both the bolometric and non-bolometric ones. This relation is expressed as the following way,

$$\delta V = I_B \frac{\partial R}{\partial T} \Delta T + R \frac{\partial I}{\partial T} \Delta T, \quad (1)$$

where  $\delta V$  represents the output voltage arisen from the laser irradiation,  $I_B$  and  $R$  are a bias current and the resistance of a sample, respectively.  $\Delta T$  means the rising temperature by heating effect due to the laser irradiation. The first term of right hand in this equation indicates bolometric response which result from an increase of the sample's temperature. On the other hand, the second term of right hand in this equation means nonbolometric response. The lower part of Fig. 1 shows the magnitude of both the bolometric and the nonbolometric which is normalized to peak value. These values are calculated according to the expression (1). We have investigated the frequency dependence of the ratio of a bolometric signal to the total one,  $S_B/S_{\text{TOTAL}}$ , as shown in Fig. 2. At the region of low modulation frequency, this ratio is constant, because the bolometric signal dominates over the total signals. But it is found that the bolometric signal gradually decreases from the modulation frequency of about 100 kHz and the nonbolometric one dominates at the higher frequency.

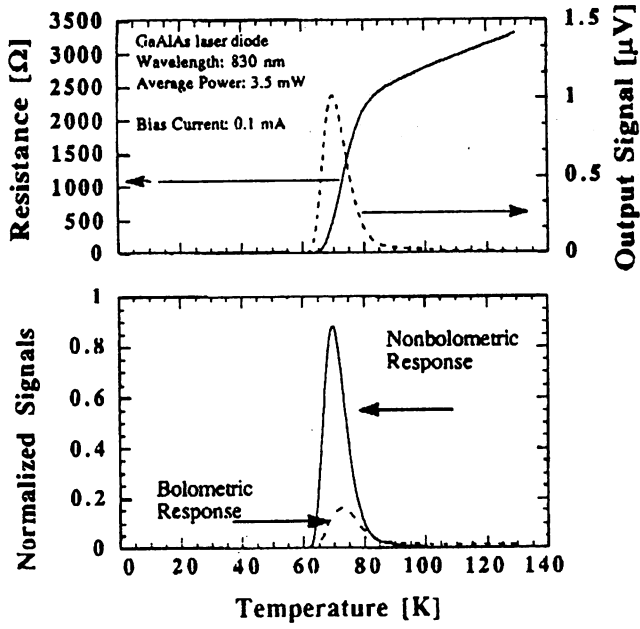
According to the non-equilibrium theory of Kaplan *et al.*<sup>151</sup> which is based on BCS theory, it is estimated that modulation frequency of the laser to 20 GHz can be achieved. Moreover, if the pairing mechanism of electrons in high- $T_c$  superconductors is based on the electron-electron interaction, not an electron-phonon one, it can be expected that optical response time becomes much shorter. Therefore, it is expected that this constricted superconducting film can

be used as a novel wavelength-intensitively ultra-fast detector for accurate frequency measurement.

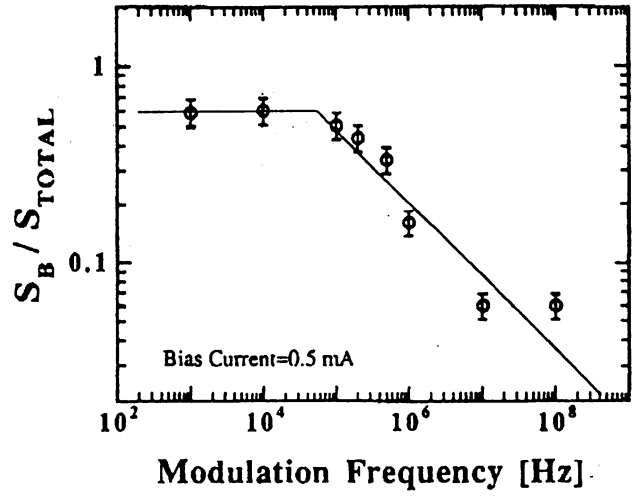
1. M. G. Forrester *et al.*, Appl. Phys. Lett. **53**, 1332 (1988).
2. K. Tanabe *et al.* Jpn. J. Appl. Phys. **29**, L466 (1990).
3. M. Kourogi *et al.*, Proceedings of CLEO '91, Baltimore, 470 (1991).
4. Y. Higashino *et al.*, (1991) Proceedings of the Third International Superconducting Electronics Conference (ISEC '91), Glasgow, in press.
5. S. B. Kaplan *et al.*, Phys. Rev. B **14**, 4854 (1976).

**PWe091 Nonbolometric Optical Response of  $\text{DyBa}_2\text{Cu}_3\text{O}_{7-x}$  Epitaxial Thin Films for a Wavelength-Insensitively Fast Photo-Detector**

Y. HARADA, K. NARUSHIMA, M. SANO, M. SEKINE, and M. OHTSU, The Graduate School at Nagatsuta, Tokyo Institute of Technology, 2459 Nagatsuta Midori-ku, Yokohama 227, Japan; Y. HIGASHINO, Yokogawa Electronic Corporation, 2-9-32 Nakacho, Musashino-shi, Tokyo 180, Japan



PWe091 Fig. 1: The optical response of a sample under the irradiation of laser with the modulation frequency of 1 MHz.



PWe091 Fig. 2: Modulation frequency dependence of the ratio of a bolometric signal to the total one,  $S_B / S_{TOTAL}$ .

## Estimation of Frequency Accuracy and Stability in a Diode Laser-Pumped Rubidium Beam Atomic Clock Using a Novel Microwave Resonant Method

Hiroyuki FURUTA and Motoichi OHTSU

Graduate School at Nagatsuta, Tokyo Institute of Technology,  
4259 Nagatsuta, Midori-ku, Yokohama, Kanagawa 227

(Received August 6, 1991; accepted for publication September 21, 1991)

Experiments on a diode laser-pumped rubidium (Rb) beam atomic clock are carried out. A novel microwave resonance method (HORR) with a conventional cylindrical cavity is used. On the basis of the experimental results, the expected frequency accuracy of  $1.4 \times 10^{-12}$  is theoretically estimated with this clock. A frequency stability as high as  $7.8 \times 10^{-13} \tau^{-1/2}$  is also estimated.

**KEYWORDS:** diode laser, rubidium atomic clock, frequency accuracy, frequency shift, frequency stability

### §1. Introduction

Highly precise and compact rubidium (Rb) atomic clocks have been required for various applications, *e.g.*, the signal sources for the Global Positioning System (GPS) satellites, and the Integrated Services Digital Network (ISDN) systems. For the improvement of their performance, Rb atomic clocks pumped by diode lasers have been investigated.<sup>1-4)</sup> Consequently, the frequency stability of Rb atomic clocks has drastically been improved.

On the other hand, the frequency accuracy of Rb atomic clocks is still limited. Owing to the AC Stark effect and the collisions of Rb atoms, *e.g.*, the collisions between Rb and buffer gas atoms, frequency shifts are induced. The light shift (AC Stark effect) can be compensated,<sup>4)</sup> or can be avoided by spatially separating interaction regions of atoms with lightwaves and microwaves. However, as long as the buffer gases are used in small glass cells, it is impossible to remove the frequency shifts induced by the collisions of Rb and the buffer gas atoms. It is also difficult to remove the frequency shift induced by the collisions of Rb atoms with glass cell walls. Since such frequency shifts have deteriorated the frequency accuracy of the clocks, conventional Rb atomic clocks have not been employed as primary frequency standards. In this connection, we proposed a diode laser-pumped Rb beam atomic clock for achieving high frequency accuracy.<sup>5)</sup>

The lineshape characteristics of a microwave resonance signal are important since it is used as the frequency reference and discriminator for the microwave frequency stabilization of an atomic clock. We proposed a novel Rabi magnetic resonance method using modal patterns of microwave magnetic fields inside a cylindrical cavity.<sup>6)</sup> This method has the advantage that Rabi resonance spectral lineshapes similar to those in Ramsey resonance can be generated with the help of a compact and simple microwave cavity, which is stable against ambient changes and easily designed. We call this novel resonance a higher-order-mode-attributed Rabi magnetic resonance (HORR).

In this paper, we discuss the frequency accuracy of a novel Rb atomic clock frequency-stabilized onto a HORR spectrum. So far the frequency accuracy of Rb atomic clocks has not been estimated nor evaluated well. This is the first demonstration of its estimation. The frequency shifts and stability of the clock are also evaluated from the results of both experimental and theoretical analyses.

### §2. Experimental Setup and Operation of Clock

A diode laser-pumped Rb beam atomic clock using HORR is shown in Fig. 1. Here only the main body of the system is shown, since the details of the system are given in Fig. 1 of ref. 6. The essential points are as follows. The cavity mode was the TE<sub>012</sub> mode; the cylindrical axis of the cavity (Line A-A') was placed perpendicular to the atomic beam trajectory (Line B-B') (see Fig. 1(a)).

Figure 2 shows an energy level diagram of rubidium-87 (<sup>87</sup>Rb) and the definitions of the symbols for each transition of the <sup>87</sup>Rb D<sub>2</sub> line. Optical pumping of Rb atoms was done using the transition  $F=2-F'=2$  (transition p, see Fig. 2) of the <sup>87</sup>Rb D<sub>2</sub> line with the diode laser LD1. The optical pumping changed the population difference between the hyperfine levels  $|F=1, m_F=0\rangle$  and  $|F=2, m_F=0\rangle$  (clock transition) in the ground state of <sup>87</sup>Rb atoms. The atoms make magnetic dipole transitions at 6.834 GHz while going through the microwave cavity. The spectral lineshapes of the magnetic resonance were observed through the detection of the population change in one of the hyperfine levels in the ground state. Hence effective state selection by optical pumping with LD1 was important for the microwave interaction. The population change was detected through the change in the fluorescence intensity of <sup>87</sup>Rb atoms pumped with the diode laser LD2. The frequency of LD2 was tuned to the recycling transition  $F=2-F'=3$  (transition q). The optical pumping on this transition increases the fluorescence intensity, which increases the signal-to-noise ratio ( $S/N$ ). The frequencies of diode lasers LD1 and LD2 for the optical pumping and detection were stabiliz-



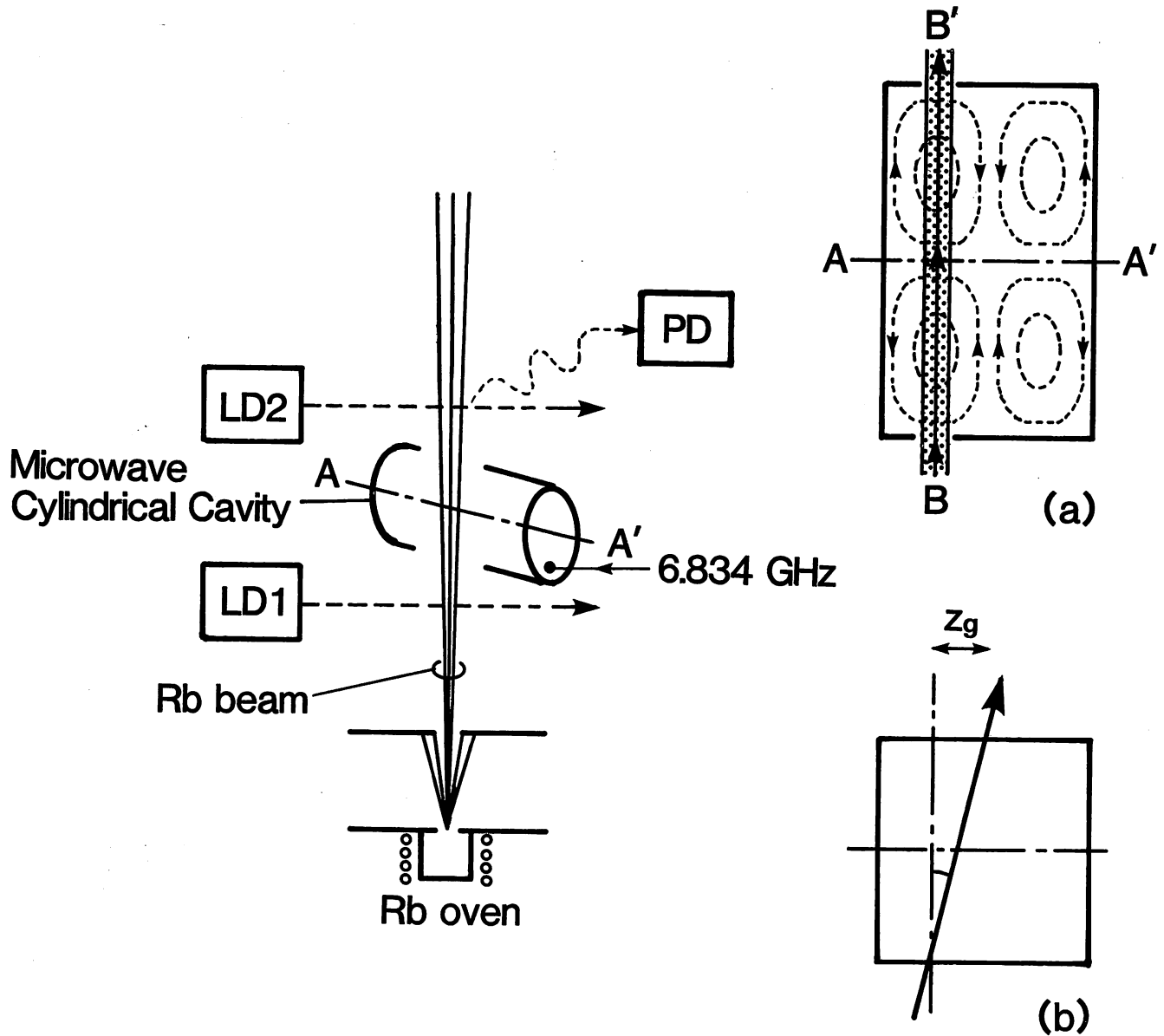


Fig. 1. Experimental setup for a diode laser-pumped Rb beam atomic clock with the novel microwave resonance method HARR, and cross-sectional view of cavity: modal pattern (a); misalignment of atomic beam trajectory (b).

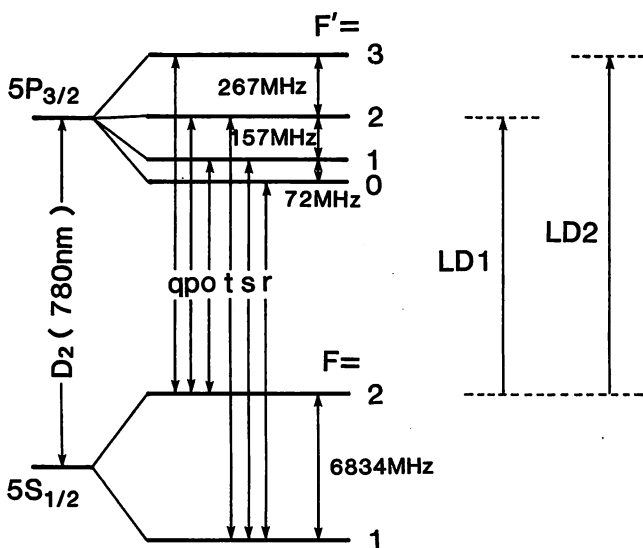


Fig. 2. Energy level of a  $^{87}\text{Rb}$  atom.

ed electrically to the linear absorption spectral lines of  $^{87}\text{Rb}$  atoms in glass cells.<sup>7)</sup>

Figures 3(a) and 3(b) show examples for experimental and calculated results of HARR spectral lineshapes, respectively. Figure 3(a) is a copy of the center part of the spectral profile of Fig. 4(b) in ref. 6. Experimental result (a) was a phase-sensitively detected signal from a lock-in amplifier. Calculated result (b) was obtained as a result of the numerical calculation given in ref. 6. It is worth noting that Fig. 3(b) represents the precisely calculated resonance curve of the Rb beam interacting with the microwave magnetic field. The amplitude of the field has a profile of the 1st kind of Bessel function of 0th order, whereas the calculated results in ref. 6 were obtained using the approximated modal profile of microwaves composed of three constant fields (see Fig. 2(c) of ref. 6). Figures 3(a) and 3(b) show good agreement between the calculation and the experiment.

The frequency of a voltage-controlled crystal oscillator

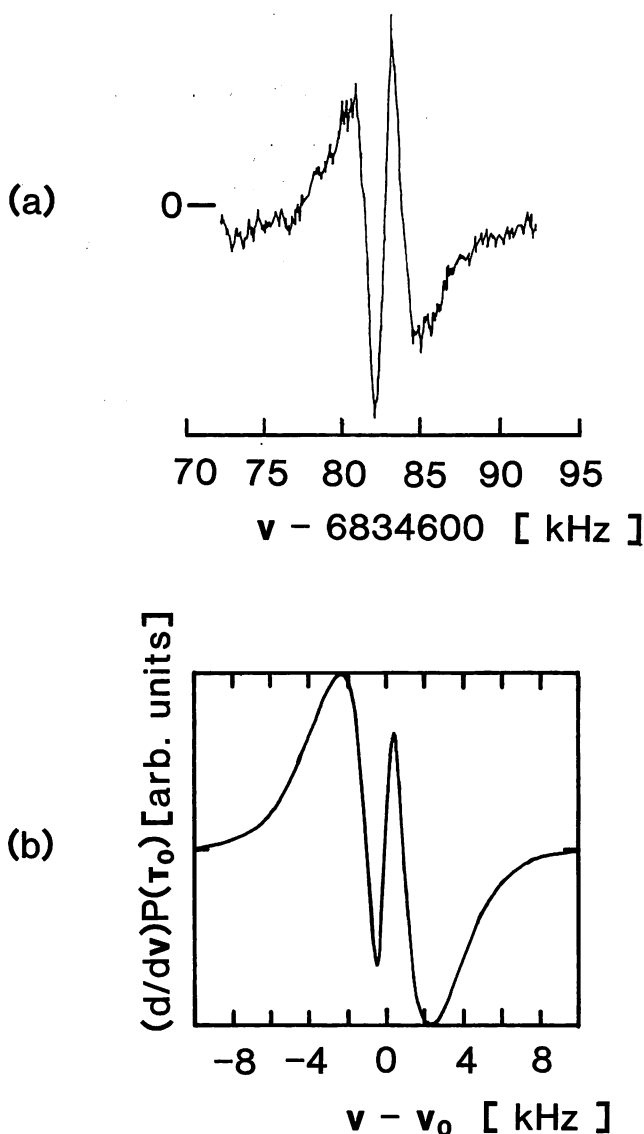


Fig. 3. Examples of the derivatives of HARR spectral lineshapes: experimental (a) and calculated (b) results. The experimental result was obtained by phase-sensitive detection at modulation frequency 420 Hz. Rb oven temperature was  $T_{\text{Rb}}=433$  (K).

(VCXO) was stabilized using the resonance spectral lineshape obtained in the experimental setup of Fig. 1. The frequency of VCXO (5 MHz) was measured with a time interval counter (SRS, SR 620-01). A commercial Rb atomic clock (Fujitsu, FC 6017 A) was used as a reference oscillator. The frequency of the Rb atomic clock was calibrated with the TV color subcarrier (NTSC, 3.58 MHz) and the rf standard (JG2AS: 40 kHz). The output signal from the time interval counter was sent to a personal computer (NEC, PC-9801 VM) through a serial interface RS-232 C. The frequency fluctuation/stability was evaluated from the results processed by the computer.

Figure 4 illustrates the results of the square root of the Allan variance<sup>8)</sup> as a function of the averaging time  $\tau$ . The frequency stability of  $1.2 \times 10^{-11}$  was obtained at  $\tau=100$  (s). The results show that the frequency fluctuations of the stabilized VCXO were reduced to about one-tenth of those in free-running VCXO over the range

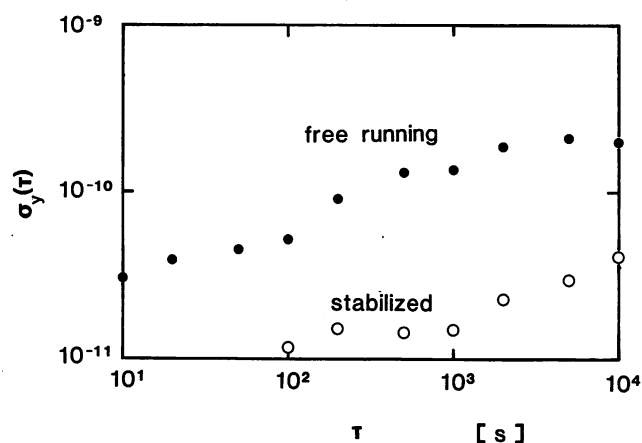


Fig. 4. Measured results of frequency stability of VCXO frequency locked to a HARR lineshape. The results are square roots of Allan variances of measured frequency fluctuations against the reference frequency of conventional Rb atomic clock, and plotted as a function of integration time  $\tau$ . The symbols  $\circ$  and  $\bullet$  correspond to the results under frequency-stabilized and free-running conditions, respectively.

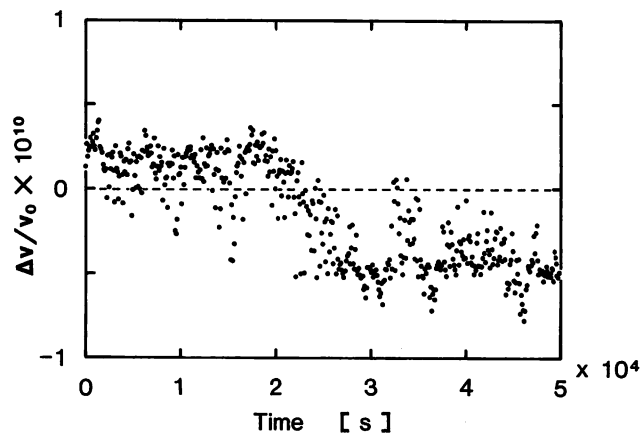


Fig. 5. Measured results of frequency fluctuation of VCXO frequency locked to a HARR lineshape. The results are plotted as a measuring time sequence. The reference frequency from a conventional Rb atomic clock was calibrated by comparing with the frequency of TV color subcarrier.

$100(\text{s}) \leq \tau \leq 10000$  (s).

Figure 5 shows the measured result of frequency drift characteristics for our clock in comparison with the reference. From this figure, a frequency drift of  $3.6 \times 10^{-12}$ /hour was seen. The standard deviation of 500 samples with the gate time of 100 s was calculated to give the fractional frequency fluctuation of  $3.0 \times 10^{-11}$ . This can be understood as the medium-term frequency stability. The frequency slip seen at 20000 s was ascribed to an accidental surge or signal offset. Except for this slip, the frequency of stabilized VCXO was maintained very stable.

Generally, the frequency accuracy is evaluated in comparison with a precisely calibrated standard frequency. The frequency of cesium (Cs) atomic clocks have been calibrated by the international time comparison. On the other hand, in Rb atomic clocks, no time comparison has

been carried out. There is no international agreement on their resonance frequencies. Only one document reported a measured frequency of Rb magnetic resonance with an accuracy of 0.5 Hz.<sup>9)</sup> Therefore, we tried to estimate the frequency accuracy of our Rb beam atomic clock. Provided that an averaged value of measured frequency in Fig. 5 was a true value of resonance frequency, the frequency stability represented by a standard deviation  $\sigma$  of frequency fluctuation in the figure gave the frequency accuracy of  $3\sigma \approx 10^{-10}$  as the accuracy in the present work.

### §3. Estimation of Frequency Accuracy/Shift

#### 3.1 Effect of collisions of Rb atoms

Collisions between alkaline atoms cause relaxations of the population of the energy levels and of the coherence between quantum states. These relaxations induce hyperfine transition frequency shifts, which are proportional to the atom density.

The angular frequency shift  $\Delta\omega_{se}$  due to the spin-exchange collision is calculated from the following equation:<sup>10)</sup>

$$\Delta\omega_{se} = -\frac{1}{4}(\rho_{1,1} - \rho_{2,2})n\bar{v}_r\bar{\lambda}_{ex}, \quad (1)$$

where  $\bar{v}_r$  is the mean relative velocity of the atoms and  $\bar{\lambda}_{ex}$  is the spin-exchange frequency shift cross section. In accordance with the discussion presented in ref. 10,  $\bar{\lambda}_{ex}$  is, at most, as large as that of spin-exchange cross section  $\bar{\sigma}_{ex}$ . In Rb atoms,  $\bar{\sigma}_{ex}$  is  $2.54 \times 10^{-18}$  (m<sup>2</sup>).<sup>10)</sup> Collisions in an atomic beam are approximately one-third as frequent as in a gas cell, i.e.,  $n = 0.336 n_b$ .<sup>11)</sup> In the perfect state

selection by optical pumping,  $|\Delta\omega_{se}|$  has been calculated and is shown with a dashed-and-dotted line in Fig. 6 as a function of the oven temperature  $T_{Rb}$ . Here the frequency shift was normalized to the angular frequency  $\omega_M$  of the microwave transition. From this figure, one can see that the frequency shift caused by collisions of atoms in the atomic beam is about  $5 \times 10^{-13}$  at  $T_{Rb} = 430$  (K), and is small enough to obtain a frequency accuracy of  $1 \times 10^{-12}$ , which is the typical value for commercial Cs atomic clocks.

Background atoms exist in the vacuum chamber (or the beam tube), and their densities are not negligible in the estimation of the frequency shift. The magnitude of frequency shift cross section  $\bar{\sigma}_{N_2}$  for the collision between Rb atoms and nitrogen molecules (N<sub>2</sub>) is  $7.4 \times 10^{-26}$  (m<sup>2</sup>),<sup>10)</sup> and is negligibly small as compared with the cross section  $\bar{\lambda}_{ex}$ . In the worst case where most of the remaining background pressures are of Rb atoms and the vapor pressure of background Rb atoms is the same as the vacuum pressure of  $1.0 \times 10^{-6}$  Torr, the density of background Rb atoms is  $3.1 \times 10^{16}$  (m<sup>-3</sup>). Using eq. (1) and  $\bar{v} = 3.8 \times 10^2$  (m/s), the normalized fractional frequency shift is estimated as  $1.8 \times 10^{-10}$ . The frequency shifts corresponding to other pressures are shown by the broken lines A ~ D in Fig. 6.

An example of total collisions is shown as a solid line for the vacuum pressure of  $1.0 \times 10^{-9}$  Torr. A frequency accuracy of  $1 \times 10^{-12}$  can be obtained under the condition in which the vacuum pressure is  $10^{-9}$  Torr and the oven temperature is less than 400 K.

#### 3.2 Cavity phase shift in HERR spectra

The frequency shift induced by the HERR spectral deformation is discussed in this subsection, since it is used as a frequency discriminator for the frequency stabilization of VCXO. In what follows, the effects of collisions of Rb atoms with other gases, other Rb atoms, and glass/chamber walls are neglected. The considered frequency shifts correspond, therefore, to the frequency shifts caused by the cavity phase difference, just as end-to-end phase shift in conventional Ramsey resonance. We consider two kinds of frequency shifts here, i.e., those due to 1) distribution of the cavity modal pattern and 2) misalignment of the atomic beam trajectory.

##### 3.2.1 Cavity pulling effect and contributions from other cavity modes

A frequency shift is induced from overlaps of various cavity resonance modes, i.e., the overlaps between the desired TE<sub>012</sub> mode and other TE modes. There are no frequency shifts in each resonance spectrum coupled with any one of the resonance modes of the cavity. To confirm this, representative resonance spectra for the TE<sub>212</sub> mode and the TE<sub>112</sub> mode were calculated. Figures 7 and 8 show examples of the calculated (a) and the experimental results (b). They confirm that these lineshapes are symmetric with respect to the centers. If the cavity phase difference in each mode is always 0 or  $\pi$ , the resonance frequency shift is not induced, noting that the resonance signal with the phase difference  $\pi$  takes a minimum at the center frequency, i.e., the center is observed at a bottom (or a valley) of the lineshape.

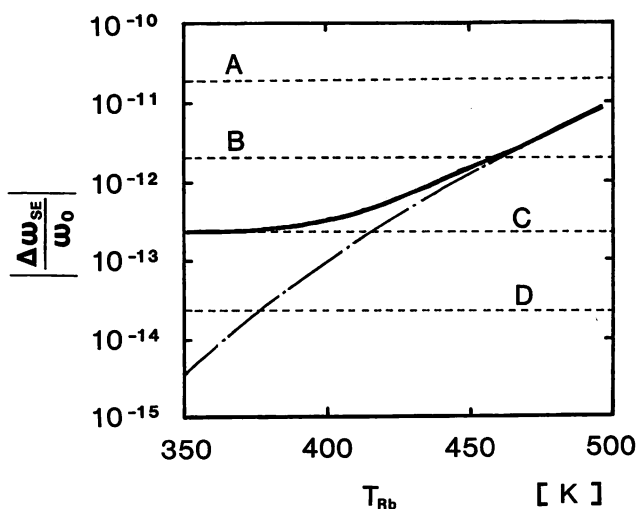


Fig. 6. Frequency shifts caused by collisions of atoms as a function of Rb oven temperature. A dashed-and-dotted line and broken lines correspond to frequency shifts caused by collisions of Rb atoms in an atomic beam with Rb atoms of the beam and atoms of several background pressures, respectively. The shifts were estimated from the spin-exchange effect. Collisions with the background atoms were assumed all as Rb atoms considering the worst situation. The oven aperture was 3 mm, and the atomic beam 15 cm away from the oven was considered. The broken lines A, B, C and D represent the results for the background pressures of  $1.0 \times 10^{-7}$ ,  $1.0 \times 10^{-8}$ ,  $1.0 \times 10^{-9}$  and  $1.0 \times 10^{-10}$  Torr, respectively. An example of total collision is shown as a solid line for the vacuum pressure of  $1.0 \times 10^{-9}$  Torr.

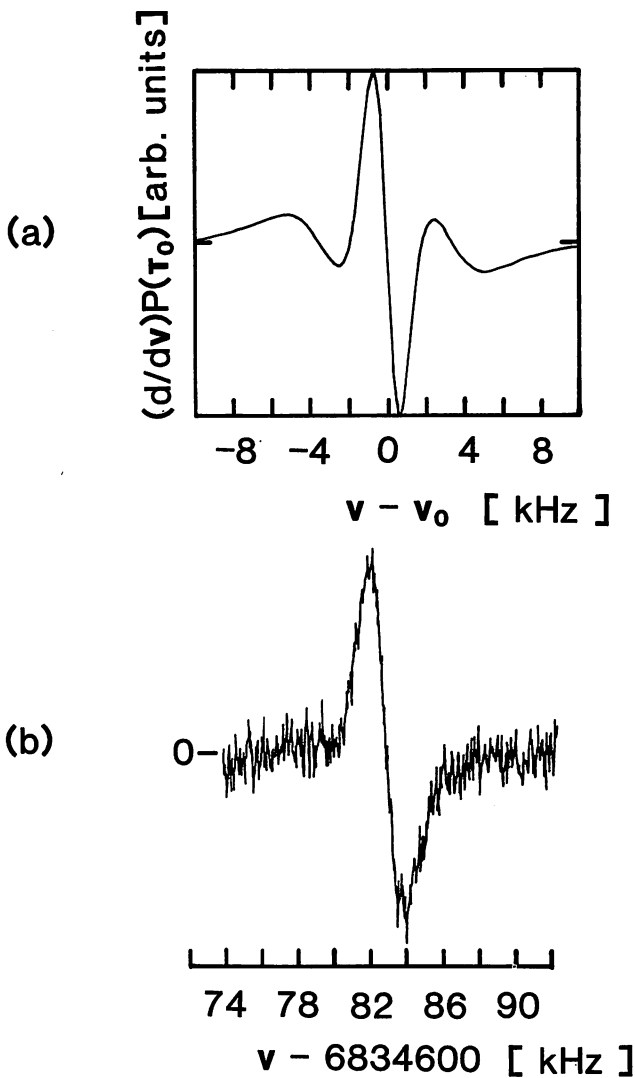


Fig. 7. Examples of the derivatives of HERR spectral lineshapes using a microwave cavity of TE<sub>212</sub> mode: calculated (a) and experimental (b) results.

However, overlap of two resonance spectra induces frequency shift because there are cavity pulling effects. When the desired TE<sub>012</sub> mode is tuned, the other modes must be detuned. The frequency shift caused by the cavity pulling effect for a passive oscillator is expressed as<sup>10)</sup>

$$\omega_R - \omega_0 = \left( \frac{Q_c}{Q_M} \right)^2 (\omega_c - \omega_R), \quad (2)$$

where  $\omega_0$ ,  $\omega_c$  and  $\omega_R$  are the transition angular frequency of the atom, the resonance angular frequency of the cavity and the resonance angular frequency of the atom, respectively. The values  $Q_c$  and  $Q_M$  are the quality factors of the cavity and the atomic microwave resonances, respectively.

The nearest resonance mode is TE<sub>212</sub>. At  $Q_c = 1500$  and  $Q_M = 6.8$  (GHz)/3 (kHz)  $\sim 2.3 \times 10^6$ , the frequency shift in the resonance lineshape for the TE<sub>212</sub> mode, which is 400 MHz away from the TE<sub>012</sub> mode, is  $3.9 \times 10^{-9}$ . The overlap of the TE<sub>212</sub> mode on the TE<sub>012</sub> mode spectral lineshape induces a frequency shift of  $1.3 \times 10^{-13}$  provided that each resonance mode has a Lorentzian lineshape with the same intensity. The effects of the other TE

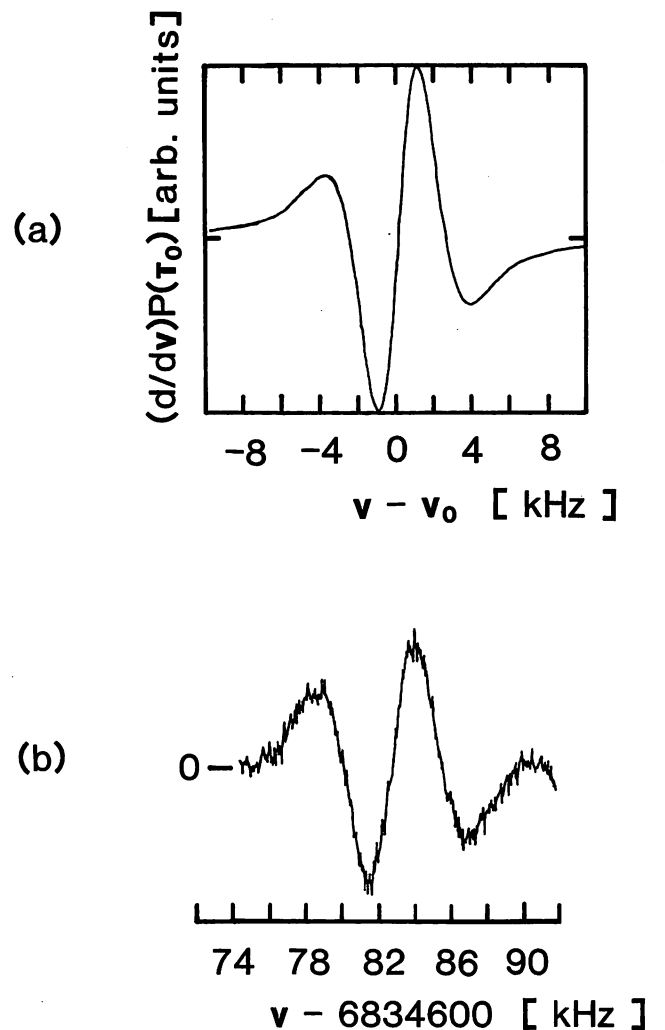


Fig. 8. Examples of the derivatives of HERR spectral lineshapes using a microwave cavity of TE<sub>112</sub> mode: calculated (a) and experimental (b) results.

modes are neglected since they are farther away and their relative intensities are much smaller. Thus the overlap effect of other cavity resonance modes cannot be the main causes for deterioration of the frequency accuracy to as low as  $1 \times 10^{-12}$ .

In the higher  $Q_c$  of the cavity, the frequency shift becomes larger and the more sensitive cavity tuning is necessary. On the contrary, for instance, at  $Q_c = 1000$  and with 0.1 MHz of cavity detuning, the frequency shift caused by the cavity pulling effect becomes  $4 \times 10^{-13}$ , and the frequency shift caused by the overlap of the TE<sub>212</sub> mode reaches  $3 \times 10^{-13}$ . This means that such undesired modes must be suppressed in the cavity design. It has been known among microwave engineers that, such undesired modes can be reduced using  $\lambda/4$  mode filters.<sup>12)</sup>

### 3.2.2 Misalignment of atomic beam trajectory

A frequency shift is induced by a cavity phase shift due to the misalignment of the atomic beam trajectory. The magnitude of microwave magnetic field amplitude varies with a change in the atomic beam trajectory, by which the HERR spectral lineshapes are deformed. However, as long as the phases of magnetic field do not change in

Table I. Frequency shifts on a diode laser-pumped Rb beam atomic clock using a HERR lineshape for the frequency stabilization.

Item	Present	Improved
Collisions of atoms	$1.8 \times 10^{-10}$ (at $10^{-6}$ Torr)	$< 3.0 \times 10^{-13}$ (at $10^{-9}$ Torr, $T_{\text{Rb}} < 400$ (K))
Cavity pulling	$1.0 \times 10^{-12}$ (at $Q_c = 1500$ , 0.1 MHz detuning)	—
Neighboring modes	$1.3 \times 10^{-13}$	—
Misaligned atomic beam	$1.6 \times 10^{-16}$ (at $z_g = 1$ (mm))	—

the cavity, the deformation of HERR lineshapes induces no frequency shift. Only the phase variation causes a frequency shift in HERR spectra. The phase variation of the field at the end of the cavity is expressed as

$$\Phi(z_g) = \alpha_g z_g \tan\left(\frac{\pi z_g}{\lambda_g/2}\right), \quad (3)$$

where  $z_g$  is the magnitude of the misalignment (defined in Fig. 1(b)),  $\lambda_g$  is the wavelength in the cavity along the axis, and  $\alpha_g$  is the loss of energy in the cavity.<sup>10)</sup> For the cavity of  $Q_c = 1500$ ,  $\lambda = 4.4$  (cm), and  $\lambda_g = 5.2$  (cm),  $\alpha_g$  takes  $5.6 \times 10^{-2}$  ( $\text{m}^{-1}$ ). The misalignment of  $z_g = 1$  (mm) (10 mrad.) yields the phase difference  $\Phi(z_g) = 6.8 \times 10^{-6}$  (rad/s). It corresponds to a negligibly small frequency shift of  $1.6 \times 10^{-16}$ .

### 3.2.3 Frequency accuracy

Table I shows the list of evaluated frequency shifts.

The frequency accuracy has been defined as “fractional uncertainty in determining an atomic transition frequency of the free atom” and is expressed by  $3\sigma$  limits for statistically determined frequencies.<sup>13)</sup> The “atomic transition frequency of free atom” is, in general, an unknown value. The frequency accuracy is estimated statistically, on the basis of the assumption that the reproducibility is sufficiently high. Therefore, the frequency accuracy, as well as the frequency reproducibility, is estimated by evaluating the frequency shift of the statistical value observed with certain fluctuation.

To summarize the above discussion, a frequency shift of  $1.8 \times 10^{-10}$  in Table I was estimated as the frequency accuracy in the present experimental situation. When the ultrahigh vacuum chamber reaching  $10^{-9}$  Torr is used, we can expect the frequency accuracy to be  $1.4 \times 10^{-12}$  for the present Rb atomic clock frequency-stabilized onto HERR spectra. It is worth noting that the magnitude of frequency shift caused by cavity pulling, which limits the present accuracy, can be reduced to the value determined by the frequency tuning technique of cavity resonance. So far, the frequency accuracy of Rb atomic clocks has not been estimated nor evaluated well. This is the first demonstration of the estimation.

## §4. Improvement of Frequency Stability

Improvement of frequency stability is expected by increasing  $S/N$  of frequency discrimination with effective optical pumping and detection. Optical pumping by diode lasers can improve detection sensitivity of the

microwave resonance line and the microwave frequency stability through two techniques, i.e., 1) increase in signal intensity with the use of more atoms effectively state-selected, and 2) reduction of noise by suppressing intensity and frequency noise of diode lasers. In ref. 6, the latter has already been mentioned. Here, the former, i.e., increase in signal intensity is mainly described.

### 4.1 Increase in signal intensity

The effect of diode laser optical pumping for the state selection of  $^{87}\text{Rb}$  atoms was derived using the time-dependent rate equations of ref. 14. The time-dependent results of the population difference  $\Delta n$  are shown in Fig. 9.  $\Delta n$  is the fractional population difference between the clock transition levels, i.e., the  $m_F = 0$  ground-state hyperfine sublevels, of the total population of  $^{87}\text{Rb}$  atoms. The results were obtained for one-laser pumping of several tunings and polarizations. Figures 9(a) and 9(b) represent the results for  $\pi$ -polarized and  $\sigma$ -polarized light, respectively. The laser power density  $P_L$  and the field spectral linewidth  $\Delta\nu_L$  are assumed to be 10 ( $\text{mW}/\text{cm}^2$ ) and 20 (MHz), respectively.  $\Delta n$  quickly reaches a steady-state value after a lightwave-atom interaction time of  $3 \mu\text{s}$ . Then an almost complete

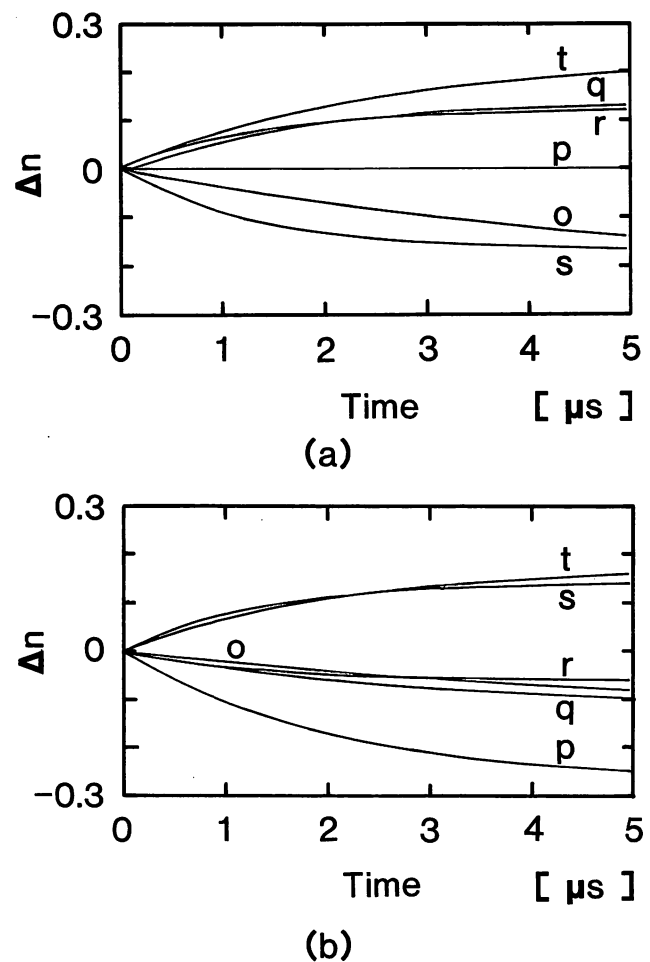


Fig. 9. Time evolution of the fractional population difference  $\Delta n$  between the  $m_F = 0$  ground-state sublevels. Optical pumping is performed with one laser. Optical power density  $P_L = 10$  ( $\text{mW}/\text{cm}^2$ ) and linewidth  $\Delta\nu_L = 20$  (MHz).  $\pi$ - (a) and  $\sigma$ -polarized (b) transitions of optical pumping.

depopulation of one of the two  $m_F=0$  sublevels is achieved, except for the two transition schemes, i.e., those on transitions  $F=1-F'=1$  (transition s, see Fig. 2) and p, which are both with  $\pi$ -polarized lights. In these two cases  $\Delta F=F'-F=0$  transitions occur and, irrespective of the laser intensity, no  $m_F=0$  sublevels can be depopulated because the transition probability is zero for  $\Delta F=0$ ,  $m_F=0$  transitions. The maximum pumping efficiency is obtained with the transition p:  $\sigma$ -polarized light, when  $\Delta n$  reaches  $-27\%$ . Compared with  $-15.5\%$  of Cs atoms pumped by a single laser,<sup>14)</sup> the result of Rb atoms is larger. With a  $\pi$ -polarized light, for the transition  $F=1-F'=2$  (transition t), it yields the maximum  $\Delta n$  of  $20\%$ . It should be noted that optical pumping was observed in the Zeeman sublevels even for the recycling transitions. Figures 9(a) and 9(b) show this effect; i.e., one of the  $m_F=0$  sublevels depopulates and the change in the fractional population difference  $\Delta n$  between the clock transition levels is not negligible.

In the two-laser pumping scheme, the results of  $\Delta n$  are seen in Fig. 10. The two-laser pumping scheme is, in general, used with the following concepts. One laser populates one of the hyperfine levels in the ground state. Then the other laser of  $\pi$ -polarization depletes all the ground-state sublevels except for that of  $m_F=0$ , according to the transition probabilities.<sup>15)</sup> It is worth noting that the second laser must be tuned to an optical  $\Delta F=0$  transition and  $\pi$ -polarized. On this transition, since the probability of transition between  $m_F=0$  Zeeman sublevels is zero, an efficient population transfer to a

$m_F=0$  ground-state sublevel is achieved. Figure 10 shows all the possible schemes of the time evolution of  $\Delta n$  when the values of  $P_L$  and  $\Delta\nu_L$  are the same with those of Fig. 9. From this result, the essential features of two-laser pumping are confirmed and examined. The discussions are as follows.

(i) As compared with one-laser pumping, it takes longer periods of interaction until the population difference  $\Delta n$  reaches its steady state. In this respect, the most efficient pumping scheme shall be chosen to obtain larger  $\Delta n$ . As seen in Fig. 10, in the interaction periods of  $20\ \mu\text{s}$ , the larger values are obtained with the two pumping schemes, i.e., those on 1) transitions s:  $\pi$ -polarized and p:  $\sigma$ -polarized, and 2) transitions t:  $\pi$ -polarized and p:  $\pi$ -polarized. The values of  $\Delta n$  for each optical pumping are as large as  $-68\%$  and  $80\%$ , respectively. It should be noted that, only with the second optical pumping scheme can  $\Delta n$  reach almost  $100\%$  with the adequate condition changes of lasers.

(ii) Note that, compared with Cs atoms, the configurations with the pumping on transitions s:  $\sigma$ -polarized and p:  $\pi$ -polarized cannot reach a  $50\%$  fractional population difference in  $^{87}\text{Rb}$  atoms. The transition probability of spontaneous radiation from the excited state  $F'=1$  to the ground state  $F=1$  is five times as large as that to  $F=2$ , and the population of atoms is concentrated to the Zeeman sublevel  $|F=1, m_F=1\rangle$  or  $|F=1, m_F=-1\rangle$ , which has no corresponding sublevels to be transferred.

(iii) As mentioned in (i), two-laser pumping schemes

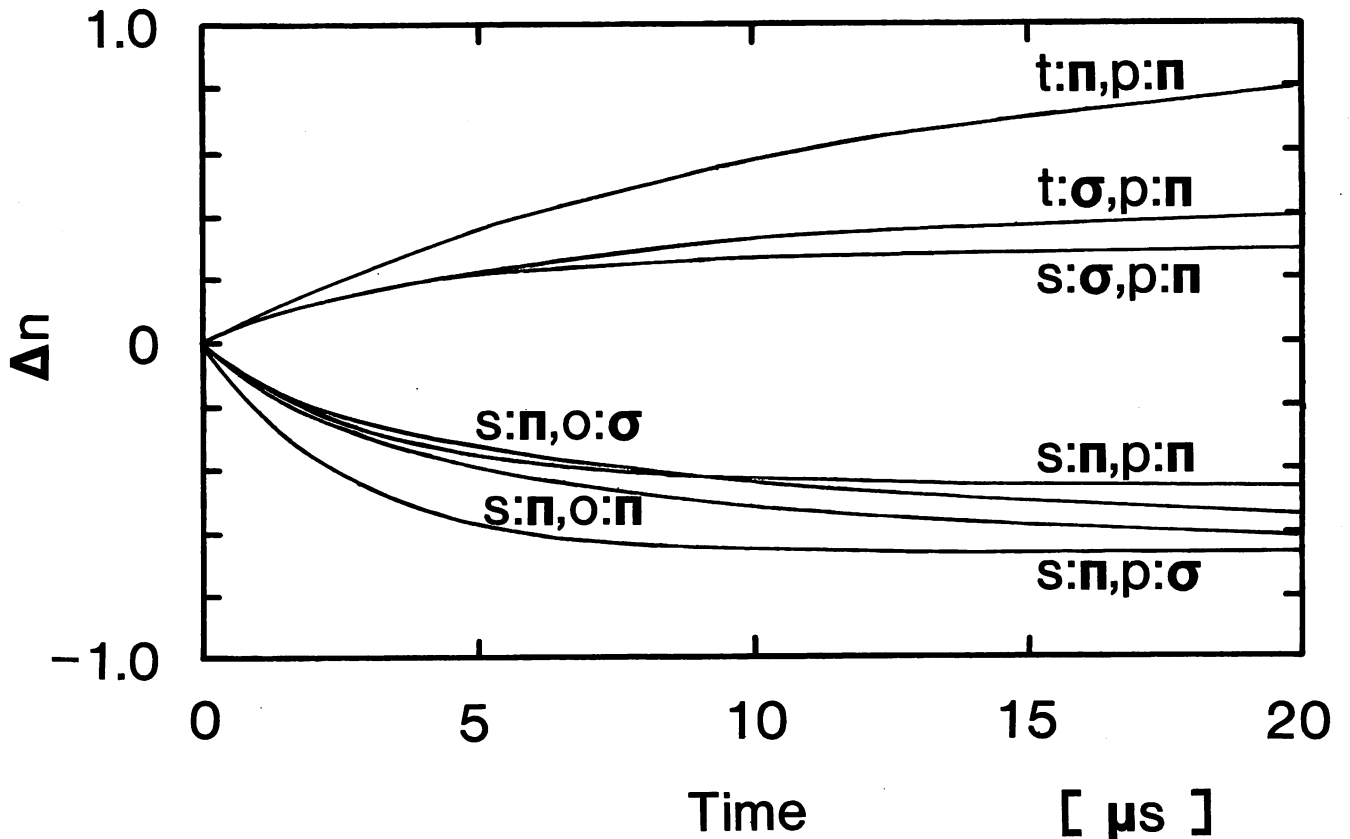


Fig. 10. Time evolution of the fractional population difference  $\Delta n$  in two-laser optical pumping.  $P_L=10\ (\text{mW}/\text{cm}^2)$  and  $\Delta\nu_L=20\ (\text{MHz})$  for each laser.

need longer interacting periods to approach the steady state as compared with the single-laser pumping scheme of Fig. 9. The pair of transitions t:  $\pi$ -polarized and p:  $\pi$ -polarized is the most efficient pair of pumping transitions, with which the population difference  $\Delta n$  reaches 98% in the steady state after an adequate interaction period (excitation period). The excitation period is varied with the change of the ratio between the optical power density and the spectral linewidth of the laser, i.e.,  $P_L/\Delta\nu_L$ . The excitation period becomes shorter as  $P_L$  becomes larger or as  $\Delta\nu_L$  becomes narrower. In practice, large  $P_L$  induces power broadening due to the saturation of pumping, where the efficiency of optical pumping decreases. The leakage of optical pumping takes place with the neighboring transitions owing to the spectrally broadened atom-lightwave interactions. In this connection, diode lasers of the narrower spectral linewidths shall be used; i.e., smaller  $\Delta\nu_L$  is required to shorten the excitation periods. In order to have a steady-state value of  $\Delta n$  after  $3\ \mu\text{s}$  of excitation at  $P_L=5\ (\text{mW}/\text{cm}^2)$ ,  $\Delta\nu_L=0.5\ (\text{MHz})$  is required. Such coherent diode lasers can be obtained stably and easily by using the electrical feedback<sup>16)</sup> or the optical feedback technique with a confocal Fabry-Perot interferometer.<sup>17,18)</sup>

Some results of optical pumping were experimentally examined. In the present work, the state selection was achieved with a one-laser pumping scheme. In this scheme, the largest population difference is produced by the pumping on the transition p:  $\sigma$ -polarized. The comparison with the results pumped on the other transitions is seen in Figs. 11(a) and 11(b). The microwave resonance signal intensities are plotted as functions of frequencies of pumping lasers of  $\pi$ - and  $\sigma$ -polarizations, respectively. The number of atoms in the hyperfine sublevel  $|F=2, m_F=0\rangle$  does not decrease by the excitation of transition p:  $\pi$ -polarized since the transition probability for this transition is zero. Consequently, the population difference between the levels  $|F=1, m_F=0\rangle$  and  $|F=2, m_F=0\rangle$  cannot be produced. No increase in the observed signal intensity can be expected. On the contrary, the transition p:  $\sigma$ -polarized excitation can depopulate the sublevel  $|F=2, m_F=0\rangle$  to zero. Much larger signal intensity can be obtained by this transition as compared with other transitions.

In order to increase the effects of optical pumping, the optical intensity and the field spectral linewidth of the diode laser, as well as choosing the transition lines, should be optimized. Since we used the lasers with free-running spectral linewidths in this work, the laser power density dependence of the microwave resonant signal intensity (population difference) was investigated. Figure 12 shows the results. The microwave resonant signal intensity was increased by increasing the laser intensity, and the saturation of signal intensity was observed at  $P_{L,\text{pump}}=10\ (\text{mW}/\text{cm}^2)$ . The comparison of transition schemes in Fig. 12 confirmed the theoretical analysis. The transition p:  $\sigma$ -polarized excitation achieved the maximum signal intensity of microwave transition with the maximum population difference. The magnitudes of the signal intensities by the optical pumping schemes on the transitions  $|F=2-F'=1$  (transition o):  $\pi$ -polarized and

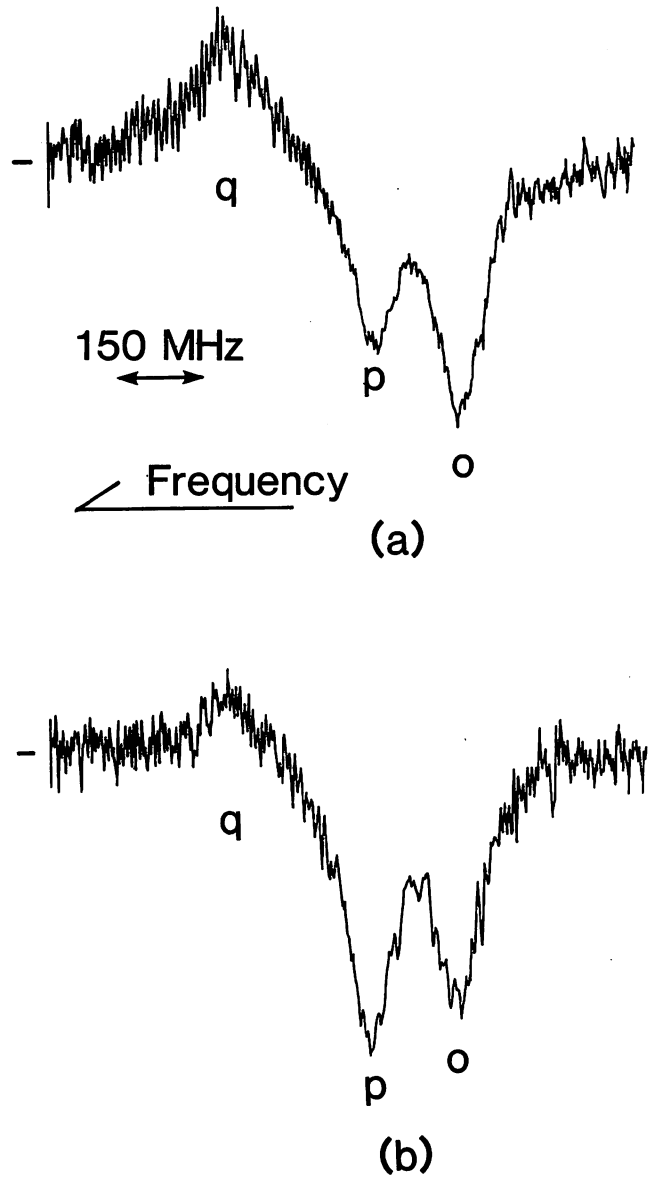


Fig. 11. Examples of HORN strength as a function of pumping laser frequency: for  $\pi$ - (a) and  $\sigma$ -polarized (b) transitions.

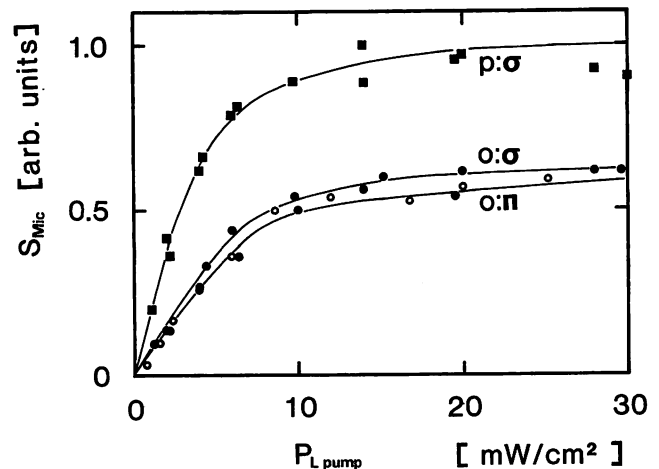


Fig. 12. The absolute value of HORN strength  $S_{\text{Mic}}$  as a function of pumping laser power density  $P_{L,\text{pump}}$ .

o:  $\sigma$ -polarized were both about 60% that of the transition p:  $\sigma$ -polarized excitation. The value obtained with pumping by the  $\pi$ -polarized transition agreed with the theoretical value, while that by the  $\sigma$ -polarized became much larger. This difference was attributed to the leakage of optical pumping by the transition p:  $\sigma$ -polarized due to the broader spectral linewidth of the diode laser.

#### 4.2 Frequency stability

A HERR spectral lineshape has the form shown in Fig. 13, whereas Fig. 3 shows the derivative of a HERR spectral shape. In a passive-type atomic clock whose VCXO frequency is stabilized to this spectral lineshape, we investigated the attainable frequency stability. As illustrated in this figure, the detected fluorescence intensity and the background light intensity are represented by  $I_{pa}$  and  $I_{pb}$  respectively. Then the microwave resonant signal is given by  $I_{ps} = I_{pa} - I_{pb}$ . The strength of the resonance fringe defined as the height between the central peak and an adjacent bottom of the central fringe is given by  $I_{pv}$ . The linewidth  $\Delta\nu_M$  of the resonance spectral lineshape is defined as the ‘‘full width at half-maximum (FWHM)’’ of the fringe.  $\nu_{0\leftrightarrow 0}$  is the microwave resonance frequency of the clock transition of the  $^{87}\text{Rb}$  atom and is 6.834 GHz. In this case, the microwave frequency stability of the atomic clock is expressed as<sup>19,20)</sup>

$$\sigma_y(\tau) = (\sqrt{2} M \nu_{0\leftrightarrow 0})^{-1} \tau^{-1/2}, \quad (4)$$

where  $\sigma_y(\tau)$  is the square root of the Allan variance,  $\tau$  is the integration time, and  $M$  is a parameter given by

$$M = 2 \left[ \frac{I_{pb} + I_{pv}}{2I_{pb} + I_{pv}} \right] \frac{I_{pv}}{\sigma_I} \frac{B^{1/2}}{\Delta\nu}. \quad (5)$$

Here,  $\sigma_I$  is the standard deviation of the noise at the fringe peak and  $B$  is the noise bandwidth. In eq. (5),  $I_{pv}/\sigma_I$  can be considered as  $S/N$ .

If the intensity and the frequency fluctuations of diode lasers can be neglected, the  $S/N$  of microwave resonance signals is limited by the shot noise of the atomic beam, the atom-to-photon conversion noise, the photon-to-photoelectron conversion noise, the stray-light-added noise, and the photodiode noise. It is expressed as<sup>21)</sup>

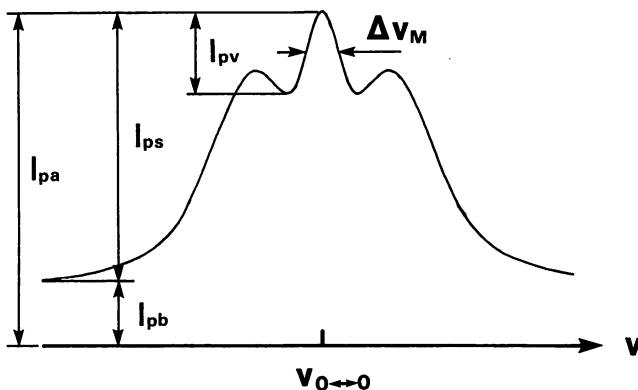


Fig. 13. A model of HERR spectral lineshape and definition of each parameter.

$$\left( \frac{S}{N} \right)^2 = \frac{(\bar{I}_a)^2}{2F(\bar{I}_a + \bar{I}'_s + F_A \bar{I}'_n)B}, \quad (6)$$

where  $\bar{I}_a$  is the atomic beam flux, and  $F$  is the noise factor of the particle conversion process and is given as

$$F = 1 + \frac{1}{\beta\gamma\eta}. \quad (7)$$

$\beta$  is the mean number of fluorescence photons emitted per atom,  $\gamma$  and  $\eta$  are the collection efficiency of fluorescence photons and the quantum efficiency of the photodetector, respectively. The quantum efficiency  $\eta$  of the photodiode for the 780 nm wavelength is 79.5%.  $\bar{I}'_s$  and  $\bar{I}'_n$  are the fictitious atomic fluxes equivalent to the effects of the stray-light-added noise and the photodiode internal noise, respectively, and are given by

$$\bar{I}'_s = \frac{\bar{I}_s}{\beta^2\gamma^2\eta + \beta\gamma}, \quad (8)$$

and

$$\bar{I}'_n = \frac{(P_n R)^2}{2e^2(\beta^2\gamma^2\eta^2 + \beta\gamma\eta)}. \quad (10)$$

Here,  $\bar{I}_s$  is the flux of the stray photons, which is estimated as  $\bar{I}_s = 1.2 \times 10^9$  ( $\text{s}^{-1}$ ) in the experimental situation.<sup>21)</sup>  $P_n$  and  $R$  are the noise equivalent power and the radiative sensitivity, respectively. In the present photodiode (Hamamatsu Photonics S2387-66R),  $P_n$  and  $R$  are  $2.2 \times 10^{-15}$  (W/Hz) and 0.5 (A/W), respectively.  $F_A$  is the noise factor of the amplifier used for current-voltage conversion of the photodiode detected signals. The practical value  $F_A = 4$  is used here.

The observed microwave resonance signals are considered to vary with the change of optical pumping efficiency for the initial state selection and for the signal detection. The efficiency of optical pumping is taken into account in the following. The fluorescence signal  $F_d$  is calculated as<sup>14)</sup>

$$F_d = \int_0^T \Gamma \sum_i n_{e1i} dt. \quad (11)$$

$\Gamma$  is the spontaneous emission decay rate and is given as the inverse of the lifetime in the excited state ( $\tau_p = 27$  (ns)).  $n_{e1i}$  is the temporal population of atoms in the excited state during the time  $dt$ . When the stray-light-added and the photodiode noises can be neglected,  $I_{pa}$  is the  $F_d$  of on-resonance for the microwave transition, while  $I_{pb}$  is the  $F_d$  of off-resonance.

The photon number emitted per atom  $\beta$  was figured out with the calculated values of  $I_{ps}$  and  $\Delta n$ . The optical power density  $P_{L\text{probe}}$  and the field spectral linewidth  $\Delta\nu_{L\text{probe}}$  of the laser (LD2 in Fig. 1) used for the signal detection were considered to be 10 (mW/cm<sup>2</sup>) and 20 (MHz), respectively. The interaction time for the detection was 3.3  $\mu\text{s}$ . The transition q ( $F=2-F'=3$ ):  $\sigma$ -polarized was chosen for the optical pumping with LD2. Thus,  $\beta = 6.6$  (photon/atom) was calculated using the relation

$$\beta = \frac{I_{ps}}{0.611\Delta n}, \quad (12)$$



where the factor 0.611 is the microwave transition rate of the HERR at the optimal condition.<sup>6)</sup>

As was discussed in §4.1, it was assumed that the state selection of atoms was carried out with nearly 100% efficiency by two-laser pumping. The  $S/N$  calculated from eq. (6) is  $1.8 \times 10^5$  (105 dB) in the noise bandwidth of 1 Hz. The transitions for the state selection were the transition t:  $\pi$ -polarized and the transition p:  $\pi$ -polarized. The values for the atomic flux  $\bar{I}_a$  and the collection efficiency  $\gamma$  were fixed to be  $1.5 \times 10^{11}$  (atom/s) and 15%,<sup>22)</sup> respectively, which were chosen for the experimental situation. Inserting  $I_{pv}=0.2I_{ps}$  and  $I_{pb}$  (obtained from eq. (11)) into eq. (4), the frequency stability

$$\sigma_y(\tau) = 7.8 \times 10^{-13} \tau^{-1/2} \quad (13)$$

was obtained where  $\Delta\nu_M = 2$  (kHz) was used.

Improvement of photodiode noise characteristics, increase in collection efficiency of fluorescence, and reduction of stray light achieve the ultimate frequency stability of this system, which is limited by the shot noise of the atomic beam. In this case,  $S/N$  reaches

$$\left(\frac{S}{N}\right)^2 = \frac{\bar{I}_a}{2B}. \quad (14)$$

With the same condition of optical pumping,  $S/N$  in the 1 Hz noise bandwidth is  $2.7 \times 10^5$  (109 dB). Then the frequency stability reaches

$$\sigma_y(\tau) = 3.9 \times 10^{-13} \tau^{-1/2}. \quad (15)$$

An additional method to improve the  $S/N$  for the frequency discrimination of microwaves is the reduction of the noise  $N$ , as described at the beginning of this section. Coherence characteristics of a diode laser are superior to those of a conventionally used rf Rb lamp. Introduction of center frequency stabilization of a laser reduced the fluctuation of its frequency. Considering the result of ref. 7, however, the residual frequency fluctuation of the pumping laser still causes the intensity noise of the microwave resonance signal of a clock, and about 20 dB of frequency (FM) noise should be reduced additionally. An FM noise reduction of a diode laser in the restricted bandwidth near a modulation frequency presents an idea. In a preliminary experiment of a diode laser-pumped Rb atomic clock, the improvement of  $S/N$  in the microwave resonance signals was examined with such an FM noise reduction of the pumping laser.<sup>6)</sup> That is, the frequency stability of an atomic clock was improved in accordance with the FM noise reduction of the laser. When such a partial FM noise reduction is employed with the center frequency stabilization of the pumping lasers, according to the discussion in ref. 6, it is possible to realize the microwave frequency stability shown in eq. (13) or (15).

## §5. Conclusions

In order to obtain a highly frequency-accurate Rb atomic clock, a diode laser-pumped Rb beam atomic clock was proposed. The novel microwave resonance method HERR was introduced in this clock. The microwave resonance signal characteristics similar to that of Ramsey resonance was obtained in a compact- and

stable-cavity system. The improvement of frequency accuracy in the novel atomic clock was confirmed.

Clock operation experiments in a preliminary setup of a novel Rb atomic clock were carried out. Characteristics of the HERR spectrum were examined as a practical candidate of the discriminator for the microwave frequency.

Frequency shifts observable in the system were estimated. The results are as follows:

1. Collisions of Rb atoms:  $3.0 \times 10^{-13}$ , at  $1.0 \times 10^{-9}$  Torr of vacuum.
2. Cavity pulling:  $1.0 \times 10^{-12}$ , at  $Q_c$  (cavity) = 1500 and  $Q_M$  (atomic resonance) = 6.8 (GHz)/3 (kHz) with 0.1 MHz of cavity resonant frequency detuning.
3. Combination of other resonance modes cavity-pulling:  $1.3 \times 10^{-13}$ , for TE<sub>212</sub> mode.
4. Misalignment of Rb atomic beam trajectory:  $1.6 \times 10^{-16}$ , at 10 mrad of misalignment.

Therefore, by using the present microwave resonance method, a frequency accuracy of  $1.4 \times 10^{-12}$  is expected. It is worth noting that the magnitude of frequency shift caused by cavity pulling, which limits the present accuracy, can be reduced to the value determined by the frequency tuning technique of cavity resonance.

An optical pumping scheme with diode lasers improves the microwave frequency stability of the Rb beam atomic clock. The following frequency stability was derived as the expected performance with the practical techniques:

$$\sigma_y(\tau) = 7.8 \times 10^{-13} \tau^{-1/2}.$$

As stated above, the frequency accuracy of a Rb atomic clock was investigated for the first time. Construction of a practical system for the present Rb beam atomic clock, which has a high-vacuum chamber, small stray light and high collection efficiency of fluorescence, will improve the frequency stability, and the time comparison as with Cs atomic clocks will reveal the high frequency-accuracy as seen in this work.

## Acknowledgements

The authors would like to thank Dr. K. Nakagiri and Mr. J. Umezumi of the Communication Research Laboratory for their valuable comments, and Mr. K. Chiba, Mr. H. Sumiyoshi and Mr. Y. Nakajima of Fujitsu, Ltd. for their support with the experiments. They also thank Dr. K. Nakagawa, Dr. C.-H. Shin, and Mr. H. Kusuzawa of their institute for their valuable discussions.

## References

- 1) M. Feldman, J. C. Bergquist and L. L. Lewis: *Proc. 35th Annu. Symp. Frequency Control* (IEEE, Ft. Monmouth, New Jersey, 1981) p. 625.
- 2) M. Hashimoto and M. Ohtsu: *IEEE J. Quantum Electron.* **QE-23** (1987) 446.
- 3) M. Hashimoto and M. Ohtsu: *J. Opt. Soc. Am. B* **6** (1989) 1777.
- 4) M. Hashimoto and M. Ohtsu: *IEEE Trans. Instrum. Meas.* **IM-39** (1990) 458.
- 5) H. Furuta, K. Nakagawa and M. Ohtsu: *Conf. Precision Electromagnetic Measurements (CPEM '90) Dig.* (IEEE, Ottawa, Canada, 1990) p. 428.
- 6) H. Furuta, H. Suzuki and M. Ohtsu: *Jpn. J. Appl. Phys.* **30** (1991) 596.
- 7) H. Furuta and M. Ohtsu: *Appl. Opt.* **28** (1989) 3737.

- 8) D. W. Allan: Proc. IEEE **54** (1966) 221.
- 9) M. Arditi and P. Cerez: IEEE Trans. Instrum. Meas. **IM-21** (1972) 391.
- 10) J. Vanier and C. Audoin: *The Quantum Physics of Atomic Frequency Standards*, Volumes 1&2 (Adam Hilger, Bristol and Philadelphia, 1989).
- 11) D. M. Lubman, C. T. Rettner and R. N. Zare: J. Phys. Chem. **86** (1982) 1129.
- 12) A. DeMarchi, R. E. Drullinger, and J. H. Shirley: *Proc. 44th Annu. Symp. Frequency Control* (IEEE, Baltimore, Maryland, 1990) p. 34.
- 13) R. E. Beehler and D. J. Glaze: IEEE Trans. Instrum. Meas. **IM-15** (1966) 48.
- 14) G. Avila, V. Giordano, V. Candelier, E. de Clerq, G. Theobald and P. Cerez: Phys. Rev. A **36** (1987) 3719.
- 15) M. Arditi, I. Hirano and P. Tougne: J. Phys. **D11** (1978) 2465.
- 16) M. Kourogi, C.-H. Shin and M. Ohtsu: IEEE Photon. Technol. Lett. **3** (1991) 496.
- 17) B. Dahmani, L. Hollberg and R. Drullinger: Opt. Lett. **12** (1987) 876.
- 18) C.-H. Shin and M. Ohtsu: Opt. Lett. **15** (1990) 1455.
- 19) V. Giordano, A. Hamel, G. Theobald, P. Cerez, C. Audoin and V. Candelier: Metrologia **25** (1988) 17.
- 20) R. F. Lacey, A. L. Helgesson and J. H. Holloway: Proc. IEEE **54** (1966) 170.
- 21) V. Giordano, V. Candelier, A. Hamel, C. Audoin, G. Theobald and P. Cerez: Opt. Commun. **67** (1988) 287.
- 22) N. Dimarcq, G. Theobald and P. Cerez: *Proc. 4th European Frequency and Time Forum* (Scientific Communities of Neuchatel and Besancon, Neuchatel, 1990) FS-04-2 p. 373.

# あなたの時計はいま何時？

大津元一

時間という特殊な量を正確に測る原子時計の性能が30年ぶりに飛躍的に向上した。その性能向上はさらに半導体レーザー時計にも及ぶ。これらの時計は基礎物理研究の手法をも変え得る強力な武器になりつつある。

「私の腕時計はきわめて正確である。なぜなら、“いつも”3分“進んでいる”からである。」この言葉の中に本稿で述べようとする内容が集約されている。つまり“いつも”というのはこの時計の時間の“安定度”が高いということである。さらに、“進んでいる”というのはこの時計が真の時刻を示さないこと、すなわち、“確度”が高くないということである。統計学や誤差論の分野で使われてる述語を用いると、安定度は偶然誤差、確度は系統誤差に相当する。以上の説明により安定度、確度の意味を理解していただけたならば、以下では「あなたの時計はいま何時？」の問いに正確に答えることができるような安定度、確度の高い時計をいかにして実現するか、さらにこれが何に使われるかについて述べることにしよう。

## 日時計から原子時計へ

古代の人類は天空の動き、日時計、砂時計などを使って時を計っていた。中世から近代にかけて機械工業が発達したが、同時に遠洋航海も盛んになり、1日に1秒くらいしか狂わない高性能な航海用時計が必要になった。この需要により精密な機械時計が発達した。20世紀に入ってからは電子技術の発達とともに時計も電子化され、さらに高性能な水晶時計が使われるようになった。

ここで時間のもつ特徴について簡単に触れておいた方がよいだろう。質量、温度、電圧、などの物理量と比較すると、時間は一定に保持することができない。すなわち時間は流れていて止めることができない。しかし、それを測定することは可能である。また、通常“時間”という言葉のもつ意味は二通

りである。第一は、定義された原点を基にした、時の流れの中での時間座標としての値で、これは“時刻”とよばれる。第二は、時計をストップウォッチとして使って測定を行う2時点の間隔である。天空の動き、日時計、は前者を測定するものであり、砂時計以降、ここで述べる原子時計は後者を測定するものといえる。とくに、本稿の後半で述べるような広い範囲にわたる応用が可能になってきたのは、原子時計によって後者の意味をもつ“時間”を正確に測る方法が発展したためである。

古賀逸策の先駆的な研究で知られる水晶時計とは水晶が一定の周波数の弾性振動をすることを利用して電子発振器をつくり、その発振周波数を分割して1ヘルツの出力信号を得、これによって時計の秒針を動かす装置である。これは高性能の発振器として基礎科学の研究の道具に、また、天体観測、人工衛星の制御と追尾、さらには通信・放送・計算機におけるクロックパルスの同期、などに広く使われている。

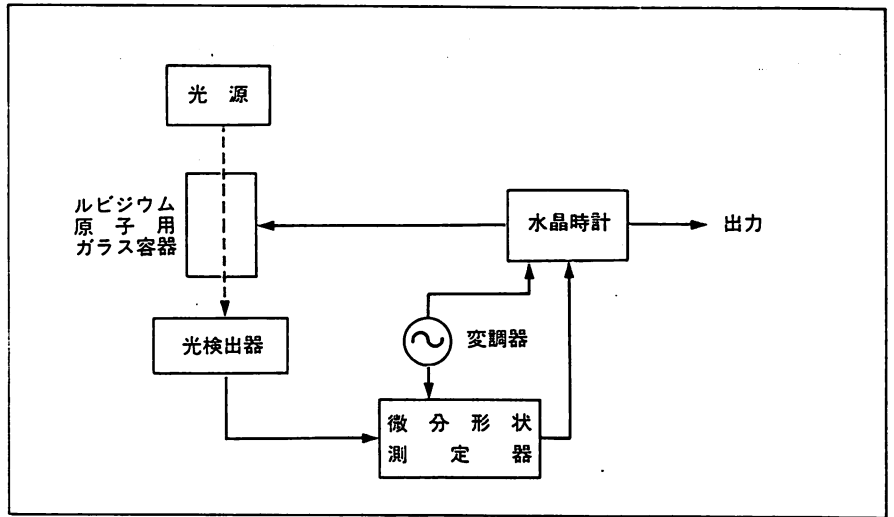
水晶時計は高い安定度をもつが、確度は低い。それは水晶の大きさ、形によって振動周波数が異なるからである。高い確度を得るために発明されたのが原子時計である。これは原子を構成する電子がその2つのエネルギー準位間を遷移することによって生じる電磁波を使うものである。遷移に関与する2つのエネルギー差  $E_a, E_b$  の差をプランクの定数  $h$  で割った値  $\nu_B (= (E_a - E_b)/h)$  がその電磁波の周波数に対応し、これは“ボーア周波数”とよばれている。これは原子構造によって決まる原子固有の値をとるので、これを使えば安定度、確度、ともに高い時

計が実現する。

### 受動形の原子時計

ここでは、私の研究グループが手がけた原子時計、すなわちルビジウム (Rb) 原子時計について概説する。〈図1〉に装置を示す。これは水晶時計の安定度を向上させるためにルビジウム原子を周波数基準として使っている装置であることに注意していただきたい。この理由によりルビジウム原子時計は“受動形原子時計”とよばれる。この装置では水晶のもつ1つの性質、すなわち、水晶に電圧を加えると弾性振動周波数がわずかに変わること、を利用する。一方、ルビジウム原子の最外殻電子のエネルギー準位を〈図2〉に示す。基底準位中の2つの超微細準位 ( $F=1, 2$ ) 間のボーア周波数は6.8ギガヘルツであり、これを周波数基準として利用する。つまり、水晶時計の周波数がルビジウム原子のボーア周波数に等しくなるように、水晶に加える電圧を制御する。

水晶に加える制御電圧を得るために2種類の電磁波とルビジウム原子との間の共鳴現象(二重共鳴とよばれる)を利用する。まず、水晶時計の出力信号をガラス容器中のルビジウム原子に加える。同時に、基底準位中の  $F=1$  準位と励起準位とのエネルギー差に相当するボーア周波数にほぼ等しい周波数をもつ電磁波をルビジウム原子に加える。このボーア周波数は385テラヘルツ(1テラヘルツ=1000ギガヘルツ)であるので、この電磁波とは波長780ナノメートルの光にほかならない。この光を吸収して励起準位に上げられた(光励起という)電子はすぐ基底準位中の  $F=1$  または  $2$  に落ちる。しかし、



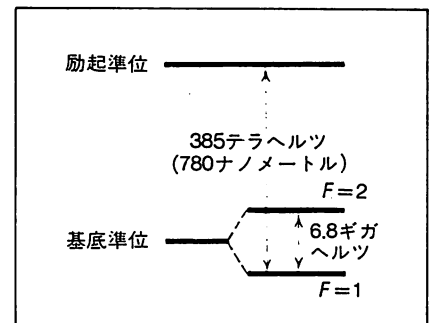
$F=1$  に落ちた電子数は再び光励起されるので、光励起によって基底準位中の  $F=1, 2$  の準位の電子数に著しい差が生じる。

ここで、 $F=1, 2$  の準位間のボーア周波数にほぼ等しいマイクロ波が水晶時計から加えられているので、 $F=1$  準位の電子はこのマイクロ波を吸収して  $F=2$  準位に遷移し、または  $F=2$  準位の電子はこのマイクロ波により刺激されて誘導放出により  $F=1$  準位に遷移する。これにより  $F=1$  準位の電子数が変化する。したがって、 $F=1$  準位から励起準位へ光励起される電子数が変化するので、ルビジウム原子を通り抜ける光のパワーが変化します。この変化量は水晶時計の周波数とボーア周波数6.8ギガヘルツとの差に比例するので、これを光検出器で測定すれば、検出器出力が上記の制御電圧となる。

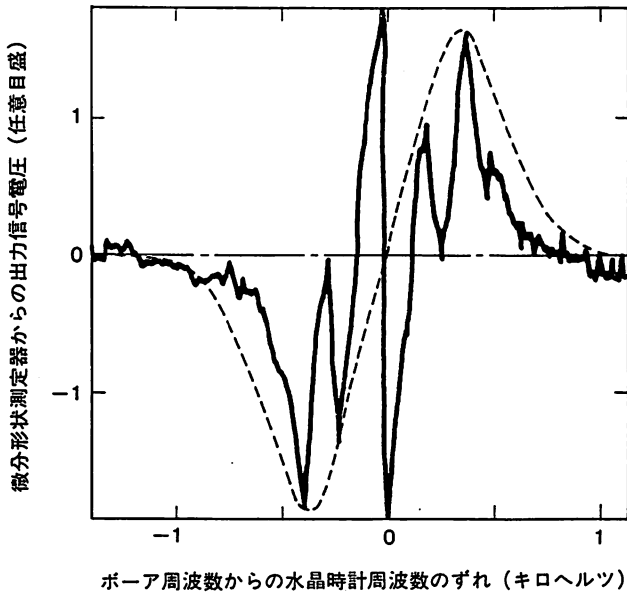
ルビジウム原子時計は構造が簡単、小型であるので実用的な原子時計として広く用いられてきた。周波数の安定度は  $1 \times 10^{-11} \sim 1 \times 10^{-13}$  に達している。すなわちこの時計が1秒狂うのに要する時間は3千年~30万年である。フランスのカストラー(Kastler)はこのような原子時計の基礎に関する研究で1966年にノーベル物理学賞を得ている。

一方、精度は水晶時計より良いがその正確な値はわかっていない。それは光励起用光源として単色性のない放電ランプを用いていること、ルビジウム

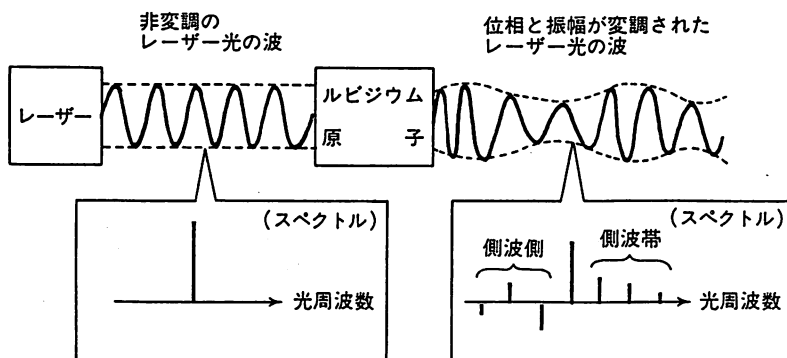
〈図1〉 ルビジウム (Rb) 原子時計の装置  
ルビジウム原子のスペクトルは水晶時計を安定化する周波数基準として用いられる。ガラス容器中のルビジウム原子を通過した光のパワーを検出する光検出器からの出力信号を微分形状測定器に加え、その出力を水晶時計の自動制御に使う。



〈図2〉 ルビジウム原子中の電子のエネルギー準位  
基底準位の  $F=1, 2$  準位間の遷移のボーア周波数を周波数基準に使う。波長780ナノメートルの光は  $F=1, 2$  の電子数に大きな差を与えるために使われる。



(a)



(b)

〈図3〉 (a)二重共鳴スペクトル形状の微分曲線

実線は半導体レーザーを用いて得られた結果。破線は放電ランプによる従来の結果。横軸はポーア周波数(6.8ギガヘルツ)からの水晶時計周波数のずれ。

(b)マイクロ周波数が変調されていることによるルビジウム原子通過後の光の変調の様子

変調された光は側波帯をもつ。

原子同士の衝突、ルビジウムとほかの原子との衝突、などにより精度の評価が困難なためである。

### レーザーを使ったルビジウム原子時計：飛躍的な進歩

光通信、衛星通信、高品位テレビ、これらを組み合わせた大容量情報伝送システムが実用化されつつある現在、さらに高性能のルビジウム原子時計が必要となってきた。この需要にこたえるために私の研究グループの橋本実、古田浩之は1984年より以下に述べるような新しい方法を試みた。

まず、安定度をさらに向上させるた

めに、放電ランプの代わりに半導体レーザーを使った。半導体レーザーの光は単色性が高く、また、半導体レーザーに流す電流を変えるとレーザー周波数も容易に変化するので、放電ランプに比べるとはるかに優れた光源である。これを使い、二重共鳴スペクトル形状の微分を測定すると〈図3a〉の実線に示すような特異な曲線が得られた。破線は放電ランプを使って得られた結果である。横軸は水晶時計からのマイクロ周波数とルビジウム原子のポーア周波数との差である。この微分を表す曲線はポーア周波数のところで横軸と交差するので、ポーア周波数を正確に見つけるのに適している。スペクトルの微分を得るためにはマイクロ周波数を1キロヘルツ程度の低周波で変調し、光検出器出力を微分形状測定器(位相敏感検波器ともよばれている\*)に加えればよい。図の縦軸はその出力値を表す。

実線で示されている特異な曲線は単色性のよいレーザー光を使った結果、マイクロ波からレーザー光への変調移乗が生じたために得られたものである。つまり、微分を測定するためにマイクロ波周波数を変調した結果、基底準位の  $F=1$  にいる電子数が変調され、その結果、ルビジウム原子を透過する光の位相と振幅が変調を受ける。変調された光は〈図3b〉下部のスペクトル図に示されるように非変調時の周波数のほかにいくつかの側波帯をもつ。このような複数の周波数をもつ光がルビジウム原子と相互作用するので側波帯間で互いに干渉が起こる。二重共鳴スペクトルの微分曲線上に現れた脈動はこの干渉を表している。この曲線はポーア周波数を横切るとき、破線

\*1 位相敏感検波器とは入力信号と参照信号とを入力すると、入力信号のうち参照信号周波数と同じ周波数をもつ成分のみを選択的に増幅する機能をもつ電子回路である。したがって、その出力には次に示すように微分曲線が得られる。すなわち、二重共鳴スペクトルの形状曲線を表す入力信号を  $V(f)$  とする。ここで、 $f$  は水晶時計の発振周波数である。この周波数を振幅  $\Delta f$ 、変調周波数  $f_m$  で変調すると、入力信号は  $V(f + \Delta f \cdot \cos(2\pi f_m t))$  となる。これは次のように級数展開される。

$V(f + \Delta f \cdot \cos(2\pi f_m t))$

$$= V(f) + \left(\frac{dV}{df}\right) \{\Delta f \cdot \cos(2\pi f_m t)\} - \frac{1}{2} \left(\frac{d^2V}{df^2}\right) \{\Delta f \cdot \cos(2\pi f_m t)\}^2 + \dots$$

したがって、位相敏感検波器出力は  $V(f)$  の微分  $dV/df$  に比例する。

よりはるかに急峻な傾きをもっているので、ポーア周波数をより正確に見つけることができる。したがって、この微分形状測定器出力は水晶時計の制御電圧として使うのにきわめて有利である。このように単色性の優れた光を使うことによってルビジウム原子を介したマイクロ波から光への変調移乗現象を観測し、かつ利用することができた。この結果、安定度は従来より10倍良くなった。

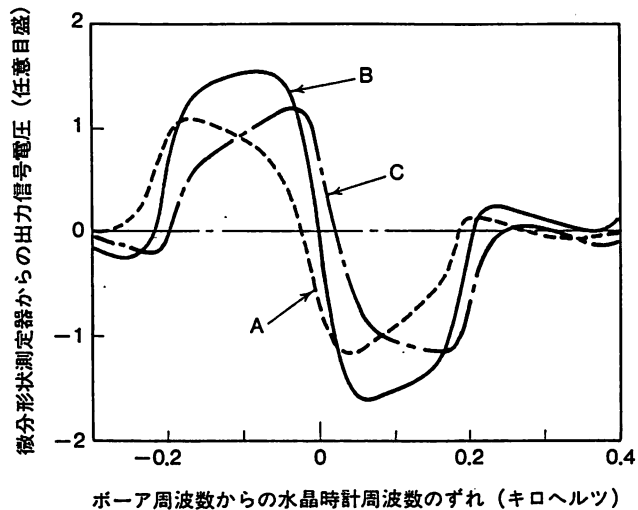
この微分測定の際に混入する最大の雑音は半導体レーザーの光の“周波数ゆらぎ”，および光検出器で光パワーを測定するときが発生する“量子雑音”，であることが見出された。そこで、半導体レーザーの電流を自動制御して光周波数揺らぎを非制御時の  $1 \times 10^{-4}$  以下の大きさまで抑圧することにより、光検出器の量子雑音のみで制限される安定度に達した。この安定度は従来のルビジウム原子時計の安定度より約1000倍良い。

ルビジウム原子に光を当てるとルビジウム原子固有のポーア周波数からわずかにずれた周波数をもつ原子時計になってしまう。このことは測定手段が測定対象の状態を乱してしまうことを意味する。なぜなら、光の高周波電界によってルビジウム原子のエネルギー準位がわずかにずれてしまうからである(交流シュタルク・シフトとよばれる)。そのずれに応じて<図4>に示すように二重共鳴スペクトルの形状も歪む。ずれの大きさは光のパワーと周波数に依存するので、光のパワーや周波数がゆらげば、ずれの量も変動する。このずれが精度を制限する主要因の1つである。それだけでなく、長い月日にわたり原子時計を動かせたときの安

定度も制限する。そこで、スペクトル形状の歪みを短時間のうちに測定して、この歪みがなくなるような特殊な自動制御を半導体レーザーに施す方法を考案した(これを自己同調法とよんでいる)。その結果、このずれの量を従来の1/40以下まで抑圧することができた。

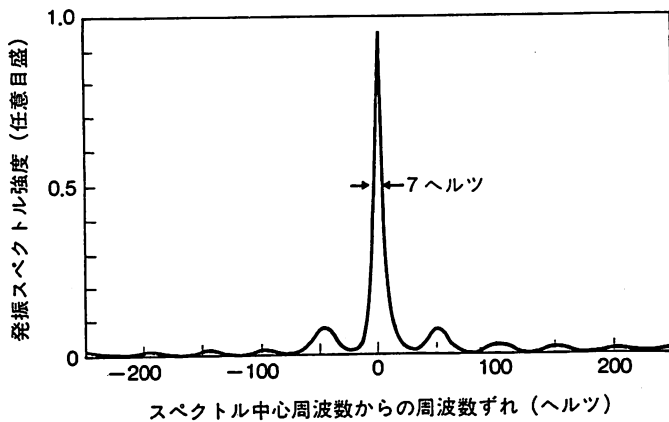
精度を制限するもう1つの要因は原子間の衝突である。衝突によりルビジウム原子のエネルギーが変化し、ポーア周波数もわずかにずれる。そこで、衝突を避けるためにガラス容器中のルビジウム原子を使うのではなく、高真空容器中でルビジウム原子を平行ビーム状に飛ばして使った。その結果、精度を向上させ、かつそれを定量的に評価できるようになり、 $1.3 \times 10^{-12}$  の値を得た。これは衝突のない真のルビジウム原子のポーア周波数の値からわずかに0.009ヘルツしかずれていないことを意味する。

この研究では半導体レーザーのもつ優れた単色性、制御性を積極的に利用



<図4> レーザー周波数の値によって変形したルビジウム原子の二重共鳴スペクトル形状

<図3a>の実線と同様の曲線の中心部分を拡大したものの。曲線A, B, Cはレーザー周波数が<図2>の基底準位、励起準位間のエネルギー差に対応するポーア周波数385テラヘルツからおのおの+1.2キガヘルツ, 0ヘルツ, -1.2キガヘルツずれた場合の測定結果。曲線A, Cの形が歪んでおり、中心で横軸と交差するマイクロ周波数もずれていることがわかる。



〈図5〉 自動制御された半導体レーザーの発振スペクトル形状

横軸はスペクトルの中心周波数 361 テラヘルツ (波長 830 ナノメートルに相当)からの周波数のずれを表す。このスペクトルの幅は安定度を表す尺度の1つであり、ここでは世界のトップデータ、7ヘルツ、が得られている。これは自動制御しない場合の安定度に比べ、10万倍良いことに対応する。

し、きわて高い性能を得た。以上のような安定度、確度の飛躍的な向上は過去30年にわたって得られなかったが、半導体レーザーの性能向上などにより今回実現した。実現の背景には高度情報化社会からの需要の高まりがある。

### ■ 時計としてのレーザー

受動形原子時計からさらに発展させて、原子から発生する電磁波自身を使って発振器をつくれれば高性能の時計が期待できる。これは“能動形原子時計”とよばれるが、この電磁波がマイクロ波であればメーザー、光であればレーザーにはかならない。ここでは時計としてのレーザーについて概説する。

実は市販のレーザーは必ずしも高性能の時計としては使えない。それは周波数の安定度、確度が上記の受動形原子時計をしのぐほど高くないからである。そこで、〈図1〉のように水晶時計を自動制御するのと同様の装置が必要となる。つまり、〈図1〉中の水晶時計をレーザーと見なした場合、ルビジウム原子に対応する周波数基準として、メタン、ヨウ素、カルシウムなどの原子、分子が使われている。これらの原子、分子のスペクトル形状の幅ができるだけ細いものを使えば、ボーア周波数を高精度で見つけられるので高い確度を実現するために有利である。このために最近では、レーザー冷却、光糖蜜、イオントラップ、などの新しい手法が活発に研究されている(これらの手法

についてはパリティ別冊 No.8 光科学を参照)。

### ■ スーパー共振器の使用

さて、安定度のみが非常に高いレーザー時計が必要な場合には上記の原子、分子の代わりに鏡を2枚向き合わせた光共振器、すなわちファブリーペロー共振器の共振周波数を周波数基準として使うこともできる。この共振周波数は共振器の長さによって決まるが、熱膨張係数の小さい材料を使って2枚の鏡を強固に保持する治具をつくれれば高い安定度が得られる。最近では反射率が99.999997%以上の鏡を使ったファブリーペロー共振器が実現しており、“スーパー共振器”ともよばれている。鏡の反射率が高いので共振スペクトルの幅は原子、分子のスペクトルの幅よりも狭い場合がある。米国国立標準局のホール(Hall)らはこれを使い、気体レーザーの一種であるヘリウムネオンレーザーの周波数を自動制御し、 $1 \times 10^{-16}$ よりよい安定度を得ている。すなわち、このレーザー時計が1秒任うのに要する時間は約3億年以上である。

最近では、原子物理学から工業的応用まで広く使われている半導体レーザーを時計として使うために、私の研究グループの久保木勝彦、申哲浩、興梠元伸が1983年以降周波数の自動制御を試み、優れた性能を実現した。〈図5〉はファブリーペロー共振器を周波数基準として使って得られた半導体レーザーの発振スペクトル形状を示す。発振スペクトルの幅の値は安定度を表す尺度の1つであり、レーザーの単色性の高さを表すとも考えられる。この図に示す幅の値、7ヘルツ、は世界のトップデータである。自動制御をしないとこ

の幅の値は約1メガヘルツなので安定度が約10万倍向上したことになる。自動制御システムの性能向上により近い将来約0.001ヘルツの幅が実現すると予測されている。

### 限りなく増大する需要

次世代の通信、放送などのシステムには安定度と精度の高い原子時計が必須装置である。一方、基礎科学分野ではきわめて多くの応用がある。まず、相対論効果の実測である。たとえば原子時計をジェット機に搭載し、東まわりで世界1周した後、地上の原子時計と時刻比較すると、約59ナノ秒の遅れが観測された。

遠く離れた2地点で宇宙遠方にある電波星または人工衛星から送られてくる電波を受信し、その受信時刻差を測定すれば2地点間の距離が精密に測定できる。この測定のためには原子時計が不可欠である。この測定装置は超長基線電波干渉計(VLBI: Very Long Baseline Interferometer)とよばれ、たとえば日本列島の位置が刻一刻動していることを測定するのに使われている。年間数センチメートルの地殻変動、数10センチメートルの地球潮汐の影響を知ることができ、海洋性地震などの長期的地震予知に役立つ。このVLBIで電波を受信するとき、太陽の付近を通過した電波は屈折する。このような相対論効果はVLBIで測定可能であり、また正確な距離測定にはこの相対論効果を補正する必要があることもわかっている。

安定度の高いレーザーの光で干渉計をつくり、空間の均一性についてマイケルソン-モーレーの実験、さらにまた、重力波検出の試みがなされている

が、これらも相対論効果の検証にはほかならない。これらの相対論効果は従来は天文現象を利用して測定されていたが、原子時計、とくにレーザーを使うと地上の実験室でも可能となる。すなわち、実験室で模擬宇宙が実現する。

原子物理学の研究でも原子時計が必須装置として活用されている。原子を構成している粒子、すなわち電子、陽子、中性子間の弱い相互作用の存在が電弱理論によって予言されており、この存在を検証するために従来、加速器を用いた大がかりな高エネルギー実験装置が使われていた。しかし、周波数の自動制御されたレーザーを用いた分光測定装置によっても実験的検証が可能であることがわかってきた。すなわち、弱い相互作用により原子の波動関数のパリティ保存が成立しなくなるので、これにより誘起される微弱な光学的遷移をこのレーザーによって測定する。最近では自動制御された半導体レーザーを用いて鉛原子の磁気双極子遷移スペクトルを測定し、そのさいパリティ非保存によって誘起される光の偏光状態変化を精密に測定した例がある。このほか、原子核の研究にも自動制御された半導体レーザーが使われはじめている。すなわち、実験室で高エネルギー実験が実現する。

さらに、私の研究グループでは自動制御された半導体レーザーを、蔣曙東の開発した“フォトン走査トンネル顕微鏡”とよばれる超高倍率顕微鏡システムと組み合わせ、原子1個ずつを捕獲、操作する“原子ピンセット”をつくり、単原子結晶成長、単原子メモリーを実現することを試みている。

### もっと光を！

安定度、精度の高い原子時計、レーザー時計は単に時間を正確に測定する発振器、ストップウォッチ、としてのみでなく、前節で述べたように極限的な新科学技術分野を実現するための突破口を鋭く切り開くメスとして使われる。その結果、これらの新分野が開発されると、これらの時計の自動制御のための新しい周波基準も見出され、安定度、精度がさらに向上する。すなわち、これらの時計の研究と極限的な新科学技術研究とは車の両輪をなす関係にある。

宇宙の誕生の瞬間からマイクロ波、光は宇宙に満ち満ちているので、これを利用しない手はないだろう。とくにレーザーを時計と捉えて悠久の時の流れを研究し利用するのは魅力的である。冒頭で述べたように、時間とは特殊な量であって、これについて議論するには物理学のみではなく哲学や生物学、さらに心理学的な観点をも必要とする。過去にニュートン、ベルグソン(Bergson)、アインシュタイン、渡辺慧らが時間について論じており、いまだに議論のつきない深遠な興味深い問題である。

一方、デモクリトスの主張以来、物質の基本構成要素の探求の結果として原子が研究・利用された結果、原子からマイクロ波、レーザー光が発生し、高精度の時計が実現した。さらに進んで、最近ではマイクロ波、光を使って新しい物質を創生する試みが活発化している。

すなわち、現在は光と物質の統合的研究・応用の黎明期である。今後の発展に必要なのはより高性能の時計であ



る。いままさに「もっと光を！ もっと時計を！」の声が高まっている。

本原稿の準備に際し、有益なご意見を賜った職業訓練大学校寺町康昌教授に深く感謝致します。

参考文献

- 1) P. Kartaschoff: *Frequency and Time*, Academic Press, (1978) (和訳として, 福與人八、大浦宣徳、倉持内武: 時と周波数, 講談社, 1980).
- 2) 大津元一: レーザーと原子時計, オーム社

(1986).

- 3) 大津元一: コヒーレント光量子工学, 朝倉書店(1990).
- 4) C. -H. Shin and M. Ohtsu: *Opt. Lett.*, 15, No. 24, 1455 (1990).
- 5) 蔣曙東, 富田直幸, 大津元一: *光学*, 20, No. 3, 134 (1991).
- 6) Ch. Salomon and J. L. Hall: *Journal of Optical Society of America B*, 5, No.8, 1576 (1988).
- 7) バリティ別冊 No.8 光科学(1991).
- 8) アンリ・ベルクソン(平井啓之訳): *ベルクソン全集 I, 時間と自由*, 白水社(1965).
- 9) 渡辺慧: *時間の歴史—物理学を貫くもの—*,

東京図書(1973).

- 10) R. Morris; *Time's Arrows: Scientific Attitudes Toward Time*, Simon and Schuster, New York (1984) (和訳として, 荒井喬: *時間の矢*, 地人書館, 1987).

# The Passive Ring Resonator Fiber Optic Gyro Using Modulatable Highly Coherent Laser Diode Module

Tohru Imai, Ken-ichi Nishide,

Hideo Ochi\*, Motoichi Ohtsu\*

Tokyo Aircraft Instrument  
Co.,Ltd, Komae city, Tokyo  
201, Japan

\*Tokyo Institute of Technology,  
Yokohama city, kanagawa  
227, Japan

## ABSTRACT

For the light source of the passive ring resonator fiber optic gyro (RFOG), we have developed 1.3  $\mu\text{m}$  highly coherent laser diode module (HCLDM) using resonant optical feedback from a compact hemispherical reference cavity. The HCLDM had the 100 KHz linewidth and was frequency-modulated by directly modulating the injection current. A FM spectroscopy technique was employed for the rotation sensing. The resolution of the present RFOG system was estimated to be  $0.9 \times \tau^{-1/2}$  (deg./hour) (where  $\tau$  is the integration time of measurement) from the signal-to-noise ratio of the demodulated signal.

## 1. INTRODUCTION

Various types of fiber optic gyros (FOG's) based on the Sagnac effect have been developed for rotation sensing<sup>1-3</sup>. Among them, a passive ring resonator fiber optic gyro (RFOG) is advantageous because of its high sensitivity. However, the RFOG requires a high-coherence light source as well as a high finesse ring resonator. A laser diode (LD) possessing highly efficient direct FM capability is a useful light source for RFOG because the power consumption is low and the volume of the gyro system can be reduced<sup>4</sup>. However, a solitary LD does not have a sufficiently narrow spectral linewidth for the RFOG, and has a large magnitude of FM noise which seriously deteriorate the gyro sensitivity. Thus, in the early stage of the works on RFOG<sup>5</sup>, a He-Ne laser was used to achieve the sensitivity as high as 0.5 deg./hour.

In this paper, we describe a light source and a rotation rate measurement technique. For the light source of RFOG, we have developed a highly coherent laser diode module (HCLDM) with the 100 kHz linewidth using the optical feedback from a hemispherical reference cavity. We employed a FM spectroscopy technique in order that the system was free from the IM noise of the LD.

## 2. DEVELOPMENT OF HCLDM

For the light source of the RFOG, a LD should meet the following requirements:

High coherence ; the linewidth must be narrower than 100 kHz<sup>4</sup>.

Stability ; laser frequency must be free from the effects of ambient temperature variations and mechanical vibrations.

Modulation capability ; the optical frequency must be controlled and modulated by varying the injection current.

The conventional methods of improving coherence by optical feedback from an external reflector have several problems, i.e., they could induce chaotic instabilities and external cavity modes, by which it is difficult to maintain the coherence very high for a long time and to modulate lasing frequency. In order to solve these problems, we employed the optical feedback from an external reference cavity<sup>6</sup>.

## 2.1 Structure of a HCLDM

A HCLDM employed optical feedback from a compact hemispherical reference cavity<sup>6</sup>. Figure 1 shows the structure of the HCLDM for which a 1.3  $\mu\text{m}$  wavelength DFB-LD was used. The hemispherical cavity was made of BK7 glass and its diameter was 10 mm, which corresponded to the free spectral range of 10 GHz. The reflectivity of the two surfaces was 90 %, and the measured value of the finesse was 10. The backward output radiation from the temperature-controlled LD was coupled off-axis with the hemispherical cavity via a collimator lens, a mirror attached to PZT, and a mode-matching lens. This cavity acted as an optical bandpass filter and, thus, the laser light was spectrally purified. All the elements were installed on a Super-Invar plate.

Since the light built-up in the cavity returns to the LD, the lasing frequency is locked to the resonance frequency of this cavity. Thus, the field spectral linewidth becomes very narrow and the center frequency of the field spectrum is also stabilized. Under this optical self-locking condition, we observed the resonance spectral profile of the cavity by sweeping the injection current of the LD. By this observation, it was found that frequency locking range of the HCLDM was about 4.5 GHz which depended on the feedback optical power.

It should be noted that the strict phase coincidence between the feedback and emitted lights is not required in the present optical feedback scheme because of its optical self-locking nature. Although the phase could be controlled by varying the voltage applied to the PZT attached to the mirror, the optical feedback was maintained very stable by the present module for a more than 5 hours without controlling the PZT voltage. This is because the total system of the HCLDM was made very compact.

## 2.2 Performances of HCLDM

Figure 3 shows the field spectral profile of the HCLDM which was measured by the delayed self-heterodyne method. The linewidth of about 100 kHz was obtained, which was 2,000 times narrower than that of the free-running laser. Among several HCLDM's fabricated in the present study, the narrowest linewidth was 25

kHz.

Figure 4 shows the magnitude of the reduced FM noise achieved by the HCLDM<sup>8</sup>, which was calculated by using numerical values for the presently fabricated HCLDM system. It is found that the FM noise reduction ratio was 30 dB, which agreed with the experimental results within the Fourier frequency range lower than 400 MHz. It is also seen from this figure that the peak of the FM noise at the relaxation oscillation frequency was reduced because the feedback bandwidth, limited by the free spectral range of the cavity, was larger than this frequency.

The direct FM efficiency of the HCLDM was measured to be 100 MHz/mA and 10 MHz/mA at the modulation frequency of 100 Hz and 10 MHz, respectively. Although, these values were 1/15 times that of the free-running LD, they were sufficiently large for the application to the present RFOG system. As is shown by Fig. 5, the HCLDM has the volume of 216 cc and was operated in a stable manner without applying the phase-control-feedback even though the ambient temperature varied from 20°C to 30°C.

### 3. FIBER RING RESONATOR

Figure 6 shows the transfer functions of the transmission-mode and reflection-mode Fabry-Perot interferometer<sup>9</sup>. Since the transfer function of the reflection-mode has a wider bandwidth and a smaller phase change than that of the transmission-mode, it is advantageous to design a wide-band negative electrical feedback loop to track the resonance frequency to the laser frequency. In addition, by considering the loss of the resonator, this mode is also advantageous because its throughput is larger than that of the transmission-mode. Based on these characteristics, the reflection-mode was employed for the RFOG system.

We fabricated a fiber ring resonator shown in Fig. 7 by using a polarization-maintaining fiber of 4.7 m long ( free spectral range is about 44 MHz ). The value of the finesse was calculated to be 50 by considering the values of the coupling ratio and excess loss in the coupler, and of the loss of the fiber itself.

At the splice point in the resonator, the principle axes of the fiber were rotated by an angle of 90 degree with respect to each other<sup>10,11</sup>. As will be shown in Fig. 9, two polarizers were installed in front of the input-output fiber ends to produce the same polarization as the incident light and to prevent the other eigenstate of polarization induced by 90 degree rotation in the resonator.

### 4. FM SPECTROSCOPY TECHNIQUE

When the optical carrier frequency  $\nu_c (= \omega_c / 2\pi)$  is modulated by modulation frequency  $f_m (= \omega_m / 2\pi)$  with a maximum frequency deviation of  $\Delta \omega / 2\pi$ , the instantaneous angular frequency  $\omega$  is given by

$$\omega = \omega_c + \Delta \omega * \cos \omega_m t \quad (1)$$

The electric field of light is expressed as

$$E_m(t) = \exp(j\omega t + m \sin \omega_m t)$$

$$= \sum_{n=-\infty}^{\infty} J_n(m) \exp(j\omega t + jn\omega_m t) \quad (2)$$

where  $m$  is the modulation index ( $= \Delta \omega / \omega_m$ ).

The transfer function of the reflection-mode of the resonator, normalized to  $\Delta \nu / 2$  and  $\Delta \nu$  is the FWHM, is given by

$$R(f) = \frac{j(\nu_0 - f)}{1 + j(\nu_0 - f)}, \quad (3)$$

where  $\nu_0$  is the resonance frequency and  $f$  is the detuning from the resonance frequency. By noting that the amplitudes of the sidebands higher than the 3rd order is negligibly small for  $m = 1$ , the electric field emitted from the resonator is expressed as

$$E_s(t) = \sum_{n=-2}^{+1} J_n(m) \frac{j(f + nf_m)}{1 + j(f + nf_m)} \exp(j\omega t + jn\omega_m t). \quad (4)$$

Detecting this electric field by a photo detector, the output signal from the detector, possessing the frequency  $\omega_m / 2\pi$ , is given by

$$I_s = \frac{2 * J_n * J_{n+1}}{[1 + (f + nf_m)^2] * [1 + (f + (n+1)f_m)^2]}$$

$$* \left( \begin{array}{l} [(f + nf_m)^2 * (f + (n+1)f_m)^2 + (f + nf_m) * (f + (n+1)f_m)] * \cos \omega_m t \\ - [(f + nf_m)^2 * (f + (n+1)f_m) - (f + nf_m) * (f + (n+1)f_m)^2] * \sin \omega_m t \end{array} \right). \quad (5)$$

As is shown by Fig. 8, the spectral profile of the quadrature component in this expression represents the dispersive shape, which can be used as a frequency discriminator to lock the laser frequency to the resonant frequency of the fiber resonator. To improve the accuracy of calculation, the sidebands up to the ninth components were taken into account, by which it was found that the maximum slope of the dispersive shape is achieved when

$$FSR/2 > f_m > 2.5 * \Delta \nu \quad \text{and} \quad m = 1.08. \quad (6)$$

Figure 8 shows the spectral profiles of the in-phase and quadrature components of the photo detector output by using these values of the parameters. As has been popularly known<sup>12,13</sup>, the FM spectroscopy technique has several advantages, e.g., the effects of the FM and IM noises of the light source can be reduced by using a high modulation frequency, wide bandwidth of the

system can be realized, and so on. By these advantages, this technique is promising to achieve a very high sensitivity of the RFOG.

## 5. GYRO SYSTEM

Figure 9 shows a block diagram of the present RFOG system. After the laser light from the HCLDM passed through a 60 dB optical isolator, it was splitted into the two beams by the fiber coupler C1. An E/O modulator (EOM) was used to modulate the phase of the one beam in order to improve the bias stability by suppressing the optical carrier frequency component under the appropriate rf voltage applied to the EOM.

The output beams from the fiber resonator, i.e. a sensing loop, were detected by photo detectors PD1 and PD2. Double balanced mixers DBM1 and DBM2 were used to extract the quadrature component of the demodulated output signals from PD1 and PD2. The output from the DBM1 was used to lock the laser frequency to the fiber resonator by controlling the injection current of LD, and that from the DBM2 was used as the output signal from the gyro system to measure the rotation rate.

Figure 10 shows the profile of the quadrature component from the photo detector PD1 measured by fixing  $f_m = 5$  MHz and  $m = 1.0$ , which agreed with the optimum condition given by eq.(6). To estimate the sensitivity of the RFOG, the S/N value of the demodulated signal from the DBM1 was measured. Figure 11 shows the measured result by the rf spectrum analyzer with the resolution bandwidth of 3 KHz. The peak at the center of this figure represents the demodulated signal. From this figure, it is found that  $S/N = 38$  dB, which means that the  $S/N = 55$  dB under the unity bandwidth of the spectrum analyzer. By using this value of the S/N, residual tracking error of the laser to the resonance frequency of the fiber resonator, was derived from a formula<sup>14</sup>

$$\delta \nu (\tau) = \frac{0.11 * \Delta \nu}{(S/N)} * \tau^{-1/2} = 0.35 * \tau^{-1/2} \text{ (Hz)}, \quad (7)$$

where  $\delta \nu (\tau)$  and  $\tau$  represents the square root of the Allan variance and the integration time of measurement, respectively. Thus, the sensitivity of the RFOG, limited by the tracking error of the laser frequency was estimated by using eq.(7) as

$$\Omega_{\min} = \delta \nu (\tau) * \frac{\lambda}{2R} = 0.9 * \tau^{-1/2} \text{ (deg./hour)}, \quad (8)$$

where the wavelength ( $\lambda$ ) of LD was  $1.3 \mu\text{m}$  and the diameter ( $2R$ ) of the fiber resonator was fixed to be 10 cm. This value shows that it should be possible to measure earth rotation in the integration time of less than 1 sec.

For reference, The shot noise limited tracking error of the laser frequency was estimated as

$$\delta \nu_s(\tau) = \frac{e \{1 - E J_0^2(m)\} \Delta \nu^2}{8 I^2 J_0^2(m) J_1^2(m) E^2} \tau^{-1/2}$$

$$= 5.6 \times 10^{-5} \tau^{-1/2} \quad (\text{Hz}), \quad (9)$$

where E is the throughput of the reflection-mode of the ring resonator, I is the dc photo current, and e is the electron charge. By this value, the shot noise limited sensitivity of the RFOG is estimated to be  $1.5 \times 10^{-4} \tau^{-1/2}$ , which means that the present system is promising to achieve a very high sensitivity of rotation sensing. It should be noted that the FM spectroscopy technique is promising for achieving the shot noise limit, because the system is free from the effect of the IM noise of the light sources. Based on this property, it can be expected that the sensitivity as high as given by eq.(9) can be achieved in the near future, by improving the performances of the servo-control circuits of the present system.

## 6. CONCLUSION

We have developed the coherent light source, HCLDM, with the linewidth of 100 KHz and used it in the RFOG system. Among the two modes of the fiber resonator, the reflection-mode was preferred. The sensitivity of the RFOG system was estimated to be  $0.9 \tau^{-1/2}$  (deg./hour) by the evaluation of the S/N value of the demodulated signal, which was obtained by employing the FM sideband locking technique. The shot noise limited sensitivity was estimated as  $1.5 \times 10^{-4} \tau^{-1/2}$  (deg./hour).

## 7. ACKNOWLEDGMENTS

We would like to thank K. Nakahama, the head of R&D department of Tokyo Aircraft Instruments Co. Ltd. for his encouragement, K. Nakagawa, C.-H. Shin, M. Kurogi, and W. Wang of Tokyo Institute of Technology for their valuable discussions.

## 8. REFERENCES

- 1.S.Ezekiel and H.J.Arditty, "Fiber-optic rotation sensors," MIT Conference Proceedings on Fiber-Optic Rotation Sensors 1981.
- 2.B.Culshaw, I.P.Giles, "Journal of Physics E: Scientific Instruments, Vol.16(1), pp5-15, 1983.
- 3.R.A.Bergh, H.C.Lefevre and H.J.Shaw, "An overview of fiber-optic gyroscopes," Journal of Lightwave Technology, Vol.LT-2(2), pp91-107, 1984.
- 4.M.Ohtsu and S.Araki, "Using a 1.5- $\mu$ m DFB InGaAsP laser in a passive ring cavitytype fiber gyroscope," Applied Optics, Vol.26, No.3, pp464-470, 1987.
- 5.R.E.Meyer and S.Ezekiel, "Passive fiber-optic ring resonator for rotation sensing," Optics Letters, Vol.8(12), pp644-646, 1983.
- 6.B.Dahmani, L.Hollberg and R.Drullinger, Optics Letters,

Vol.12(11), pp876-878, 1987.

7.L.Hollberg and M.Ohtsu, "Modulatable narrow-linewidth semiconductor lasers," *Appl.Phys.Lett.*53(11), pp944-946, 1988.

8.T.Imai, K.Nishide, C.H.Shin and M.Ohtsu, "High coherent laser diode module with  $1.3\mu\text{m}$  DFB-LD," 38th Spring meeting, Jpn. Soc. of Appl. Phys, 1991.

9.M.Ohtsu, M.Murata and M.Kouroggi, "FM Noise Reduction and Subkilohertz Linewidth of an AlGaAs Laser by Negative Electrical Feedback," *IEEE Journal of Quantum Electronics*, Vol.26, No.2, pp231-241, 1990

10.G.A.Sanders, R.B.Smith and G.F.Rouse, "Novel polarization-rotating fiber resonator for rotation sensing applications," in *Proc. SPIE OE/FIBERS '89*, Boston, USA, 1989, paper 1169-74.

11.K.Takiguchi and K.Hotate, "Manner to Reduce the Bias of Optical Passive Ring-resonator Gyro Caused by the Misalignment of the Polarization Axis in the Resonator (II)," Technical report of IEICE, Jpn, OQE89-137, pp19-24, 1989.

12.R.Carrol, C.D.Coccoli, D.Cardarelli, G.T.Coate, "The Passive Resonator Fiber Optic Gyro and Comparison to the Interferometer Fiber Gyro," *Proc.SPIE* Vol.719, pp169-177, 1986.

13.W.Lenth, "High Frequency Heterodyne Spectroscopy with Current-Modulated Diode Lasers," *IEEE Journal of Quantum Electronics*, Vol.QE-20, NO.9, pp1045-1050, 1984.

14.J.Vanier and L.Bernier, "On the Signal-to-Noise Ratio and Short-Term Stability of Passive Rubidium Frequency Standards," *IEEE Trans. Instrum. and Meas.* Vol.IM-30, No.4, pp277-282, 1981.

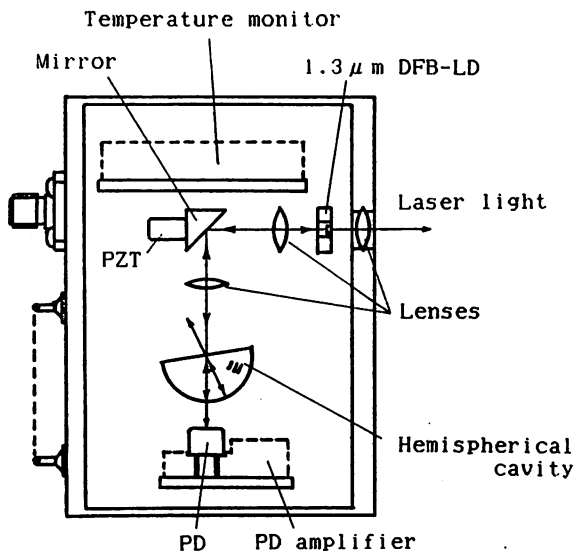


Fig. 1 Structure of HCLDM.

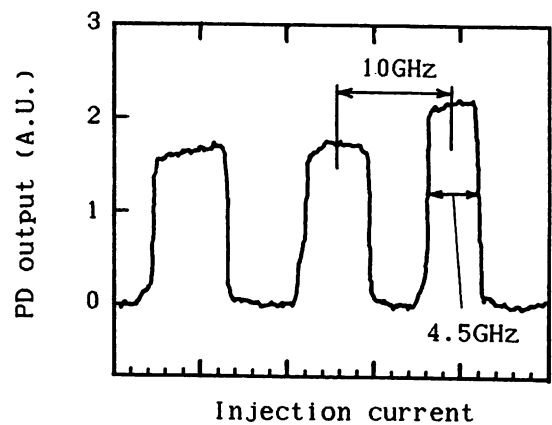


Fig. 2 Spectral profile of the hemispherical reference cavity measured as a function of the injection current of the LD under optical feedback condition.



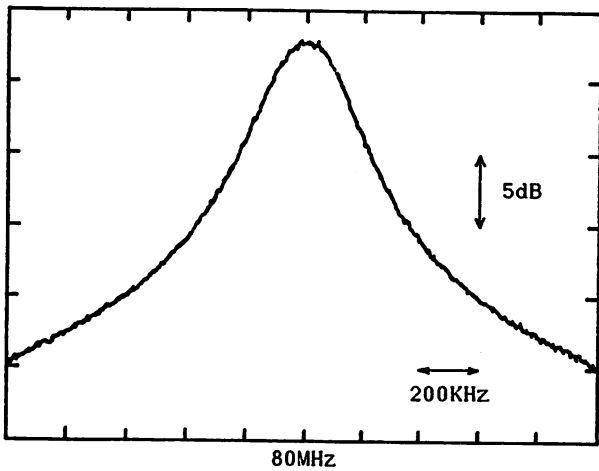


Fig. 3 Field spectral profile of the HCLDM under optical feedback condition measured by the delayed self-heterodyne method with the optical fiber of 2 km long.

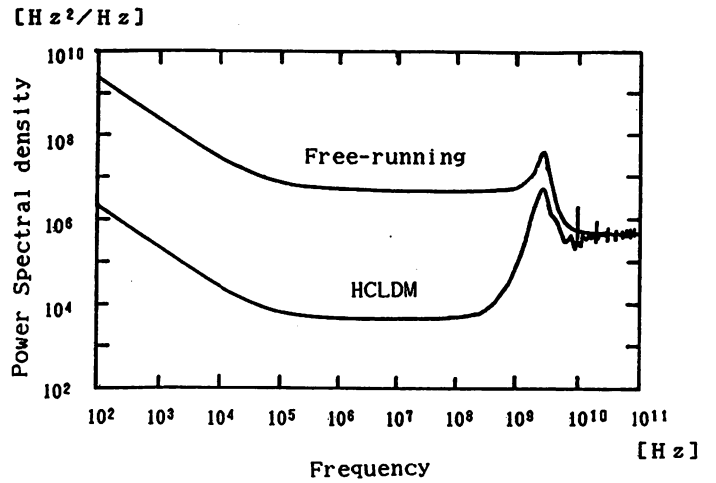


Fig. 4 Calculated results of the power spectral densities of the FM noise of the free-running LD and HCLDM.

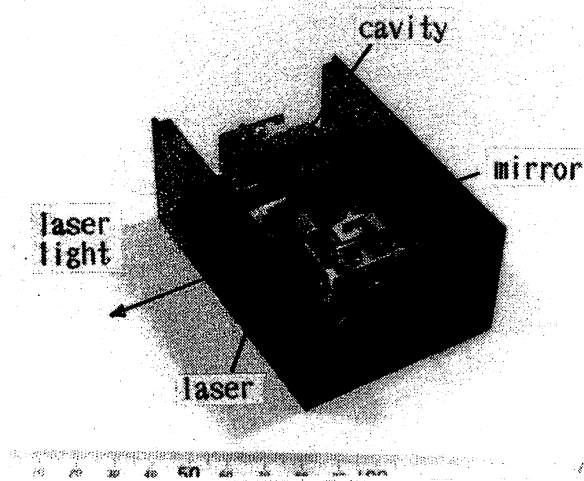


Fig. 5 Photograph of the HCLDM. The dimension was 90 mm(L), 60mm(W), and 40 mm(H).

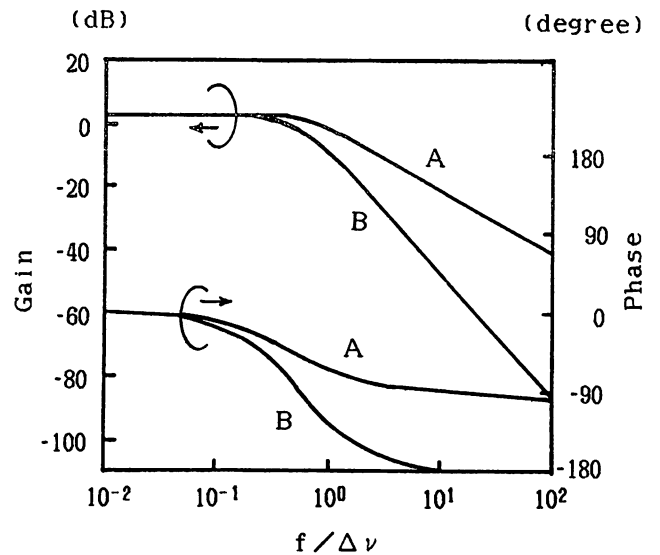


Fig. 6 Calculated transfer functions of a Fabry-Perot interferometer. Curves A and B represents the results for the reflection-mode and transmission-mode, respectively.

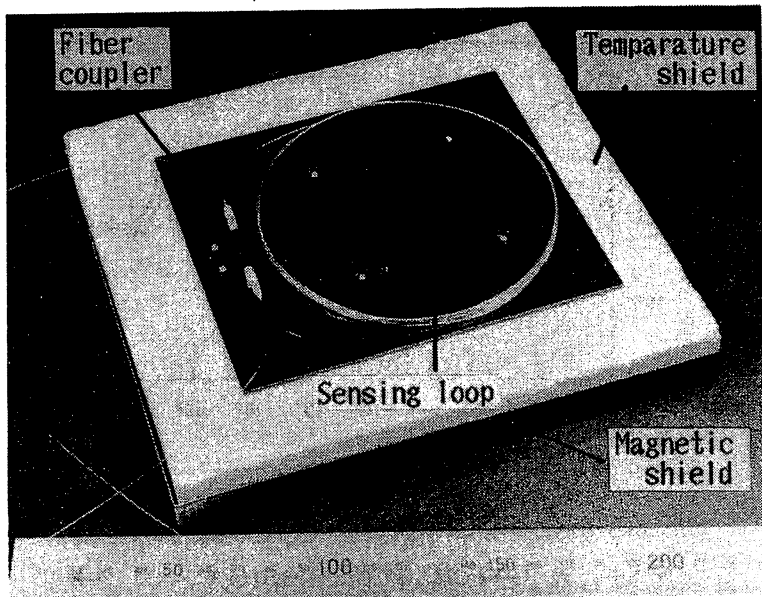


Fig. 7 Photograph of the fiber ring resonator with a PANDA fiber of 4.7m long. Its free-spectral range and finesse were 44 MHz and 50, respectively.

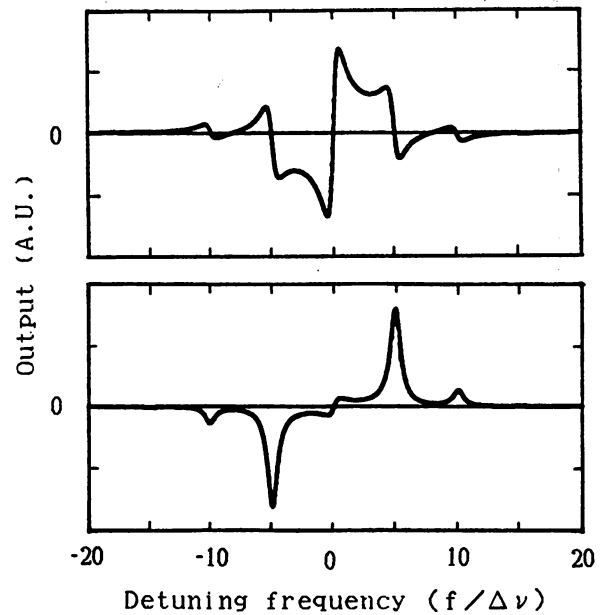


Fig. 8 Calculated spectral profile of demodulated signal from the fiber ring cavity. The upper and lower traces represents the in-phase and quadrature component, respectively.

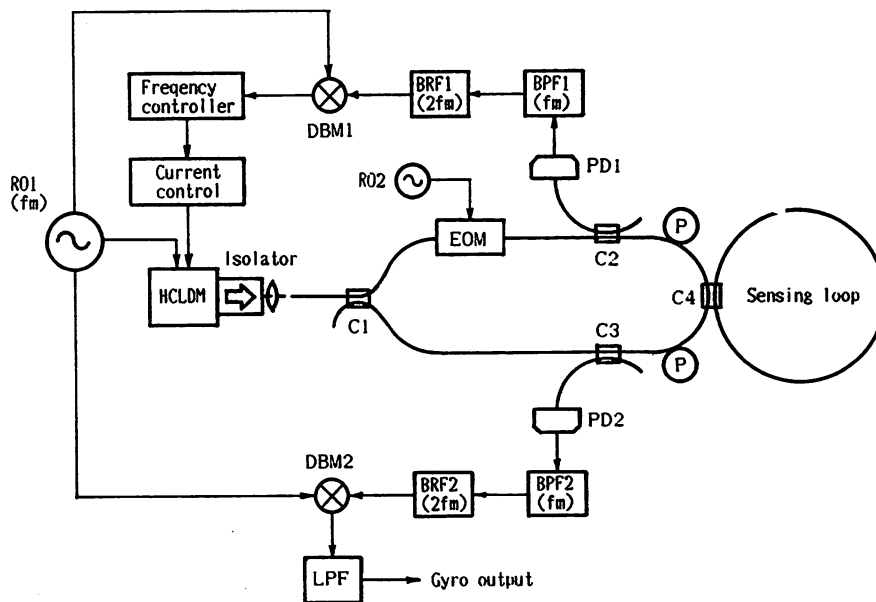


Fig. 9 Experimental setup of the RFOG using the FM spectroscopy technique.  
 C1-C4: Fiber couplers. P: Polarizer. BPF: Bandpass filter. BRF: Band rejection filter. LPF: Low pass filter. DBM1, DBM2: Double balanced mixers. R01, R02: rf oscillators. PD1, PD2: Photo detectors. EOM: E/O modulator.

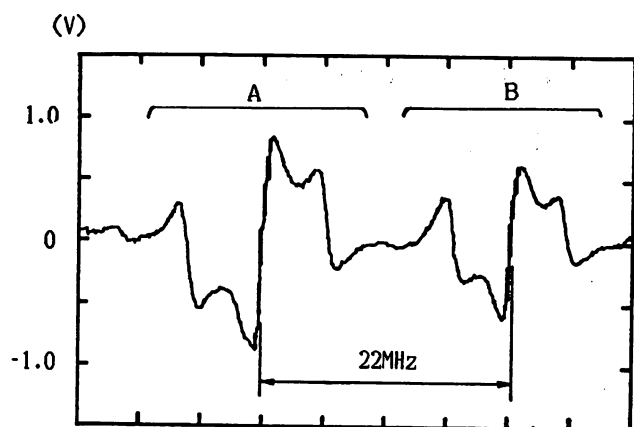


Fig. 10 Measured spectral profiles of the in-phase component of the demodulated signal. The modulation frequency and index were fixed to be 5 MHz and 1.0, respectively. A: For the main polarization mode of the fiber. B: For the quadrature polarization mode of the fiber.

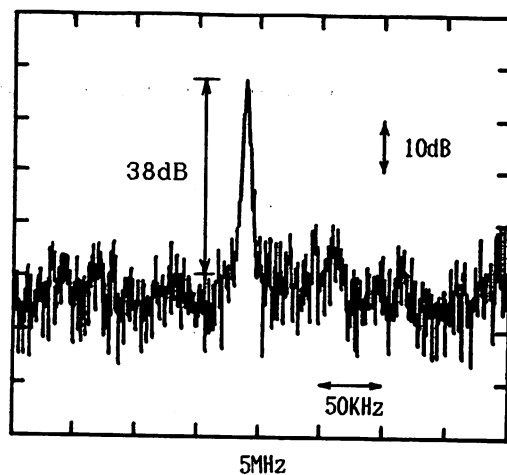


Fig. 11 CRT display trace of the rf spectrum analyzer observed to estimate the S/N value of the demodulated signal, where  $f_m$  and resolution bandwidth were 5 MHz and 3 kHz, respectively.

## A Photon Scanning Tunneling Microscope Using an AlGaAs Laser

Shudong JIANG, Naoyuki TOMITA, Hisao OHSAWA<sup>1</sup>  
and Motoichi OHTSU

*Graduate School at Nagatsuta, Tokyo Institute of Technology,  
4259 Nagatsuta, Midori-ku, Yokohama, 227*

*<sup>1</sup>Nikon Corporation, Nishi-Ohi 1-Chome, Shinagawa-ku, Tokyo 140*

(Received May 9, 1991; accepted for publication July 20, 1991)

A novel super-resolution photon scanning tunneling microscope (PSTM) using diode lasers and optical fibers was demonstrated to measure the samples with submicron structure in a noncontact and nondestructive manner. A reproducible method for fabrication of the fiber probe with the tip curvature radius of 80 nm is reported. The step with the height of 9 nm, optical disk with submicron-sized pits similar to moth-eye structure, and latex particles with 80 nm in diameter have been observed. To the best of our knowledge, this is the smallest particle size resolved by the PSTM.

**KEYWORDS:** optical microscope, nm-resolution, near-field, tunneling photon, evanescent wave, sub-micron aperture, diode laser, fiber probe

### §1. Introduction

In recent years, the remarkable progress in biochemistry and semiconductor device fabrication has made the development of noncontact, nondestructive microscopy with high resolution necessary. The photon scanning tunneling microscope (PSTM), which combines the advantages of both a conventional optical microscope and a scanning tunneling microscope, has received much attention. There are two kinds of PSTM (also known as the near-field scanning optical microscope (NSOM)) with the ability to circumvent the diffraction limit which have been reported by several research groups. For example, One type known as NSOM, forces incident light through a submicron-sized aperture and obtains the submicron resolution.<sup>1-3)</sup> However, even in the ideal case, it has been proven that the total flux transmitted by a small aperture is proportional to  $a^{-4}$  ( $a$  is the radius of aperture).<sup>4)</sup> As a result, a high-power laser, photon counting, and prolonged integration time of measurement had to be used in the system, but the improvements in resolution and sensitivity are still below the expectations. Another type, known as PSTM, uses a probe with a submicron-sized aperture at one end to detect the evanescent field modified by the sample surface.<sup>5-8)</sup> However, the use of the bulky gaslaser, which is the only form reported hitherto, makes the PSTM more cumbersome than the compact STM, and the technical difficulty in fabrication of the probe, which is the key component in lateral resolution determination, prevents high resolution being achieved.

In this paper, we report a novel PSTM system<sup>9)</sup> in which the diode lasers can be directly high-speed-modulated to make the system more compact ( $25 \times 20 \times 12 \text{ cm}^3$ ) and reduce the measuring time. In experiments, a step of 9 nm in height, a moth-eye structure optical disk with submicron sized pits, and latex particles with the diameter of 80 nm were successfully resolved. This is the smallest particle size resolved by PSTM to the best of our knowledge. The reproducible fabrication of a very sharp fiber probe with a tip radius of curvature of

80 nm is also reported.

### §2. Experimental

It is well known that when a laser beam is incident to a boundary between two homogeneous media of different refractive indices under the condition of internal total reflection, an evanescent field is generated within the range  $z < \lambda$ , where  $z$  is the normal distance from the boundary. When the light wave is treated as photons, the evanescent field generation can be regarded as a tunneling effect in which the photons cross the boundary of the potential barrier. The height of the potential barrier which confines the photons is determined by the difference between the refractive indices of the two media. A high normal resolution may be expected because the observation probability of the tunneling photons decreases exponentially with increasing as the distance. On the other hand, when the field of the photon is destructively measured by an probe with a aperture smaller than the wavelength, the accuracy of measurement of the photon momentum can be expressed as<sup>1)</sup>

$$\Delta p = \hbar k \cdot (\Delta \lambda / \lambda) = h/a \quad (1)$$

where  $\hbar = h/2\pi$ ,  $h$  is the Planck constant,  $k$  is the wave number of the light and  $a$  is the aperture diameter. According to the Heisenberg uncertainty principle, the minimum uncertainty of the position measurement of the photons is determined by the aperture and becomes

$$\Delta x = a/2\pi \quad (2)$$

From eq. (2), it can be understood that the lateral resolution is higher than the diffraction limitation, and is only dependent on the aperture diameter.

Figure 1 shows the schematic diagram of the presently proposed PSTM. The light source is a 30 mW AlGaAs diode laser with the wavelength of 780 nm (LT024MD, TOSHIBA). As the beam is incident to the surface of the prism on which the sample is set under the total internal reflection condition, the evanescent field is generated. Such a field, depending on the topography of the sample, is picked up by a fiber probe which has a subwavelength

aperture at one end, and is detected by a photomultiplier (R928, HAMAMATSU) using synchronous phase-sensitive detection. Scanning is realized in the monolithic high-precision wide-range translation condition<sup>10)</sup> by a multicomponent parallel spring on which the prism is set,

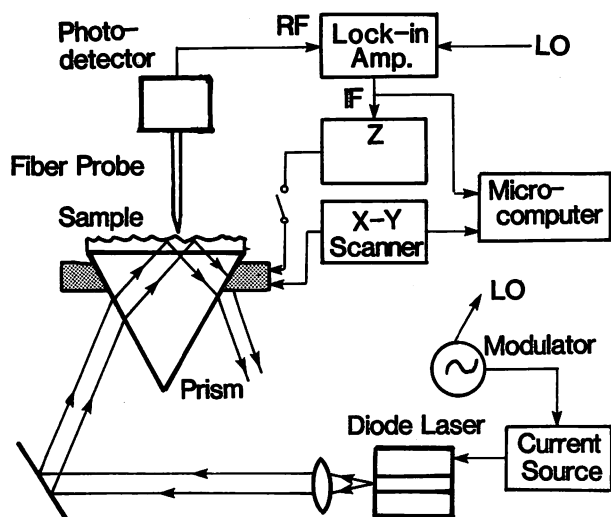


Fig. 1. The setup of our PSTM. Power of the diode laser is 30 mW.

and the scanning scope is  $15 \mu\text{m} \times 15 \mu\text{m}$  laterally and  $5 \mu\text{m}$  normally. The probe is driven close to the sample in the  $z$  direction by the piezoelectric device on which the fiber probe is mounted.

Reproducibility of a very sharp fiber probe is indispensable to fabrication of the submicron sized aperture for the high lateral resolution. A single-mode optical fiber of 800 nm wave-length processed by a selective etching technique using ammonium-fluoride-buffered hydrofluoric acid is used to fabricate the probe. The diameters of core and cladding are  $5 \mu\text{m}$  and  $125 \mu\text{m}$  respectively. Because of the difference in the  $\text{GeO}_2$  doping concentration, the etching rate of the cladding in this buffered solution is higher than that of the core, and so the fiber end becomes conical. The base of the fabricated cone is equal to the core cross section, and the height and the curvature radius of the tip end can be adjusted by varying the etching time, the concentration of hydrofluoric acid, and the solution temperature. From the results of a series of measurements, the optimum etching solution was found to consist of 1 part 50% hydrofluoric acid buffered in 3 parts of 40% ammonium fluoride and 1 part of water. Figure 2 shows SEM images of various probe end sharpness versus etching time. The ingredient ratio of the solution is  $\text{NH}_4\text{F}:\text{HF}:\text{H}_2\text{O}=3:1:1$

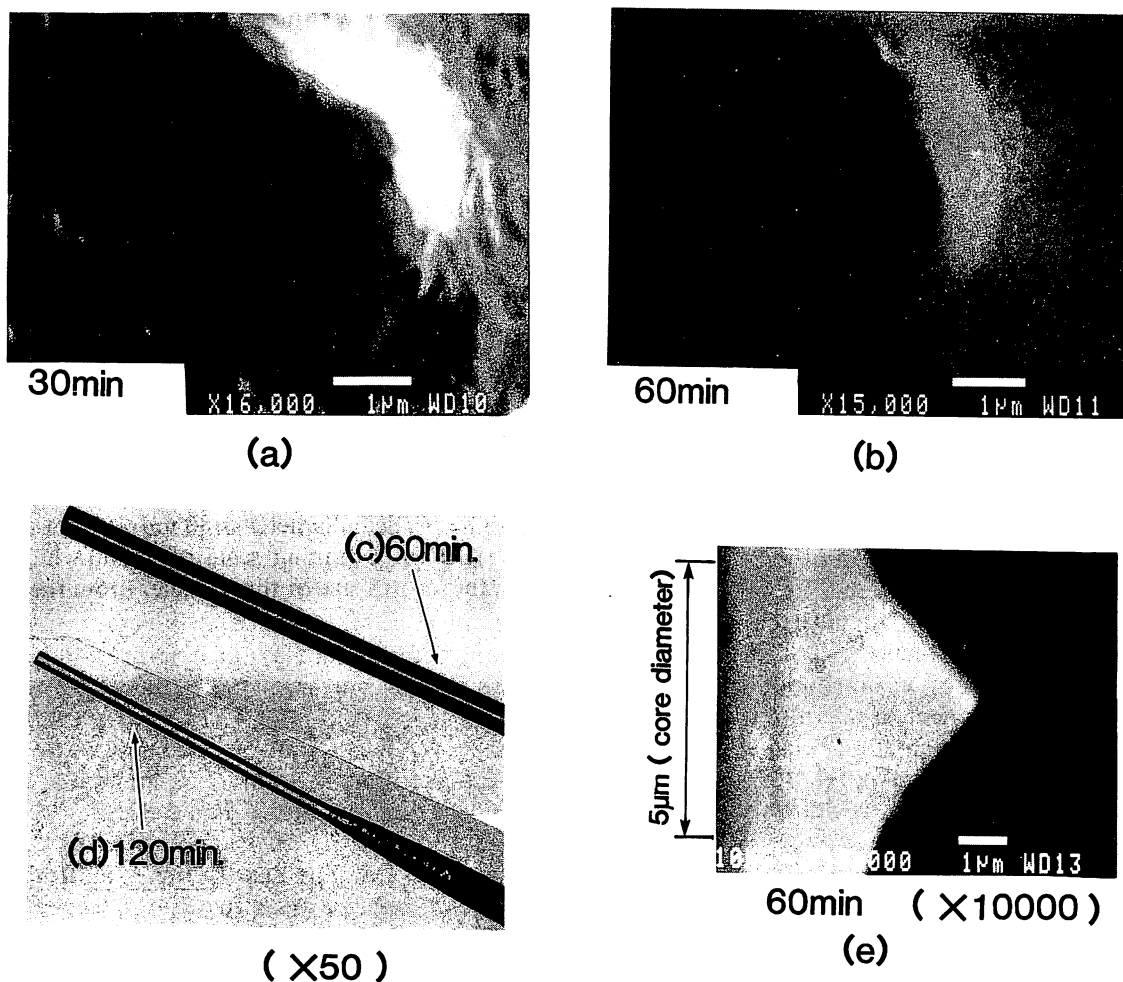


Fig. 2. SEM images of the probe end sharpness versus etching time. The diameters of core and cladding are  $5 \mu\text{m}$  and  $125 \mu\text{m}$ , respectively. The ingredient ratio of the solution is  $\text{NH}_4\text{F}:\text{HF}:\text{H}_2\text{O}=3:1:1$ . The etching time is (a) 30 min, (b), (c) and (e) 60 min, and (d) 120 min.

and etching times are 30 min, 60 min, and 120 min, respectively. Comparing Fig. 2(a) and Fig. 2(b), we can see that in the case of 30 min., the end of the fiber is still trapezoidal, but in the case of 60 min, the end of the fiber becomes conical. With longer etching (e.g., 120 min, see the comparison between Fig. 2(c) and Fig. 2(d)), the radius of curvature of the top is rarely changed further, but the etching of the cladding along the fiber still occurs, and this increases the undesired scattering of light from the side of the fiber and impairs the signal-to-noise ratio (SNR). Using this ingredient ratio, the optimal etching time is about 60 min. Figure 2(e) shows the SEM image, with the magnification of  $1.8 \times 10^4$ , of the probe top in this optimum case. The curvature radius is estimated as 80 nm by measuring the geometrical profiles of the SEM images of a number of fiber probes which are fabricated by the same method. As far as we know this is the smallest fiber probe tip in PSTM. Experiments<sup>11</sup> also indicate that smaller curvature of the fiber end can be fabricated by further optimizing the ingredient ratio of the solution.

### §3. Results and discussion

As the evanescent field decays exponentially in the  $z$  direction, the sharpened fiber tip can also be considered as an effective aperture. The fiber probe, shown in Fig. 2(e), which is used in the experiment described later, is only sharpened without making aperture. From the results of the experiment, the effective aperture radius is estimated to be nearly the same order of curvature radius as the fiber tip. In the experiments, all of the observations are in the height-constant condition, i.e., the  $z$  direction open feedback, and the height of the fiber probe remains constant during the scanning.

The first experiment demonstrated the decay of the evanescent field for various sample-tip separations. The incidence angle of the laser beam is  $45^\circ$ , and the separation is changed by the PZT voltage. From the results

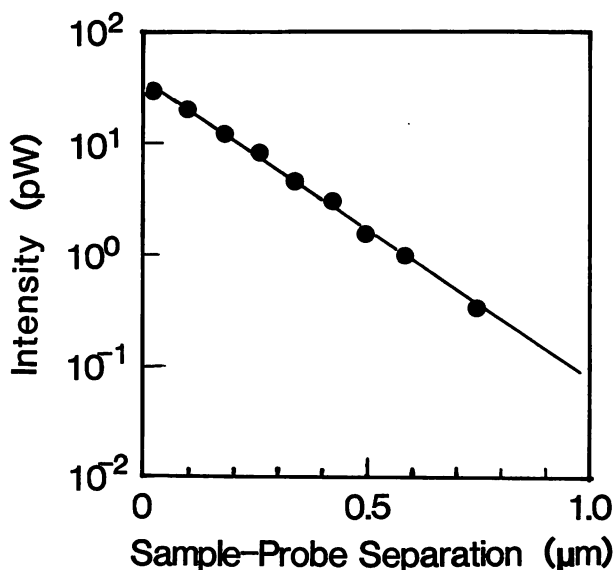


Fig. 3. Decay of evanescent field with separation variation between sample and tip. The dots are measured values.

shown in Fig. 3, we can see that the intensity of the evanescent wave decays exponentially with the increases separation between sample and tip, and the maximum pick-up power is 30 pW.

An example of the high normal resolution of our PSTM is given in Fig. 4. The sample under test is a prism with half its surface coated by a  $\text{SiO}_2$  thin film with a thickness of 9 nm. The time constant  $T$  of the phase-sensitive detection is 12.5 ms and the modulation frequency of the diode laser is 5 kHz. The edge of the film was observed, and the scanning range was  $7 \mu\text{m} \times 12 \mu\text{m}$ . From Fig. 4, it can be seen that because a step as thin as 9 nm is resolvable, the detailed information on the local structure of the edge of the coating can be obtained; this could not be obtained by other microscopes such as the laser interferometric microscopes. Furthermore, higher normal resolution also can be expected by increasing  $T$ , because the detected white noise magnitude is proportional to  $1/T^{-1/2}$ .

Proof of our ability to obtain information over a wide range with the shorter measurement time of our PSTM is given in Fig. 5, which shows the measured results of the optical disk with submicron sized pits similar to the moth-eye structure. Figure 5(a) shows the SEM image of such a disk. The pitch of the gratinglike profile used for laser beam tracking is  $1.4 \mu\text{m}$ , and the diameter of the pit is about 300 nm. Figure 5(b), (c) and (d) display the PSTM images with different scanning ranges of  $5.5 \times 4.5 \mu\text{m}$ ,  $2.8 \times 2.0 \mu\text{m}$ , and  $1.4 \times 1.0 \mu\text{m}$ , respectively. The pits correspond to the blue holes in the color photograph (Fig. 5(c)). From (b), the pitches of the grating are found to be  $1.4 \mu\text{m}$  from the full scanning scale of  $5.5 \mu\text{m}$ , and the diameter of the pit is 280 nm, estimated from the full scanning scale of  $2 \mu\text{m}$ . Since the submicron structures on the CD surface lead to scattering and produce serious background noise in the pick-up signal, the fluctuating profile besides the pits in the figure can be regarded as the result of such noise.

Figure 6 shows the measured results of latex particles of 80 nm diameter. However, the latex particles were distributed on the prism, as is explained schematically by Fig. 6(a). The measured image is shown in Fig. 6(b). The scanning area is  $1 \mu\text{m} \times 1 \mu\text{m}$ , and the time constant is 4 ms. The particle diameter is 80 nm–100 nm as estimated from the full scanning scale of  $1 \mu\text{m}$ , which coincides with the known size of the particle. From these results, it

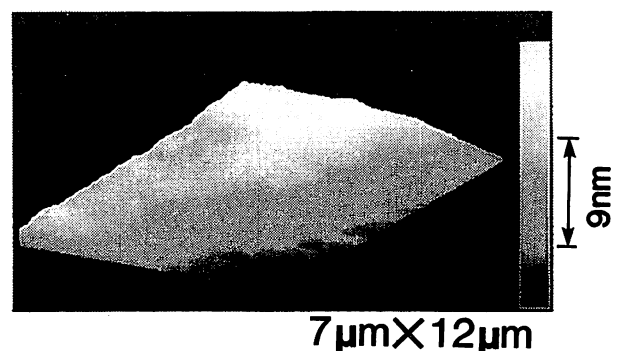


Fig. 4. The image of a 9 nm step height.

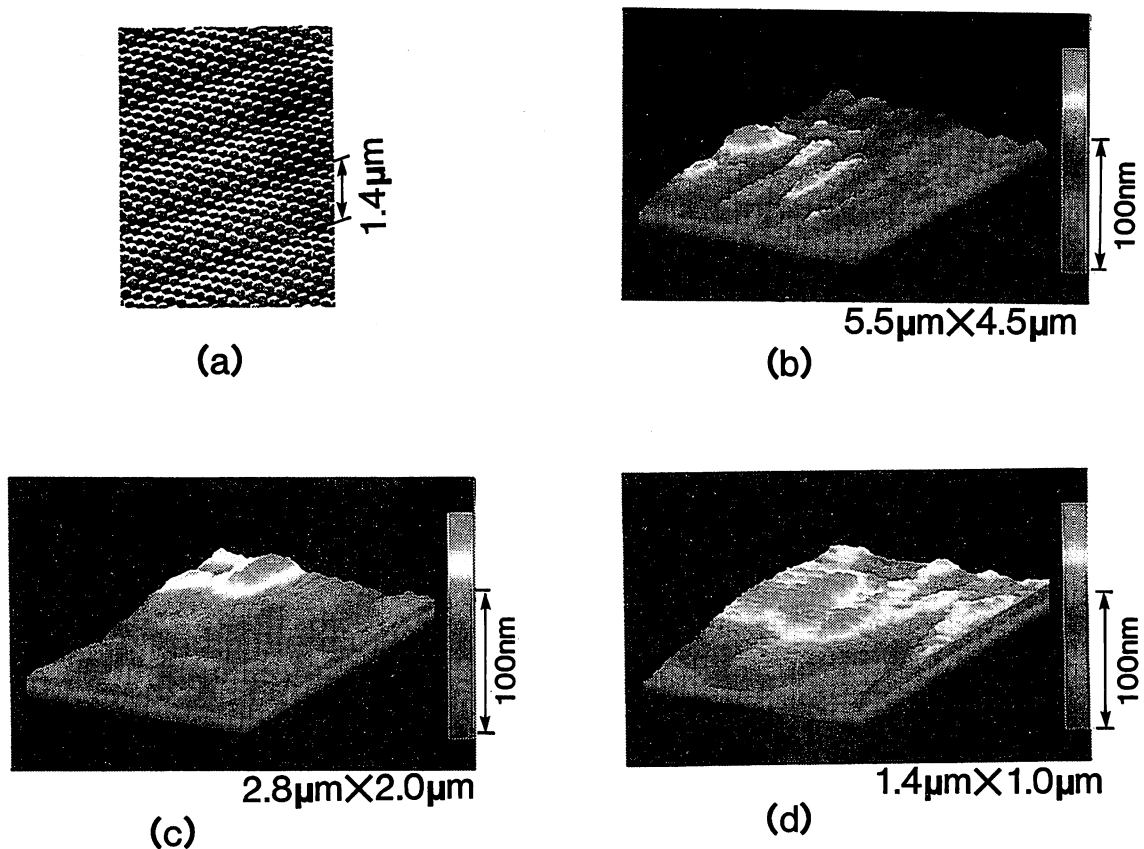


Fig. 5. The measured results of the optical disk with submicron sized pits similar to moth-eye structure. (a) The SEM image of such a disk. The pitch of the gratinglike profile is  $1.4 \mu\text{m}$ , and the diameter of the pit is about  $300 \text{ nm}$ . (b) (c) and (d) The PSTM images with different scaling ranges:  $5.5 \times 4.5 \mu\text{m}$ ,  $2.8 \times 2.0 \mu\text{m}$  and  $1.4 \times 1.0 \mu\text{m}$ , respectively.

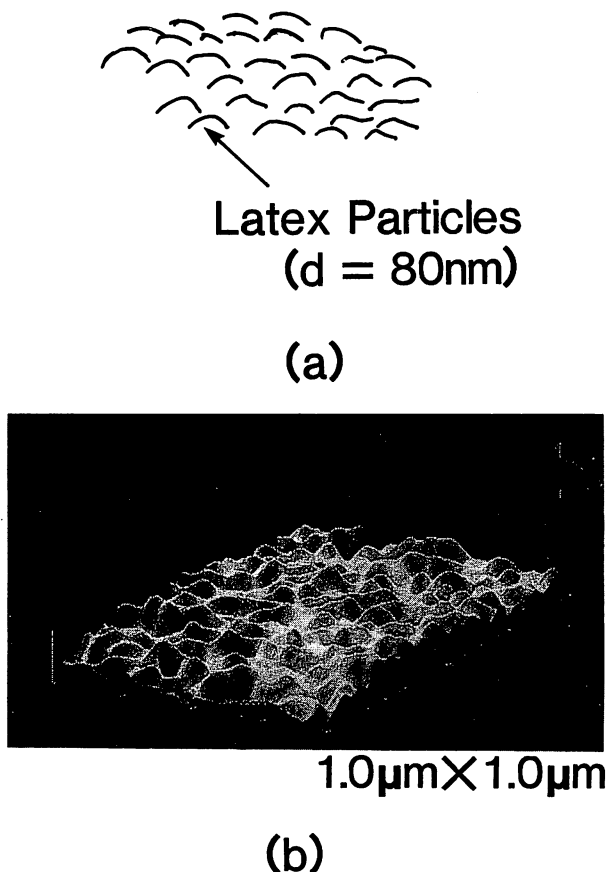


Fig. 6. Measured results of latex particles with diameter of  $80 \text{ nm}$ .

can be seen that a lateral resolution smaller than the radius of the curvature of fiber tip ( $80 \text{ nm}$ ) can be obtained.

#### §4. Summary

A novel photon scanning tunneling microscope using diode lasers and optical fibers is described and samples with submicron structure were measured in a noncontact and nondestructive manner. The fiber probe with the radius of curvature of  $80 \text{ nm}$  sharpened by etching is used in the experiment. The step height of  $9 \text{ nm}$ , optical disk with submicron-sized pits similar to moth-eye structure, and latex particles  $80 \text{ nm}$  in diameter have been measured. Future improvement of the lateral resolution of the present PSTM requires reliable and reproducible fabrication technology to produce a fiber probe with a nm-sized aperture.

On the other hand, for solving the problem of the limitation of the resolution resulted from the low pickup power in the PSTM system described above, a type of reflection-resonance PSTM has been proposed.<sup>12,13</sup> Details will be examined in a later paper.

#### Acknowledgments

The authors wish to thank Dr. H. Yamada (NRLM) and Dr. K. Nakagawa (Tokyo Inst. Tech.), for their discussions at the beginning of this work, Mr. T. Fujii, Mr. M. Suzuki (Nikon), Dr. S. Miyamoto (Fujikura) and Dr. S. Kodato (Anritsu) for their help with system com-

position and probe fabrication and Prof. A. Ikai (Tokyo Inst. Tech.), for the samples supplying and discussions on biochemistry.

### References

- 1) U. Durig, D. W. Pohl and F. Rohner: *J. Appl. Phys.* **59** (1986) 3381.
- 2) E. Betzig, M. Isaacson and A. Lewis: *Appl. Phys. Lett* **51** (1987) 2088.
- 3) E. Betzig and J. K. Trautman: *Science* **251** (1991) 1468.
- 4) H. A. Bethe: *Phys. Rev.* **66** (1944) 163.
- 5) R. C. Reddik, R. J. Warmack and T. L. Ferrell: *J. Am. Phys. Soc.* **39** (1989) 767.
- 6) R. C. Reddick and R. J. Warmack: *Rev. Sci. Instrum.* **61** (1990) 3669.
- 7) D. Courjon, K. Sarayeddine and M. Spajer: *Opt. Commun.* **71** (1989) 23.
- 8) D. Courjon and J. M. Vigourreux: *Appl. Opt.* **29** (1990) 3741.
- 9) S. Jiang, N. Tomita, K. Nakagawa and M. Ohtsu: *Proc. CLEO'91., USA* (Optical Society of America, Washington, D.C., 1991) p. 420.
- 10) T. Fujii, M. Suzuki, M. Miyashita, M. Yamaguchi, T. Onuki, H. Nakamura, T. Matsubara, H. Yamada and K. Nakayama: *J. Vac. Sci. & Technol.* **B9(2)**, Mar/Apr (1991) 666.
- 11) H. Ghafoori-shiraz and T. Asano: *Opt. Lett.* **11** (1986) 537.
- 12) M. Ohtsu, K. Nakagawa, S. Jiang and N. Tomita: *Proc. OEC'90., Tokyo, 1990* (Institute of Electronics, Information and Communication Engineers, Japan, 1990) p. 166.
- 13) S. Jiang, N. Tomita, K. Nakagawa and M. Ohtsu: *Proc. OEC'90., Tokyo, 1990* (Institute of Electronics, Information and Communication Engineers, Japan, 1990) p. 170.



## Nanometric Scale Biosample Observation Using a Photon Scanning Tunneling Microscope

Shudong JIANG, Hisao OHSAWA<sup>1</sup>, Kazunobu YAMADA,  
Togar PANGARIBUAN, Motoichi OHTSU, Kensaku IMAI<sup>2</sup>  
and Atsushi IKAI<sup>2</sup>

Graduate School at Nagatsuta, Tokyo Institute of Technology,  
4259 Nagatsuta, Midori-ku, Yokohama 227

<sup>1</sup>Nikon Corporation, 6-3 Nishi-Ohi 1-chome, Shinagawa-ku, Tokyo 140

<sup>2</sup>Faculty of Bioscience and Bioengineering, Tokyo Institute of Technology,  
4259 Nagatsuta, Midori-ku, Yokohama 227

(Received March 17, 1992; accepted for publication May 16, 1992)

A T4 bacteriophage with a tail diameter of about 9 nm was observed for the first time in an atmospheric condition without a metal film coating, by means of a superresolution photon scanning tunneling microscope (PSTM) using a fiber probe. Fiber probes with cone angles of 25°–100° and their minimum curvature radii less than 10 nm were fabricated and the angle variance was less than 0.5°. The normal resolution of such a PSTM was evaluated to be less than 1 nm, and the lateral resolution, limited by the curvature radius of the fiber probe, was estimated to be within 20 nm.

**KEYWORDS:** optical microscope, biosample, nanometric resolution, near-field, tunneling photon, evanescent wave, submicron aperture, fiber probe

### §1. Introduction

Because of the diffraction limit of conventional optical microscopes, submicron sized biological samples must be measured by means of electron microscopy or scanning tunneling microscopy. In preparation for measurement using these microscopes, samples must be processed, *e.g.*, by coating with metal films, and they must be installed in a high vacuum chamber or fixed on metal coated substrates.<sup>1,2)</sup> On the other hand, photon scanning tunneling microscopy (PSTM) offers the capability of measuring live biosamples in a nondestructive, noncontact manner.

We have previously reported such a system and some of its measurement results. The system, which utilized a 300-nm pits diameter moth-eye optical disk, and 80-nm-diameter latex particles, employed a diode laser and a sharpened fiber probe.<sup>3,4)</sup> In this paper, we present for the first time, an evaluation of the normal and lateral resolutions of the PSTM system, and demonstrate the results of submicron-sized T4 bacteriophages observed by such an optical method. Since the lateral resolution of the PSTM depends on the cone angle or the curvature radius at the top of the sharpened fiber probe, fabrication of a sharpened fiber-probe is indispensable. Therefore we also show improved fiber probes which were fabricated by ourselves.

### §2. System and Pick-up Efficiency

The experimental setup for our biosample observation was virtually identical to the system shown in Fig. 1 of ref. 4. The diode laser light (15 mW power and 780 nm wavelength) is incident to a prism on which the T4 bacteriophage is fixed by a drying technique. Since the spatial power distribution of the evanescent field, generated on the sample under the condition of total internal reflection, depends on the three-dimensional

topography of the sample, the evanescent field power was picked up by a fiber probe and detected by the phase-sensitive detection method in order to measure the sample profile, for which the diode laser power was directly modulated with a modulation frequency of 5 KHz.

For estimating the pick-up efficiency of this system, the model shown in Fig. 1 is used, where  $E_1$  is a monochromatic optical electric field, and  $n_1$ ,  $n_2$ , and  $n_3$  are the refractive indices of the media 1, 2, and 3 respectively. The evanescent field is picked up by a probe with a cone angle  $\theta$ , and considering the symmetry of such a model about the  $z$ -axis, tunneling of the evanescent field can be simplified two-dimensionally. A completely flat sample surface is also assumed for simplicity.

When  $E_1$  reaches the boundary between media 1 and 2 with an angle  $\phi_1$ , which satisfies the total internal reflection condition, the transmission field in medium 3

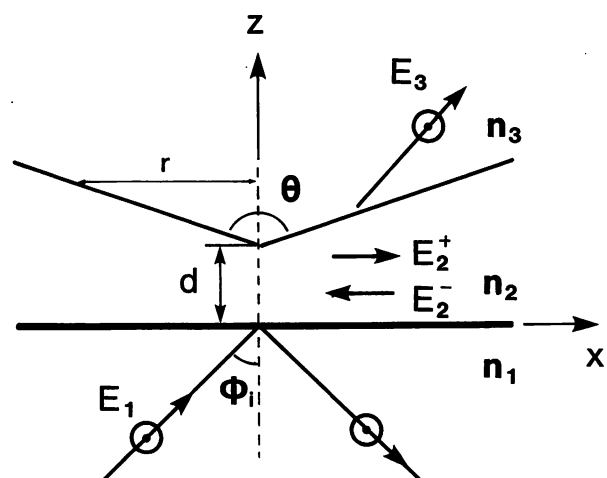


Fig. 1. Model of the estimation of pick-up efficiency of the probe with the cone angle.

created by the tunneling effect can be obtained by the boundary conditions imposed at  $z=0$  and  $z=d+x/\tan(\theta/2)(=D)$ .

The wave number vectors ( $k$  vector) of  $E_1$ ,  $E_2$ , and  $E_3$  are supposed to be independent of the  $\theta$ ; and supposing  $n_1=n_3=n$ ,  $n_2=1$ , we derived the theoretical expression for the intensity ratio of  $E_3$  to  $E_1$  as

$$T(x) = \left| \frac{E_3}{E_1} \right|^2 = \frac{4\gamma^2 n^2 \cos \phi_i}{4\gamma^2 n^2 \cos^2 \phi_i + (1-n^2)^2 \sinh^2(2\pi\gamma D/\lambda)} \quad (1)$$

where  $\lambda$  is the wavelength of the incident light,  $\phi_i$  is the incident angle and  $\gamma = ((n \sin \phi_i)^2 - 1)^{1/2}$ . Then, the pick-up power of the evanescent field can be expressed, through integrating the electric field contribution over the entire side of the cone, as

$$P = \frac{n\epsilon_0 c}{2} |E_1|^2 \int_0^{2\pi} \cos \zeta \, d\zeta \int_0^a T(x) x \, dx \quad (2)$$

where  $\epsilon_0$  is the permittivity in vacuum, and  $a$  is the core radius of the fiber which is  $2.5 \mu\text{m}$  when the single-mode fiber is used.

The estimations obtained by eqs. (1) and (2) are shown in Fig. 2. Figure 2(a) shows the pick-up power versus the sample-probe separation. It can be seen that the power decays exponentially when the sample-probe separation increases, and the decay rate is independent of the cone angle, which is confirmed by our experimental results described in Fig. 4. Figure 2(b) shows the relative pick-up power, which is normalized to the value of the pick-up power by the entire probe, as a function of  $r$  (see Fig. 1 for its definition). With the increase of  $r$ , the relative pick-up power increases more slowly. From the result

given in Fig. 2(b), a probe with a cone angle  $\theta$  can be considered to have a sub-wavelength effective aperture which implies that the pick-up power is dominantly received by the top of the probe and the diameter of such an aperture becomes smaller with smaller  $\theta$ .

### §3. Experiment and Discussion

To fabricate fiber probes with small cone angles for higher resolution, a selective etching technique using ammonium fluoride ( $\text{NH}_4\text{F}$ )-buffered hydrofluoric acid (HF) solution was used. Several types of  $\text{GeO}_2$ -doped single-mode fibers for the 800 nm wavelength with different doping rates have been investigated. Because the etching of the  $\text{SiO}_2$  cladding is faster than that of the core in which the  $\text{GeO}_2$  is doped, the cladding was removed and the core end becomes conical. The cone angle or the curvature radius at the top of the sharpened core can be adjusted by varying the  $\text{GeO}_2$  doping concentration in the fiber core, the etching time, and the concentration of the etching solution.<sup>5)</sup> Examples of the fiber probe which were fabricated using the different concentrations of etching solution and  $\text{GeO}_2$  doping rates are shown in Fig. 3. The  $\text{GeO}_2$  doping concentration in the core of the fiber shown in Fig. 3(a) is 3.6 mol%, and that of the fibers shown in Figs. 3(b), 3(c) and 3(d) is 23 mol%. It can be seen that the cone angles are  $100^\circ$ ,  $45^\circ$  and  $25^\circ$ , respectively, and the fibers with larger doping rate have smaller cone angles. By increasing the magnification of the scanning electron microscopic (SEM) pictures (see Fig. 3(d)), the smallest curvature radius at the top of the core of these fiber probes was roughly estimated to be less than 10 nm. However, it should be noted that the SEM resolution was not sufficiently high so as to obtain the value precisely. Via a series of etching experiments, these fiber probes were found to be fabricated with a reproducibility of  $\Delta\theta=0.5^\circ$ . Details of the relationships between cone angles and the etching time, the concentration of the

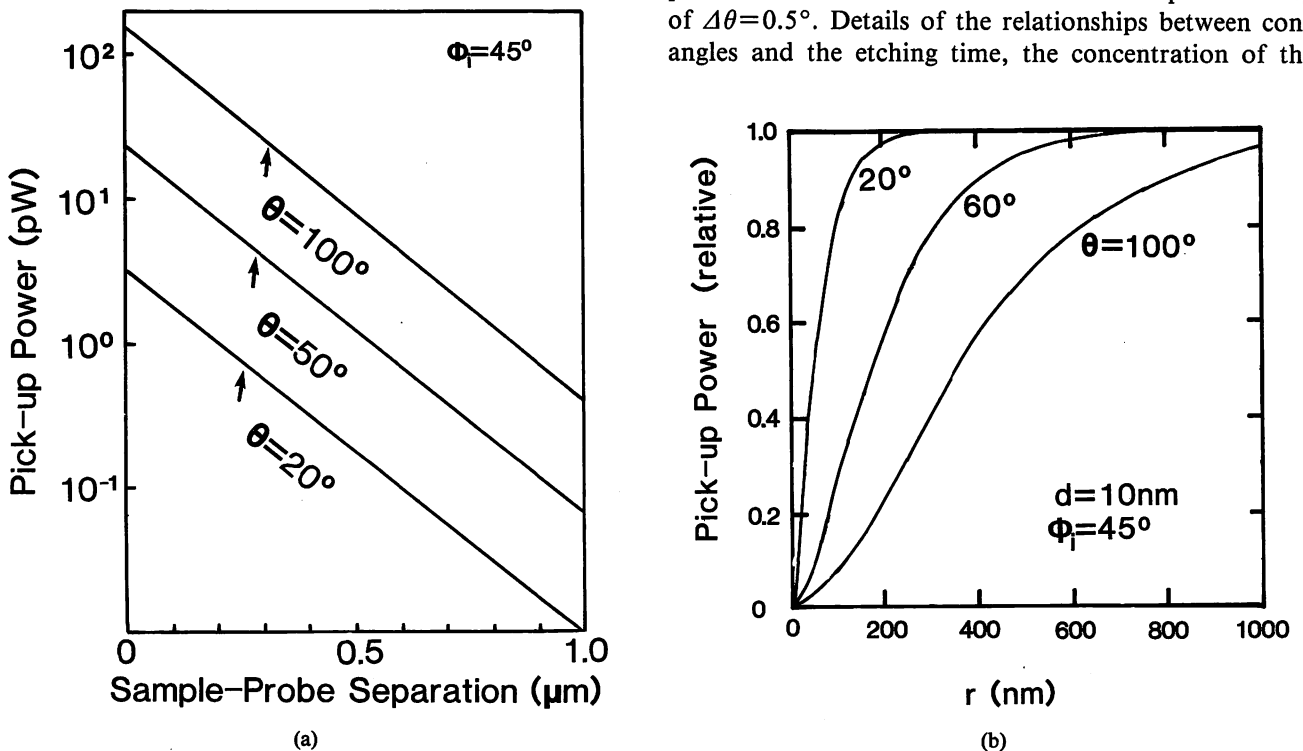


Fig. 2. Estimation results of the pick-up efficiency. (a) Pick-up power versus the sample-probe separation. (b) Relative pick-up power, which is normalized to the value of the pick-up power by the entire probe, as a function of  $r$ .

etching solution and the solution temperature will be published elsewhere.\*

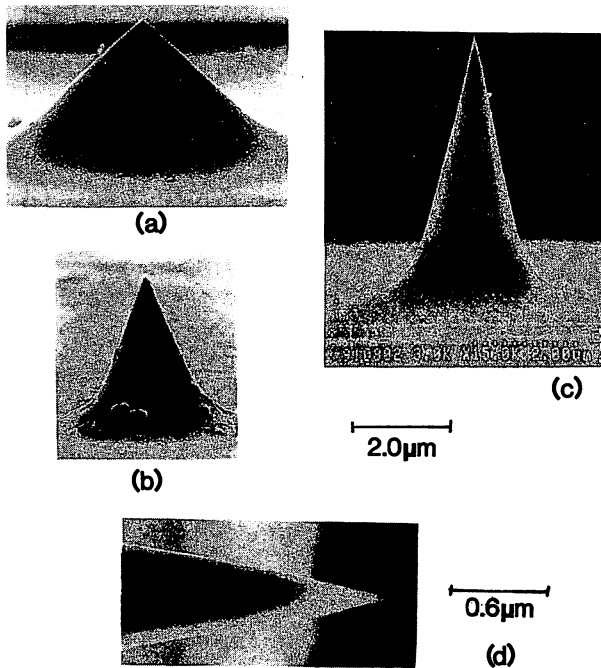


Fig. 3. The SEM image of the fiber probes which were fabricated by different concentrations of the fiber core and etching solution. The etching solution temperature is 22°C. (a), (b), and (c) The probes with the cone angle of 100°, 45°, and 25°, respectively. (d) The SEM image with larger magnification of the probe with the cone angle of 25°.

For comparison of the pick-up efficiency and the normal resolution of the system using the fiber probes with different cone angles, the evanescent field at different sample-probe separation was picked up and its power was measured by the fiber probes shown in Figs. 3(a), 3(b) and 3(c) (probes 1, 2 and 3, respectively). Figure 4 shows that the pick-up power decays exponentially with increasing the sample-probe separation, and the decay rate which is determined by the incident angle  $\phi_i (=45^\circ)$  is independent of the cone angle.

The normal resolution  $\Delta z$  depends on the normally resolved intensity variation, which can be expressed as

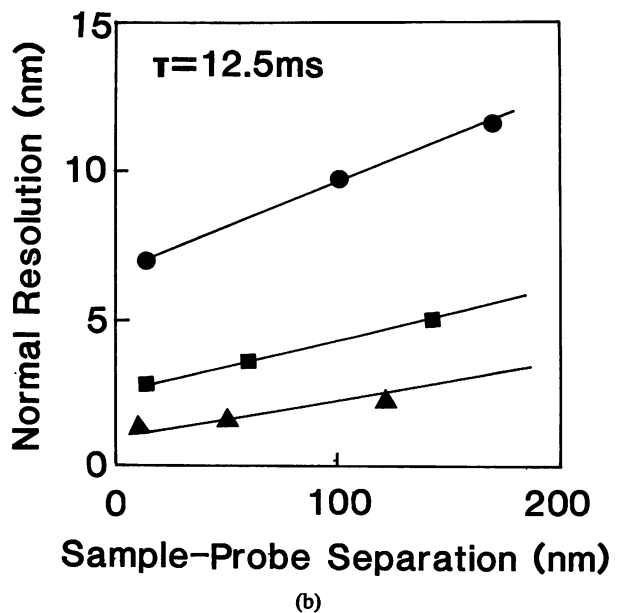
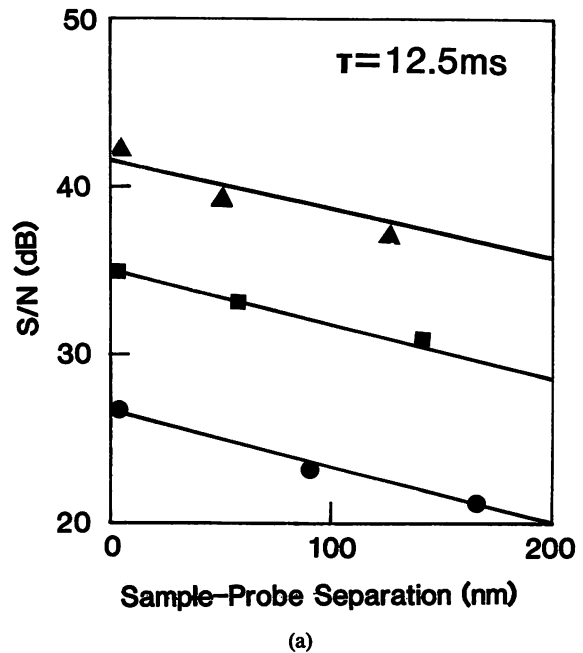


Fig. 5. Measurement results of SNR and the normal resolution of the PSTM. Measured values by fiber probes with cone angles 100°, 45°, and 25° are marked with triangles, squares and circles, respectively. (a) Measurement results of SNR at the different sample-probe separations. The measurements were carried out by using a lock-in amplifier with a time constant of 12.5 ms. (b) Results of the normal resolution in various probing positions using different probes.

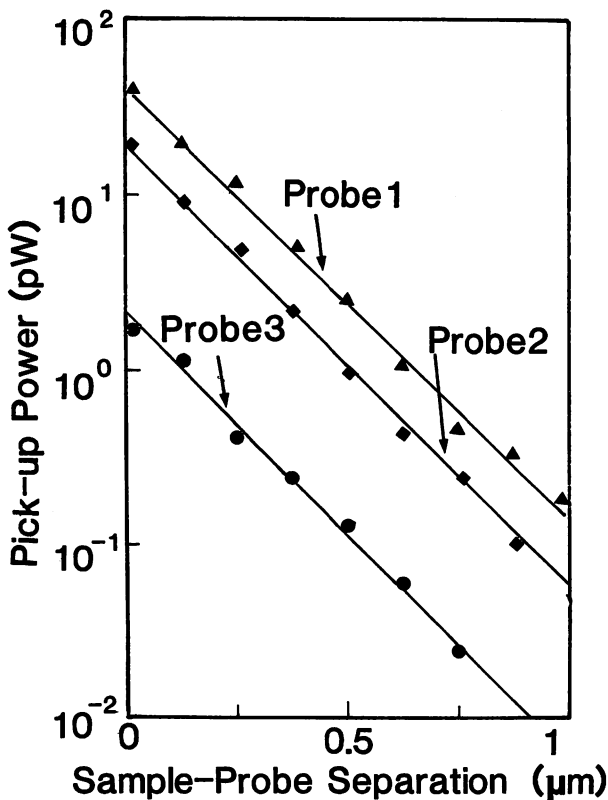


Fig. 4. A comparison of the pick-up performance of the probes with different cone angles.

\*T. Pangaribuan, K. Yamada, S. Jiang, H. Ohsawa and M. Ohtsu: submitted to Jpn. J. Appl. Phys.

$$\Delta z = (1/\eta)(1/SNR). \quad (3)$$

In this expression,  $\eta$  is the slope of the line in Fig. 4 and  $SNR$  is the signal-to-noise ratio of the system under the condition of particular time constant  $\tau$  of the lock-in amplifier used for the measurement.

Figure 5(a) shows the measurement results of the  $SNR$  in the case of  $\tau = 12.5$  ms at the different sample-probe separations. At the same sample-probe separation, the  $SNR$  obtained by the probe with a larger cone angle by which larger power can be picked up is higher than that of the probe with a smaller cone angle. By the same probe,  $SNR$  decreases as the sample-probe separation increases because the evanescent field decays exponentially. Furthermore, it should be noted that the value of  $\Delta z$  is proportional to  $\tau^{-1/2}$  in measurement<sup>6)</sup> because the system noise is mainly generated from the detector and can be approximately considered to be white noise. However, considering the thermal drift of the system caused by environmental temperature variation, the maximum time constant was empirically found to have an optimal value at 12.5 ms under the present experimental conditions.

Results of normal resolutions at various sample-probe separations using probes 1, 2 and 3 are shown in Fig. 5(b). At the same sample-probe separation, the normal resolution is lower using the probe with a smaller cone angle while the lateral resolution can be higher. Therefore, it can be seen that there is a trade-off between the lateral resolution and the normal resolution of the system.

Figure 6 gives the limitations of the  $SNR$  determined by a light source and photodetector. The values marked with triangles, squares and circles are the measured  $SNR$  values using probes 1, 2 and 3, respectively. Line A is the

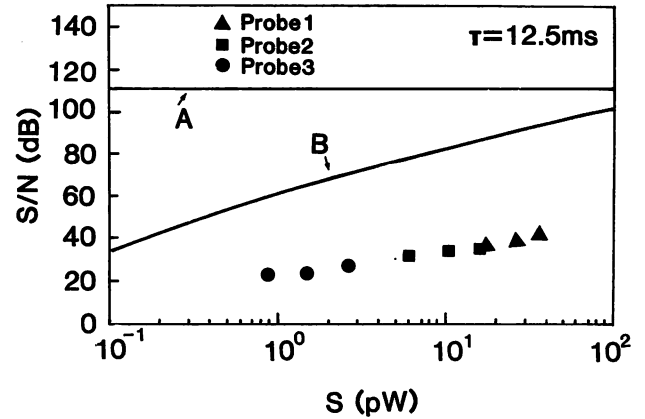


Fig. 6. Limitations of  $SNR$  determined by a light source and photodetector. The values marked with triangles, squares and circles are the measured  $SNR$  using probes with different cone angles. Line A is the measured equivalent  $SNR$  of the magnitude of the laser power fluctuations, and line B is the calculated  $SNR$  of the photomultiplier.

measured equivalent  $SNR$  of the magnitude of the laser power fluctuations, and curve B is the calculated  $SNR$  determined by the photomultiplier. The measured values of the  $SNR$  of our system are more than 20 dB lower than that limited by the detector noise and can be considered as the effects of environmental mechanical vibration and sample-probe separation variation resulting from temperature fluctuation. We can also conclude that the normal resolution will be improved tenfold after the influences from the environment are well isolated, and will be further improved by reducing the noise of the photodetector.

To confirm the improvement of the lateral resolution

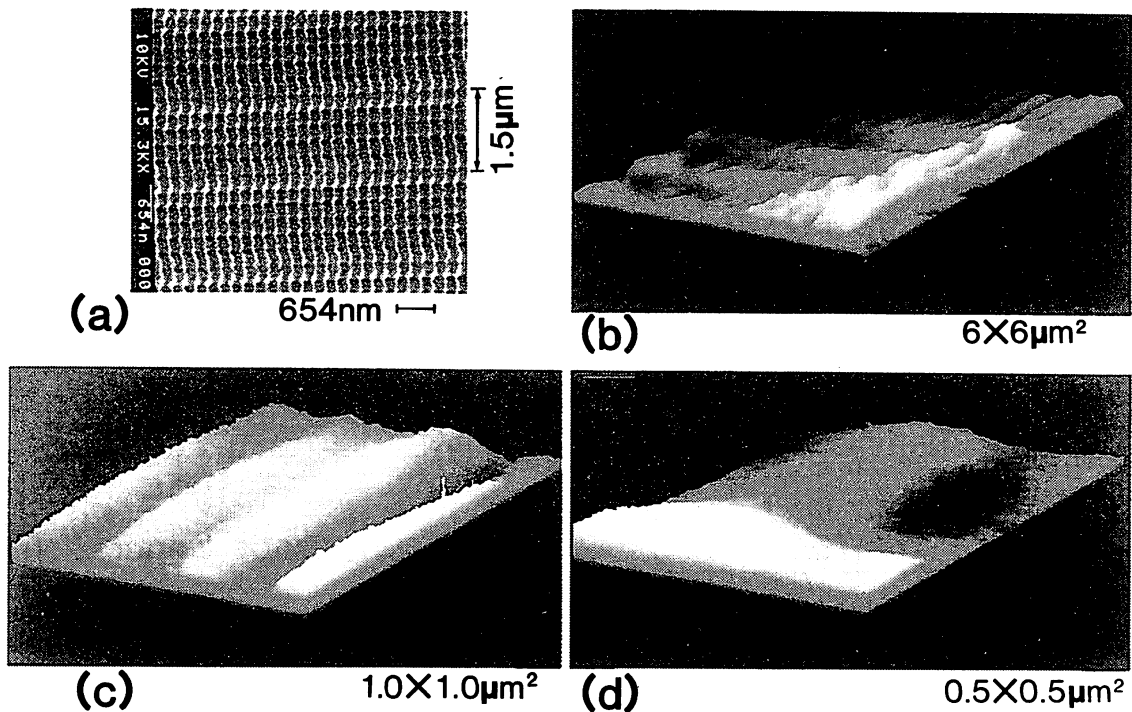


Fig. 7. Measured results of the optical disk with submicron-sized pits similar to the moth-eye structure using probe 2. (a) The SEM image of such a disk. (b), (c) and (d) The PSTM images at different magnifications.

by using the fiber probe with a small cone angle, an optical disk with submicron-sized pits similar to the moth-eye structure was measured using probe 2. Figure 7(a) is the SEM image of such a disk. The pitches of the grating like profile in the  $y$  and  $x$  direction are  $1.5 \mu\text{m}$  and  $300 \text{ nm}$ , and the diameter of each pit is about  $300 \text{ nm}$ . Figures 7(b), 7(c) and 7(d) are the PSTM images at different magnifications. We can see the grating-like structure in the  $y$  and  $x$  direction in the magnifications of Figs. 7(b) and 7(c), respectively, and the pit in the magnification of Fig. 7(d). Comparing Fig. 7 with the results in Fig. 5 of ref. 4, which were measured by probe 1, it is clearly seen that the resolution is improved by using the probe with a small cone angle.

Using probe 3, T4 bacteriophages were observed. The

structure of T4 is schematically given in Fig. 8(a). The nominal size of the icosahedral head is  $85 \text{ nm}$  by  $115 \text{ nm}$ , and the diameter and the length of the tail are about  $9 \text{ nm}$  and  $98 \text{ nm}$ , respectively.<sup>7)</sup> The sample was prepared by depositing a droplet of dilute phosphate-buffered saline (PBS) ( $50 \text{ mM Na}_2\text{HPO}_4$ ,  $25 \text{ mM KH}_2\text{PO}_4$ ,  $70 \text{ mM NaCl}$ ,  $1 \text{ mM MgSO}_4$ , pH 7.2) onto a prism in air and drying with an aspirator. The number of T4 bacteriophages contained in the solution total about  $2.7 \times 10^{13} / \text{ml}$ . Figure 8(b) shows the SEM image of the diluted T4 bacteriophage sample. The PSTM image is shown in Fig.

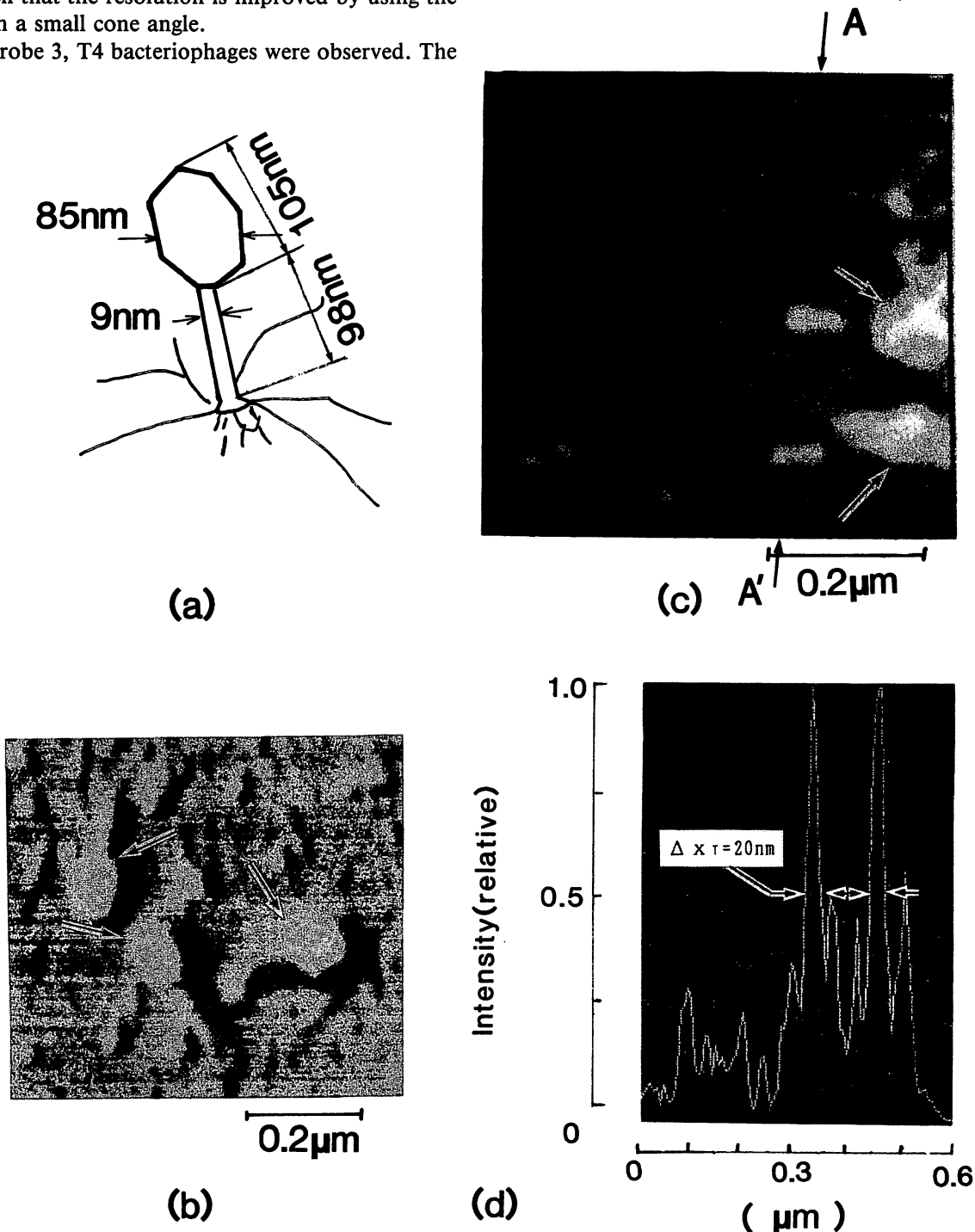


Fig. 8. Images of the T4 bacteriophage. (a) The structure of the T4. (b) SEM image of the T4 sample. (c) PSTM image using the probe with a cone angle of  $25^\circ$ . The scanning range is  $0.6 \times 0.6 \mu\text{m}^2$ . (d) Relative intensity in the cross section corresponding to the tails of the two observed T4 bacteriophages.

8(c). The scanning range is  $0.6 \mu\text{m} \times 0.6 \mu\text{m}$  ( $=64 \times 64$  pixels), the line-scan speed is 1.5 s and the time constant of the lock-in amplifier is 12.5 ms. Heads and tails of two T4 bacteriophages were clearly identified. Figure 8(d) gives the relative intensity in the cross section corresponding to the tails of the two observed T4 bacteriophages along line A-A' in Fig. 8(c). The lateral resolution of such an observation is 20 nm; the lateral resolution here is defined as the full width at the half-maximum of the detected signal intensity. It should also be noted that such a lateral resolution was affected by the scan step length, which was about 9.4 nm in the measurement, and the lateral resolution limited by the curvature radius of the fiber probe can be estimated to be within 20 nm.

#### §4. Conclusions

A Bacteriophage T4 with a tail diameter of about 9 nm was successfully observed for the first time by means of the photon scanning tunneling microscope. Such a successful observation resulted from the fact that a fiber probe with a cone angle as small as  $25^\circ$ , and a curvature radius of smaller than 10 nm has been achieved. The fiber probes used in our experiments were reproducibly fabricated with an angle variance of less than  $0.5^\circ$ . The

normal resolutions of our PSTM were evaluated to be less than 1 nm, and the lateral resolution, limited by the curvature radius of the fiber probe, was estimated to be within 20 nm.

#### Acknowledgments

The authors wish to thank Dr. S. Miyamoto (Fujikura) for his help with fiber probe fabrication and Professor F. Arisaka (Tokyo Institute of Technology), for supplying the biosample.

#### References

- 1) F. Arisaka, S. Takeda and S. Ishii: *Biochemistry* **29** (1990) 5057.
- 2) J. G. Mantovani, D. P. Allison, B. B. Reddik and K. Bruce Jacobson: *J. Microsc.* **158** (1990) Pt 1, 109.
- 3) S. Jiang, N. Tomita, K. Nakagawa and M. Ohtsu: *Proc. CLEO'91, USA* (Optical Society of America, Washington, D.C., 1991) p. 420.
- 4) S. Jiang, N. Tomita, H. Ohsawa and M. Ohtsu: *Jpn. J. Appl. Phys.* **30** (1991) 2107.
- 5) S. Jiang, N. Tomita, H. Ohsawa and M. Ohtsu: *Proc. A. M. OSA '91, USA* (Optical Society of America, Washington, D.C., 1991) p. 65.
- 6) P. Kartaschoff: *Frequency and Time* (Academic Press Inc., London, 1978) Chap. 2.
- 7) C. K. Mathews, E. M. Kutter, G. Mosig and P. B. Berget: *Bacteriophage T4* (American Society for Microbiology, Washington, D.C., 1983) p. 11.

## レーザー解説

## フォトン走査トンネル顕微鏡

大津元一\*・蔣曙東\*・大澤日佐雄\*\*

(1991年8月6日 受理)

## Photon Scanning Tunneling Microscope

Motoichi OHTSU\*, Shudong JIANG\* and Hisao OHSAWA\*\*

(Received August 6, 1991)

The authors' studies on photon scanning tunneling microscope (PSTM) are reviewed. Normal and lateral resolutions achieved by a transmission-type PSTM are estimated as high as 2-nm and 5-nm, respectively. To improve the performance of the system, several methods are proposed, e.g., a novel reflection-resonance-type PSTM is advantageous to improve the resolution. Advanced application systems are also proposed, and especially, a possibility of using the PSTM system as a single-atom-level crystal growth is discussed.

**Key Words;** Photon, Microscope, STM, Semiconductor laser, Crystal growth.

## 1. まえがき

光による新しいセンシング, プロセッシング, を行なうためには光の持つ特性を再考する必要がある。光を波と見なしたとき, その特性は周波数(光パルス幅), パワー, 偏光, によって記述され, 現在までにレーザーを用いてこれらの性能は著しく向上している<sup>1)</sup>。しかし, まだ取り残されているのは光の空間的局在および, 光をフォトンと見なしたときのエネルギーの最少単位 $h\nu$ を活用する方法である。

我々は数年前に以上のような考察をもとにフォトン走査トンネル顕微鏡(PSTM: Photon Scanning Tunneling Microscope)の研究を開始

した。まず, 光の波長より小さい寸法の空間に光を局在させることにより回折限界を越える超解像顕微鏡が実現する。さらに, この顕微鏡の視野内の試料は少数個の原子からなり得るので,  $h\nu$ の値が小さくても(特に共鳴相互作用を利用すれば), これらの原子に与える摂動エネルギーが大きくなり得る。

したがって, 摂動エネルギーが小さい場合には, PSTMを非接触・非破壊で超解像形状測定可能な顕微鏡として, さらに摂動エネルギーが大きい場合には極微プロセッシングのための加工機として使える。特に, 後者に関しては単原子レベルの結晶成長などの可能性がある。

PSTMでは近視野での光学的測定技術を使う

\*東京工業大学 総合理工学研究科 (〒227 横浜市緑区長津田4259)

\*\*株式会社ニコン開発本部研究所 (〒140 品川区西大井1-6-3)

\*Graduate School at Nagatsuta, Tokyo Institute of Technology (4259 Nagatsuta, Midori-ku, Yokohama 227)

\*\*Research Laboratory, NIKON Corp. (1-6-3 Nishi-Ohi, Sinagawa-ku, Tokyo 140)

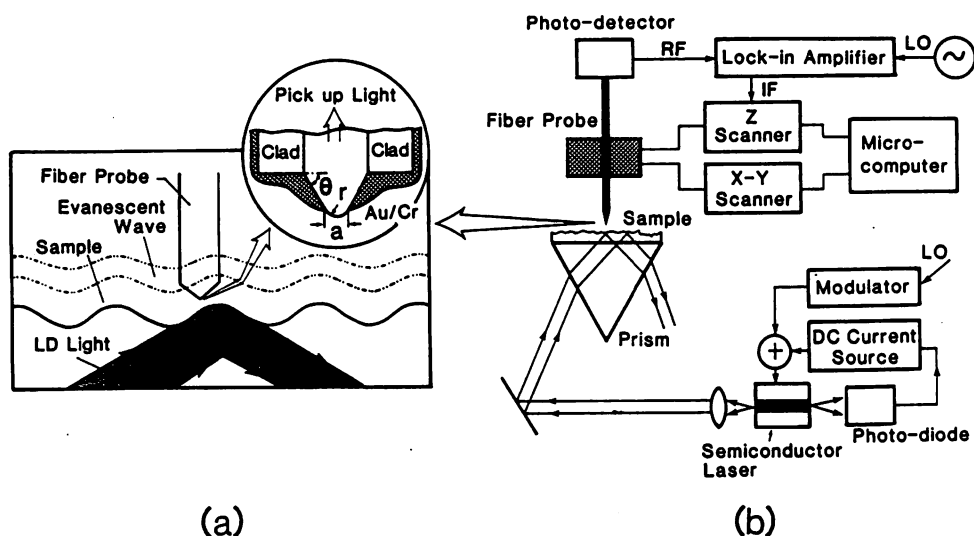


Fig. 1 Transmission-type photon scanning tunneling microscope (T-PTSM). (a) The principle of operation. (b) Block diagram of the system.

ので近視野顕微鏡 (NFM: Near Field Microscope)<sup>2-8)</sup>とも呼ばれる。NFMはすでに長い歴史をもつが、それらは装置性能、実用性、プロセッシングへの応用可能性、などの点で未だ発展途上である。この点を改善したPSTMはNFMとは著しい差を有するといえる。しかし現在のところ、PSTMとNFMとの区別、分類、さらにそれらの名称についての厳密な定義が必ずしも十分ではなく、今後整理されるべきである。

以下ではPSTMに関する我々の研究を中心に概説するが、その内容の一部については、すでに公表されている著者らの解説記事<sup>9-11)</sup>と重複することを予めお断りさせて頂きたい。

## 2. PSTMの原理

Fig. 1 (a)にPSTMの基本原則を示す。顕微鏡としての試料の面内方向( $x-y$ 軸方向)分解能を向上させるためには光の波長 $\lambda$ より小さい直径 $a$ をもつ開口をプローブとして使う。一方、厚み方向( $z$ 軸方向)の分解能を向上させるためには全反射時に発生するエバネッセント光を利用する。エバネッセント光は $z$ 軸方向に指数関数的に減衰するので $z \ll \lambda$ なる近視野での測定が必要である。近視野では回折が無視でき、上記開口により超解像が実現する。すなわち、こ

の開口によって光の空間的局在を実現して面内形状に関する情報を抽出し、開口を通り抜けた光のパワー測定によってその情報を検出する。これは、ファブリ・ペロー共振器などの光周波数復調器の透過光パワーを測定すれば光周波数に関する情報を抽出できることと同等である。

光をフォトンと見なして以上の原理を考えると、 $a \ll \lambda$ なる開口を通して光をピックアップすることはフォトンの運動量測定誤差 $\Delta p$ を大きくし( $\Delta p/p = h/a$ ;  $h$ はプランクの定数)、位置測定誤差を $\Delta x$ を減少させることに対応する( $\Delta x \geq a/2\pi$ )。一方、エバネッセント光の検出は、開口を試料に近づけることにより試料面におけるフォトンのトンネリング障壁の高さを減少させること、すなわち、開口によってエバネッセント光の場を破壊することにより検出していることに対応する。

我々の用いているプローブは先端を研磨した光ファイバーである。これをFig. 1 (b)に示すように $x-y$ 軸方向に走査しながら、光パワーを測定し、計算機により適当な画像処理を施した後、CRTディスプレイ上に表示する。これらの走査、表示システムは従来のSTMと同様である。



### 3. PSTMのシステムと実験結果

まず, Fig. 1 (b)に示すような透過形PSTM (T-PSTM)について記す。T-PSTMはレーザー光のパワー密度が高いことを利用したものであり, 試料表面形状の測定はエバネッセント光のパワーを測定することにより行われる。T-PSTMを光通信システムと対応させると強度変調-直接検波方式に対応する。したがって, システム構成は簡単かつ小形(本体体積 $1.000\text{cm}^3$ 以内)であるが, 低パワーのエバネッセント光を測定するので, 従来は感度が低く, 分解能も制限されていた。しかし, 我々はAlGaAsレーザーに出力光が一定になるような自動制御を施し, かつ単一モード光ファイバーをプローブとして用いることにより検出パワーを増大することができた。T-PSTMを用いると試料表面の局所的な光化学反応を強制的に誘起させて, その結果を測定すること, さらに, レーザー波長を掃引すれば局所的な分光分析, 組成分析, などが期待できる。Fig. 1 (b)ではレーザーパワーの直接変調・位相敏感検波方式が示されているが, この他に, プローブのz軸方向走査用のピエゾ・アクチュエータを変調し, 位相敏感検波する方式, さらに, フォトンカウンティング法など, 種々の方法が可能である。半導体レーザーの直接変調帯域は1GHz以上に及ぶので他のSTMシステムに比べ, 高速測定可能な利点を有する。

高い面内分解能を得るために微小開口を持つ光ファイバー・プローブを使っている。このファイバー先端の微小開口の製作方法は従来いくつか提案されているが(ラテックス球による方法<sup>2)</sup>, 石英棒の先端を尖らす方法<sup>3)</sup>, ピペット法<sup>5)</sup>など), 未だ加工精度と再現性が低い。一方我々の製作方法は次のようなものである。単一モード光ファイバーのコア先端を弗酸を用いた選択エッチングによって尖らせる。次にクロム及び金の薄膜を蒸着し, さらにプラズマエッチングあるいはSTMプローブの先端との放電によりコア先端の一部を露出させ, 微小開

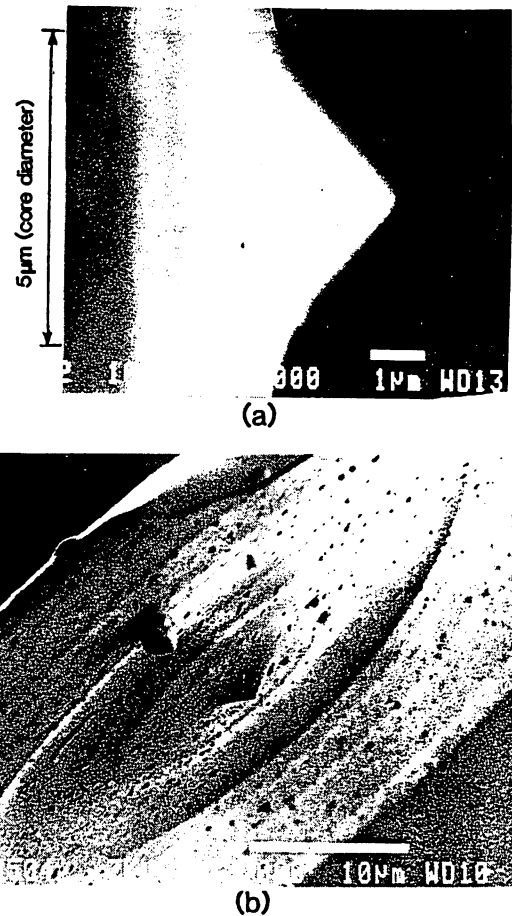


Fig. 2 SEM picture of an optical fiber with a shaped core<sup>10)</sup>. (a) Side view. (b) Bird's-eye view.

口とする。Fig. 2には先端を尖らせ, 金属薄膜を蒸着した後のSEM写真を示す<sup>10)</sup>。ファイバー・コア先端部の尖り角度(Cone angle)は約100度, また曲率半径は約80nm以内と推定される。金属薄膜の蒸着, さらに開口形成についてはまだ必ずしも十分な再現性が得られていないが, 数10nm以下の開口径が可能であることも指摘されている<sup>4)</sup>。さらに, ファイバー先端をより鋭く尖らせれば電界蒸発法も可能である<sup>12)</sup>。選択エッチングによるファイバー・コアの先鋭化はファイバーの比屈折率差 $\delta$ に依存する。Fig. 2でも用いた波長 $0.8\mu\text{m}$ レーザー用の通常の単一モードファイバーでは $\delta=0.36\%$ であるが, 非線形光学用ファイバーでは $\delta$ の値は2.3%に達する。これを用い, Fig. 2よりも

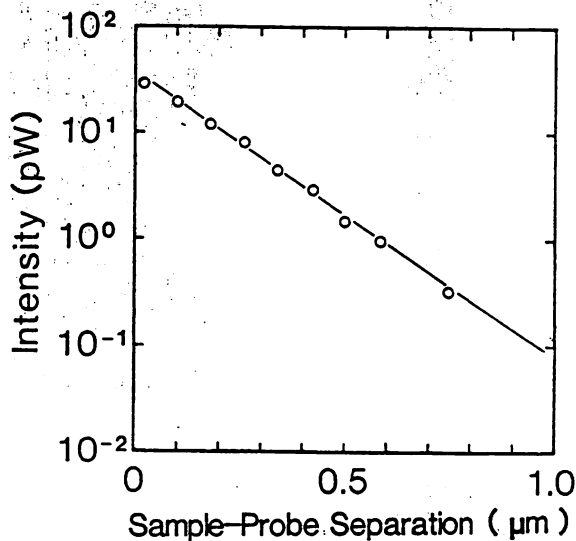


Fig. 3 Measured result of the relation between the sample-probe separation and picked-up evanescent power of the T-PSTM<sup>16)</sup>.

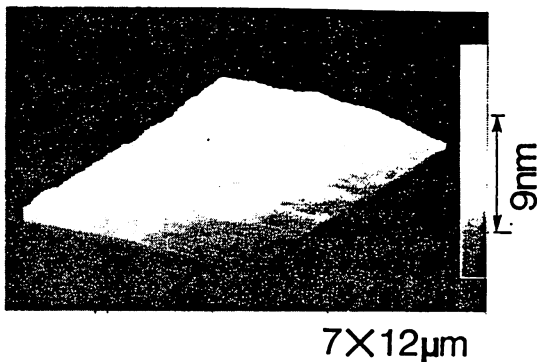


Fig. 4 Measured profile of the edge of the SiO<sub>2</sub>-thin film of 9-nm thickness<sup>16)</sup>.

さらに鋭い先端が最近実現し、尖り角度は約25度になっていることが確認されている<sup>13)</sup>。

Fig. 3 にプローブと試料マウント用プリズム面との間隔と、エバネッセント光パワーとの関係の測定結果を示す。試料入射時のレーザーパワーは数mWである。測定されたエバネッセント光パワーは数10pWである。両パワー値の比は従来のNFMシステム<sup>2-7)</sup>に比べて100倍以上の高い値になっている。さらに、開口周囲の金属蒸着膜からの表面プラズモンを使えば、さらに高い光パワーが得られることが確認されている<sup>14,15)</sup>。この場合、面内分解能が低下する恐

れがあるが、測定感度が向上するので、さらに小さな開口を使うことが可能となり、むしろ分解能が向上すると期待されている。Fig. 1 (b) のプリズムの上面の半分に蒸着した厚さ9 nm のSiO<sub>2</sub> 薄膜の端部の形状測定を行った結果を Fig. 4 に示す<sup>16)</sup>。Fig. 5 (a) には深さ約80nm、直径約300nmのピットを有する Moth-eye 光ディスク表面のSEM写真を示す<sup>16)</sup>。この光ディスク表面には周期1.4 μmの案内溝が設けられている。さらに、厚さ約12nmのプラチナ薄膜が蒸着されているが、ほぼ透明である。Fig. 5 (b)~(c)はT-PSTMでの測定結果である<sup>16)</sup>。倍率を上げて行くと、図(b)では上記の案内溝が見られ、(c),(d)ではピットが見られる。Fig.6は直径80nmのラテックス球をプリズム表面に固定した試料の測定結果である<sup>16)</sup>。この場合ラテックス球は互いに凝集し、真球から歪んだ状態になっているが、多数のラテックス球が明瞭に観測される。Fig.7はバクテリオファージT<sub>4</sub>の像である<sup>13)</sup>。従来はSEM観測により、この形状は頭部直径が65~95nm、尾部は長さ約95nmの細い線状であることがわかっていたが、今回PSTMにより初めて染色せずに観測することに成功している。

以上の一連の測定結果において、測定時の信号S/N値より、厚み方向分解能2 nm以内、面内分解能5 nm以内、と推定されている。ただし、これらの値は位相敏感検波方式における測定時定数 $\tau$ が1 ms~100msの場合の結果である。半導体レーザーが高速変調可能であることをより積極的に利用すればこの $\tau$ の値はさらに小さくなり、高速測定の特長を生かすことができる。システムの雑音の基本要因は光検出時のショット雑音、すなわち白色雑音なので、S/N値は $\tau^{-1/2}$ に比例する。従って、 $\tau$ を大きくすれば、さらに高い分解能が期待される。

#### 4. 性能向上のための課題

T-PSTMは簡単なシステムであるが、微小な光パワーを測定するので、感度が低く、従って分解能も制限される。この問題を解決するため

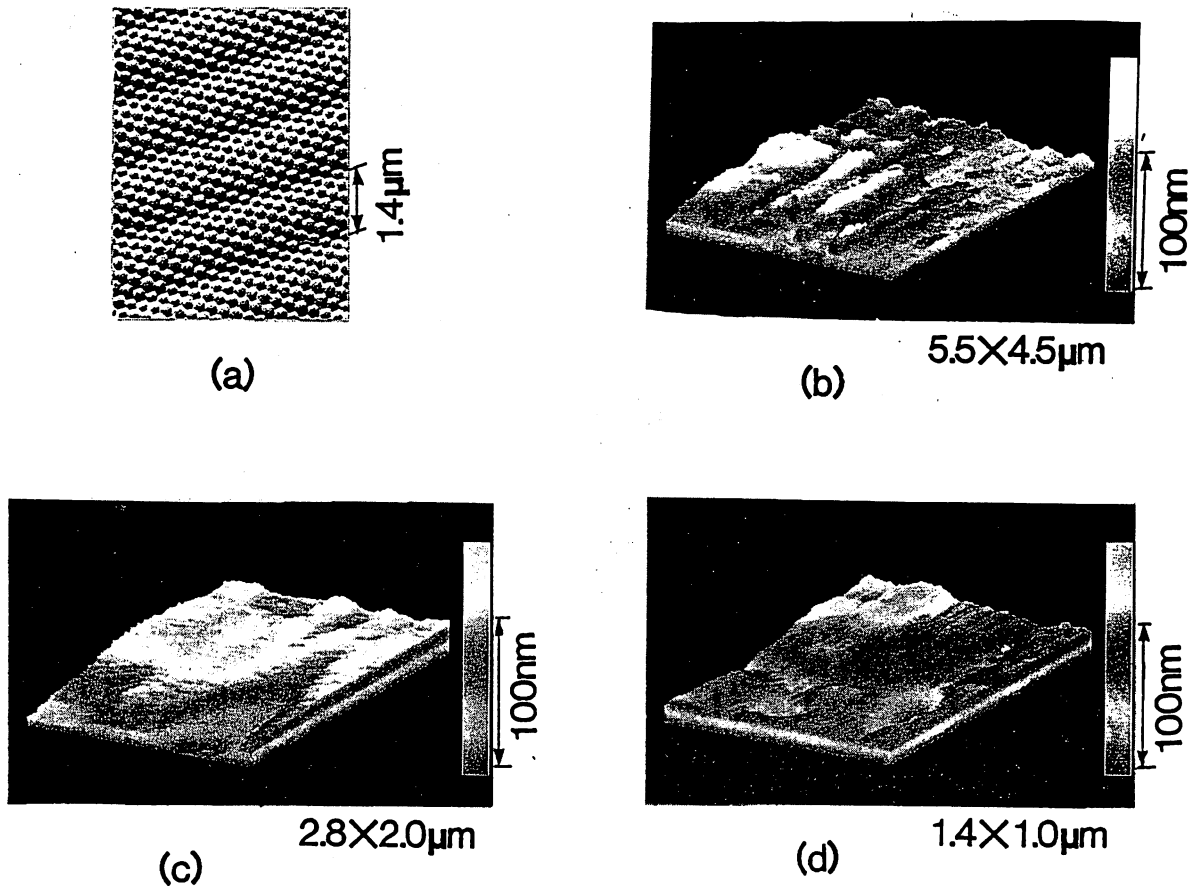


Fig. 5 Measured profile of the Moth-eye-type optical disc surface, on which pits of 80-nm depth and 300-nm diameter are fabricated<sup>16)</sup>. (a) SEM picture. (b)-(d) Measured profile by the T-PSTM by increasing the magnification power.

に我々は反射共振形PSTM (RR-PSTM) を提案している<sup>15,17)</sup>。Fig. 8 (a)にRR-PSTMの基本構成を示す。レーザー光を導波路形共振器に入射させ、レーザー周波数が共振器の共振周波数に一致するようにレーザーを制御しておく。共振器の2つの端面のうち、試料に面した端面には微小開口を設け、これをプローブとして用いる。共振器を試料に接近させると、開口からのエバネッセント光が近接試料表面によって撓動を受ける。その結果、共振器端面の複素反射率が試料の表面形状によって変化し、共振周波数がシフトする。これにより上記のレーザーの周波数もシフトするので、これを基準レーザーあるいは他の共振器とのヘテロダイン信号周波数シフト測定により求める。すなわち、RR-PSTMはレーザーの高コヒーレンス特性を

活用したものであり、試料形状は周波数シフトの測定により求められる。Fig. 8 (b)に(a)の変形として、半導体レーザー自身をプローブとして用いるシステムの原理図を示す。すなわち光増幅機能を有するプローブであり、(a)の半導体レーザーと共振器の役割を一つの半導体レーザーにより実現させる方法の一つとして我々が提案しているものである<sup>15,17)</sup>。

周波数測定はすべての物理量測定のうちで最高精度になり得ることは衆知の通りであるので、これはT-PSTMのもつ感度に関する問題点を解決するものである。すなわち、これは周波数変調-ヘテロダイン検波方式を採用したコヒーレント光通信システムに対応する。RR-PSTMにより、さらに高い分解能をもつセンシングが可能と考えられる。ショット雑音限

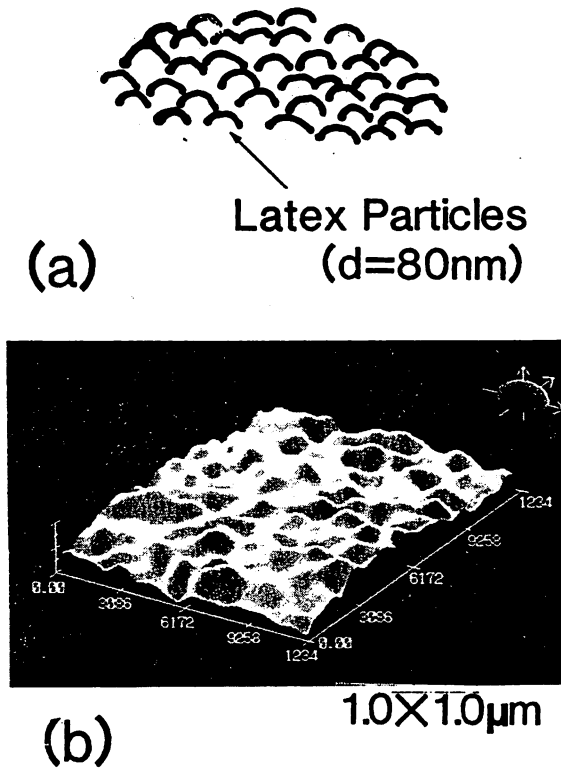


Fig. 6 Measured profile of the latex particles with 80-nm diameters which were densely fixed on a glass substrate<sup>16)</sup>. (a) Schematic explanation. (b) Measured profile.

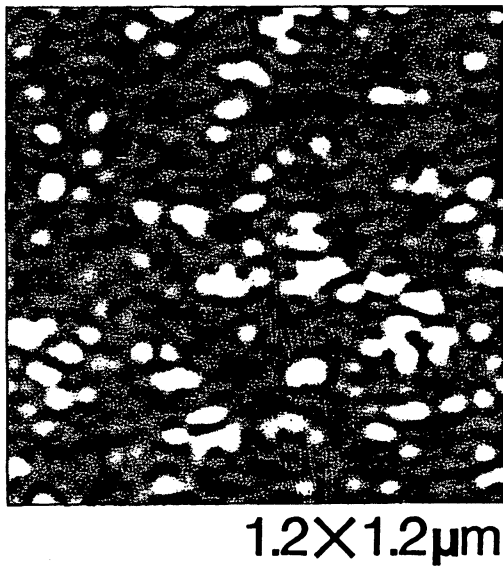


Fig. 7 Measured profile of the bacteriophage T<sub>4</sub><sup>13)</sup>.

界での分解能はT-PSTMよりも1桁以上よいことが推定されているが<sup>17)</sup>、これを実現するため

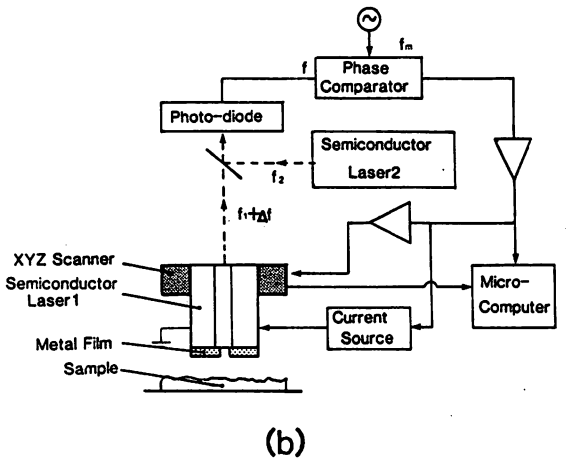
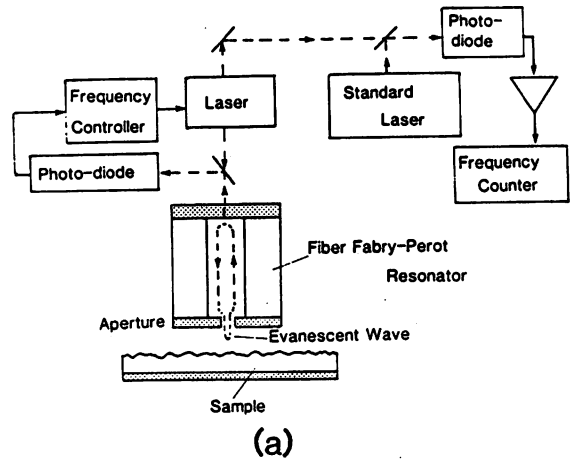


Fig. 8 Reflection-resonance-type PSTM<sup>15,17)</sup>. (a) The system employing the heterodyne-detection with a standard laser. (b) The system using a semiconductor laser as a probe.

には約10Hzの光周波数シフトを検出しなければならない。従って、RR-PSTMを実現するための要素技術として高フィネスの短共振器や、高コヒーレンス半導体レーザー、光位相同期ループが必要である。高コヒーレンス半導体レーザーとしてはすでに線幅7 Hzが実現しており<sup>18)</sup>、ヘテロダイン形光位相同期ループの周波数安定度も $1 \times 10^{-18}$ を実現している<sup>19)</sup>。さらに $1 \times 10^{-16}$ のレーザー周波数安定度も実現している<sup>20)</sup>。これらの技術を利用すれば上記の光周波数シフト値は十分検出可能である。

マイクロ波を用いた予備的なシミュレーション実験により、すでに厚み方向および面内方向

分解能として各々  $5 \times 10^{-3} \lambda$ ,  $5 \times 10^{-2} \lambda$  が得られている<sup>17)</sup>。これらの値はT-PSTMに比べ、すでに優れており、今後、測定条件の改良により一層の分解能向上が期待される。

この他、PSTMの性能向上には次のような課題の克服が必要と考えられる。

(1) 近視野波動光学理論の確立：近視野領域でのマクスウェル方程式を適切な境界条件で解く近視野波動光学理論はまだ十分発達していない。原子大きさ程度の分解能が実現すると、光に対して物体表面とは何か、境界条件とは何か、などについての詳細な検討を行い、感度、分解能の相互関係を明らかにする必要がある。

(2) 試料の固定法の確立：特にラテックス球のような微小粒子やバクテリオファージなど、有機、生体試料をガラス面上に固定する際、凝集を防ぐための再現性の高い技術の確立が重要となる。

(3) 要素作成技術の確立：再現性のある微小開口作成法として、エレクトロン・エッチング法<sup>21)</sup>、電界蒸発法<sup>12)</sup>、などの技術を利用するとともにファイバー先端をより先鋭化する加工法の開発が必要である。これには、3節で述べたように比屈折率差の大きなファイバーなど、PSTM用の特殊ファイバーの開発が望まれる。また、半導体プレーナー加工技術を利用して平板上に微小開口を作り、プローブとして用いることも可能である。RR-PSTMの場合、高フィネスの短共振器が必要であるが、現在までに単一モードファイバーを用いて、誘電体多層膜蒸着により、共振器長2 mm以下、フィネス200以上の値が報告されている<sup>22)</sup>。また、スーパー共振器ではフィネス  $1 \times 10^6$  も実現している<sup>23)</sup>。今後、さらにプレーナー技術(イオン交換、イオン注入)による高安定、低損失導波路形短共振器の実現が期待できる。Fig. 8の共振器の代わりに半導体レーザーの端面に微小開口を作ったものを使えば、これは光増幅機能も備えたプローブとなる<sup>15,17)</sup>。

(4) 新しい測定方式の探索：

(a) 開口合成法の使用可能性の探求：すでに製作されているマルチコア・ファイバー<sup>24)</sup>、またはプレーナー・プロセス技術を用い、近接した複数個のプローブをモノリシックに製作し、マルチ・プローブとして用いる。これにより得られた試料形状測定結果に含まれる各プローブ間の相関を抽出することにより、単一プローブよりも高い分解能が期待される。同様の可能性は従来のSTMにも得られることがわかっている。この場合、モアレ・パターンに類似の画像が得られるので、計算機処理により分解能はさらに向上し得る。光の特徴について従来の常識的な知識から推定するとPSTMの分解能はSTMのそれに匹敵するほど高くなり得ないのではないかとの憶測もあるが、光のもつ特徴を利用することにより原子レベルの分解能を得ることも不可能ではないと考えられる。

(b) 量子雑音限界の打破：PSTMはヘテロダイン検波法などを採用できるので、ショット雑音限界(量子雑音限界)が比較的容易に達成可能である。この意味でPSTMは量子効果の現れやすいシステム、すなわち quantum microscope (量子顕微鏡)、ということができよう。分解能および感度限界は当面この量子雑音により制限されるが、光子数スクイズド状態、位相スクイズド状態<sup>25)</sup>、の光を使用すれば、それぞれT-PSTM, RR-PSTMはこの雑音限界を越える super-quantum microscope になり得る。

## 5. 可能な応用範囲

現在のPSTMの分解能は光学顕微鏡と電子顕微鏡(SEM, STMなど)との中間の値をとり、かつ視野が比較的広いので非接触・非破壊・実時間の形状センサーとして有用である。前節最後にも指摘したようにこのセンサーとしての分解能はさらに向上し得る。また、後述のように加工機としても機能し得るので、以下のような広い分野での応用可能性を有する。

(1) 有機エレクトロニクス分野：有機超薄膜などの表面形状の広視野観測、かつ光源波長を掃引して各部分での局所的な構造解析。

(2) 生命理工学分野：生体細胞膜、DNA、特に種々のウイルス<sup>26)</sup>などの形状の非破壊動特性測定。複数個のプローブを用いた生体細胞膜中の刺激の伝搬特性の評価、ゲート機構の解明。細胞プロセッシング(例えば、従来使われていたレーザー顕微鏡<sup>27)</sup>の代わりにPSTM用のプローブを使い、細胞の特定の位置にレーザー光を照射して細胞に穴を開け、細胞へのDNAの打ち込み精度を向上させる)。DNAよりも小さな寸法の試料を操作するピンセットとしての利用。

(3) 光メモリー、記録：相転移形光磁気ディスクの評価。この場合は屈折率のみ変化するので、原子間力顕微鏡 (AFM: Atomic Force Microscope), STMでは測定不可能であり、PSTMが不可欠といえる。短波長レーザーを使ったPSTMによりフォトクロミック材料表面へのサブミクロン刻線。

(4) 半導体理工学分野：結晶表面に吸着した原子、分子層の評価、単原子層結晶成長制御、超高密度集積回路 (ULSI) の評価およびトリミング、局所的レーザーアニール、結晶表面上の原子中のsp混成軌道の斜め方向からの光の打ち込みによる光電子放出。極微半導体の量子サイズ効果の評価。

(5) 精密機械理工学分野：マイクロマシンの駆動、制御(以下に述べる(4)の原理と同様、光の放射圧を利用)。

ここで、(4)に関連して、我々が提案している単一原子操作および結晶成長の手法を以下に概説する<sup>28,29)</sup>。フォトンの最小エネルギー $h\nu$ が小さくとも、操作対象のエネルギーが小さければ、光照射による摂動エネルギーは相対的に十分大きく、PSTMは超微細加工機として働く。すでにSTMをキセノンの単一原子の操作に使う試みが報告されているが<sup>30)</sup>、PSTMでは適当な波長の光源を選べば半導体産業において重要な原子にも適用可能な加工機となり得る。これは三段階からなる。まず、第一段階としては真空中で気体原子集団にレーザー光を照射し、レーザー冷却および光糖蜜の手法により原子の

熱運動の等価原子温度を低下させる<sup>31)</sup>。第二段階としてRR-PSTMのプローブをこの冷却原子集団に近づける。冷却原子がプローブから出射するエバネッセント光場に飛び込んだとき、この原子をエバネッセント光のもつ双極子力により形成されるポテンシャルの井戸に捕獲する。安定な捕獲のためには実際には対向する複数のプローブの対を用いる。第三段階としてプローブを移動し、捕獲した原子を冷却結晶基板上に移動する。そして、さらにもう一つの押し出し用プローブを用意しておき、これから光を出射させ、原子を加速・加熱して押し出し、結晶基板上に付着・固定させる。ここで、問題となる点は安定なポテンシャル井戸の形成法およびそれに必要なレーザー光パワーである。この概略値を知るために、セシウム原子を例にとって計算した結果、光糖蜜中の原子温度が0.1mKのとき、開口径 $a/\lambda = 1 \times 10^{-2}$ なるピックアップを用いれば、プローブへの必要入射パワーは約1mWでよいことがわかった<sup>28,29)</sup>。この値は既存の半導体レーザーにより実現可能である。ごく最近、この考え方を支持する関連実験結果が報告された<sup>32)</sup>。ただし、この報告では我々のような微小開口プローブを用いてはいないので、必要レーザーパワーは1W以上であった。従って、単一原子結晶成長には光糖蜜とともに微小開口プローブが必須要素であると言えよう。この方法の類形として、結晶基板上に原子を一個ずつ積み上げ、単一原子レベルの細線 (Atomic Tower, Whisker) や Quantum Point の形成、などが考えられる。

## 6. おわりに

従来十分には実現していなかった光の空間的局在を利用し、超解像センサー、極微プロセッサとして働き得るPSTMについて、我々の研究を中心にご紹介した。光技術を補助手段として使っている高分解能顕微鏡としてAFMがあるが、これに対し、PSTMは光を主手段として使い、光でなくては実現しない超高性能を実現していると言えよう。AFMでは原子間力は距

離の $-2$ 乗で変化するが、PSTMではエバネッセント光パワーは指数関数的に変化するので厚み方向分解能を向上させる上で有利である。4.(4)節で述べたように測定方式を注意深く検討すれば面内分解能も原子レベルに達する可能性がある。今後、このような手法は極限技術にますます利用されていくと考えられる。特に、近視野波動光学は未開発の分野であり、量子光学の手法と組み合わせればさらに新奇な極限光学システムの実現も可能である。

これらのシステムに必要な要素として、半導体レーザー、光ファイバー、光集積回路、などがあるが、これらの要素の開発のいくつかは我が国が世界をリードしていることを考慮すると、PSTMは我が国が先頭に立って研究すべき課題であるといえる。PSTMをセンサーとしてのみ使うと自ずからその波及効果は制限されるが、使用範囲をプロセッサまで拡大すれば、その波及効果は大きい。PSTMも従来の各種のSTMと同様、学際的な研究課題である。光学分野だけに留まらず、他分野との協力が研究発展のための必須条件といえる。逆にこのような協力により研究が発展すれば、光学が広範な分野の新しい科学技術の基幹研究分野となり得る。現在の光学はこのような過渡的な状況に差し掛かっていると思われるので、この好機を逃すべきではないと思われる。

#### 謝辞

光ファイバーに関しご討論頂いた藤倉電線(株)の宮本末広氏に感謝致します。また、本研究を進める上でご協力頂いた、本学学生富田直幸(現在、日産自動車(株))、P. トガル、藤江嘉彦、山田和延の各氏、さらにご討論頂いた中川賢一博士に感謝致します。

#### 参 考 文 献

- 1) 大津元一：コヒーレント光量子工学，朝倉書店，東京，1990。
- 2) U. C. Fischer, U. T. Durig and D. W. Pohl: Appl. Phys. Lett., 52 (1988) 249.
- 3) U. Durig, D. W. Pohl and F. Rohner: J. Appl. Phys., 59 (1986) 3318.
- 4) R. C. Reddick, R. J. Warmack and T. L. Ferrell: Phys. Rev. B, 39 (1989) 767.
- 5) E. Betzig, M. Issacson and A. Lewis: Appl. Phys. Lett., 51 (1987) 2088.
- 6) D. Courjon and J. M. Vigoureux: Appl. Opt., 29 (1990) 3734.
- 7) J. M. Guerra: Appl. Opt., 29 (1990) 3741.
- 8) 岡本隆之，山口一郎：光学，19 (1990) 682.
- 9) 蔣曙東，富田直幸，大津元一：光学，20 (1991) 134.
- 10) 大津元一：Opt. E. 138 (1991) 90.
- 11) 大津元一：日本光学会，第28回サマーセミナー予稿集，(1991年8月)。
- 12) 西川治：応用物理，50 (1981) 807.
- 13) 蔣曙東，大澤日佐雄，P. トガル，山田和延，今井健策，猪飼篤，大津元一：応用物理学会講演会予稿集，(1991年10月)発表予定。
- 14) 富田直幸，蔣曙東，藤江嘉彦，中川賢一，大津元一，大澤日佐雄，大津元一：応用物理学会講演会，(1991年3月)，30pQ2/II。
- 15) S. Jiang, N. Tomita, K. Nakagawa and M. Ohtsu: Technical Digest of Conf. on Lasers and Electro-Optics, Baltimore, May 1991, paper no. CTh05.
- 16) S. Jiang, N. Tomita, H. Ohsawa and M. Ohtsu: Jpn. J. Appl. Phys., 30 (1991) 9月号，印刷中。
- 17) S. Jiang, N. Tomita, K. Nakagawa and M. Ohtsu: Proc. of the 3rd Optoelectronics Conference, MakuHari Messe, 1990, paper no. 12D1-3.
- 18) C.-H. Shin and M. Ohtsu: Opt. Lett., 15 (1990) 1455.
- 19) C.-H. Shin and M. Ohtsu: IEEE Photon. Tech. Lett., 2 (1990) 297.
- 20) D. Hils and J. L. Hall: Proc. of Frequency Standards and Metrology Sympo., ed. by A. De Marchi, Springer-Verlag, Berlin, (1988) 162.
- 21) P. F. Marella and R. F. Pease: Appl. Phys. Lett., 54 (1989) 2366.
- 22) J. Stone and L. W. Sultz: Electron. Lett., 23 (1987) 781.
- 23) J. Bergquist, NIST, USA, 私信, 1991.
- 24) M. Fukuma, I. Ogasawara, A. Nishimura and S. Suzuki: Proc. of the 6th International Conf. on Integrated Opt. and Opt. Fiber Commun., January 1987, Reno, Nevada, paper no. W17.
- 25) 矢島達夫：「光の量子効果」，(「量子力学と新技術」，第9章)，日本物理学会，培風館，(1987) 182.

- 26) K. Tanaka, A. Ikai and K. Kameyama: *J. Bio. Chem.*, 263 (1988) 16209.
- 27) 粕谷敬宏, 塚越幹郎: *応用物理*, 57 (1988) 1035.
- 28) 大津元一, 蔭曙東, 富田直幸, 中川賢一, 藤江嘉彦: *応用物理学会講演会予稿集*, (1990年9月) 27aL9/Ⅲ.
- 29) S. Jiang, N. Tomita, K. Nakagawa and M. Ohtsu: *Tech. Digest of Conf. on Lasers and Electro-Optics*, Baltimore, May 1991, paper no. CThO5.
- 30) D. M. Eigler and E. K. Schweizer: *Nature*, 344 (1990) 525.
- 31) D. Sesko, C. G. Fan and C. E. Wieman: *J. Opt. Soc. Am. B*, 5 (1988) 1225.
- 32) M. A. Kasevich, D. Weiss and S. Chu: *Opt. Lett.*, 15 (1990) 607.



特集●極限に挑む

# 光 STM による極微細加工技術

大津 元一

光が圧力をもっていることは古くから知られている。その圧力はきわめて小さいが、微粒子に対しては無視できない力を及ぼす。たとえば、彗星の尾がいつも太陽と反対の方向に向いているのは、太陽からの光の圧力で吹き飛ばされて、なびいているからと考えられている。このように天体现象では光の圧力の効果はよく知られている。ひるがえって、レーザー光について考えると、これは輝度とパワー密度が大きいので、微粒子に対しては大きな力を及ぼす。この原理についてはすでにいくつかの解説記事に記されているので<sup>1)2)</sup>、本稿では従来とは異なった特性をもつ光を作り、これによって原子1個ずつの運動を制御することについて述べる。

最近光により原子集団の運動を制御し真空中に捕獲する方法（「レーザー冷却による光糖蜜生成法」と呼ばれている<sup>3)</sup>）、さらにはマイクロ波電磁場を援用して1個のイオンの運動を制御し捕獲する方法（「イオントラップ法」と呼ばれている<sup>4)</sup>）が活発に研究され、とくに後者は1989年にノーベル物理学賞の受賞対象となったが、1個の中性原子の運動を制御することはまだ行われていない。本稿ではこれについての我々の提案と予備研究について紹介し、極微細加工技術への応用の可能性を示す。なお、この記事の内容の一部は他誌での解説の内容<sup>4)</sup>と重複することをご了承ください。

## 原子操作の道具としての光

レーザー光を1個の原子の運動制御の道具として使うには次の2項目を実現しなければならない。

- ①光周波数 $\nu$ を対象原子のもつ共鳴周波数 $\nu_r$ の値に設定でき、かつ $\nu$ の揺らぎが小さく、時間的に変動しないこと。
- ②光のエネルギーが極微空間に局在しており、エネルギー密度、エネルギー密度の空間的変化率、波数ベクトルの値、波数ベクトルの空間的変化率が大きいこと。

この2項目を実現するには周波数軸上および空間座標軸上で独特な性質をもつ光を発生させなければならない。

①を実現するために我々は半導体レーザーの注入電流、温度を自動制御し、さらに非線形光学素子を用いた周波数変換により $\nu$ を広範囲にわたり掃引し、 $\nu_r$ の値に設定することができた。同時に $\nu$ の揺らぎも抑圧できた。その結果、レーザーの発振スペクトル線幅 $\Delta\nu$ (揺らぎの少なさを表す尺度)の値として250 Hzを得ている<sup>5)</sup>。この $\Delta\nu$ の値は自動制御を施さない場合のレーザー固有の量子揺らぎの値の約 $1 \times 10^{-4}$ の値である（このようにレーザー固有の量子力学的揺らぎ以下の揺らぎをもつ光は「ハイパー・コヒーレント光」と呼ばれている<sup>6)</sup>）。さらに光学的制御も併用することにより $\Delta\nu=7\text{Hz}$ を得ている<sup>7)</sup>。ここで使ったレーザーの波長は830 nmなので $\nu=3.6 \times 10^{14}$  (Hz)であり、したがって、 $\nu/\Delta\nu=5 \times 10^{13}$ なる大きな値が得られたことになる（このスペクトル形状は図1中の挿入図に示されている）。図1には最近の我々の発振スペクトル線幅の狭窄化の実験の進歩の様子を示す。これらは世界のトップデータになっており、自動制御装置の改良により近い将来約58 mHzの値の実現が見込まれている<sup>8)</sup>。以上の詳細は文献9, 10を参考にされたい。

②を実現するために我々はフォトン走査トンネル顕微鏡のシステムを開発している<sup>11)</sup>。これは光の波長 $\lambda$ より小さな寸法をもつ試料形状を測定することができる光学顕微鏡である。図2(a)に示すように試料裏面から全反射条件を満たす入射角度でレーザー光を入射すると試料表面にはエバネッセント光と呼ばれる表面波が発生するのは衆知のとおりである<sup>12)</sup>。エバネッセント光は試料表面からの距離 $z$ の増加とともに急激に減少するので、 $z < \lambda$ なる位置で光パワーを測定すればそのパワー変化量から試料厚み方向の形状変化を高精度で測定できる。その際、直径が $\lambda$ より小さい開口を通過したエバネッセント光のパワーを測定する。 $z < \lambda$ なる位置では光の回折現象は生じないので開口を通過したエバネッセント光は開口直

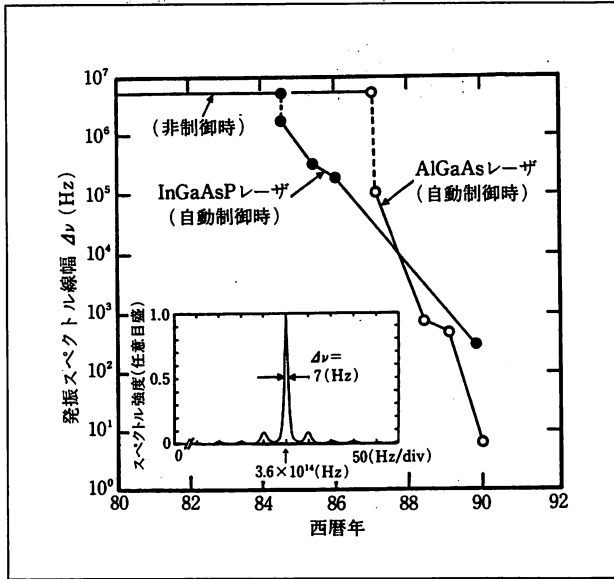


図1 半導体レーザーの発振スペクトル線幅  $\Delta\nu$  の狭窄化の研究の進歩の様子

下の試料表面から発生したものである。したがって、試料面内の形状測定の分解能は  $\lambda$  ではなく開口直径によってきまる。従来の光学顕微鏡の分解能は光の回折現象のために、 $\lambda$  程度の値であることは古くから知られている光学の常識であるが<sup>12)</sup>、ここではエバネッセント光、すなわち極微空間に局在した光を用いることによってこの常識をくつがえし、高分解能が実現する。

我々はエッチングにより先端を先鋭化した光ファイバを開口として用いている。光ファイバ先端の曲率半径  $a$  が  $\lambda$  以下であれば通常の伝搬光は先端を通過し得ず（光導波路の用語を使うと「遮断」していると表現できる）、通過するのはエバネッセント光のみであるので、開口よりも先端を先鋭化した光ファイバを用いる方が加工技術上および次節で示す応用上都合がよい。写真1にその光ファイバ先端の電子顕微鏡写真を示す<sup>12)</sup>。先端角は25度である。先端曲率半径  $a$  は10 nm以内と推定されるが、電子顕微鏡の分解能が不十分なほど小さくなっている。この光ファイバ（以後「ファイバ・プローブ」と呼ぶ）を図2 (b) に示すようにピエゾアクチュエータにより試料上方  $z \approx 10 \sim 20$  nm で試料面内方向に走査して試料形状を測定する。ここで光源として使っている半導体レーザーの波長  $\lambda$  は780 nmである。ファイバ・プローブの走査方法は従来の走査トンネル顕微鏡と同様であるが、本装置は空気中でも測定できること、非導電性試料でも測定できることなどの利点を有する。写真2は直径80 nm(約

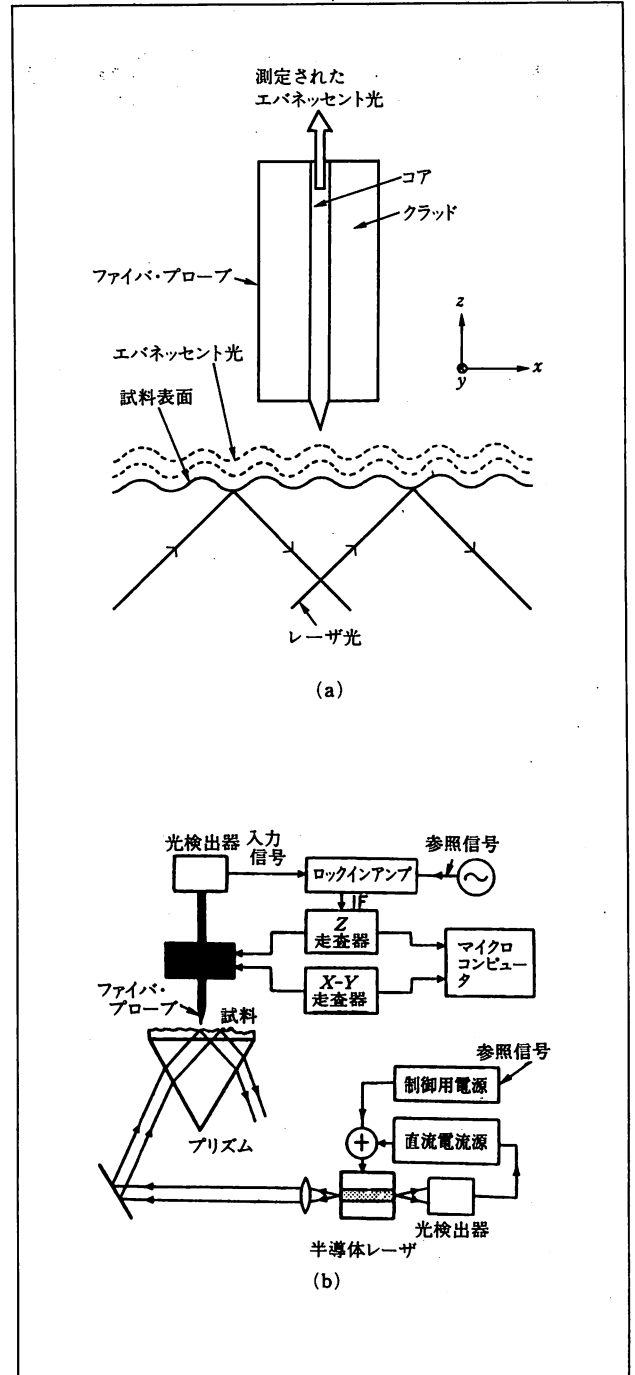
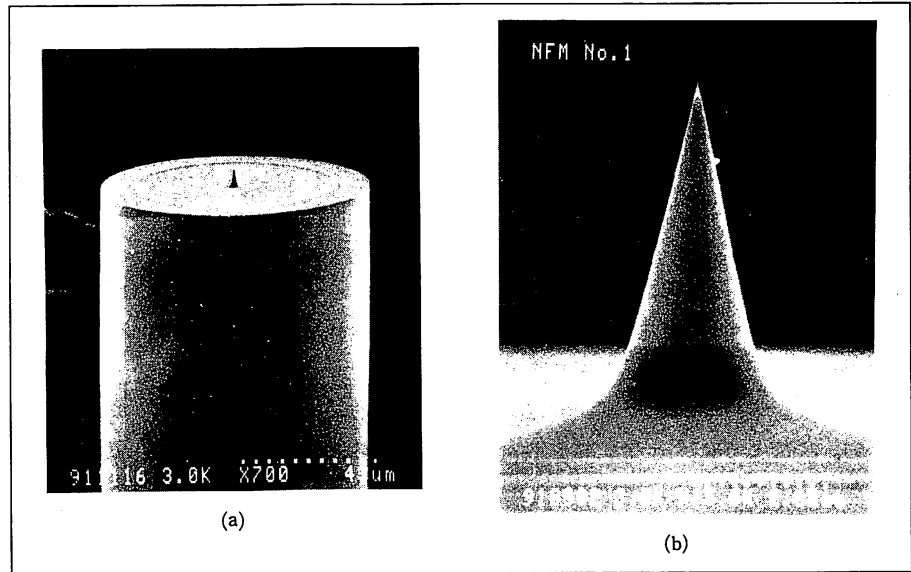


図2 フォトン走査トンネル顕微鏡の説明。(a)原理図。(b)装置図

$\lambda/10$ の値) のラテックス球（ポリスチレン球）をガラス板の上に多数並べたものの像を示す<sup>11)</sup>。通常、ラテックス球はガラス板上では互いに凝集してしまうために、多数の球が測定視野の中にみえ、一部分は変形してしまっている。しかし、明瞭な像が得られていることがわかる。

さらに、生体試料の1つであるバクテリオファージ

写真1 コア先端を先鋭化した光ファイバの電子顕微鏡写真。(a)ファイバ端全体図。ファイバ直径は約90  $\mu\text{m}$ 。(b)尖らせたファイバ先端の拡大図。写真の幅は5.6  $\mu\text{m}$



T4の像もこの装置により測定されている<sup>13)</sup>。これは頭部(径約100 nm)、尾部(幅9 nm、長さ100 nm)をもつがその尾部の像も明瞭に得られている。以上の一連の測定により、本装置は厚み方向分解能2 nm以内、面内分解能5 nm以内をもつと評価されている。より詳細な量子光学的議論によると、本装置の原理は原子間力走査トンネル顕微鏡と同等であり、したがって原子の寸法程度の分解能を実現することが可能であると推定されている<sup>13)</sup>。

さて、1個の原子の運動の制御・操作にはこのファイバ・プローブを用いる。つまり、ファイバ・プローブ後端からレーザー光を入射させ、先端に発生するエバネッセント光を用いる。このエバネッセント光の存在する空間は $\lambda^3$ 以下の体積内にあるので上記②を満たす。ここで、使用する光源として、我々がすでに開発している上記①を満たすものを用いる。

### 1個の原子の運動の制御・操作

真空中に浮遊する原子をファイバ先端のエバネッセント光の場の中に捕獲する。ファイバ後端から入射したレーザー光のうち通常の伝搬光はファイバ先端の尖った部分には到達せず、したがって出射しない。エバネッセント光のみがファイバ先端に絡みついている。そのパワーは小さいが、局在している空間体積が $\lambda^3$ 以下であるので、そのパワー密度の値、パワー密度の空間的変化率は大きい。さらに、その波数ベクトルはファイバ・プローブ先端表面に平行であり、その値は大きい。さらにその空間的変化率も大きい。ちなみに40 mWのパワーをもつレ

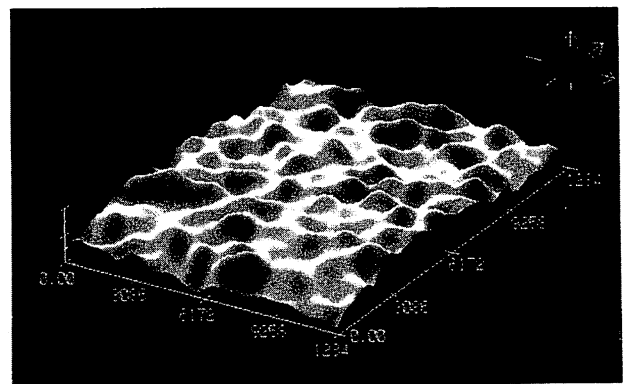


写真2 ガラス板上に固定した直径80 nmのラテックス球集団のフォトン走査トンネル顕微鏡像<sup>11)</sup>。視野の1辺は1.0  $\mu\text{m}$

ーザ光をファイバ後端から入射させると写真1のファイバ・プローブ先端のエバネッセント光のパワー密度は100 W/cm<sup>2</sup>以上にも達する。

いまレーザー周波数 $\nu$ を $\nu_r$ よりもわずかに小さい値になるように調節しておく。目安として $\nu - \nu_r \approx -(\gamma \sim 10 \gamma)$ (ここで $\gamma$ は原子共鳴線の幅)とする。この光の場に1個の原子が飛び込んだとき、原子は吸収と自然放出とを介して光と相互作用するが、この相互作用の結果生じる原子の運動状態を考える。ファイバ・プローブ先端は曲率を有するので極座標表示を用いた方が計算の際に有利と思われるが、ここでは直感的なイメージを抱いていたために直交座標系を用いて説明する。

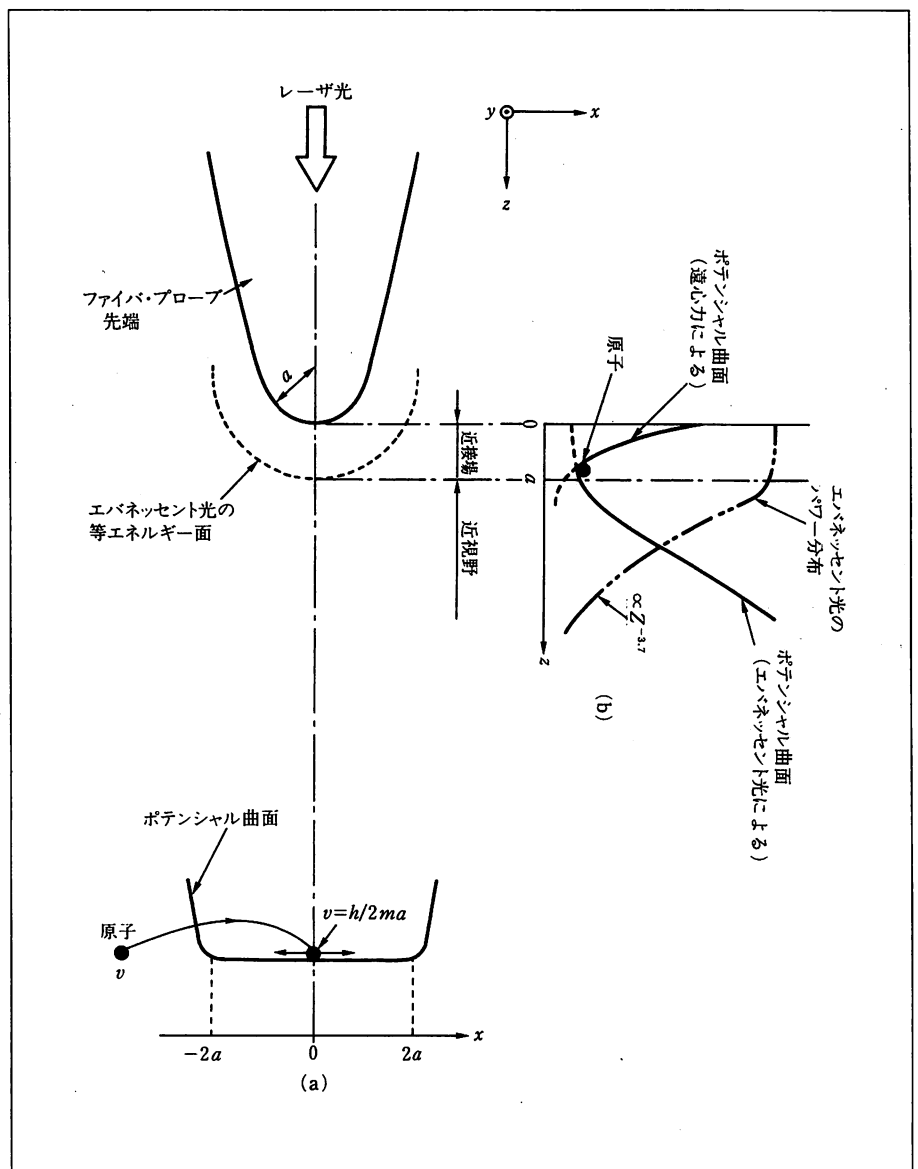
ファイバ・プローブ軸(z方向)とは垂直方向(x方向)の原子の運動状態を与えるポテンシャル曲面は図3(a)

に示すようになる。このポテンシャル中に原子が外部から  $x$  方向に速度  $v$  で飛び込む場合を考える。この原子は光の場の中に入射する位置、方向にかかわらず、必ず前方、後方から光が照射される。これはファイバ・プローブ形状の軸対称性とエバネッセント光の波数ベクトルがファイバ・プローブ表面に平行であることによる。ドブラー効果のために、原子からみると前方からの光の周波数は  $\nu + v/a$  ( $a$  は前節でも示したようにファイバ・プローブ先端の曲率半径) となる。このドブラーシフト量  $v/a$  は自由空間を伝搬する通常の光による値  $\nu v/c$  ( $c$  は光の速度) ではなく、その  $\lambda/a$  ( $\gg 1$ ) 倍であることに注意されたい。このように大きなドブラーシフトを誘起するこ

とはここで使用しているエバネッセント光のもつ特徴、すなわち、非伝搬光のもつ波数ベクトル値が大きいこと、いいかえればエバネッセント光は質量をもつ光子 (フォトン) であることに起因している。

したがって、 $\nu + v/a$  が  $\nu_r$  に等しければ原子はこの光を吸収する。その後原子は自然放出により光を発するが、その周波数は  $\nu_r$  である。したがって、これらの吸収と放出により原子はドブラーシフト  $v/a$  の大きさに比例したエネルギー量  $h\nu/a$  ( $h$  はプランクの定数) を失い、減速する。一方、後方から照射された光が原子に吸収される量子力学的確率は小さい。これはドブラーシフトの符号が上記の値の場合と逆で、かつ  $\nu < \nu_r$  となるように

図3 原子に対するエバネッセント光のポテンシャル曲面。(a)ファイバ・プローブ軸 ( $z$  軸) と垂直面内のポテンシャル曲面。(b)  $z$  軸方向のポテンシャル曲面 (エバネッセント光パワーの  $z$  方向依存性も併記している)



設定してあることによる。こうして、原子は減速しながら、ポテンシャル曲面の中央部に達し、最終速度は  $h/2ma$  ( $m$  は原子の質量) になる。

この減速した原子がポテンシャル中央部でさらに光を吸収・放出すると  $\pm h/2ma$  の速度でポテンシャル曲面内を左右に動く。このポテンシャル曲面の縁に近づくと、ポテンシャル曲面の縁部では原子の速度はファイバ・プローブ先端形状の曲率半径  $a$  の値に依存する大きさの  $z$  方向成分をもつので、後述する  $z$  方向に関する吸引力に対応するポテンシャルの影響が現れ始める。このことは図3(a)のポテンシャル曲面の縁部には高いポテンシャル障壁があることに対応し、したがって、原子はこの縁から外へは出ない。このようにして原子はファイバ・プローブ先端の  $z$  軸を中心とし、半径が  $2a$  に相当する円形面内に捕獲され、原子はこの面内のどこかに見いだされる。ここでアルカリ金属原子を例にとり、上記の最終速度  $h/2ma$  の値を求めると  $0.2\text{ m/s}$  となる。ただし、ここでは  $a=10\text{ nm}$  とした。この速度値に対応する熱運動の等価温度  $T_{eq}$  は約  $0.1\text{ mK}$  となる。すなわち、絶対零度に近い超冷却原子が1つ半径  $2a$  の面内を動き回っていることになる。

一方、光の場の中にある原子のもつポテンシャルエネルギーの  $z$  方向依存性は図3(b)のようになる。 $\nu < \nu_r$  と

なるように設定してあるので、このポテンシャルにより原子はファイバ・プローブの方へ引き付けられる引力を受ける。同図にはエバネッセント光パワーの  $z$  依存性も示した。 $0 < z < a$  の領域は近接領域 (Proximate Region) と呼ばれ、パワーは  $z$  にはよらずほとんど変化しない。 $a < z < \lambda$  の領域は近視野領域 (Near Field Region) と呼ばれ、パワーは  $z^{-3.7}$  に比例して変化する<sup>13)</sup>。すなわち、 $z \approx a$  に変曲点をもつ。したがって、原子のポテンシャル曲線も変曲点をもつので、原子はこの点で光から最も大きな力を受ける。一方、 $z < a$  では原子運動のもつ遠心力が大きくなる。したがって、原子は上記ポテンシャルによる引力があってもファイバ・プローブ表面に吸着される位置まで近づくことはない。このようにして原子はエバネッセント光によってファイバ先端から  $z \approx a$  なる位置に捕獲される。

ここで再びアルカリ金属原子を例にとり、原子の捕獲のポテンシャルの深さ  $\Delta W$  を原子の熱運動の等価温度  $T_{eq}$  ( $\equiv \Delta W/k_B$ ;  $k_B$  はボルツマン定数) により表すと、ファイバに入射するレーザーパワーが  $40\text{ mW}$  のとき、 $T_{eq}=1\text{ mK}$  となる。このことは逆に、原子を  $1\text{ mK}$  以下まで予備冷却しておかなければならないことを意味する。しかし、図4に示すように最近活発に研究が行われている「レーザー冷却による光糖蜜生成法」を使えば、原

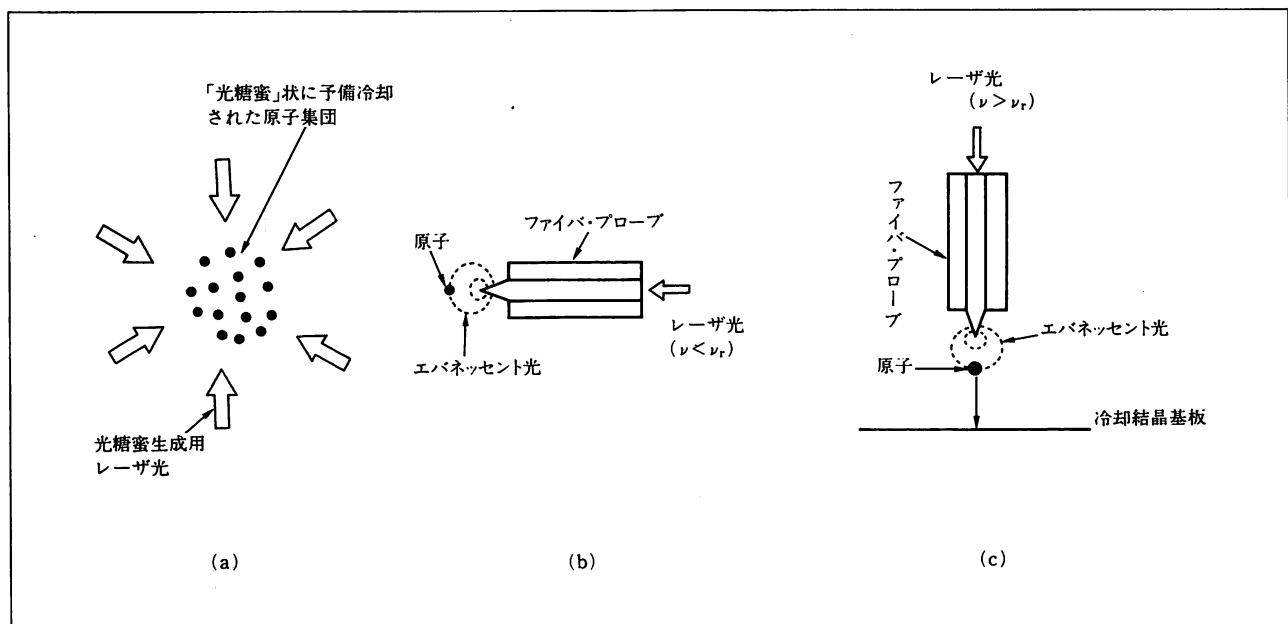


図4 単原子レベルの結晶成長法の説明。(a)第1段階、「レーザー冷却による光糖蜜生成法」による予備冷却原子集団の形成。(b)第2段階、予備冷却された原子集団中の1個の原子をファイバ・プローブ先端のエバネッセント光により捕獲。(c)第3段階、冷却結晶基板上への捕獲原子の押し出し・固定

子を数  $\mu\text{K}$  まで冷却できる<sup>1)</sup>のでこれは問題ではない。また、原子間の反発力があるので複数個の原子が捕獲されることもない。さらに原子を光の場の中に捕獲したか否かは蛍光観測などにより容易に判断できる。捕獲した原子をファイバ・プローブとともに冷却結晶基板上方に運び、 $\nu = \nu_0 + \gamma$  となるようにレーザー周波数値を増加させれば原子は加熱・加速され押し出され、基板に落下し、ファンデルワールス力またはこのほかの化学結合力により冷却結晶基板上に固定される。すなわち、単原子レベルでの結晶成長が可能である。

従来、トンネル電子を使った走査トンネル顕微鏡のプローブにより結晶基板上で原子を移動したり、原子を除去する試みが報告されているが、対象となる原子の種類が不活性気体原子などに限られている。それに対し本方法は前述の光の性質①に注意すると、対象とする原子の共鳴遷移周波数値に同調する光を用意することができる。したがって、半導体素子工学分野で重要なシリコン、ゲルマニウム、ヒ素などの原子についても適用可能であり、対象原子の種類がきわめて多い点に特長を有する。

## その他の応用の可能性と問題点

現在の半導体レーザー光パワーは1 W以上が実現しており、これらの高パワーを使うと前節の単原子結晶成長以外にも広範な応用が期待される。すなわち、サブミクロン線幅の光記録、局所的レーザーアニーリング、レーザートリミングなどである。とくにエバネッセント光のエネルギーの変化方向と波数ベクトルの方向とは異なるので、単なる原子捕獲のみでなく、微粒子の並進、回転運動などを制御することが可能である。すなわち、運動の制御の自由度が大きいためマイクロマシンの駆動などへの利用可能性を有する。さらに、生命理工学分野では蛋白分子の熱運動制御などに使える可能性もある。このように周波数揺らぎが小さく、極微空間に局在した光の応用可能範囲はひろい。

物質との相互作用を念頭においたエバネッセント光の特性の理論モデルの構築は現時点ではあまり進んでいない。それは本稿のように体積が  $\lambda^3$  以下の領域での光の振る舞いを議論する必要がある実験がなかったからである。しかし、本稿に記した実験の進歩とともにその理論モデルの構築が不可欠になった。その場合、光を波動とみなすよりも光子(フォトン)とみなした方が見通しがよい。とくにエバネッセント光は物質からわずかにしみだした光なので「トンネル光子」に対応する。我々はこ

の考えに基づいて理論モデルの構築を試みているが、この詳細については別の機会に紹介させていただければ幸いである。

## まとめ

周波数揺らぎが少なく、かつ空間的に局在した光を用いて1個の原子の運動を制御・操作するための我々の試みについて概説したものであり、極微細加工をはじめとして広範な応用が期待できるが、本研究を進歩させるには実験、理論ともに並行して遂行し、かつ学際的な相互協力が必要である。本誌の読者諸兄のご指導・ご鞭達をお願いしたい。

**謝辞** 本稿中、フォトン走査トンネル顕微鏡の理論に関しては山梨大学工学部の堀裕和先生のご指導を得た。実験に関しては本学学生、蔣曙東、P.トガール、山田和延の各氏、さらに憐ニコンの大澤日佐雄氏のご協力を得た。ここに深く感謝する。なお、本研究の一部は文部省科学研究費補助金一般研究B(課題番号03452089)により行われた。

## 参考文献

- 1) 清水富士夫：応用物理，**60** (1991) 864
- 2) 藪崎 努：パリティ，**6** (1991) 66
- 3) W.M. Itano, J.C. Bergquist, and D.J. Wineland : Science, **237** (1987) 612
- 4) 大津元一：精密工学会会誌，**58** (1992) 3号，印刷中
- 5) M. Kourogi, C.-H. Shin, and M. Ohtsu : IEEE Photonics Technol. Lett., (1991) 496
- 6) 大津元一：サイエンス，1989年3月号，64
- 7) C.-H. Shin and M. Ohtsu : Opt. Lett., **15** (1990) 1455
- 8) M. Ohtsu and N. Tabuchi : J. Lightwave Technol., **6** (1988) 357
- 9) 大津元一：“コヒーレント光量子工学”，朝倉書店(1990)
- 10) M. Ohtsu : “Highly Coherent Semiconductor Lasers”, Artech House Inc., (1991)
- 11) S. Jiang, N. Tomita, H. Ohsawa and M. Ohtsu : Jpn. J. Appl. Phys., **30** (1991) 2107
- 12) M. Born and E. Wolf : “Principles of Optics”, Fourth Edition, Pergamon Press (1970)
- 13) S. Jiang, H. Ohsawa, N. Tomita and M. Ohtsu : Tech. Digest of Annual Meeting of Opt. Soc. Am., Nov. 1991, San Jose, CA, 65
- 14) U. Durig, D.W. Pohl and F. Rohner : J. Appl. Phys., **59** (1986) 3318

(おおつ・もといち/東京工業大学大学院総合理工学研究科)

解説 ■ 大津元一\*\*

# 光による単一原子の運動制御\*

*Control of Atomic Motion by Light / Motoichi OHTSU*

Key words: laser, coherent, photon STM, Doppler-shift, trapping

## 1. ま え が き

光が圧力を持っていることは古くから知られている。その圧力はきわめて小さいが、微粒子に対しては無視できない力を及ぼす。例えば、彗星の尾がいつも太陽と反対の方向に向いているのは、太陽からの光の圧力で吹きとばされて、なびいているからと考えられている。このように天体現象では光の圧力の効果はよく知られている。ひるがえって、レーザー光について考えると、これは輝度、パワー密度が大きいので、微粒子に対して大きな力を及ぼす。この原理については本号の霜田の解説記事に記されているので、本稿では従来とは異なった特性を持つ光を作り、これによって原子1個ずつの運動を制御することについて述べる。

最近では光により原子集団の運動を制御し真空中に捕獲する方法（「レーザー冷却による光糖蜜生成法」と呼ばれている<sup>1)</sup>）、さらにはマイクロ波電磁場を援用して1個のイオンの運動を制御し捕獲する方法（「イオントラップ法」と呼ばれている<sup>2)</sup>）が活発に研究され、特に後者は1989年にノーベル物理学賞の受賞対象となったが、1個の中性原子の運動を制御することはまだ行われていない。本稿ではこれについての我々の提案と予備研究についてご紹介する。

## 2. 原子操作の道具としての光

レーザー光を1個の原子の運動制御の道具として使うには次の2項目を実現しなければならない。

① 光周波数 $\nu$ を対象原子のもつ共鳴周波数 $\nu_r$ の

値に設定でき、かつ $\nu$ の揺らぎが小さく、時間的に変動しないこと。

② 光のエネルギーが極微空間に局在しており、エネルギー密度、エネルギー密度の空間的变化率、波数ベクトルの空間的变化率、が大きいこと。

この2項目を実現するには各々周波数軸上及び空間座標軸上で独特な性質をもつ光を発生させなければならぬ。①を実現するために我々は半導体レーザーの注入電流、温度を自動制御し、さらに非線形光学素子を用いた周波数変換により $\nu$ を広範囲にわたり掃引し、 $\nu_r$ の値に設定することができた。同時に $\nu$ の揺らぎも抑圧できた。その結果、レーザーの発振スペクトル線幅 $\Delta\nu$ （揺らぎの少なさを表す尺度）の値として250 Hzを得ている<sup>3)</sup>。波長1  $\mu\text{m}$ のレーザー光では $\nu = 3 \times 10^{14}$  Hzなので、この場合、 $\nu/\Delta\nu \approx 1 \times 10^{12}$ なる大きな値が得られたことになる。この $\Delta\nu$ の値は自動制御を施さない場合のレーザー固有の量子揺らぎの値の約 $1 \times 10^{-4}$ の値である（このようにレーザー固有の量子力学的揺らぎ以下の揺らぎをもつ光は「ハイパーコヒーレント光」と呼ばれている<sup>4)</sup>）。さらに光学的制御も併用することにより7 Hzを得ている<sup>5)</sup>。これらは世界のトップデータになっており、自動制御装置の改良により近い将来約58 mHzの値の実現が見込まれている<sup>6)</sup>。

②を実現するために我々はフォトン走査トンネル顕微鏡のシステムを開発している<sup>7)</sup>。これは光の波長 $\lambda$ より小さな寸法をもつ試料形状を測定することができる光学顕微鏡である。図1に示すように試料裏面より全反射条件を満たす入射角度でレーザー光を入射すると試料表面にはエバネッセント光と呼ばれる表面波が発生するのは周知のとおりである<sup>8)</sup>。エバネッセント

\* 原稿受付 平成4年1月8日

\*\* 東京工業大学大学院総合理工学研究科（横浜市緑区長津田町4259）

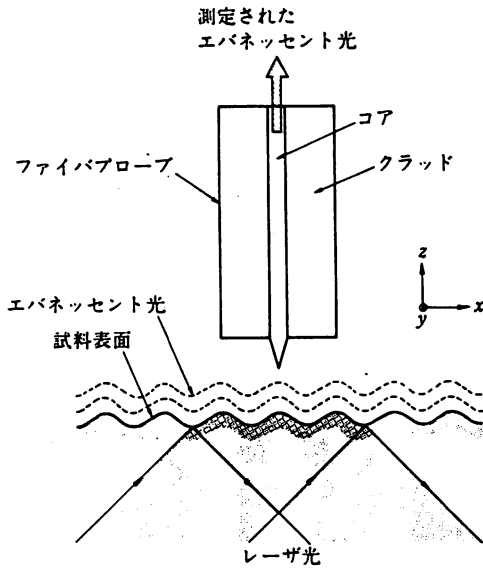
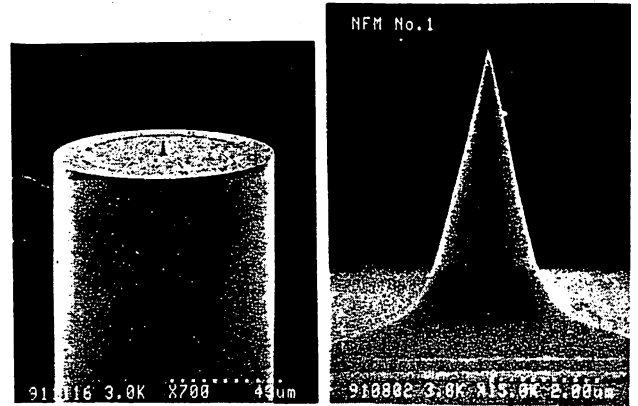


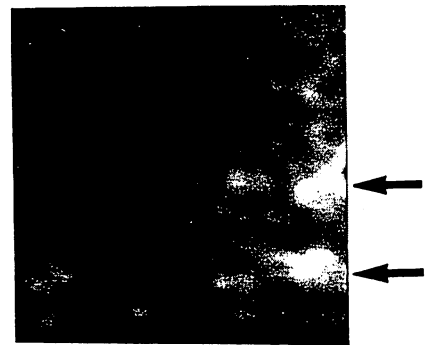
図1 フォトン走査トンネル顕微鏡の原理図

光は試料表面からの距離  $z$  の増加とともに急激に減少するので、 $z < \lambda$  なる位置で光パワーを測定すればそのパワー変化量から試料厚み方向の形状変化を高精度で測定できる。その際、直径が  $\lambda$  より小さい開口を通過したエバネッセント光のパワーを測定する。 $z < \lambda$  なる位置では光の回折現象は生じないので開口を通過したエバネッセント光は開口直下の試料表面から発生したものである。従って、試料面内の形状測定の分解能は  $\lambda$  ではなく開口直径によって決まり、従来の光学顕微鏡では得られない高い分解能が実現する。

我々はエッチングにより先端を研磨した光ファイバを開口として用いている。図2(a)にその光ファイバ先端の電子顕微鏡写真を示す<sup>9)</sup>。先端角は  $25^\circ$  である。先端曲率半径  $a$  は  $10 \text{ nm}$  以内と推定されるが、電子顕微鏡の分解能が不十分なほど小さくなっている。この光ファイバ（以後「ファイバプローブ」と呼ぶ）を試料上方  $z \approx 10 \sim 20 \text{ nm}$  で試料面内方向に走査して試料形状を測定する。ここで光源として使っている半導体レーザの波長  $\lambda$  は  $780 \text{ nm}$  である。ファイバプローブの走査方法は従来の走査トンネル顕微鏡と同様であるが、本装置は空気中でも測定できること、非導電性試料でも測定できること、などの利点を有する。図2(b)は生体試料の1つであるバクテリオファージ T4 の像をこの装置により測定した結果を示す<sup>9)</sup>。矢印で示すように頭部（径約  $100 \text{ nm}$ ）、尾部（幅  $9 \text{ nm}$ 、長さ  $100 \text{ nm}$ ）をもつ二つのバクテリオファージ T4 の像が明瞭に測定されている。これら一連の測定により、厚み方向分解能  $2 \text{ nm}$  以内、面内分解能  $5 \text{ nm}$  以内と評価されている。より詳細な量子光学的議論によると、本装置の原理は原子間力走査トンネル顕微鏡



(a)



(b)

- (a) とがらせたファイバ先端の電子顕微鏡写真<sup>9)</sup>
- (左) ファイバ端全体図。ファイバ直径は約  $90 \mu\text{m}$
- (右) とがらせたファイバ先端の拡大図。写真の幅は  $5.6 \mu\text{m}$
- (b) バクテリオファージ T4 の像<sup>9)</sup>。2本の矢印の先にバクテリオファージ T4 が2体見える。この写真の一辺は  $0.6 \mu\text{m}$

図2

と同等であり、従って原子の寸法程度の分解能を実現することが可能であると推定されている<sup>9)</sup>。

さて、1個の原子の運動の制御・操作にはこのファイバプローブを用いる。つまり、ファイバプローブ後端よりレーザ光を入射させ、先端に発生するエバネッセント光を用いる。このエバネッセント光の存在する空間は  $\lambda^3$  以下の体積内にあるので上記②を満たす。ここで、使用する光源として、我々がすでに開発している上記①を満たすものを用いる。

### 3. 1個の原子の運動の制御・操作

真空中に浮遊する原子をファイバ先端のエバネッセント光の場の中に捕獲する。ファイバ後端から入射したレーザ光のうち通常の伝搬光はファイバ先端のところがった部分には到達せず、従って出射しない。エバネッセント光のみがファイバ先端に絡みついている。そのパワーは小さいが、局在している空間体積が  $\lambda^3$  以下であるので、そのパワー密度の値、パワー密度の



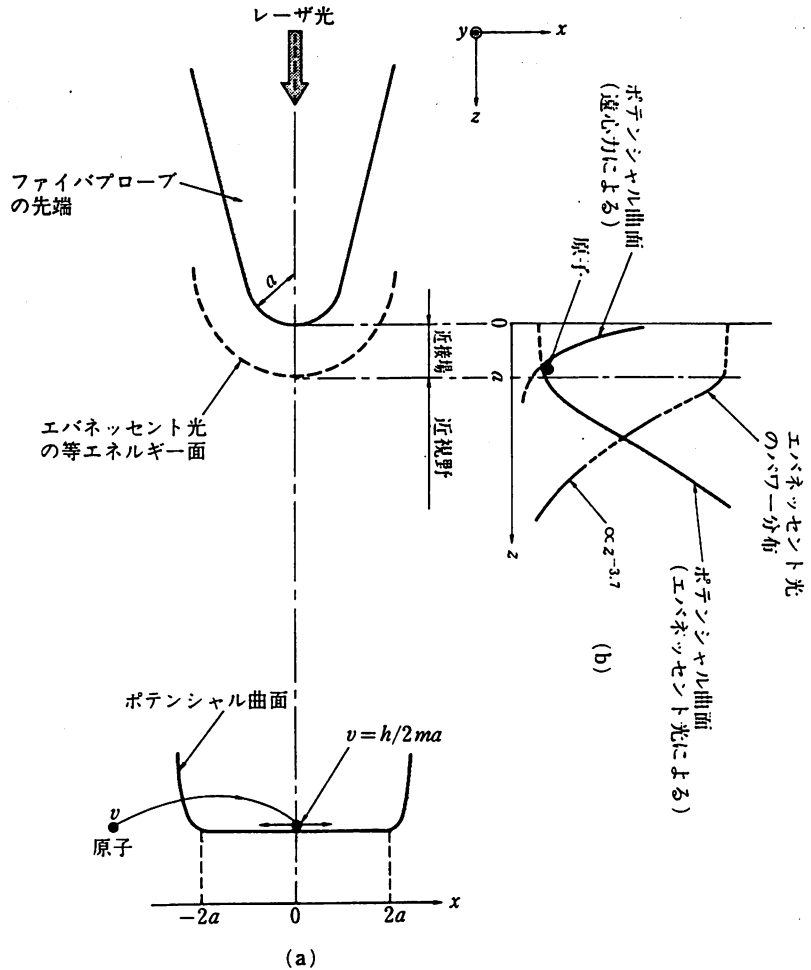
空間的変化率は大きい。さらに、その波数ベクトルはファイバプローブ先端表面に平行であり、その空間的変化率が大きい。ちなみに40 mWのパワーをもつレーザー光をファイバ後端から入射させると図2(a)のファイバプローブ先端のエバネッセント光のパワー密度は100 W/cm<sup>2</sup>以上にも達する。

いま $\nu$ を $\nu_r$ よりもわずかに小さい値になるようにレーザー周波数を調節しておく。目安として $\nu - \nu_r \approx -(\gamma \sim 10\gamma)$  (ここで $\gamma$ は原子共鳴線の幅)とする。この光の場に1個の原子が飛び込んだとき、原子は吸収と自然放出とを介して光と相互作用するが、この相互作用の結果生じる原子の運動状態を考える。ファイバプローブ先端は曲率を有するので極座標表示を用いた方が計算の際に有利と思われるが、ここでは直感的なイメージを抱いて頂くために直交座標系を用いて説明する。

ファイバプローブ軸(z方向)とは垂直方向(x方向)の原子の運動状態を与えるポテンシャル曲面は図3(a)に示すようになる。このポテンシャル中に原子が外部よりx方向に速度 $v$ で飛び込む場合を考える。

この原子は光の場の中に入射する位置、方向にかかわらず、必ず前方、後方から光が照射される。これはファイバプローブ形状の軸対称性とエバネッセント光の波数ベクトルがファイバプローブ表面に平行であることによる。ドブラー効果のために、原子から見ると前方からの光の周波数は $\nu + v/a$  ( $a$ は前節でも示したようにファイバプローブ先端の曲率半径)となる。このドブラーシフト量 $v/a$ は自由空間を伝搬する通常の光による値 $\nu v/c$  ( $c$ は光の速度)ではなく、その $\lambda/a$  ( $\gg 1$ ,  $\lambda$ は光の波長)倍であることに注意されたい。このように大きなドブラーシフトを誘起することはここで使用しているエバネッセント光のもつ特徴、すなわち、非伝搬光のもつ波数ベクトル値が大きいこと、いいかえればエバネッセント光は質量をもつ光子であること、に起因している。

従って、 $\nu + v/a$ が $\nu_r$ に等しければ原子はこの光を吸収する。その後原子は自然放出により光を発する



(a) ファイバプローブ軸(z軸)と垂直面内のポテンシャル曲面  
 (b) z軸方向のポテンシャル曲面(エバネッセント光パワーのz軸方向依存性も併記している)  
 図3 原子に対するエバネッセント光のポテンシャル曲面

が、この周波数は $\nu_r$ である。従って、これらの吸収と放出とにより原子はドブラーシフト $v/a$ の大きさに比例したエネルギー量 $h\nu/a$  ( $h$ はプランクの定数)を失い、減速する。一方、後方から照射された光が原子に吸収される量子力学的確率は小さい。これはドブラーシフトの符号が上記の値の場合と逆で、かつ $\nu < \nu_r$ となるように設定してあることによる。こうして、原子は減速しながら、ポテンシャル曲面の中央部に達し、最終速度は $h/2ma$  ( $m$ は原子の質量)になる。

この減速した原子がポテンシャル中央部でさらに光を吸収・放出すると $\pm h/2ma$ の速度でポテンシャル曲面内を左右に動く。このポテンシャル曲面の縁に近づくと、ポテンシャル曲面の縁部では原子の速度はファイバプローブ先端形状の曲率半径 $a$ の値に依存する大きさのz方向成分をもつので、後述するz方向に関する吸引力に対応するポテンシャルの影響が現れ始める。このことは図3(a)のポテンシャル曲面の

縁部には高いポテンシャル障壁があることに対応し、従って、原子はこの縁から外へは出ない。このようにして原子はファイバプローブ先端の $z$ 軸を中心とし、半径が $2a$ に相当する円形面内に捕獲され、原子はこの面内のどこかに見いだされる。ここでアルカリ金属原子を例にとり、上記の最終速度 $h/2ma$ の値を求めると $0.2\text{ m/s}$ となる。ただし、ここでは $a=10\text{ nm}$ とした。この速度値に対応する熱運動の等価温度 $T_{\text{eq}}$ は約 $0.1\text{ mK}$ となる。すなわち、絶対零度に近い超冷却原子が1つ半径 $2a$ の面内を動き回っていることになる。

一方、光の場の中にある原子の持つポテンシャルエネルギーの $z$ 方向依存性は図3(b)のようになる。 $\nu < \nu_c$ となるように設定してあるので、このポテンシャルにより原子はファイバプローブの方へ引き付けられる引力を受ける。同図にはエバネッセント光パワーの $z$ 依存性も示した。 $0 < z < a$ の領域は近接領域(Proximate Region)と呼ばれ、パワーは $z$ にはよらずほとんど変化しない。 $a < z < \lambda$ の領域は近視野領域(Near Field Region)と呼ばれ、パワーは $z^{-3.7}$ に比例して変化する<sup>10)</sup>。一方、 $z < a$ では図3(a)のポテンシャル曲面内を動きまわる際に原子が受ける遠心力が大きくなる。従って、原子は上記ポテンシャルによる引力があってもファイバプローブ表面に吸着される位置まで近づくことはない。このようにして原子はエバネッセント光によってファイバ先端から $z=a$ なる位置に捕獲される。

ここで再びアルカリ金属原子を例にとり、原子の捕獲のポテンシャルの深さ $\Delta W$ を原子の熱運動の等価温度 $T_{\text{eq}}$ ( $\equiv \Delta W/k_B$ ;  $k_B$ はボルツマン定数)により表すと、ファイバに入射するレーザーパワーが $40\text{ mW}$ のとき、 $T_{\text{eq}}=1\text{ mK}$ となる。このことは逆に、原子を $1\text{ mK}$ 以下まで予備冷却しておかなければならないことを意味する。しかし、最近活発に研究が行われている「レーザー冷却による光糖蜜生成法」を使えば、原子を数 $\mu\text{K}$ まで冷却できる<sup>11)</sup>のでこれは問題ではない。また、原子間の反発力があるので複数個の原子が捕獲されることもない。さらに原子を光の場の中に捕獲したか否かは蛍光観測などにより容易に判断出来る。捕獲した原子をファイバプローブとともに冷却結晶基板上方に運び、 $\nu = \nu_c + \gamma$ となるようにレーザー周波数値を増加させれば原子は加熱・加速され押し出され、基板に落下し、ファンデルワールス力またはその他の化学結合力により冷却結晶基板上に固定される。すなわち、単原子レベルでの結晶成長が可能である。

#### 4. その他の応用可能性と問題点

現在の半導体レーザーの光パワーは $1\text{ W}$ 以上が実現しており、これらの高パワーを使うと前節の単原子結晶成長以外の広範な応用が期待される。特に、エバネッセント光のエネルギーの変化方向と波数ベクトルの変化方向とは異なるので、単なる原子捕獲のみでなく、微粒子の並進、回転運動などを制御することが可能である。従ってマイクロマシンの駆動などへの利用可能性を有する。さらに、生命理工学分野では蛋白分子の熱運動制御などに使える可能性もあり、周波数揺らぎが小さく、極微空間局在した光の応用可能範囲は広い。

物質との相互作用を念頭においたエバネッセント光の特性の理論モデルの構築は現時点ではあまり進んでいない。それは本稿のように体積が $\lambda^3$ 以下の領域での光の振舞いを議論する必要がある実験がなかったからである。しかし、本稿に記した実験の進歩とともにその理論モデルの構築が不可欠になった。この場合、光を波動とみなすよりも光子(フォトン)と見なした方が見通しがよい。とくにエバネッセント光は物質からわずかにしみだした光なので「トンネル光子」に対応する。我々はこの考えに基づいて理論モデルの構築を試みているが、この詳細については別の機会にご紹介させて頂ければ幸いである。

#### 5. ま と め

周波数揺らぎが少なく、かつ空間的に局在した光を用いて1個の原子の運動を制御・操作するための我々の試みについて概説した。この試みはわが国で生まれ育っているものであり、新しい精密工学分野をはじめとして広範な応用が期待できるが、本研究を進歩させるには実験、理論ともに平行して遂行し、かつ学際的な相互協力が必要である。本稿の読者諸兄のご指導・ご鞭撻をお願いしたい。

#### 謝 辞

本稿中、フォトン走査トンネル顕微鏡の理論に関しては山梨大学工学部の堀裕和先生のご指導を得た。実験に関しては本学学生、蔭曙東、P.トガール、山田和延の各氏、さらに(株)ニコンの大澤日佐雄氏のご協力を得た。ここに深く感謝いたします。なお、本研究の一部は文部省科学研究費補助金一般研究B(課題番号03452089)により行われた。

## 文 献

- 1) 清水富士夫：原子のレーザー冷却とその周辺技術，応用物理，60，9 (1991) 864.
- 2) W. M. Itano, J. C. Bergquist and D. J. Wineland：Laser Spectroscopy of Trapped Atomic Ions, Science, 237, (Aug. 1987) 612.
- 3) M. Kourogi, C. -H. Shin and M. Ohtsu：A 250 Hz Spectral Linewidth 1.5  $\mu\text{m}$  MQW-DFB Laser Diode with Negative-Electrical-Feedback, IEEE Photonics Technol. Lett., 3, 6, (1991) 496.
- 4) 大津元一：ハイパー・コヒーレント光の実現，サイエンス，日経サイエンス社，1989年3月号，p. 64.
- 5) C. -H. Shin and M. Ohtsu：Stable Semiconductor Laser with a 7-Hz Linewidth by an Optical-electrical Double-feedback Technique, Opt. Lett., 15, 24, (1990) 1455.
- 6) M. Ohtsu and N. Tabuchi：Electrical Feedback and its Network Analysis for Linewidth Reduction of a Semiconductor Laser, J. Lightwave Technol., 6, 3, (1988) 357.
- 7) S. Jiang, N. Tomita, H. Ohsawa and M. Ohtsu：A Photon Scanning Tunneling Microscope Using an AlGaAs Laser, Jpn. J. Appl. Phys., 30, 9 A, (1991) 2107.
- 8) M. Born and E. Wolf：Principles of Optics, 4th Ed., Pergamon Press, Oxford, (1970) 47.
- 9) S. Jiang, H. Ohsawa, N. Tomita and M. Ohtsu：Photon Scanning Tunneling Microscope using Diode Lasers, Tech. Digest of Ann. Meeting of Opt. Soc. Am., San Jose, CA, (Nov. 1991) 65.
- 10) U. Doring, D. W. Pohl and F. Rohner：Near-field Optical-scanning Microscopy, J. Appl. Phys., 59, 15, (1986) 3318.

## ■ 著者紹介



1978年3月東京工業大学大学院博士課程修了。工学博士。レーザー制御，フォトンSTM，量子光学，非線形光学などを研究

光ピンセットで1個の原子を自在に操る

# 顕微鏡 ルネッサンス「フォトンSTM」で何が可能か?

——超高感度光記録、マイクロマシン駆動等、無限の応用

表面観察技術の極限は、Åオーダーの原子を観察するところまで到達している。この見えた原子を捕えたり操作しようとする試みが現在の最先端。多くの可能性を秘めた新物質創製への挑戦として注目を集めている。光ピンセットでつかむことがなぜできるのか? そのインパクトは何か? (編集部)

大津 元一

光はまっすぐ遠くまで伝搬する。とくにレーザーの場合、光ビームの単位断面積あたりのパワー密度は大きい。この特徴を利用して、光通信、光情報処理等の先端技術が育ち、さらには物質や原子の加熱にも用いられてきた。

しかし、古代の科学者デモクリトス以来、光によって1個の中性原子を冷却した例は皆無であった。これを実現し、かつ原子の位置を制御・操作するためには、遠くまで伝搬する「普通の光」を使うのではなく、これから説明する「極微空間に局在した光」を使えばよいことが最近わかってきた。すなわち「原子操作技術の幕開け」の時代の到来である。

さらにこの光を使うと、光学の常識を覆す高い倍率(高い分解能)の光学顕微鏡が実現する。したがって、今日は「顕微鏡のルネッサンス」の時代でもある。ここでは単一中性原子操作の可能性について論ずるが、それに先立ち、原子操作のための道具としての新しい顕微鏡、「フォトン走査トンネル顕微鏡(フォトンSTM: Photon Scanning Tunneling Microscope)」について述べる。

## 顕微鏡が限界を超えた!!

——光学の常識をくつがえす

光を波としてとらえると、これは自由空間をまっすぐ進むが、もし板に開けられた微小な穴(開口と呼ばれ

る)があると、それを通り抜けた光波は広がることはよく知られている。これは「回折」と呼ばれる現象である。

開口の直径 $a$ が小さいほど回折の効果は顕著である。この性質のために、従来の光学顕微鏡では、光の波長 $\lambda$ より小さい寸法をもつ試料の像はぼやけてしまい、観察不可能であった。そこで、微小な試料を見るには電子顕微鏡を用いたり、最近ではトンネル電子を利用した走査トンネル顕微鏡(STM)が発明されている。しかし、これらは試料に金属膜を蒸着し、かつ試料を高真空中に置く必要があるため、非接触・非破壊の観察は不可能である。

われわれはこれらの欠点を補い、かつ光学の教科書に古くから記されている回折による限界を打破し、光の波長よりも小さい寸法をもつ試料を観測するための顕微鏡(すなわち光学の常識をくつがえす顕微鏡)を考案・開発している。

第1図に示すように試料裏面からレーザー光を入射させ全反射が起こるようにする。

このとき光学の教科書にあるように、試料表面にはエバネッセント光と呼ばれる表面波が発生する。エバネッセント光は普通の光とは異なり、物質表面からみついでいて、遠くへは伝搬しない。すなわち「極微空間に局在した光」である。その光パワーは試料表面からの距離 $z$ とともに急激に減少するので、 $z < \lambda$ の領域でのみ観察可能である( $\lambda$ : 光の波長)。そこでこの領域(近

東京工業大学 大学院総合理工学研究科 教授 工博  
(オオツ モトイチ)

視野領域と呼ばれる)に開口を置き、開口を通り抜けたエバネッセント光パワーを測定すれば、そのパワー変化量は試料面粗さを表しているので $z$ 方向に沿った試料面形状の測定精度(分解能と呼ばれる)は非常に高くなる。

一方、冒頭に記した回折現象は $z > \lambda$ となる領域(遠視野領域と呼ばれる)でのみ起こる現象なので、近視野では $a \ll \lambda$ の場合でも開口を通り抜けたエバネッセント光は広がらない。すなわち、開口の真下にある試料表面から発したエバネッセント光のパワーだけが測定できる。したがって試料面内の形状測定の分解能は従来の光学顕微鏡とは異なり、光の波長ではなく開口直径で決まる。

以上がフォトン STM の動作原理であるが、光をフォトン(光子)とみなすと、開口を通り抜けたエバネッセント光とは、試料形状、開口と試料との距離、開口径等によって決まる確率で生じるフォトンの(試料内部から開口の後ろへの)トンネル効果と考えることもできる。

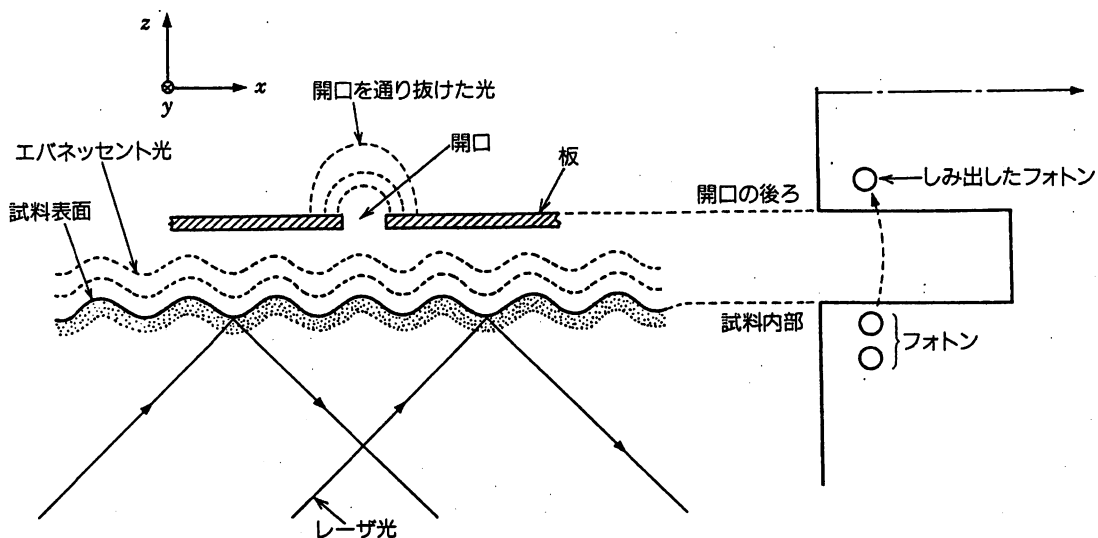
このような微小開口をもった板を試料表面上(普通 $z \approx \lambda/100$ である)で走査し、各位置で開口を通り抜けたエバネッセント光パワーを測定し、計算機のディスプレイ上に表示すれば高分解能が得られ、空气中で、か

つ非接触・非破壊で測定できる超高分解能の光学顕微鏡となる。実際には開口の代わりに鋭く研磨されたコアをもつ光ファイバを用いてもよく、かつその製作方法はより簡便・高精度である。この場合、分解能はコア先端部の曲率半径によって決まることがわかっている。

第2図(a)、(b)は化学エッチング法によりコア先端を先鋭化したファイバ端面とそのコア部を拡大した電子顕微鏡写真である。これより先端角度20度、曲率半径10nm以内が実現していることがわかる。ただし、曲率半径は非常に小さく、コア先端はこのような高倍率の電子顕微鏡を使ってもぼやけて見える。

このファイバを走査しながらその先端からピックアップしたエバネッセント光パワーを測定することにより第3図に示すような直径 $\lambda/10$ (ただし $\lambda = 800\text{nm}$ )のポリスチレン製微小粒子集団<sup>(3)</sup>、さらには極微生物試料の代表例であるバクテリオファージ T4の像等を初めて光によって観測することができた。

普通の光学顕微鏡ではこの写真全体がぼやけた小さな点のように見えるだけである。これら一連の測定結果により、試料厚み方向、面内方向の分解能はそれぞれ2 nm 以内、5 nm 以内と見積もられている。これは世界最高の性能であり、装置の細部改良により分解能



(a) 試料裏面からレーザー光を全反射するように入射させるとエバネッセント光が試料表面に発生する。開口を通りぬけるエバネッセント光のパワーを測定することで、表面の形状がわかる。

(b) 光をフォトンとみなしたときのフォトンのトンネル効果。

第1図 フォトン STM の動作原理

はさらに向上すると考えられている。

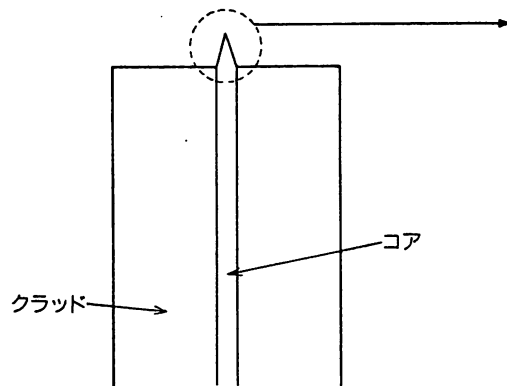
### 単一中性原子を操作する

このような驚異的な分解能をもつ光学顕微鏡が実現したが、あえて極言すれば、私は顕微鏡にはあまり興味はない。人間が他の動物と異なるのは道具を使って新しい物を作ることができる点なので、この考え方に基づくと、すでに自然界にある物質を顕微鏡を使って観測・評価することは人間らしい行動としては不十分である。

私の興味は、前節で示したフォトン STM 用のファイバプローブを「光ピンセット」という道具として用いて、真空中に浮遊する単一中性原子を捕獲し、ひいて

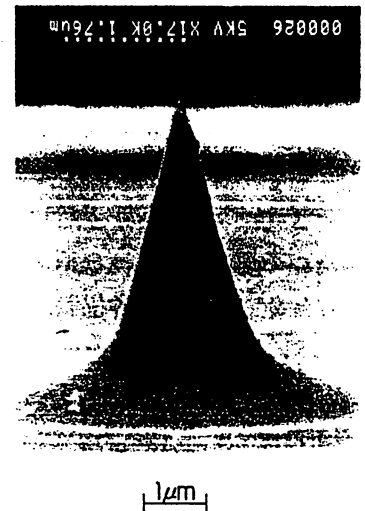
は単一原子レベルでの結晶成長を行う(新しい物を作る)ことにある。ではその可能性はどのようなだろう。

第4図に単一原子捕獲の原理を示す。フォトン STM の場合とは反対にファイバ後端からレーザ光を入射する。先端の曲率半径は光波長よりはるかに小さいので「普通の光」は先端まで達しない。先端にはエバネッセント光だけがからみついている。この光は遠くへ伝搬しないので、「重いフォトン」と考えられる(普通の光は質量0のフォトンである)。エバネッセント光に原子が飛び込んでくると、重いフォトンとの衝突を繰り返して原子の熱運動エネルギーは減少し、原子は冷却される。ファイバ後端から入射するレーザのパワーを30 mW(CD プレーヤ用半導体レーザのパワーと同等)、フ

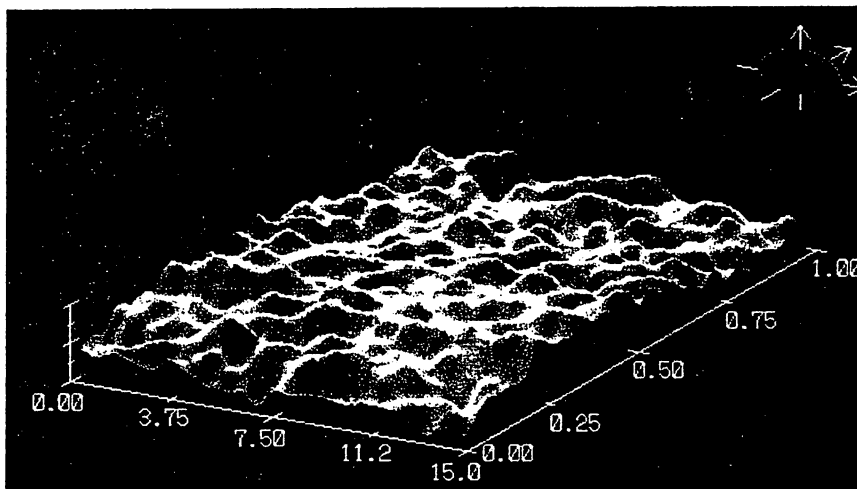


第2図 コア先端を先鋭化した光ファイバ

(a) 断面形状(コア径: 3 $\mu$ m、クラッド径: 90 $\mu$ m)



(b) コア先端の電子顕微鏡写真



第3図 直径80nmのポリスチレン球集団がガラス表面に密集している状態の観測結果<sup>(3)</sup>

ファイバの先端曲率半径15nmとすると冷却された原子の温度は約80 $\mu$ K、そのときの熱運動速度は約15cm/s、と推定されている(0 K=-273 $^{\circ}$ C)。このように極低温まで冷却された原子はファイバ先端付近をゆっくり運動しており、これにより遠心力が働くので、ファイバ先端に付着することなく、エバネッセント光中でブラウン運動する。

原子を安定に捕獲するためには捕獲のポテンシャルが十分深くなければならないが、この方法では真空中を室温で飛び回っている原子を捕獲できるほど深くない。上記の実験条件では700 $\mu$ K以下の温度の原子だけが捕獲される。この温度はずいぶん低いように思われるかもしれないが、最近では普通のレーザー光を使って真空中に浮遊している中性原子の集団を数 $\mu$ Kまで冷却する技術が開発されており<sup>(1)(2)</sup>、これを使って原子集団を700 $\mu$ K以下まで予備冷却することは容易である。したがって、そのような予備冷却原子集団中の一つの原子をファイバプローブで捕獲できる。

詳細は省略するが、この捕獲法は原子の熱運動の速度選別機能も有しており、また原子間には互いに反発する力が働くので1個の原子だけが捕獲される。原子が捕獲されたか否かは原子から発する蛍光を観測すればわかる。蛍光測定感度はきわめて高いことは従来か

ら知られており、単一原子からの蛍光も測定できる。

また、以上の議論は、実はレーザー光の周波数 $\nu$ ( $\lambda=800\text{nm}$ の光の周波数は約 $400\text{T Hz}$ 、すなわち $4 \times 10^{14}\text{ Hz}$ )を原子のエネルギー構造によって決まる原子固有の共鳴周波数 $\nu_r$ よりわずかに低周波側(約10MHz、すなわち $1 \times 10^7\text{ Hz}$ )に固定した場合( $\nu < \nu_r$ )に成り立つ。一方、わずかに高周波側( $\nu > \nu_r$ )に固定すると原子は捕獲されず、逆に押し出される。

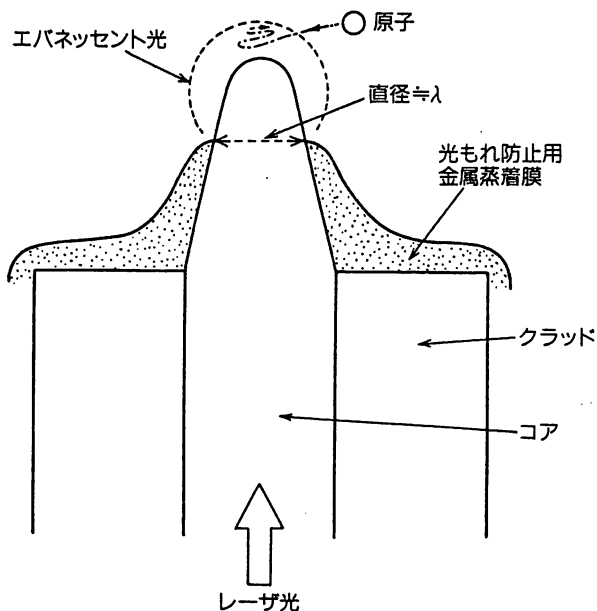
これを利用して、まず $\nu < \nu_r$ の状態ですべて単一原子を捕獲し、冷却された結晶基板の上方にファイバごと移動し、次に $\nu > \nu_r$ とする。そうすると原子は押し出され、加速・加熱されて結晶基板の上に落ち、固定される。すなわち基盤の上に基石を置くように単原子レベルでの結晶成長ができる。また、このように光を使って原子を操作する方法の利点は、対象となる原子の種類が多いことである。例えば、適当な波長のレーザーを用意しておけば半導体産業に重要なシリコン等の原子を捕獲することができる。

## 「常識」は破るためにある ——新しい光と物質を作る

ここで紹介したフォトンSTMのアイディアは、1920年代にすでにアインシュタインが友人に宛てた手紙の中にしたためてあったといわれている。しかし、これを実現する試みが始まったのは1980年代に入ってからである。私は6年前、アメリカの研究所で仕事をしていたときファイバの先鋭化を試みようとしたが、周囲の研究者からは「難しい点が多すぎるのでやめたほうがよい」と言われた。

しかしあきらめきれず、帰国後私の研究室の学生諸君と試みると、みごとに尖ったファイバができた。純真で忍耐強く才気溢れる学生諸君に感謝したい。さらに私がいち早くこのような新しい分野に参入できたのは、わが国の産業界が世界に誇る高品質の光ファイバ、ならびに半導体レーザー光源を使うことができたからである。その意味で単一中性原子操作とフォトンSTMはわが国で生まれ育ったまったく新しい分野といえる。

エバネッセント光を微小開口でピックアップする装置は非常に単純なので、「この研究はコロンブスの卵ではないか?」と思われるかもしれない。しかし、古く



第4図 フォトンSTM用のファイバプローブ先端のエバネッセント光による単一中性原子捕獲の原理

からその存在を知られていたエバネッセント光の実体は実はあまりわかっていない。とくに重いフォトンなどという概念はなかった。さらに量子力学的な考察を加えると光と物質とはあまり区別がつかないものであること、フォトンSTMの動作原理はトンネル電子を使った上記のSTMとなんら異なるものではないこと、等の新事実もわかってきた。つまり、原理的にはフォトンSTMの分解能はSTM等の分解能と同等で、原子1個ずつを分離観測できる能力を有する。

このように本稿で述べた話題はエバネッセント光と称する極微空間に局在した光を発生・利用する新しい試みといえる。さらにこの光により原子を操作できれば新しい極微物質が作れる。新しい物質ができればそこからさらにまた新しい性質をもった光が生ずる。光と物質とは車の両輪をなすように相互作用しながら、その特性が進歩していく。新しい光と物質を創製する

ことの作業はきわめて魅力的で若々しい。その波及効果も、極微結晶工学、超高密度光記録、ひいては原子メモリ(一つの原子に1ビットの情報を記憶させ、読み出す)、極微生体試料の操作、マイクロマシンの駆動、等多岐にわたる。

ご注意いただきたいのは、教科書等々書いてある「常識」は、打破できないことはないということである。それに気づくか否かが問題なので、常々「教科書を読むのではなく書くつもりで研究しよう」と自戒している。

#### 参考文献

- (1) 大津元一：「コヒーレント光量子工学」、朝倉書店(1990年)
- (2) M.Ohtsu: "Highly Coherent Semiconductor Lasers", Artech House, Co., Boston (1992)
- (3) S.Jiang, N.Tomita, H.Ohsawa and M.Ohtsu: "A Photon Scanning Tunneling Microscope Using an AlGaAs Laser", Jpn.J.Appl.Phys., Vol.30, No.9A, p.p.2107-2111 (Sept.1991)



11:00am

---

**TuO2 Photon scanning tunneling microscope using diode lasers**

S. Jiang, H. Ohsawa, N. Tomita, and M. Ohtsu

*Tokyo Institute of Technology, Ohtsu Laboratory, Graduate School at Nagatsuta, 4259 Nagatsuta, Midori-ku, Yokohama, Japan*

A novel superresolution photon scanning tunneling microscope (PSTM) using diode lasers and optical fibers has measured a submicron structure sample in a noncontact and nondestructive manner. Diode lasers, which can be directly high speed modulated, are used to make the system more compact ( $25 \times 20 \times 12 \text{ cm}^3$ ) and the measuring time shorter. The principle of the operation is that the evanescent field (tunneling photon) depending on the topography of the sample is picked up by a fiber probe on which the sub-wavelength aperture is fabricated. The top of the fiber probe was sharpened by HF selective etching to achieve 80-nm radius of curvature. A stepped  $\text{SiO}_2$  thin film 9 nm high optical disk with submicron sized pits similar to a moth-eye structure was observed. Furthermore, 80-nm diameter latex particles have also been observed. These are the smallest size particle resolved by the PSTM, to the author's knowledge. A reflection-resonance type PSTM is proposed for solving the problem with the low power picked up in a transmission-type PSTM (demonstrated above), which limits the measurement sensitivity.

*Nikon Corp., 6-3 Nishi-ohi 1-Chome, Shinagawa-ku, Tokyo, Japan*

**Reference**

1. S. Jiang, N. Tomita, K. Nakagawa, and M. Ohtsu in *Conference on Lasers and Electro-Optics*, Vol. 10 of the 1991 OSA Technical Digest Series (Optical Society of America, Washington, D.C., 1991), paper CThO5.

PHOTON STM, APPLICATIONS TO BIOTECHNOLOGY AND  
SINGLE ATOM CRYSTAL GROWTH

M. OHTSU

Graduate School at Nagatsuta, Tokyo Institute of Technology  
4259 Nagatsuta, Midori-ku, Yokohama 227, JAPAN

A transmission-type photon scanning tunneling microscope (T-PSTM) and a reflection-resonance-type PSTM (RR-PSTM) for higher resolution were proposed[1-3]. Figures 1(a) and (b) represent the setup of the systems. For the T-PSTM, a fiber probe was fabricated by using a single-mode optical fiber specially designed for nonlinear optics. Figure 2 shows the top of the sharpened fiber. The minimum cone-angle as small as 21 degree was achieved. The curvature radius for this fiber was estimated to be smaller than 10 nm. By using this fiber-probe, images of three-dimensional profiles of several samples, i.e., a SiO<sub>2</sub> thin film, a moth-eye-type optical disk (Fig. 3), and the bunched group of latexes (Fig.4), were observed. For the RR-PSTM, numerical analyses and simulation experiments by using a 44 mm wavelength microwave confirmed that the resolution higher than that of the T-PSTM can be expected.

As an application to biology, the profile of a bacteriophage T4 was observed by the T-PSTM. Figure 5(a) shows the images of spherical heads and bodies of two bacteriophages, which are the results of the first successful measurement in the world. By comparing the SEM picture given by Fig.5(b), it can be confirmed that the resolution of the present T-PSTM is as high as that of the SEM[3]. Through these measurements, the normal and lateral resolutions of the T-PSTM were estimated to be higher than 2 nm and 5 nm, respectively, which are, to the author's knowledge, the highest record of the PSTM documented so far.

Higher resolution and shorter measurement time can be expected by increasing the modulation frequency of the diode laser. An advanced method to fix the biological sample is under developed to improve the reproducibility of the measurements. A system to measure dynamic properties of a biological sample is also under development by using a multi-core fiber-probe.

A novel technique of manipulating atomic particles can be realized by a highly localized evanescent field produced at the extremity of the nanometric fiber-probe by the laser light propagating in the fiber[4]. As is shown by Fig.6, the interaction of atoms with the localized evanescent field shows several remarkable features. Due to extraordinary large and spatially-modulated wave-vector of the field, an atom absorbing an evanescent photon in the proximity region is recoiled strongly in the direction parallel to the probe surface. When the field frequency is detuned red to the atomic resonance, the atom is always decelerated laterally and accelerated normally to the probe surface. Due to rapid intensity decrease in the near field region, a relatively strong dipole attractive force acts on the atom normally to the probe surface when the field frequency is

red-detuned. In addition, the spontaneous emission is anisotropic due to spatially normal to the probe tip. These features suggest that a potential well is formed at the contiguous region between the proximate and near fields.

A calculation for the alkali-atoms shows that an atom with the thermal velocity 30 cm/s is trapped in an evanescent field produced by a fiber-probe of 15 nm curvature-radius irradiated by laser light with spectrum covering 0 - 30 MHz lower wing of the resonance. In this condition, the recoil momentum for one evanescent photon absorption equals the atomic momentum. The centrifugal force due to recoil of the evanescent photon is balanced by the dipole attractive force in the near-field region. The spontaneous emission in the passage of the evanescent field forces the atom into the potential well, which require the pre-cooling temperature of 0.3 mK for a saturation-intensity excitation and is feasible by using optical molasses. The atom is not adsorbed on the probe surface because of the normal repulsive force in the proximity region.

The fundamental process of the PSTM is described by a short-range interaction via evanescent photons scattered from/to propagating photons. To describe this process, it is advantageous to use a quantum optical approach by using the Feynman's diagrams, which is applicable to all of SXM's. This interaction should be treated explicitly, which has not yet been fully developed in the conventional theories[5-7].

#### Acknowledgments

The author thanks Prof. A. Ikai of Tokyo Inst. Tech. for providing him with biological samples. He indebted to Prof. H. Hori of Yamanashi Univ. for his theoretical discussions. A part of this work was supported by the Grant-in-Aid (number 03452089).

#### References

- [1] M. Ohtsu, K. Nakagawa, S. Jiang, and N. Tomita, Optoelectronics Conference, July 1990, Makuhari, Japan, 12D1-1
- [2] S. Jiang, N. Tomita, H. Ohsawa, and M. Ohtsu, Jpn. J. Appl. Phys., 30 (1991) 2107
- [3] S. Jiang, H. Ohsawa, N. Tomita, and M. Ohtsu, Annual Meeting of Opt. Soc. Am., Nov. 1991, San Jose, Tu02
- [4] H. Hori, S. Jiang, M. Ohtsu, and H. Ohsawa, submitted to International Quantum Electronics Conference, Vienna, June 1992
- [5] C. Girard and M. Spajar, Appl. Opt., 29 (1990) 3726
- [6] C.R. Carniglia and L. Mandel, Phys. Rev.D, 3 (1971) 280
- [7] B.B. Dasgupta and R. Fuchs, Phys. Rev. B, 24 (1981) 554

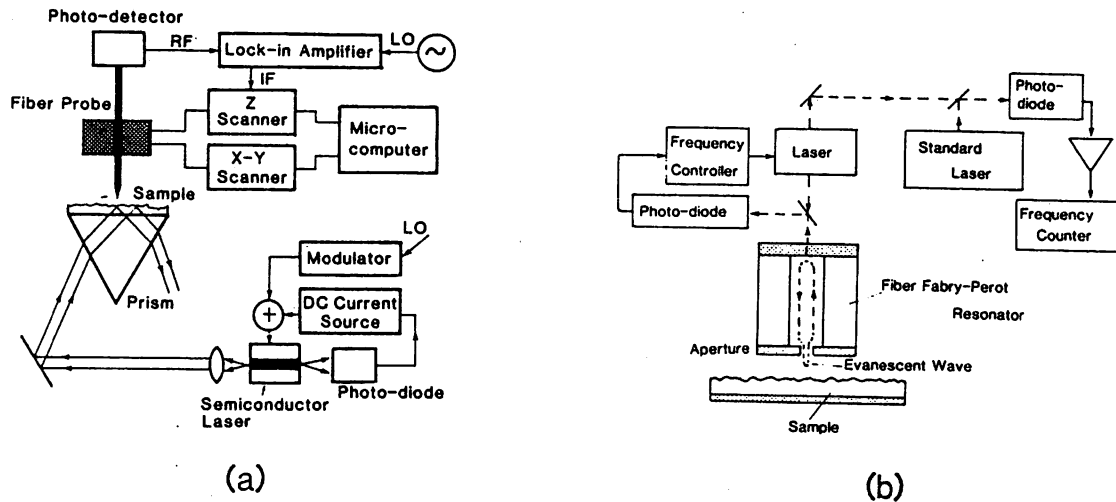
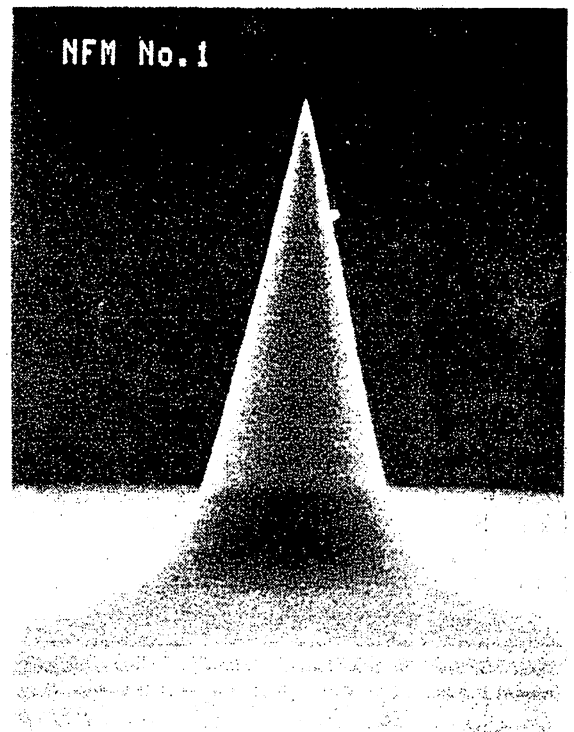


Fig.1

Experimental setup of PSTM's[1-3].  
 (a) Transmission-type. (b) Reflection-resonance-type.



(a)



(b)

Fig.2

SEM-pictures of the fiber-probe[3]  
 (a) Diameter of the clad is 90 um. (b) Magnified picture of (a).  
 Width of this picture is 5.6 um.

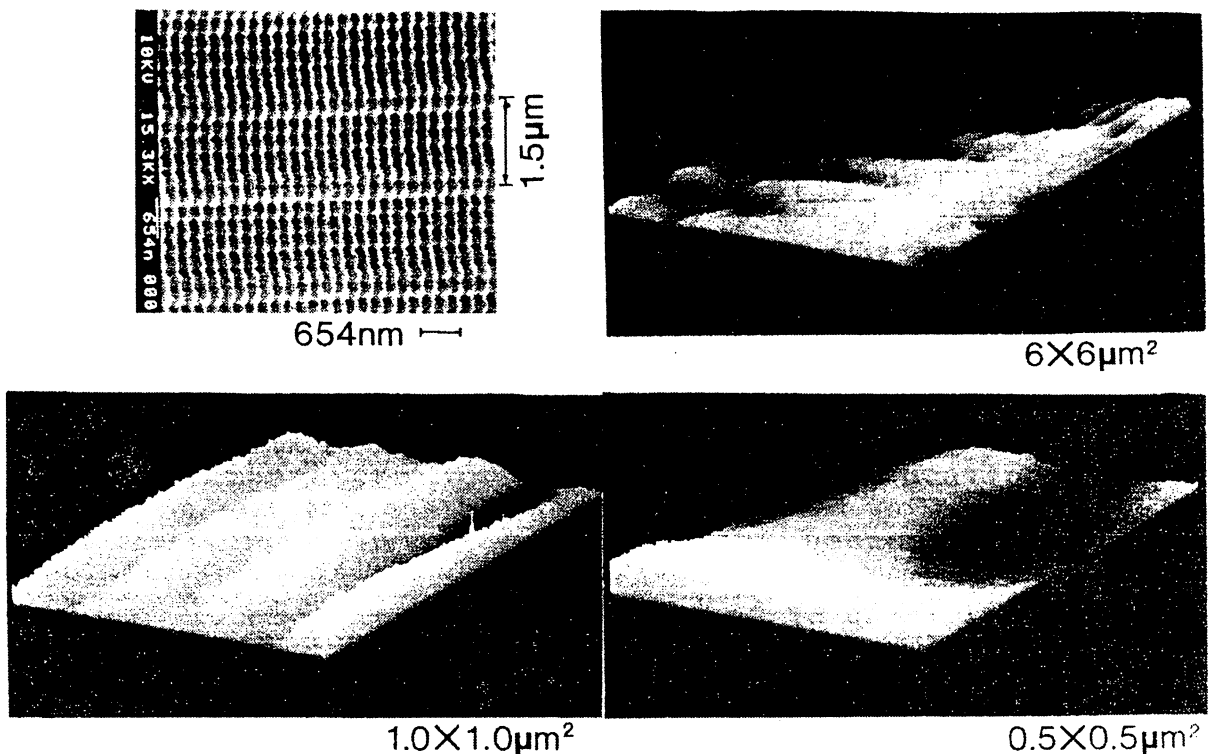


Fig.3

Profiles of a moth-eye optical disk[3].  
 Upper-left: SEM-picture. Other three pictures were taken by the T-PSTM with several magnifications.

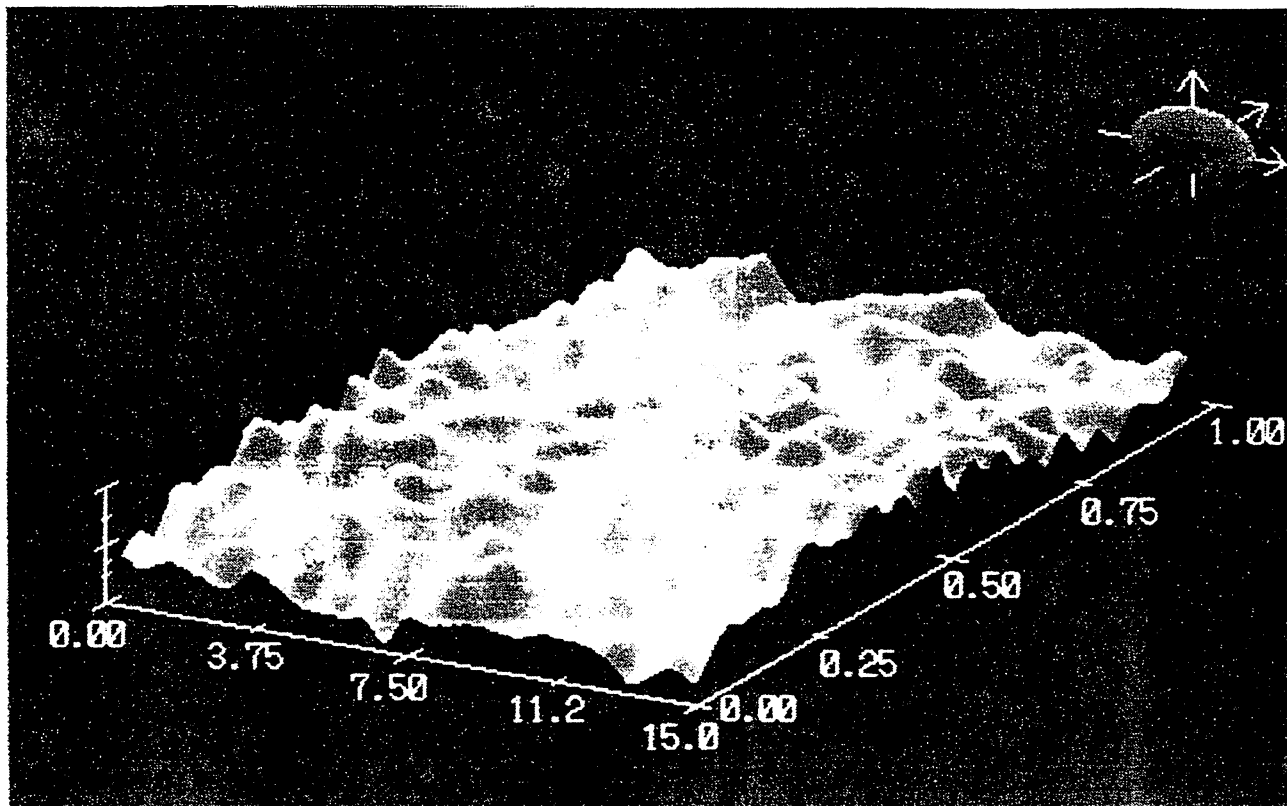


Fig.4

Profiles of the bunched group of the latexes. The diameter of each latex is 80 nm[2]

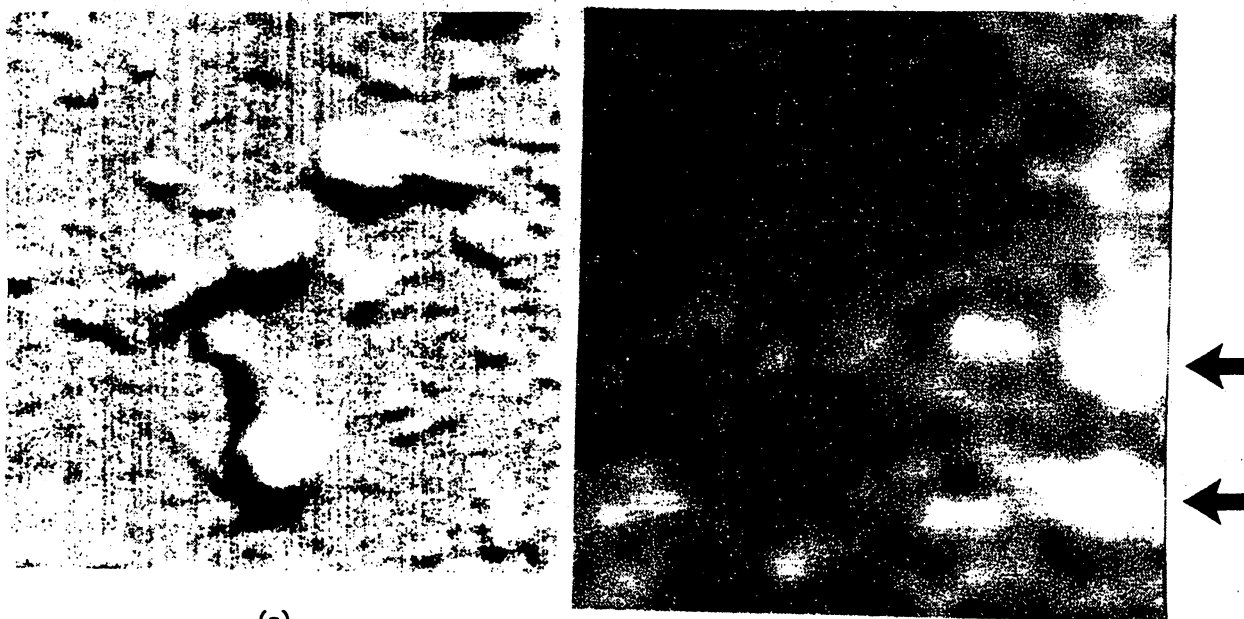


Fig.5 (a)

(b)

Profiles of bacteriophages T4[3]

(a) SEM-picture. (b) Images indicated by arrows represent two bacteriophages. Dimensions of these two pictures are  $0.6 \mu\text{m} \times 0.6 \mu\text{m}$ .

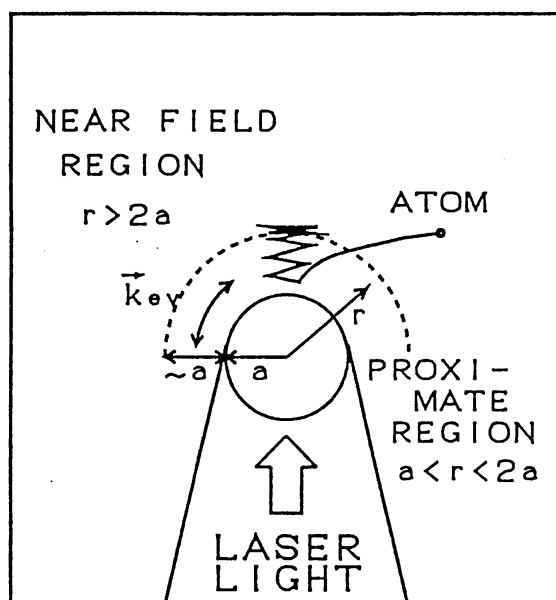


Fig.6

The schematic diagram of the evanescent field in the vicinity of the extremity of the fiber-probe and its interaction with an atom[4].

## PHOTON STM

M. OHTSU

Graduate School at Nagatsuta, Tokyo Institute of Technology  
4259 Nagatsuta, Midori-ku, Yokohama, Kanagawa 227, JAPAN  
Phone:+45-922-1111, Fax:+45-921-1156

The studies on photon scanning tunneling microscope ( Photon STM ) are reviewed. An optical fiber-probe with the curvature radius smaller than 5 nm and the cone angle of 20 degrees has been realized by chemical etching. Based on the observed results of three-dimensional profiles of several samples including the bacteriophage T4, the normal and lateral resolutions were estimated to be higher than 2 nm and 5 nm, respectively.

By employing the quantum optics method, a novel and intuitive model was developed to describe the evanescent field which was considered as the tunneling photons. Furthermore, the principle of operation of the photon STM was found to be equivalent to those of STM, AFM, etc., which means that the resolution of the photon STM could be up to the atomic level and a general theory of the tunneling microscope could be established.

Possibility of using the photon STM system for manipulating a single neutral atom and its application to the single-atom level crystal growth are also proposed.

radius of a sharpened fiber-probe (see Fig. 2(a)(b) for its detailed profile). Its principle of operation, employing a sharpened optical fiber-probe, is schematically explained by Fig. 1(a). Figure 1(b) shows the images of spherical head and cylindrical bodies of bacteriophages T4, which are the results of the first successful measurement in the world. This figure confirms that the resolution as high as several nanometer was achieved, which is, to the authors' knowledges, one of the highest records documented so far.

A novel technique of manipulating atomic particles can be realized by a highly localized evanescent field produced at the extremity of the nanometric fiber-probe by the laser light propagating in the fiber. The interaction of atoms with the localized evanescent field shows several remarkable features (Fig. 2(c)). Due to extraordinary large and spatially-modulated wavevector of the field, an atom absorbing an evanescent photon in the proximity region is recoiled strongly in direction parallel to the probe surface. When the field frequency is detuned red to atomic resonance, the atom is always decelerated laterally and accelerated normally to the probe surface. Due to rapid intensity decrease in the near field region, a relatively strong dipole attractive force acts on the atom normally to the probe surface when the field frequency is red-detuned. In addition, the spontaneous emission will be anisotropic due to spatial asymmetry normal to the probe tip. These features suggest that a potential well will be formed at the contiguous region between the proximate and near fields.

A calculation for the rubidium D-line shows that a Rb atom with velocity 30 *cm/s* is trapped in an evanescent field produced by a fiber-probe of 15 *nm* curvature-radius irradiated by laser light with spectrum covering 0 ~ 30 *MHz* lower wing of the resonance. In this condition the recoil momentum for one evanescent-photon absorption equals the atomic momentum. The centrifugal force due to recoil of the evanescent photon will be balanced by the dipole attractive force in the near-field region. The spontaneous emission in the passage of the evanescent field forces the atom into the potential well, which requires the pre-cooling temperature of ~ 300  $\mu$ K for a saturation-intensity excitation and is feasible by using optical molasses. The atom is not adsorbed on the probe surface because of the normal repulsive force in the proximity region.

The fundamental process of PSTM is described by a short-range interaction via evanescent photons scattered from/to propagating photons, as diagramed in Fig. 3, which is applicable to all of SXMs. This interaction should be treated explicitly, which has not been fully developed in the conventional theories.<sup>[3,4,5]</sup>

1. E. Betzig et. al., *Appl. Phys. Lett.* **59**, 3381 (1986).
2. S. Jiang et. al., *Jpn. J. App. Phys.* **30**, 2107 (1991).
3. C. Girard and M. Spajar, *Appl. Opt.* **29**, 3726 (1990).
4. C. R. Carniglia and L. Mandel, *Phys. Rev. D* **3**, 280 (1971).
5. B. B. Dasgupta and R. Fuchs, *Phys. Rev. B* **24**, 554 (1981).

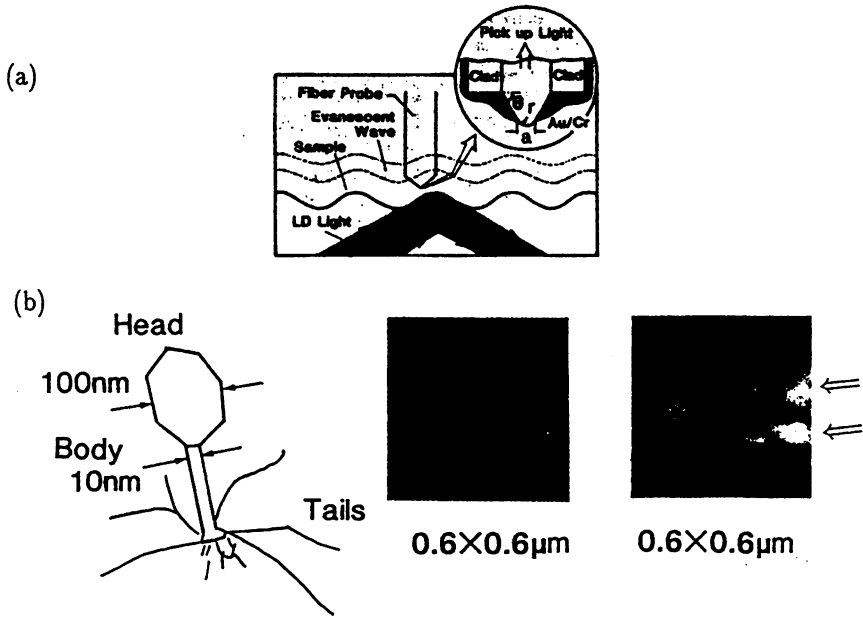
17:45

**MoM7 A Nanometer-Resolution Photon Scanning Tunneling Microscope and Proposal of Single Atom Manipulation**

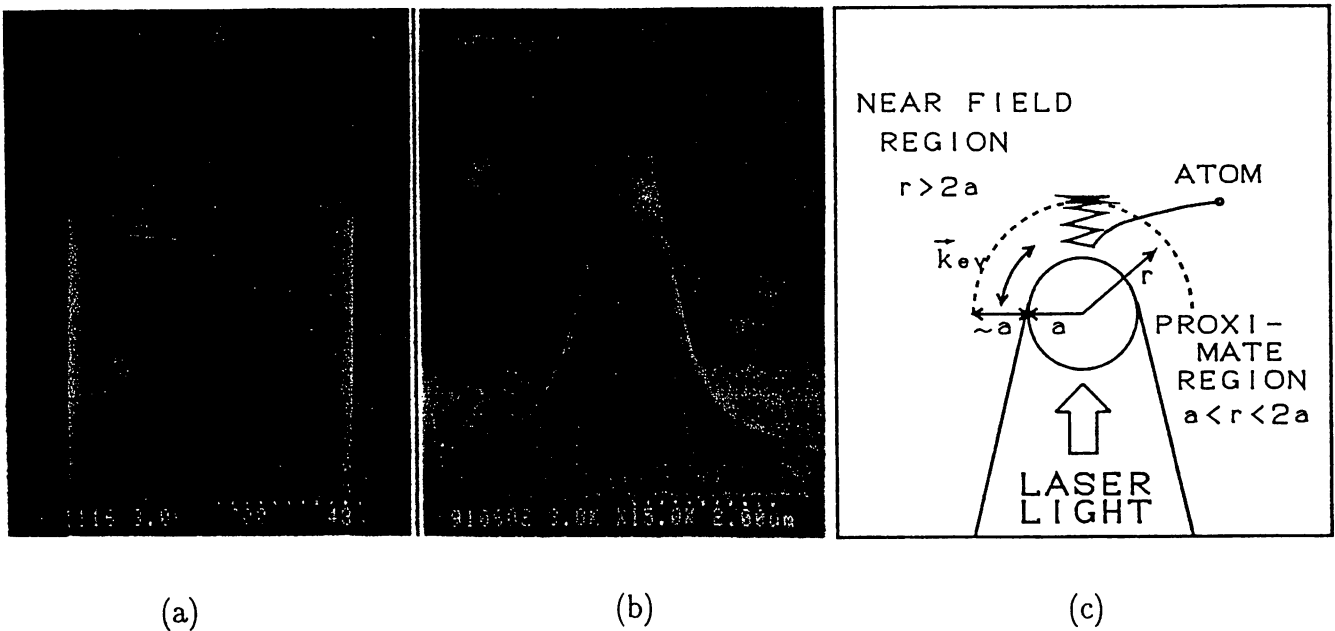
H. HORI, Faculty of Engineering, Yamanashi University, 4-3-11 Takeda, Kofu 400, Japan; S. JIANG, and M. OHTSU, Graduate School at Nagatsuta, Tokyo Institute of Technology, 4259 Nagatsuta, Midori-ku, Yokohama 227, Japan; H. OHSAWA, Nikon Corporation, Nishi-Ohi 1-Chome, Shinagawa-ku, Tokyo 140, Japan

Recent development of the photon scanning tunneling microscope (PSTM), utilizing evanescent or tunneling photons, opened a novel area of diagnosing nanometerscale objects because the resolution, being far beyond the diffraction-limit,<sup>[1,2,3]</sup> is limited only by the diameter of an aperture-probe or curvature

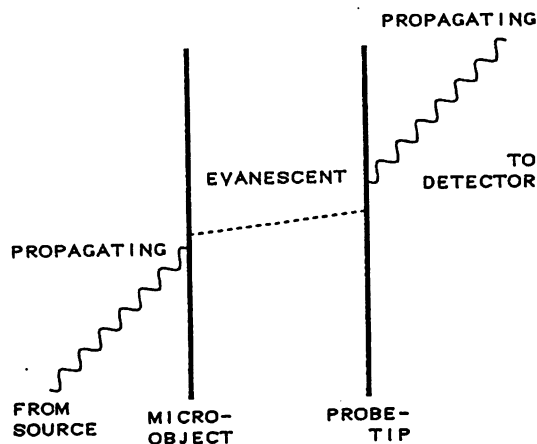




MoM7 Fig. 1: (a) Schematic explanation of the PSTM. (b) Dimensions of the bacteriophage T4 (left), images obtained by a conventional scanning electron microscope (center) and by our PSTM (right), respectively. Two bacteriophages are indicated in the PSTM image (A 780-nm wavelength diode laser was used as a light source.).



MoM7 Fig. 2: (a) The picture of the fiber-probe. Chemical etching removed the cladding and sharpened the core of the single-mode optical fiber. (b) The extremity of the fiberprobe with cone angle 25 degree and curvature-radius estimated to within 20 nm (c) The schematic diagram of the evanescent field in the vicinity of the extremity of the fiber-probe and its interaction with atoms.



MoM7 Fig. 3: A diagram describing the fundamental process of PSTM, which represents the short range interaction between micro-object and probe tip via virtual evanescent photon scattered from and into propagating photons.